TECHNICAL REPORT STANDARD TITLE PAGE

1. Report No.	2. Government Accession No.	3. Recipient's Catalog No.
FHWA/TX-81/3+284-2		

4. Title and Subtitle	5. Report Date
Pavement Roughness on Expansive Clays	January 1981
	6. Performing Organization Code

7. Author(s)	8. Performing Organization Report No.
Manuel O. Velasco and Robert L. Lytton	Research Report 284-2

9. Performing Organization Name and Address	10. Work Unit No.
Texas Transportation Institute The Texas A&M University System College Station, Texas 77843	11. Contract or Grant No. Study No. 2-8-80-284
	13. Type of Report and Period Covered Interim - September, 1979 October, 1980
12. Sponsoring Agency Name and Address State Department of Highways and Public Transportation; Transportation Planning Division P. O. Box 5051 Austin, Texas 78763	14. Sponsoring Agency Code

15. Supplementary Notes

Research performed in cooperation with DOT, FHWA.
Study Title: Pavement Roughness On Expansive Clays

16. Abstract

The patterns of pavement roughness caused by expansive clays are due largely to the underlying patterns of cracks in the subgrade soil mass. The cracks will be closer together when the soil is more active and when the climatic wetting and drying cycles have greater influence. The cracking patterns in the soil and the consequent roughness patterns are not uniform but must be characterized as a spectrum of crack spacings and wavelengths with their corresponding amplitudes.

Pavement roughness was measured by the GM Profilometer on 23 pavement sections in Texas. Two methods are used to obtain the amplitude versus wave length spectra that characterize the roughness patterns: the Fast Fourier Transform (FFT) method and the "bump counter" direct method. The two spectra are not the same nor are they expected to be. The FFT method is adopted for characterizing the roughness patterns because of its greater consistency. However, a correspondence is found between the two spectra. As a matter of convenience, the spectra are plotted as amplitude versus frequency, which is the number of wave lengths per unit length. The graphs of amplitude versus frequency were fitted by a power law equation with two constants, c and n, which are found to be correlated with each other. Unique values of c and n characterize the roughness pattern of each pavement and these, in turn, are found to depend upon the composite flexural stiffness of the pavement, time, climatic measures, and several physico-chemical soil properties. (continued on back of page)

17. Key Words	18. Distribution Statement
Pavement roughness, expansive clay soils, spectrum of crack spacings and wavelengths, amplitudes.	No Restrictions. This document is available to the public through the National Technical Information Service, Springfield, Virginia 22161

19. Security Classif. (of this report)	20. Security Classif. (of this page)	21. No. of Pages	22. Price
Unclassified	Unclassified	228	

Form DOT F 1700.7 (8-69)

PAVEMENT ROUGHNESS ON EXPANSIVE CLAYS

by

Manuel O. Velasco and Robert L. Lytton

Research Report Number 284-2

Flexible Pavement Data Base and Design

Research Study 2-8-80-284

conducted for

The Texas State Department of Highways and
Public Transportation

in cooperation with the
U.S. Department of Transportation
Federal Highway Administration

by the

Texas Transportation Institute
Texas A&M University
College Station, Texas

January 1981

ABSTRACT

The patterns of pavement roughness caused by expansive clays are due largely to the underlying patterns of cracks in the subgrade soil mass. The cracks will be closer together when the soil is more active and when the climatic wetting and drying cycles have greater influence. The cracking patterns in the soil and the consequent roughness patterns are not uniform but must be characterized as a spectrum of crack spacings and wavelengths with their corresponding amplitudes.

Pavement roughness was measured by the GM Profilometer on 23 pavement sections in Texas. Two methods are used to obtain the amplitude versus wave length spectra that characterize the roughness patterns: the Fast Fourier Transform (FFT) method and the "bump counter" direct method. The two spectra are not the same nor are they expected to be. The FFT method is adopted for characterizing the roughness patterns because of its greater consistency. However, a correspondence is found between the two spectra. As a matter of convenience, the spectra are plotted as amplitude versus frequency, which is the number of wave lengths per unit length. The graphs of amplitude versus frequency were fitted by a power law equation with two constants, c and n, which are found to be correlated with each other. Unique values of c and n characterize the roughness pattern of each pavement and these, in turn, are found to depend upon the composite flexural stiffness of the pavement, time, climatic measures, and several physico-chemical soil properties. Four soil properties are found to be necessary to predict the roughness spectra: (a) cation exchange capacity which is an indicator of the kind of mineral that is present, (b) percent clay which shows

how much clay is present in the subgrade soil, (c) exchange sodium percentage which is partly an indication of the geological environment in which the clay was deposited and partly an indication of how erodable and dispersive the soil is, and (d) the plasticity index which is a measure of the moisture reactivity of the soil. The dominant wave lengths in each of the roughness patterns are determined together with cumulative distributions of wave lengths and amplitudes for each of the pavement sections studied. Probability density functions for wavelengths are developed from these data. A method for using these wave length probabilities and the corresponding amplitude spectral equation is developed to calculate the amount of level-up material that must be placed on the pavement to achieve a smooth ride. A method of computing the amount of material that can be removed by heaterplaning and milling operating is also shown. An equation for the loss of serviceability index with time is developed and several examples are presented showing how the serviceability loss depends upon soil and pavement properties. The equation for serviceability index loss constitutes a design equation for pavements on expansive soils.

IMPLEMENTATION STATEMENT

The data, the soil tests, and the equations developed in this report are the basis of a design procedure for pavements on expansive clay. Pavement roughness due to expansive clay is dependent upon cation exchange capacity, percent clay, exchange sodium percentage, as well as the familiar plasticity index. The differential movement of an expansive subgrade is resisted by the composite flexural stiffness of the overlying pavement layers. The State Department of Highways and Public Transportation should consider acquiring the simple laboratory instrumentation that is required to measure the cation exchange capacity and exchange sodium percentage of these expansive soils.

DISCLAIMER

TABLE OF CONTENTS

TABLE OF CONTENTS (CONTINUED)

LIST OF TABLES

LIST OF TABLES (CONTINUED)

LIST OF FIGURES

LIST OF FIGURES (CONTINUED)

LIST OF FIGURES (CONTINUED)

LIST OF FIGURES (CONTINUED)

LIST OF FIGURES (CONTINUED)

LIST OF FIGURES (CONTINUED)

CHAPTER ONE

INTRODUCTION

The importance of the damage caused by expansive clays to all types of structures in many areas of the world is well known. In particular, the most evident damage to highway pavements constructed on swelling soils is the appearance of a series of waves along the pavement. The waves continue to develop until moisture equilibrium in the soil is reached (38). These patterns of pavement roughness are due largely to the underlying patterns of cracks in the subgrade soil mass. The cracks will be closer together and larger when the soil is more active and when the wetting and drying of the subgrade soil due to climatic influences and drainage is more severe. Water that enters and leaves the cracking patterns in the soil beneath the pavement is reflected upward as a series of bumps which are not uniform but must be characterized as a spectrum of wave lengths and their corresponding amplitudes. The practical consequences of this pavement roughness are loss of riding comfort and reduction in pavement service life.

Identification of expansive clays is relatively simple, as a result of the available knowledge obtained from laboratory tests dealing with the nature of these soils. However, as Gromko has pointed out, there is not yet enough information about the in-situ behavior of swelling soils (10). Specifically, the presence of these soils under highways is a major problem to designers, because to predict their effects is complex, making very difficult the determination of the most economic measure, or combination of measures, to adopt in preserving acceptable riding quality. Some of the available measures are: pre-construction

treatments of the soil, such as removing it to a certain depth, chemical stabilization with different products, or prewetting, implementation of moisture barriers (horizontal or vertical), and post-construction treatments of the pavement, such as overlay, level-up, or some form of reworking. Any of these measures is usually expensive. For example, when an upgrading work becomes necessary, not only the maintaining agency pays for it, but also the traveling public bears an indirect cost. It has been reported by Lytton that the cost to the drivers of having to reduce speed because of expansive clay roughness is in the order of $550 per lane mile per year for each inch of potential differential movement for a typical stream of traffic (ADT - 7000 vehicles/day/lane) (13). An adequate design of the pavement should take into account all of these factors and minimize the overall cost for the expected life of the roadway.

One of the world's areas where the presence of swelling materials is well documented is Central Texas (Figure 1). This area belongs to the Atlantic and Gulf Coastal Plain physiographic province, which is underlain by a sequence of sedimentary rocks and nonlithified sediments. In East-Central Texas, this sequence contains some highly expansive argillaceous rocks (19). Also, in this area soils included in the Vertisol order are abundant. The Vertisols are described by the soil scientists as having a high content of montmorillonite, showing deep wide cracks in the dry seasons, and presenting other evidence of movement.

A potentially expansive soil will actually exhibit volume changes in-situ only if soil moisture variations occur. Then, the climate and drainage conditions play an important role in the behavior of these soils,

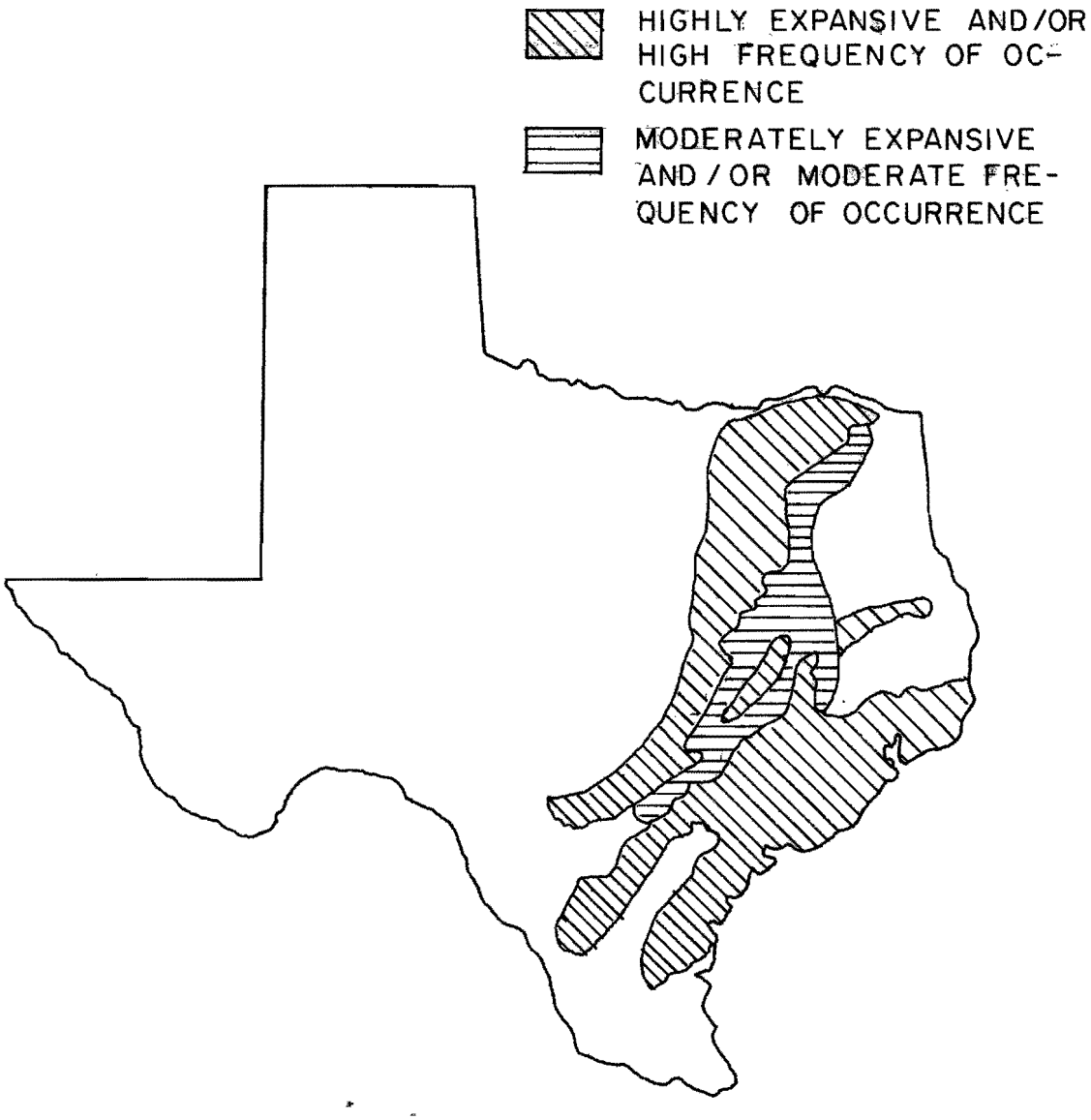

FIGURE 1. Distribution of Potentially Expansive Materials in East-Central Texas (19)

and the study of them should include some environmental indicator. One such indicator was introduced by Thornthwaite (34), using the concept of potential evapo-transpiration, defined as the amount of water which would be returned to the atmosphere if there was an unlimited supply of water to the plants and ground. Thornthwaite proposed his moisture index as

$$I_m = \frac{100\ S - 60\ d}{E_p} \quad \ldots\ldots\ldots\ldots\ldots\ldots\ldots\ldots \quad (1)$$

where

I_m = Thornthwaite moisture index

S = surplus of water, in inches

d = deficit of water, in inches

E_p = potential evapo-transpiration, in inches

A positive Thornthwaite moisture index indicates a net surplus of soil moisture, while a negative number shows a net soil moisture deficit. In Central Texas, this index varies widely, practically between 20 and -20.

Purpose

Measurements of pavement roughness have been made on several highway sections located in 9 different areas of Central Texas, where expansive soils are present. The purposes of this study are to characterize the patterns of roughness and to analyze the relative influence of the variables involved, such as the thickness and stiffness of the pavement layers, the properties of the natural soils, environmental factors, and time.

CHAPTER TWO

PRESENT STATUS

Nature of Expansive Soils

The number of studies related to the nature and behavior of expansive soils is very extensive. Generally, these works, based on laboratory tests, have been focused on the identifiaction, classification, and prediction of heave of swelling soils (10). Recently, the U.S. Army Waterways Experiment Station has completed a comprehensive series of reports for the Federal Highway Administration (19, 22, 23, 24). These reports cover distribution surveys of expansive soils in the USA, their geology, mineralogy, and physicochemical properties, investigations of the microscale mechanisms that cause volume changes, and an evaluation of the methodology for identifying and qualitatively classifying swelling soils. The results of these studies have led to a classification based on liquid limit, plasticity index, and natural suction (23).

During the last years, the necessity for a suction-based approach to the prediction of heave has been recognized. From this standpoint, Lytton (14) proposed the suction compression index as a means to differentiate the behavior of soils. This index is expressed as:

$$\gamma_h = \frac{-\frac{\Delta V}{V_i}}{\log \frac{h_f}{h_i}} \quad \ldots\ldots\ldots\ldots\ldots\ldots\ldots\ldots \quad (2)$$

where

γ_h = suction compression index

ΔV = volume change

V_i = initial volume

h_f = final value of soil suction

h_i = initial value of soil suction

The suction compression index may be determined by several tests (17). In fact, γ_h is directly related to the COLE (coefficient of linear extensibility), obtained from a test performed routinely by the Soil Conservation Service. Furthermore, it has been reported that the COLE (and then γ_h) depends upon the type of minerals and percent clay present in the soil (17). Also, Anderson et al. (1) have found that the COLE in some Vertisols was highly correlated with the percent of fine clay and the Exchange Sodium Percentage (ESP). COLE values for Vertisols range from 0.05 in arid regions to more than 0.09 in humid regions (3). All procedures for determining γ_h (which is approximately equal to the COLE) involve suction measurements. This practice is not yet in routine use by civil engineers. To overcome this difficulty, McKeen (16) has developed a chart for predicting γ_h as a function of the Cation Exchange Activity and Activity of the soil.

Knowing the suction compression index and the expected suction changes within a soil column, it is possible to predict the heave of the column. The method has been proven to be fairly accurate for this purpose. On the other hand, observations in the field show that the response of expansive soils in the horizontal dimension is not uniform. In particular, pavement roughness is a consequence of differential heave. Although the properties of the soil are generally measured on integral samples and in the vertical direction, the be-

havior of the whole soil mass not only depends upon these properties, but also on other characteristics of the mass, like cracking fabric and horizontal variations of the soil (15).

The Gilgai Phenomenon

The genesis of the waves observed in road pavements can be understood through the study of a common landform that develops in some climatic areas with expansive clays, characterized by a pattern of mounds and depressions. This surface feature has been called "gilgai" (an Australian aboriginal term). Beckmann et al. (4) have studied several forms of gilgai and factors influencing their genesis, such as topography, climate, mineralogy, clay content, exchangeable sodium, organic matter, and plasticity. Also, Lytton et al. (15) have described the stages of development of a normal gilgai. These authors stress the importance of the cracking fabric of the soil in the appearance and behavior of the gilgaied landform.

In an originally horizontal clay deposit, cracks would appear during the dry season. In the following wet season, water will easily move down through the cracks, and the soil volume surrounding each of them will swell, forming mounds. Subsequently, surface water will be trapped in the depressions between the mounds. As the depressions are wetter than the mounds, suction gradients are induced. Water migrates from beneath the depressions (leaching salts) to the mounds and evaporates there. Pressure zones and shear failure cracks appear on the boundaries between depressions and mounds. It has been also reported that these processes create horizontal variations in the soil characteristics (3, 4, 15). The soil is darker, has lower pH, lower carbonate content,

and higher organic matter content beneath the depressions than under the mounds.

It seems reasonable in a problem where mounds and depressions are present, to define and consider variables such as wavelength and amplitude. In the literature concerning waveforms, a wavelength is defined as the horizontal distance between two successive high points. Amplitude is taken as half the vertical distance between a high point and the adjacent low point. Although there is not yet sufficient information collected about wavelength and amplitude values in gilgai areas and, especially, about which characteristics of the soil may determine these values, the data available give a general idea of the ranges of these quantities.

In Australia, gilgai forms have been observed to develop with wavelengths between 12 and 120 feet and amplitudes from less than 1 inch to about 3 feet (4). It has been also suggested by Australian soil scientists that, although it is generally believed that gilgai soils are predominantly montmorillonitic, the longest wavelengths and highest amplitudes are associated in some cases with soils with high kaolinite content or soils with a relatively low clay content (11).

Bartelli and McCormack (3) have reported that for the Houston Black clay, abundant in Central Texas, the typical wavelength is 12 feet and the amplitude averages 5 inches. Another study was carried out in two gilgai fields of Texas (Snook and Thrall) including field surveys and statistical analyses, in order to determine wavelength probability density functions (15). In both cases, it was found that

wavelengths between 10 and 20 feet had more than 50% probability of occurrence. The mean amplitude was 2.4 inches in Snook and 3.3 inches in Thrall. The soils in the two fields are highly montmorillonitic.

Also, in other areas of the work, wavelengths have been reported to vary from 10 to 200 feet and amplitudes from 1 to more than 20 inches (9).

Finally, it has been observed in Texas and Australia that when gilgai fields have been smoothed by plowing or grading, they reestablish the same patterns as before within two to eleven years (13). When a roadway is constructed on a soil that has the potential to develop gilgai, its cracking pattern will usually remain beneath the roadway, unless the soil is removed to a depth of several feet. If water has access to the soil mass, differential movements might take place and then pavement roughness will appear. For example, in the study of the gilgai fields at Snook and Thrall cited before, pavement roughness was also measured on roadway sections adjacent to the fields. Statistical analyses of these data showed that the wavelength probability density functions of the pavement roughness were similar to those determined in the gilgai fields, indicating that the same roughness patterns were developing beneath the pavement (15).

Measurement and Analysis of Road Roughness

In general, roughness technology can be divided into three aspects: methods of measurement, analysis and interpretation of data, and application of the results. The first two are aimed at obtaining a meaningful description of the roadway profile. The last one consists in the

use of this description as input in more complex analyses, such as the prediction of the dynamic tire forces of a vehicle (20), or the prediction of the Present Serviceability Rating (PSR), an arbitrary scale from 0 to 5 related to riding quality (35).

In his "State of the Art" report (2), Balmer discusses the capabilities of the most important devices that have been used to measure roughness, such as the straight edge, the multiple wheel profilometers, the GM profilometer, the CHLOE profilometer, the BPR roughmeter, and road meters. The GM profilometer, extensively used in Texas, consists of two small road wheels which are mounted on trailing arms underneath the vehicle, one in each wheelpath. The relative motion of each wheel and the vehicle body is measured by a potentiometer. Accelerometers in the vehicle body measure the vertical acceleration of the vehicle. An analog computer double integrates this information and then combines the results from the two potentiometers to obtain the true road profiles, both for the right and left wheelpaths (21).

Several methods of analysis have been developed to interpret the road profiles. One of the most frequently used is the Power Spectral Density analysis. A brief definition of the mathematical tools involved in this method is presented here.

Given y (x), a function which gives the elevation of the road profile, its autocovariance is defined as:

$$C(\ell) = \lim_{L \to \infty} \frac{1}{L} \int_{\frac{-L}{2}}^{\frac{L}{2}} y(x) \cdot y(x + \ell)\, dx \quad \ldots\ldots\ldots\ldots \quad (3)$$

where

$y(x)$ = a function which describes the road profile elevation

x = distance along the road

ℓ = lag of the variable x

L = length of the record

$C(\ell)$ = autocovariance function

It should be noticed that $C(\ell = 0)$ is the average value of $y^2(x)$. This value is called the average or total power in $y(x)$.

The power spectrum is the Fourier transform of the autocovariance function, or:

$$P(f) = \int_{-\infty}^{\infty} C(\ell) \cdot e^{-i\,2\pi\,f\ell}\, d\ell \quad \ldots\ldots\ldots\ldots\ldots (4)$$

where

$P(f)$ = power spectrum of the road profile

f = frequency in cycles per unit length (e.g., cycles/ft)

$C(\ell), \ell$ = as defined above

Furthermore, it can be demonstrated that the total power in $y(x)$ can be expressed as:

$$\text{total power} = C(\ell = 0) = \int_{-\infty}^{\infty} P(f)\, df \quad \ldots\ldots\ldots\ldots (5)$$

Then, it can be seen that the power spectrum, $P(f)$, represents the distribution over the frequency domain of the total power in $y(x)$, the road profile function. Two analytic procedures, the Indirect method

and the Direct method are available for determining power spectra. Both have been discussed by Quinn and Sattaripour (20) in their analysis of the profiles of some highway sections. The study includes curves that fit the measured power spectra. The curves are defined by an equation with two parameters developed by Zable (39).

A modification of the Power Spectral Density analysis, which gives results more easily visualized, is to take the Fourier transform of y(x) directly, in order to determine the amplitude distribution (again a function of frequency) instead of the power spectrum. Basically, this amplitude distribution is the result of decomposing the road profile into a linear combination of sinusoidal functions, each of them with a specific wavelength and amplitude. This is done by a Fast Fourier Transform (FFT) analysis, performed with the help of a digital computer. The road profile should be discretized in order to be fed into the computer, sampling it at equally spaced intervals. The analysis of this discretized sequence with the classical Fourier integral would give serious problems, but an adaptation of the Fourier's theory to discrete cases, the Discrete Fourier Transform (DFT), has been developed. The FFT is merely an algorithm for a rapid computation of the DFT. A complete description of these mathematical tools can be found in the literature (7, 20). McKeen has used this method in his study of airport pavements on expansive clays (16).

Another method of analysis is the use of filtering techniques. Digital filters are weighting functions, each of them related to a specific frequency band. When a filter is applied to the digitized road profile, the output is composed of those amplitudes of waves with-

in the frequency band defined by the filter. Williamson et al. (37) have used this approach in their study of the relationships between the measured road roughness and the Present Serviceability Rating (PSR) which has been correlated with measured pavement roughness. The PSR estimate so obtained is called the Serviceability Index (SI).

Filtering techniques are also the basis of the Amplitude-Frequency Distribution method. This method develops a tabular representation of road roughness. Each entry of the table gives the number of road profile "bumps" having a specific amplitude and frequency (6).

Summary

In this section, information about the nature and behavior of expansive soils, and about the technology available for measuring and analyzing pavement roughness has been presented. It is clear that the first step in dealing with the complexity of the design of pavements on expansive soils is to collect consistent measures of roughness and characterize them in a useful manner. Some efforts in this direction have been made in this report. Specifically, the factors influencing the development of pavement roughness on expansive soils, and their relative importance have been analyzed. This knowledge is necessary for a more rational approach to the design of pavements on these troublesome soils.

In the next chapter entitled "DATA COLLECTION", the data collected for analysis are reported. In Chapter 4, "METHODS OF ANALYSIS AND RESULTS", the pavement roughness patterns of roads built on expansive soils are characterized as a function of two parameters, and the dominant wavelengths of these patterns are studied. Empirical models are developed to predict the values of the two parameters. Also, the para-

meters are correlated with the Serviceability Index reduction. A summary of the findings of this study is presented in Chapter 5, "CONCLUSIONS AND RECOMMENDATIONS". Finally, supplementary information and a case study are presented in the Appendices.

CHAPTER THREE

DATA COLLECTION

Roadway Sections

Profiles of the right and left wheel paths of 23 pavement sections were measured with the GM Profilometer. These sections are located in 9 different areas of Central Texas, whose names and location are shown in Figure 2. An indication of the climate of these areas can be obtained from the values of the Thornwaite moisture index. These values have been recorded by county and their statistics are presented in Table 1.

The GM profilometer that was used to measure the roughness was operated by the Center for Transportation Research of the University of Texas at Austin, The device was run at 20 miles per hour in all the cases except for Smithville, where it was run at 34 miles per hour. A detailed description of the GM profilometer can be found in the report by Roberts and Hudson (21). Here, it will only be pointed out that the device is equipped with four selectable high pass filters. Filter No. 2 was chosen for the runs at 20 miles per hour. With this filter, the amplitude of the input signal is attenuated for wavelengths above 300 feet, along with some phase shift for wavelengths above 32 feet.

The road profiles, both for the right and left wheelpaths, have lengths varying from 0.2 to 4.0 miles. They were converted to digital form and stored in magnetic tapes. For this study, a segment of the available profile on each section has been analyzed. The exact locations and lengths of these segments are presented in Table 2. All of the sections are in cut, or at grade, except San Antonio 90-3, which has around 4 feet of fill, and part of San Antonio 90-1 and San Antonio 410-2.

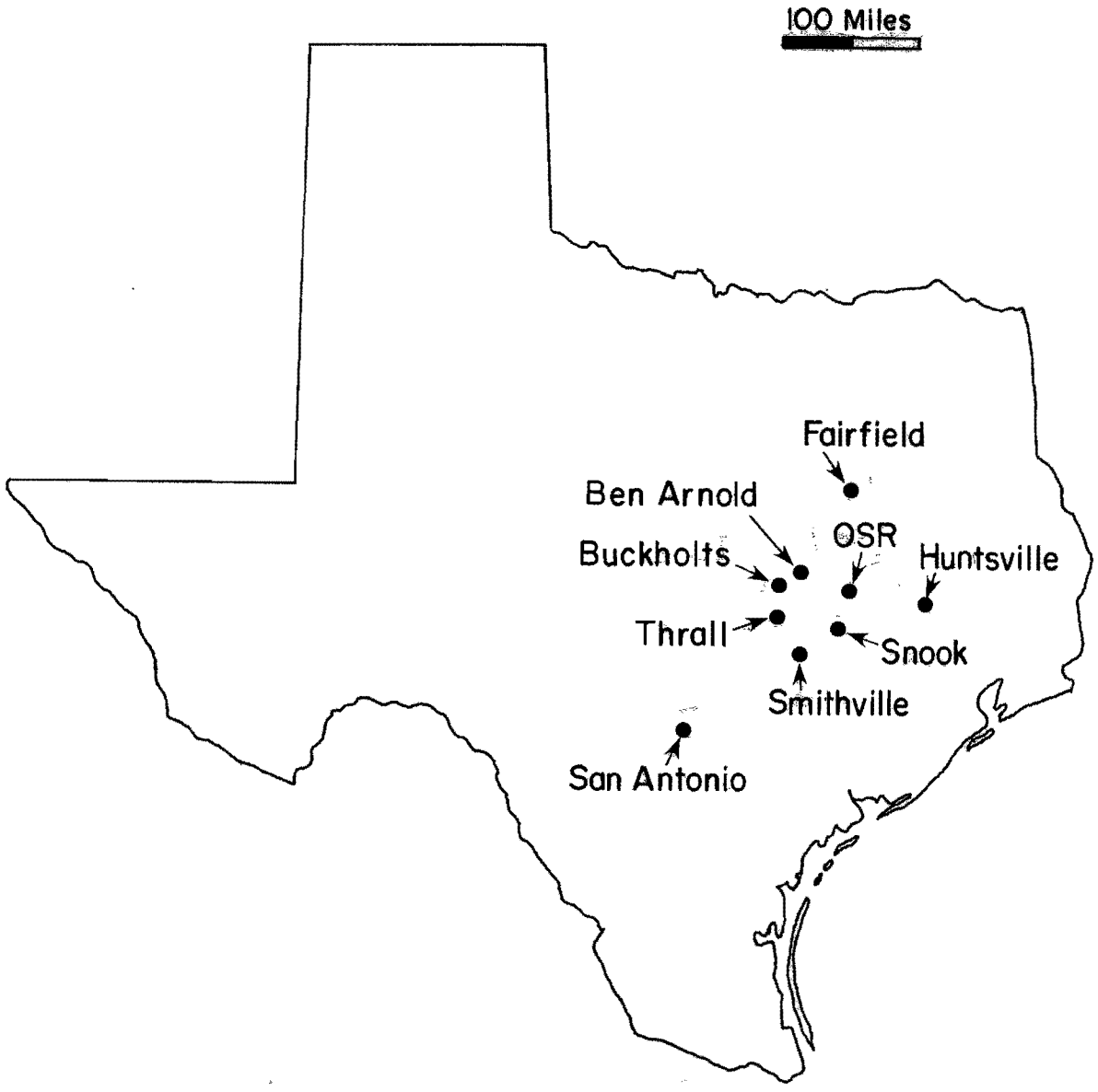

FIGURE 2. Location of Areas

TABLE 1. Thornthwaite Moisture Index

Area (1)	County (2)	Thornthwaite Moisture Index[a]				
		Mean (3)	Standard Deviation (4)	Maximum (5)	Minimum (6)	Range (7)
Huntsville	Walker	10.8	25.1	62.4	-19.5	81.9
Ben Arnold	Milam	-10.5	17.1	15.7	-37.6	53.3
Buckholts[b]	Bell	-12.5	16.7	14.8	-40.3	55.0
Buckholts[b]	Milam	-10.5	17.1	15.7	-37.6	53.3
Fairfield[b]	Freestone	9.5	22.7	39.8	-34.9	74.6
Fairfield[b]	Navarro	3.7	23.8	60.6	-30.8	91.4
Smithville	Bastrop	-10.7	19.0	34.1	-41.6	75.7
Snook	Burleson	2.1	24.2	61.5	-32.0	93.5
OSR	Brazos	4.6	23.6	57.3	-32.8	90.1
Thrall	Williamson	-12.3	15.4	17.6	-42.4	60.1
S. Antonio	Bexar	-15.7	16.5	20.4	-42.2	62.6

[a]Computed from available weather station data over 20 years.

[b]The roadway sections within this area are located in two different counties.

TABLE 2. Location of Roadway Segments

Section (1)	County (2)	Roadway (3)	Segment Location		
			Start (4)	Direction (5)	Length, in feet (6)
Huntsville 1	Walker	IH 45	Mile post 103.0	North	1896
Huntsville 2	Walker	IH 45	Mile post 105.6	North	1896
Ben Arnold 1	Milam	US 77	0.1 miles south of the intersection with FM 1963	South	1896
Ben Arnold 2	Milam	US 77	1.0 miles south of the intersection with FM 1963	South	1896
Ben Arnold 3	Milam	US 77	3.0 miles south of the intersection with FM 1963	South	1896
Buckholts 1	Bell	US 190	0.4 miles west of Milam County Line	East	1896
Buckholts 2	Milam	US 190	3.6 miles east of Bell County Line	West	1896
Fairfield 1	Freestone	IH 45	Mile post 212.2	North	1896
Fairfield 2	Navarro	IH 45	Mile post 214.1	North	1600

TABLE 2. (Continuation)

Section (1)	County (2)	Roadway (3)	Segment Location		
			Start (4)	Direction (5)	Length, in feet (6)
Smithville 1A	Bastrop	US 290	0.8 miles east of the intersection with FM 2104	West	1109
Smithville 1B	Bastrop	US 290	0.6 miles east of the intersection with FM 2104	West	1010
Snook 1	Burleson	FM 60	0.4 miles south of the intersection with FM 2039	North	1200
OSR 1	Brazos	Old S. Antonio Road	1.1 miles west of the intersection with FM 2223	West	912
OSR 2	Brazos	Old S. Antonio Road	1.6 miles west of the intersection with FM 2223	West	1896
OSR 3	Brazos	Old S. Antonio Road	2.5 miles west of the intersection with FM 2223	West	1896
Thrall 1	Williamson	US 79	2.0 miles west of Thrall city limits	West	1305

TABLE 2. (Continuation)

Section (1)	County (2)	Roadway (3)	Segment Location		
			Start (4)	Direction (5)	Length, in feet (6)
San Antonio 410-1	Bexar	IH 410	Overhead exit sign at Valley Hi	North	1896
San Antonio 410-2	Bexar	IH 410	Exit sign southbound to Valley Hi	South	1896
San Antonio 37	Bexar	IH 37	1.6 miles south to the Hackberry overpass	South	1896
San Antonio 90-1	Bexar	US 90	Station 276 + 03	East	1896
San Antonio 90-5	Bexar	US 90	Station 250 + 02	West	1896
San Antonio 90-3 (East)	Bexar	US 90	Station 205 + 99	East	1896
San Antonio 90-3 (West)	Bexar	US 90	Station 193 + 01	West	1896

The State Department of Highways and Public Transportation in Texas keeps records of the construction and subsequent repair of the pavements. These records give a fairly good idea of the maintenance problems in the sections which are the subject of this study. In Table 3, the dates of the end of construction and last resurfacing on the sections (before the profilometer was run) are presented. Also in this table, the dates when the GM profilometer was run are shown. This information will help in the analysis of pavement roughness as a time dependent problem.

Also, it may be expected that the stiffness of the pavement structure plays a major role in the development of different roughness patterns. The stiffness depends upon the type of pavement materials and depths of the surface and base courses. These data can be found in the construction records cited before. Most of the sections had asphalt concrete surfaces when the profilometer was run, except the OSR sections (which had only a double bituminous treatment) and the ones located in Huntsville, Fairfield, and San Antonio 37, with concrete pavements.

The fact that pavements are multilayered systems with different materials complicates the direct comparison of them. To overcome this problem, a simple approach was taken, determining for each pavement its "effective depth", a homogeneous quantity related to the stiffness of the materials in each layer (the greater the effective depth, the stiffer the pavement). To define this quantity, the following process was used:

First, values of the modulus of elasticity were assumed for the different materials involved. Asphalt concrete was the material chosen as a basis for subsequent comparisons. The assumed moduli of elasticity are:

E_o = modulus of elasticity for asphalt concrete = 2×10^5 psi

TABLE 3. Time Record

Section (1)	Date of Construction (2)	Date of Resurfacing[a] (3)	Date of Profilometer Run (4)	Time between (2) and (4), in years (5)
Huntsville 1	June 61	None	May 74	12.8
Huntsville 2	June 61	None	May 74	12.8
Ben Arnold 1	July 64	July 71	May 74	2.8[b]
Ben Arnold 2	July 64	July 71	May 74	2.8[b]
Ben Arnold 3	July 64	July 71	May 74	2.8[b]
Buckholts 1	June 65	August 65	May 74	8.8[b]
Buckholts 2	June 65	August 65	May 74	8.8[b]
Fairfield 1	October 68	None	May 74	5.6
Fairfield 2	October 68	None	May 74	5.6
Smithville 1A	April 67	None	May 74	6.6
Smithville 1B	April 67	None	May 74	6.6
Snook 1	October 68	February 70	November 73	3.7[b]
OSR 1	October 56	None	November 73	17.1
OSR 2	October 56	None	November 73	17.1
OSR 3	October 56	None	November 73	17.1
Thrall 1	December 62	July 71	November 73	2.3[b]
S. Antonio 410-1	September 59	June 79	June 79[c]	0[b]
S. Antonio 410-2	September 59	June 79	June 79[c]	0[b]
S. Antonio 37	August 69	None	November 79[c]	10.3
S. Antonio 90-1	November 71	None	October 75[c]	3.9
S. Antonio 90-5	November 71	None	October 75[c]	3.9
S. Antonio 90-3 (East)	November 71	None	October 75[c]	3.9
S. Antonio 90-3 (West)	November 71	None	October 75[c]	3.9

[a]Last resurfacing before the profilometer was run.

[b]In this section, the time between the date of resurfacing and the date when the profilometer was run is recorded.

[c]After this first run, more profilometer data are being taken periodically.

E_s = modulus of elasticity for surface materials (See Table 4)

E_b = modulus of elasticity for base course = 3×10^4 psi

TABLE 4. Assumed Moduli of Elasticity for Surface Materials

Material	E_s, in psi
Asphalt Concrete	2×10^5
Concrete	3×10^6
Double Bituminous Treatment	1×10^5

Second, given a pavement structure 1 inch wide (Figure 3), an equivalent configuration is defined, based on the modulus of elasticity ratios $\frac{E_s}{E_o}$ and $\frac{E_b}{E_o}$. The dimensions of this hypothetical configuration are shown in Figure 4. It should be noted here that in the roadway sections where resurfacing was done before running the profilometer, the value of the surface depth, a, includes that resurfacing.

Third, the moment of inertia, I, for the equivalent configuration is calculated using the following formula:

$$I = \sum_{i=1}^{n} I_{ci} + \sum_{i=1}^{n} \frac{E_i}{E_o} \times d_i \times (\bar{y}_i)^2$$

where n = the number of layers in the pavement

E_i, d_i = the elastic modulus and depth of the $i^{\underline{th}}$ layer of the pavement

I_{ci} = the moment of inertia of the $i^{\underline{th}}$ layer around its own centroid

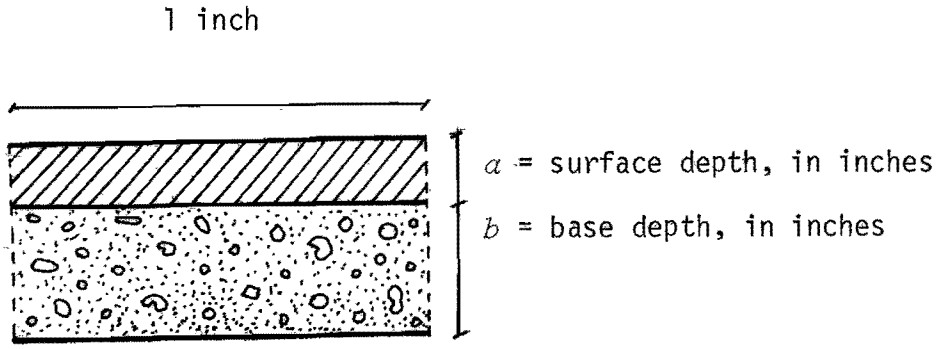

FIGURE 3. Pavement Structure

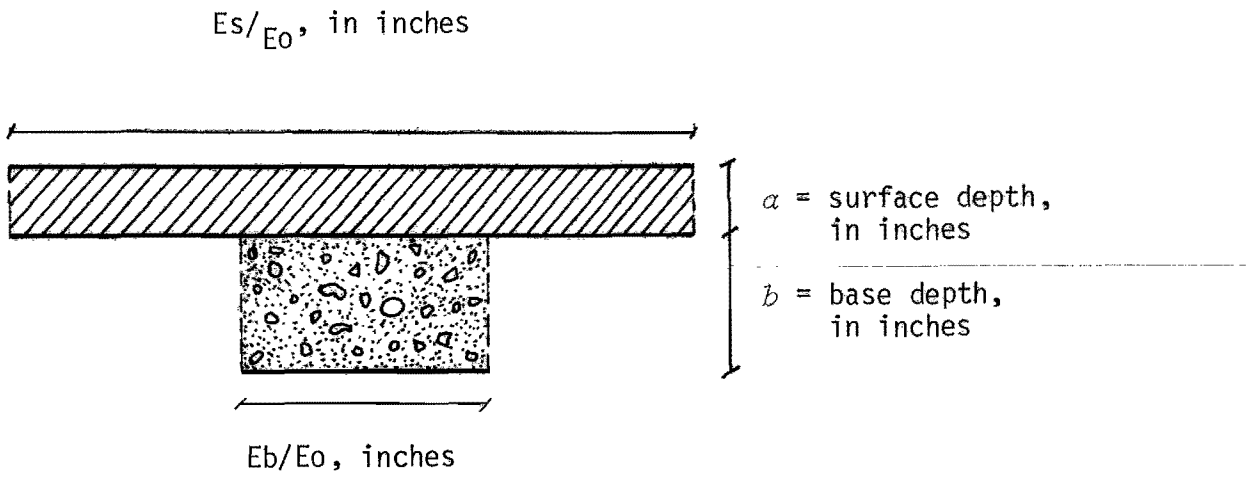

FIGURE 4. Equivalent Configuration

$\bar{y}_i$ = the distance of the centroid of the i^{th} layer from the centroid of the transformed section

Finally, the "effective depth" is defined as:

$$DEPTH = \sqrt[3]{\frac{12 \times I}{1 \text{ inch}}} \quad \ldots\ldots\ldots\ldots\ldots\ldots\ldots\ldots \quad (6)$$

where

DEPTH = effective depth, in inches

I = moment of inertia for the equivalent configuration, in inches^4

It can be seen that the effective depth of a pavement represents a single layer of asphalt concrete DEPTH inches thick, which would have the same moment of inertia as the equivalent configuration of the pavement, and then it is assumed its stiffness would be equal to that of the actual pavement. In Table 5, the calculated effective depths for the different roadway sections are presented.

Soil Properties

The Soil Conservation Service publishes a series of soil surveys by county. From this source, general information concerning the soils present in a specific area can be obtained. In particular, the pedologic classification of the natural soils underlying the 23 roadway segments can be found in some of these soil surveys reports (25, 26, 27, 28, 29, 30, 31, 32) along with several soil maps. These data are presented in Table 7. The soils in 16 roadway segments belong to the Vertisol order. Alfisols underlie the remaining 7 roadway segments. All these soils have been evaluated by soil scientists as having a high or very high shrink-swell

TABLE 5. Effective Depth of the Pavements

Section	Type of Pavement	Depth, in inches		Moduli of Elasticity Ratios		Effective Depth, in inches
		Base	Surface	Eb/Eo	Es/Eo	
(1)	(2)	(3)	(4)	(5)	(6)	(7)
Huntsville 1	Concrete	8	8	0.15	15	20.5
Huntsville 2	Concrete	8	8	0.15	15	20.5
Ben Arnold 1	Asphalt Concrete	14	2.3	0.15	1	10.9
Ben Arnold 2	Asphalt Concrete	14	2.3	0.15	1	10.9
Ben Arnold 3	Asphalt Concrete	14	2.3	0.15	1	10.9
Buckholts 1	Asphalt Concrete	16	1.6	0.15	1	11.5
Buckholts 2	Asphalt Concrete	16	1.6	0.15	1	11.5
Fairfield 1	Concrete	6	8	0.15	15	20.2
Fairfield 2	Concrete	6	8	0.15	15	20.2
Smithville 1A	Asphalt Concrete	24	1.2	0.15	1	15.6
Smithville 1B	Asphalt Concrete	24	1.2	0.15	1	15.6
Snook 1	Asphalt Concrete	7	1.1	0.15	1	5.4
OSR 1	Dbl. Bit. Treat.	6	0.6	0.15	0.5	4.0
OSR 2	Dbl. Bit. Treat.	6	0.6	0.15	0.5	4.0
OSR 3	Dbl. Bit. Treat.	6	0.6	0.15	0.5	4.0
Thrall 1	Asphalt Concrete	13	3.1	0.15	1	11.1
S. Antonio 410-1	Asphalt Concrete	21	unknown	0.15	1	---
S. Antonio 410-2	Asphalt Concrete	21	unknown	0.15	1	---
S. Antonio 37	Concrete	8	8	0.15	15	20.5
S. Antonio 90-1	Asphalt Concrete	32	3	0.15	1	20.9
S. Antonio 90-5	Asphalt Concrete	32	3	0.15	1	20.9
S. Antonio 90-3 (East)	Asphalt Concrete	23	3.5	0.15	1	17.7
S. Antonio 90-3 (West)	Asphalt Concrete	23	3.5	0.15	1	17.7

TABLE 6. Traffic Data

Section	Average Daily Traffic			Total Number of Equivalent 18K Single Axle	
	Year of Completion[a]	1975	1980	Between (2) and (3)	Between (3) and (4)
(1)	(2)	(3)	(4)	(5)	(6)
Huntsville 1	4,750	16,630	20,000	3,698,000	7,591,000
Huntsville 2	4,750	16,630	20,000	3,698,000	7,591,000
Ben Arnold 1	--	2,400	2,700	--	241,000
Ben Arnold 2	--	2,400	2,700	--	241,000
Ben Arnold 3	--	2,400	2,700	--	241,000
Buckholts 1	2,330	3,340	3,850	805,000	797,000
Buckholts 2	2,330	3,340	3,850	805,000	797,000
Fairfield 1	--	10,850	15,000	--	8,067,000
Fairfield 2	--	10,850	15,000	--	8,067,000
Smithville 1A	2,210	3,110	4,000	314,000	422,000
Smithville 1B	2,210	3,110	4,000	314,000	422,000
Snook 1	1,470	2,170	2,500	30,000	50,000
OSR 1	240	380	450	33,000	10,000
OSR 2	240	380	450	33,000	10,000
OSR 3	240	380	450	33,000	10,000
Thrall 1	2,610	4,100	4,950	823,000	618,000
S. Antonio 90-5	6,100	9,000	10,500	228,000	639,000
S. Antonio 90-3	6,100	9,000	10,500	228,000	639,000

[a]The year of completion is presented in Table 3.

TABLE 7. Soil Type

Section (1)	Soil Classification[a]			Parent Material		Shrink-Swell Potential (7)
	Series (2)	Subgroup (3)	Order (4)	Formation (5)	Period (6)	
Huntsville 1	Annona	Vertic Paleudalfs	Alfisols	Willis	Tertiary	High
Huntsville 2	Ferris	Udorthentic Chromusters	Vertisols	Fleming	Tertiary	Very High
Ben Arnold 1	Houston Black	Udic Pellusters	Vertisols	Taylor	Cretaceous	Very High
Ben Arnold 2	Heiden	Udic Chromusters	Vertisols	Taylor	Cretaceous	Very High
Ben Arnold 3	Heiden	Udic Chromusters	Vertisols	Wills Point	Tertiary	Very High
Buckholts 1	Heiden	Udic Chromusters	Vertisols	Taylor	Cretaceous	Very High
Buckholts 2	Houston Black	Udic Pellusters	Vertisols	Taylor	Cretaceous	Very High
Fairfield 1	Crockett	Udertic Paleustalfs	Alfisols	Rockdale	Tertiary	High
Fairfield 2	Crockett	Udertic Paleustalfs	Alfisols	Kincaid	Tertiary	High
Smithville 1A	Axtell	Udertic Paleustalfs	Alfisols	Yegua	Tertiary	High
Smithville 1B	Tabor	Aquic Paleustalfs	Alfisols	Yegua	Tertiary	High
Snook 1	Burleson	Udic Pellusterts	Vertisols	Alluvium	Quaternary	High
OSR 1	Wilson	Vertic Ochraqualfs	Alfisols	Yegua	Tertiary	High
OSR 2	Wilson	Vertic Ochraqualfs	Alfisols	Yegua	Tertiary	High
OSR 3	Heiden	Udic Chromusters	Vertisols	Yegua	Tertiary	Very High

TABLE 7. (Continuation)

Section (1)	Soil Classification[a]			Parent Material		Shrink-Swell Potential (7)
	Series (2)	Subgroup (3)	Order (4)	Formation (5)	Period (6)	
Thrall 1	Burleson	Udic Pellusters	Vertisols	Taylor	Cretaceous	High
S. Antonio 410-1	Houston Black	Udic Pellusters	Vertisols	Taylor	Cretaceous	Very High
S. Antonio 410-2	Houston Black	Udic Pellusters	Vertisols	Taylor	Cretaceous	Very High
S. Antonio 37	Houston Black	Udic Pellusters	Vertisols	Taylor	Cretaceous	Very High
S. Antonio 90-1	Houston Black	Udic Pellusters	Vertisols	Taylor	Cretaceous	Very High
S. Antonio 90-5	Houston Black	Udic Pellusters	Vertisols	Taylor	Cretaceous	Very High
S. Antonio 90-3 (East)	Houston Black	Udic Pellusters	Vertisols	Taylor	Cretaceous	Very High
S. Antonio 90-3 (West)	Houston Black	Udic Pellusters	Vertisols	Taylor	Cretaceous	Very High

[a]The definition of the terms used in the soil classification are presented in Appendix III.

potential. Also, information about the parent materials of the soils was obtained from a geological map (18), and it is included in Table 7. The pedological terms that are used in Table 7 are defined in Appendix III.

Soil samples were taken adjacent to the roadway segments using a manual auger, in general at depth of 1, 2, and 3 feet. A total of 60 samples were brought to the laboratory, where the following tests were performed:

1. Atterberg Limits
2. Determination of the percent clay (grain size less than 0.02 mm)
3. Cation Exchange Capacity (CEC)
4. Exchange Sodium Percentage (ESP)

The CEC and ESP tests were done following the method of Bower et al. (4).

The average test results for each roadway segment are presented in Table 8, except for San Antonio 90-3 and San Antonio 90-1, where samples of the natural soils were not taken. The results are fairly consistent with the soil types listed in Table 7 as soils having a very high shrink-swell potential. In general, these soils have average plasticity indexes equal to 35 or above. On the other hand, soils from Huntsville 1, Fairfield 1, Fairfield 2, and Thrall 1 (listed as having high shrink-swell potential) have plasticity indexes below 35.

Knowing the plasticity index (PI), CEC, and percent clay of a soil, its activity (PI%clay) and cation exchange activity (CEC%clay) can be calculated. The chart developed by McKeen (16) allows the estimation of the COLE of a soil as a function of these two quantities. The chart is shown in Figure 5. The COLE values that appear in this chart are for hypothetical soils with 100 percent clay. For real soils, these values should be corrected by multiplying by the clay content as a decimal. The

TABLE 8. Soil Tests Results

Section (1)	Percent Clay [a] (2)	Liquid Limit (3)	Plasticity Index (4)	CEC, in meq/100gm (5)	ESP. in percent (6)
Huntsville 1	27	33	15	25	6.0
Huntsville 2	50	71	49	46	2.0
Ben Arnold 1	65	82	51	74	10.0
Ben Arnold 2	69	88	54	61	3.0
Ben Arnold 3	66	75	45	64	0.9
Buckholts 1	60	79	50	48	16.1
Buckholts 2	53	57	35	44	6.0
Fairfield 1	40	45	26	39	5.0
Fairfield 2	47	46	27	38	4.0
Smithville 1A	57	68	44	52	2.3
Smithville 1B	69	84	56	54	9.7
Snook 1	57	71	44	58	0.5
OSR 1	58	58	38	50	0.6
OSR 2	50	57	35	46	0.5
OSR 3	66	80	50	74	0.7
Thrall 1	50	53	28	74	0.6
S. Antonio 410-1	53	72	42	43	15.3
S. Antonio 410-2	53	69	40	59	11.5
S. Antonio 37	49	62	38	56	4.2
S. Antonio 90-5	48	86	50	68	16.3

[a] Percent smaller than 0.002 mm.

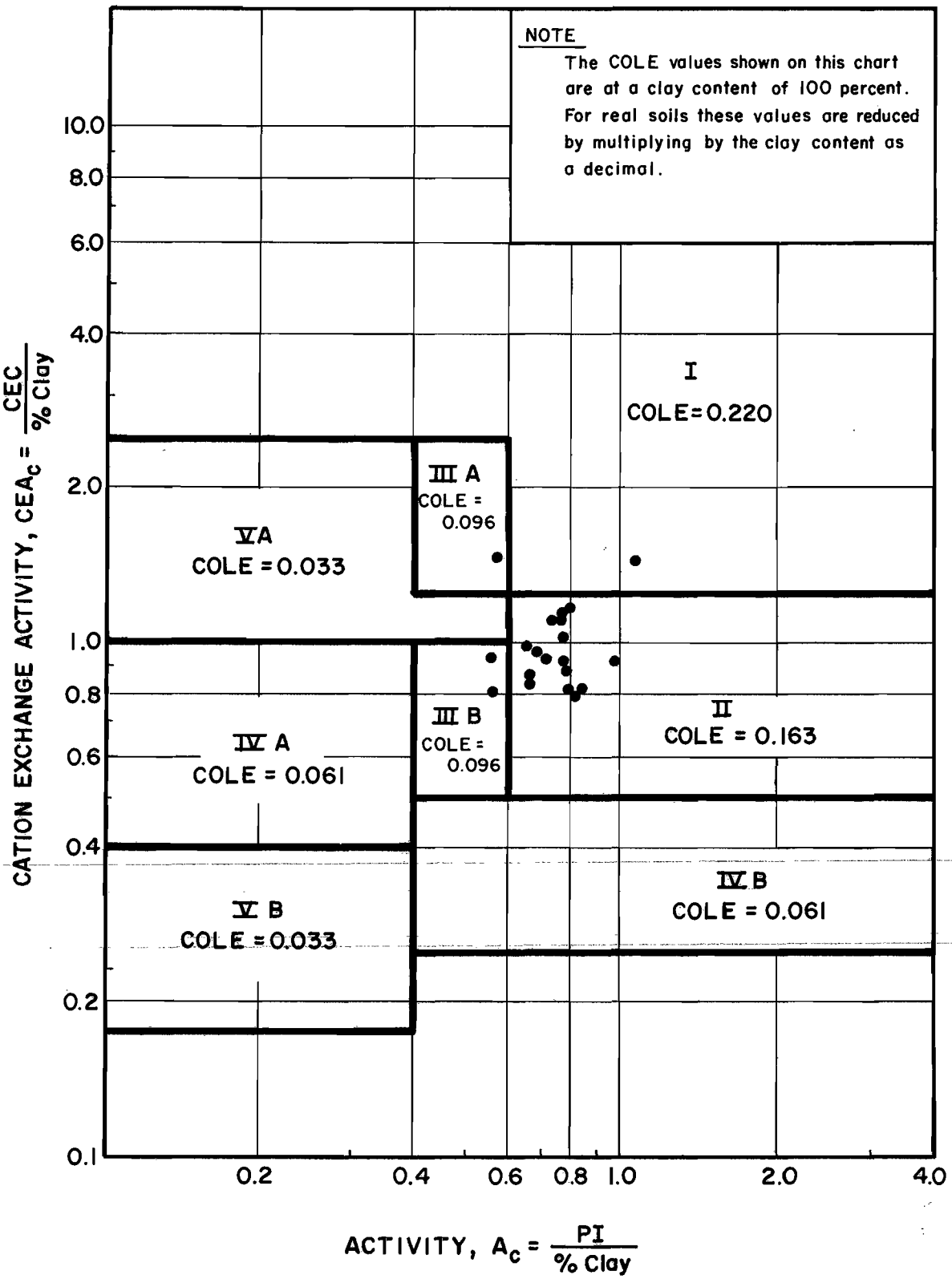

FIGURE 5. Chart for COLE Prediction (After McKeen) (16)

average activity and cation exchange activity values were calculated for the soils of each pavement section (See Table 9), and were plotted in Figure 5. It can be seen that almost all the soils lie within region II. The COLE values of these soils have been estimated with the correction for the actual clay content, and they are presented in Table 9. These COLE values are also consistent with the soil types listed in Table 7. Most of them are above 0.08 (which is a high value). The exceptions are, again, Huntsville 1, Fairfield 2, and Thrall 1.

From the data presented in Tables 7, 8 and 9, it appears that most of the pavement sections of this study were constructed on highly expansive soils.

Summary

In this section, information about 23 pavement sections has been presented. Specifically, data dealing with the climate, characteristics of the pavement, time of construction, traffic records, and subgrade soil properties have been collected.

TABLE 9. COLE Values from McKeen's Chart

Section (1)	Activity (2)	Cation Exchange Activity (3)	Region (4)	COLE (5)
Huntsville 1	0.56	0.93	III B	0.026
Huntsville 2	0.98	0.92	II	0.082
Ben Arnold 1	0.78	1.14	II	0.106
Ben Arnold 2	0.78	0.88	II	0.112
Ben Arnold 3	0.68	0.97	II	0.108
Buckholts 1	0.83	0.80	II	0.098
Buckholts 2	0.66	0.83	II	0.086
Fairfield 1	0.65	0.98	II	0.065
Fairfield 2	0.57	0.81	III B	0.045
Smithville 1A	0.77	0.91	II	0.093
Smithville 1B	0.81	0.78	II	0.112
Snook 1	0.77	1.02	II	0.093
OSR 1	0.66	0.86	II	0.095
OSR 2	0.70	0.92	II	0.082
OSR 3	0.76	1.12	II	0.108
Thrall 1	0.56	1.48	III A	0.048
S. Antonio 410-1	0.79	0.81	II	0.086
S. Antonio 410-2	0.75	1.11	II	0.086
S. Antonio 37	0.78	1.14	II	0.080
S. Antonio 90-5	1.04	1.42	I	0.106

CHAPTER FOUR

METHODS OF ANALYSIS AND RESULTS

Characterization of Pavement Roughness

The measured profiles of the roadway segments listed in Table 2 have been analyzed using the Fast Fourier Transform (FFT) method, in order to study the profiles in the frequency domain.

As was mentioned in Chapter 2, the FFT decomposes the road profile into a family of sinusoidal functions at discrete frequencies. For this study, an FFT computer program was designed to perform the following operations in each road profile:

1. Sample the profile at equally spaced intervals of 0.82 feet.
2. Take 512 of those data samples, which represent a length of 419.84 feet.
3. Apply the FFT algorithm to that length. The result obtained is the distribution of one half the amplitude values (A/2) of sinusoids at frequencies:

$$f = \frac{j}{L}, \quad j = 2, 3, 4, \ldots, N-1 \qquad (7)$$

where

f = frequency, in cycles/foot

N = number of samples = 512

L = length = 419.84 feet

4. Repeat operations 2 and 3 for 10 consecutive lengths, with the first points of each of them separated by 164 feet. Then, the 10 lengths cover 1896 feet of the road profile. In a few sections, the available profile was less than 1896 feet long. For them, a lower number of lengths with

a minor separation was considered. The minimum has been 7 lengths separated by 82 feet, covering 912 feet.

5. Average the distributions of $\frac{A}{2}$ values calculated for the different lengths, and print-out the results. This operation reduces the effect of data scattering.

It is believed that these mean spectra of $\frac{A}{2}$ over the frequency domain, besides having an easily understandable physical meaning, are a very consistent representation of the measured roughness on the pavement sections. Furthermore, the shapes of the spectra that were obtained strongly suggested that they may be fitted by curves defined by the general equation:

$$\frac{A}{2} = c\, f^{n} \quad \ldots\ldots\ldots\ldots\ldots\ldots\ldots\ldots\ldots\ldots \quad (8)$$

where

A = mean amplitude, in inches

f = frequency, in cycles/foot

c,n = parameters

Taking logarithms of both sides of the equation, it becomes the general equation of a straight line with slope equal to n and intercept equal to log c. Thus, linear regression analysis can be used, for the measured $\frac{A}{2}$ spectrum in each roadway segment, to determine the corresponding n and log c values. In this analysis, only the data for the lower 60 discrete frequencies (representing wavelengths from 208.3 feet to 6.9 feet) have been considered, as higher frequencies are not significant to the overall problem.

The obtained values of n and log c, both for the left and right wheelpaths, are presented in Table 10. All the R^2 values were above

0.90. Because in the San Antonio area a considerable number of profilometer runs at different dates are available, only the results for 4 of those runs are included in Table 10. The complete set of results for the sections in the San Antonio area is presented in Appendix VII.

The plots of the fitted curves $\frac{A}{2}$ versus f for the right wheelpaths of the different roadway segments are shown in Appendix IV. These figures include the measured $\frac{A}{2}$ values at some frequencies, and indicate where the differences with the fitted curve are greatest. As an example, one of these plots is presented in Figure 6.

Also, in Figures 7 and 8 the fitted curves for the right and left wheelpaths are shown, but now in a log-log scale, where they become straight lines, and with wavelength instead of frequency as the abscissa axis. Wavelength is the inverse of frequency. For a specific roadway segment, it can be seen from these two figures that the roughness spectra of the right and left wheelpaths are very similar. Nevertheless, for most of the sections the spectrum of the right wheelpath indicates a slightly greater roughness (greater amplitudes over the wavelength domain) than in the left wheelpath. A rough illustration of this point is given by calculating the average of the straight lines presented in Figure 7 and comparing it with the average of those in Figure 8. This comparison is shown in Figure 9. The fact that, in general, more roughness develops in the right wheelpath seems reasonable, as the right wheelpath is closer to the edge of the pavement, where greater soil moisture variations are likely to occur.

The characterization of pavement roughness on expansive soils as a function of only two parameters (c and n), greatly facilitates the study of factors influencing the development of roughness. This analysis may

TABLE 10. Log c and n Values

Section	Left Wheel		Right Wheel		Date
(1)	Log c (2)	n (3)	Log c (4)	n (5)	(6)
Huntsville 1	-4.00	-1.30	-3.61	-1.09	May, 1974
Huntsville 2	-4.19	-1.51	-3.92	-1.39	May, 1974
Ben Arnold 1	-3.70	-1.36	-3.71	-1.38	May, 1974
Ben Arnold 2	-3.91	-1.43	-3.74	-1.36	May, 1974
Ben Arnold 3	-3.88	-1.47	-3.90	-1.46	May, 1974
Buckholts 1	-3.56	-1.31	-3.61	-1.34	May, 1974
Buckholts 2	-3.82	-1.48	-3.79	-1.44	May, 1974
Fairfield 1	-3.75	-1.35	-3.57	-1.27	May, 1974
Fairfield 2	-3.73	-1.33	-3.61	-1.27	May, 1974
Smithville 1A	-3.91	-1.27	-3.94	-1.32	November, 1973
Smithville 1B	-3.90	-1.41	-3.94	-1.46	November, 1973
Snook 1	-3.75	-1.17	-3.76	-1.20	November, 1973
OSR 1	-3.00	-1.08	-3.18	-1.20	November, 1973
OSR 2	-3.32	-1.14	-3.19	-1.13	November, 1973
OSR 3	-3.26	-1.06	-2.95	-1.05	November, 1973
Thrall 1	-3.91	-1.19	-3.93	-1.24	November, 1973
S. Antonio 410-1	-3.56	-1.21	-3.57	-1.21	November, 1979
S. Antonio 37	-3.75	-1.46	-3.75	-1.43	November, 1979
S. Antonio 90-5	-4.08	-1.44	-4.15	-1.45	April, 1978
S. Antonio 90-3 (West)	-3.99	-1.39	-4.18	-1.48	April, 1978

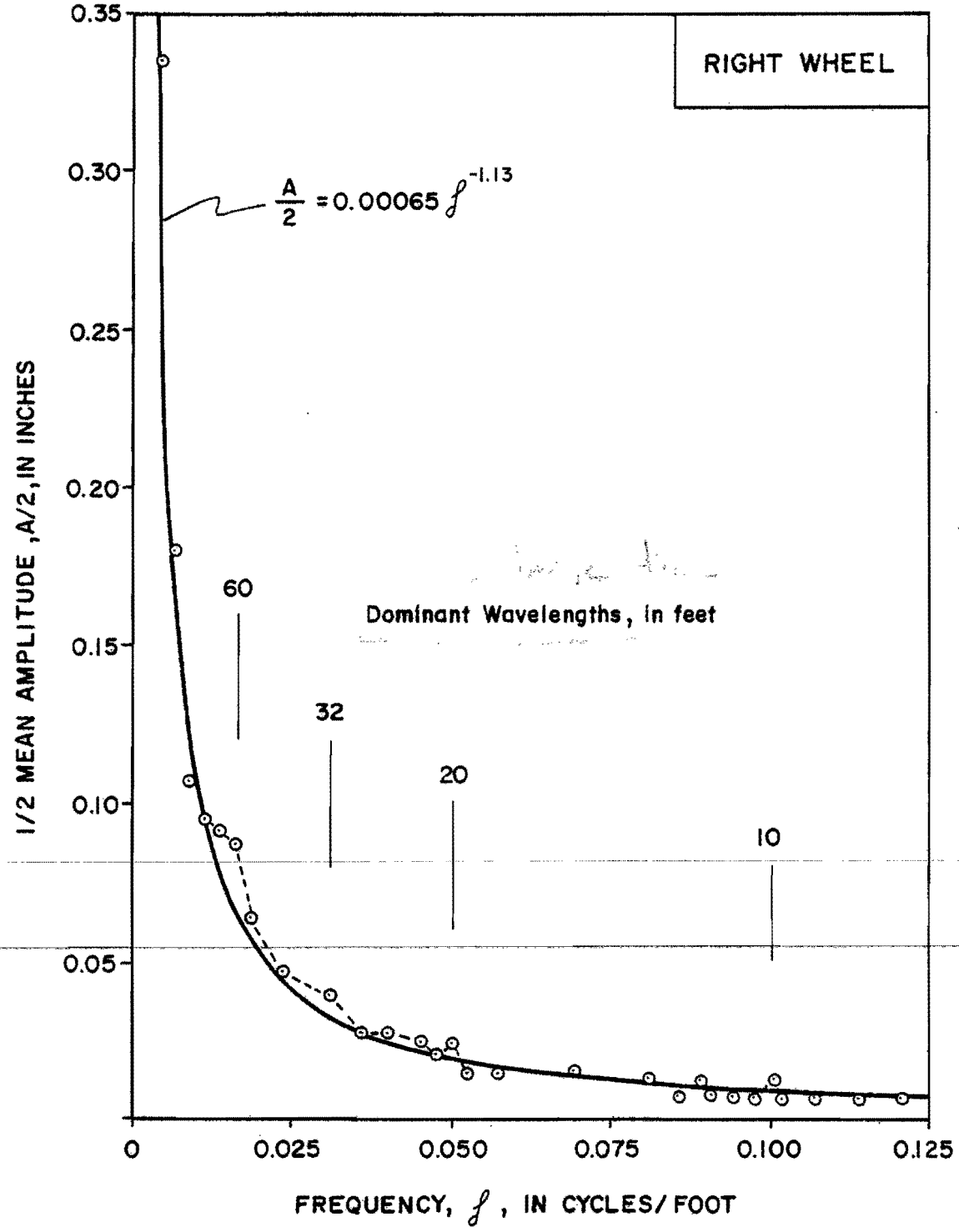

FIGURE 6. Frequency Domain Plot
(OSR 2)

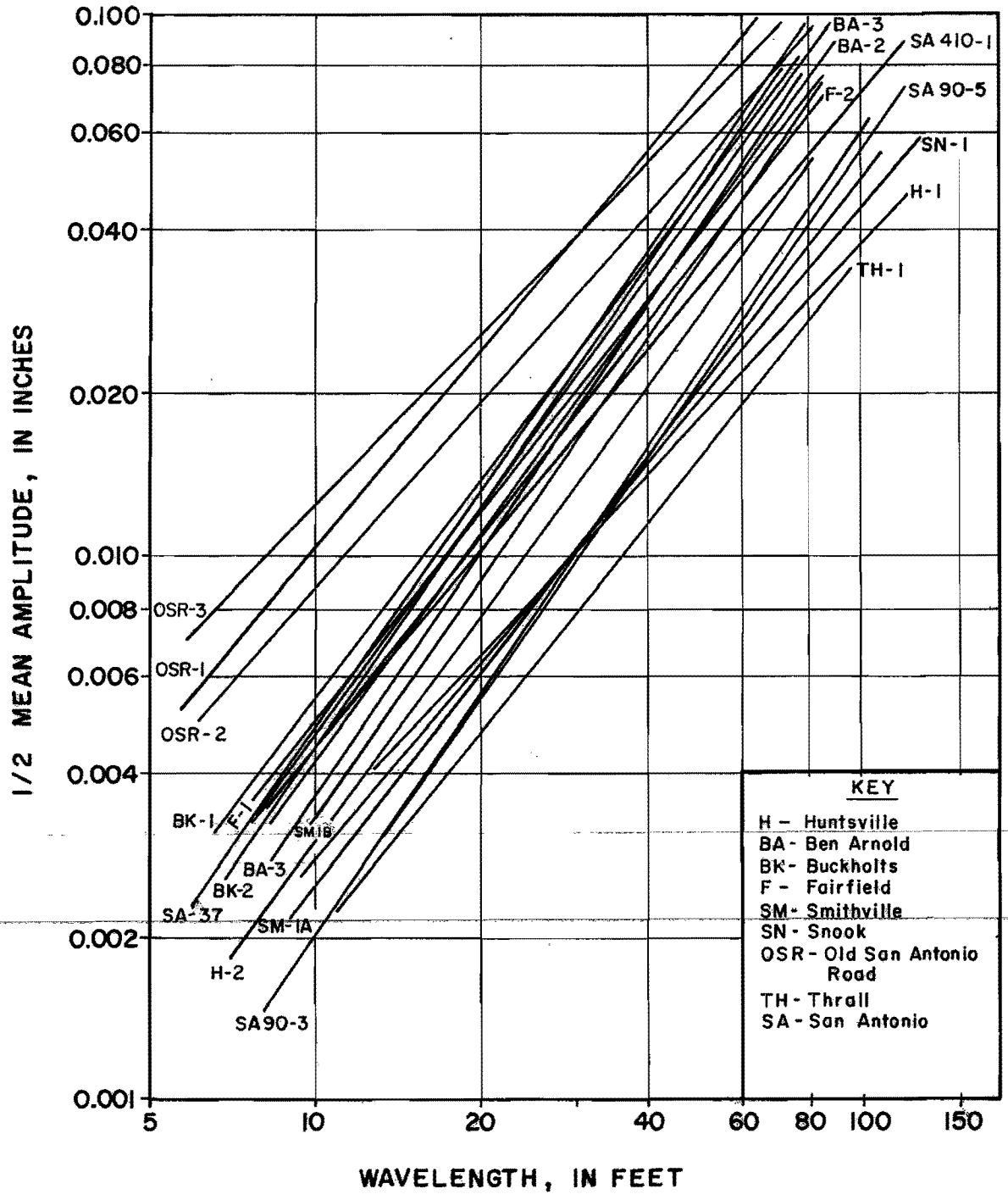

FIGURE 7. Roughness Spectra
(Right Wheelpath)

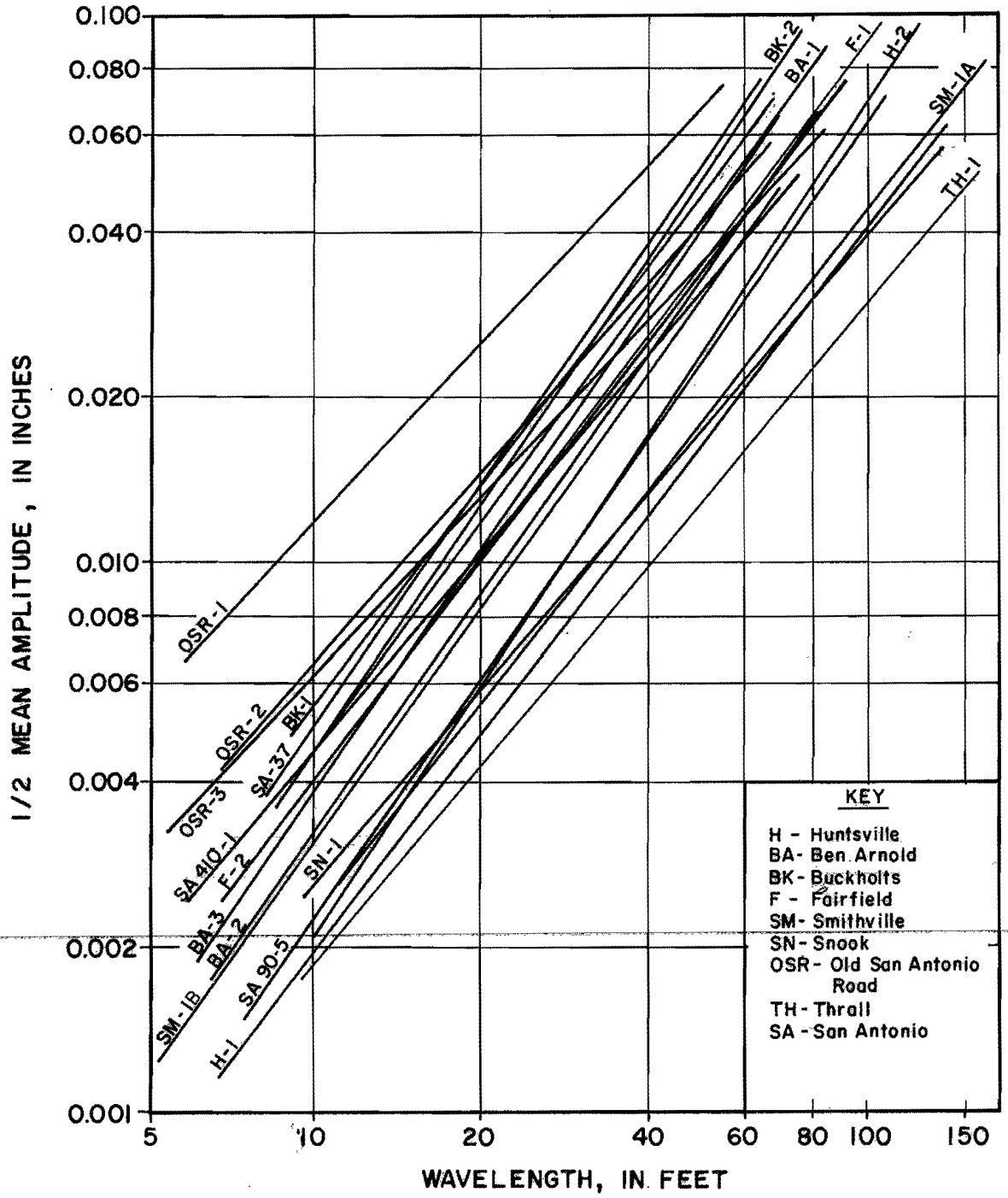

FIGURE 8. Roughness Spectra
(Left Wheelpath)

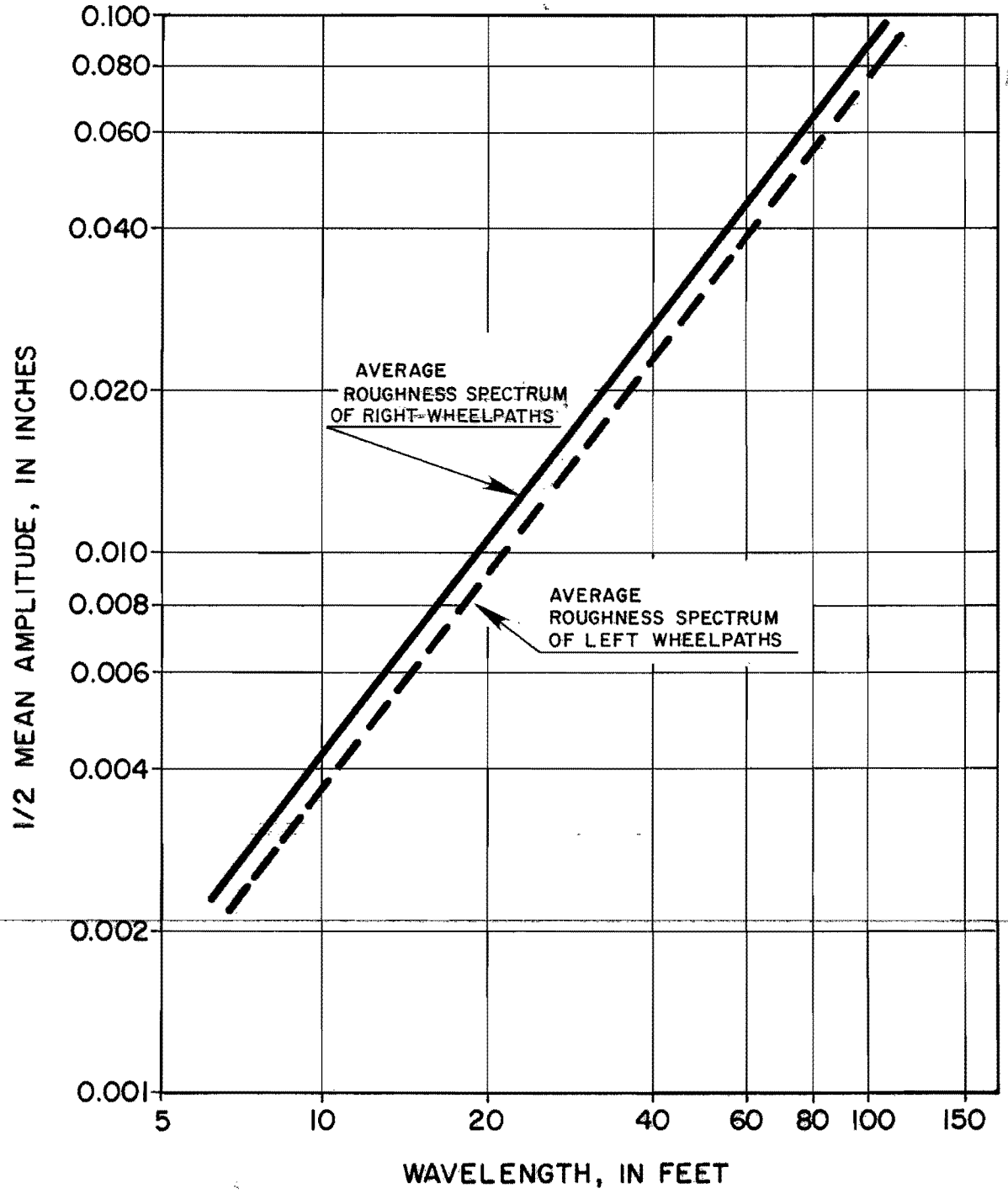

FIGURE 9. Comparison Between Right and Left Wheelpaths

have an important practical interest if the values of the parameters can be predicted and related to the Serviceability Index. These objectives will be discussed later in this report.

Dominant Wavelengths

Lytton et al. (15) and McKeen (16) have suggested that the pavement roughness spectra on expansive soils tend to show some dominant wavelengths. Although the influence of these specific wavelengths will be reflected in the values of log c and n, it is also interesting to distinguish them specifically.

A simple assumption might be made: the measured values of $\frac{A}{2}$ for these wavelengths will appear as peaks above the fitted curves in the frequency domain plots. (Appendix VI).

With this assumption, the values of the dominant wavelengths have been estimated for the right wheelpath of the different roadway segments. They are presented in Table 11. Even though the roadway sections have different characteristics, it seems that some of the dominant wavelength values are the same for a significant number of sections. To illustrate this point, a bar graph was prepared, grouping all the values included in Table 11 into 3-foot intervals and calculating the percentage of dominant wavelengths in each interval with respect to the total number of values. (See Figure 10). It appears that dominant wavelengths are more frequent between 9-12, 27-30, 36-42, 51-54, and 102-105 feet.

It should be pointed out that the described technique for estimating dominant wavelengths has two drawbacks. First, being based upon results from FFT analysis, the estimated values represent sinusoidal components of the pavement roughness, but not actual waves present in the road profile.

TABLE 11. Wavelengths of Sinusoids with Peak Amplitude (Right Wheelpath)

Section (1)	Dominant Wavelengths[a], in feet (2)									
Huntsville 1	9	11	13	16	22	30	42	52	--	---
Huntsville 2	8	11	14	17	--	28	38	52	70	---
Ben Arnold 1	-	--	--	--	--	--	--	52	--	105
Ben Arnold 2	-	--	--	--	--	--	42	--	--	105
Ben Arnold 3	-	--	--	--	--	32	--	--	--	---
Buckholts 1	-	--	12	--	--	--	--	--	84	---
Buckholts 2	-	--	--	--	--	--	42	--	--	105
Fairfield 1	-	--	--	--	--	--	--	47	--	105
Fairfield 2	-	--	12	--	--	--	--	--	--	105
Smithville 1A	-	--	--	--	--	--	42	--	--	105
Smithville 1B	-	--	--	17	26	--	38	52	84	---
Snook 1	-	--	--	--	--	--	--	--	--	---
OSR 1	8	9	--	--	--	30	38	--	--	---
OSR 2	-	10	--	20	--	32	--	--	60	---
OSR 3	-	10	12	--	26	35	--	52	--	---
Thrall 1	-	--	--	--	--	--	--	--	--	105
S. Antonio 410-1 (November 79)	-	--	12	20	--	--	--	--	--	105
S. Antonio 37	-	--	--	--	--	30	--	47	--	105
S. Antonio 90-5 (April 78)	-	--	--	--	--	--	38	52	--	---
S. Antonio 90-3 (April 78)	-	--	--	--	--	--	--	--	--	105

[a]From Fast Fourier Transform analyses

Second, given the characteristics of the input (sampling interval and number of samples) chosen in this study for the FFT analysis, the output is a distribution of sinusoids at discrete frequencies separated by 0.0024 cycles/foot. With this frequency interval, actual short waves in the road profile will be distributed over several frequencies (and their possible amplitude peaks shadowed), while, on the other hand, the "resolution" in the lower frequency region is poor. In order words, a decrease of 0.0024 cycles/foot in this region signifies (as wavelength is the inverse of frequency) an appreciable increase in wavelength. For example, the three consecutive discrete frequencies equal to 0.0119, 0.0095, and 0.0071 cycles/foot represent, respectively, sinusoids with wavelengths equal to 84,105, and 141 feet.

Because of this difficulty, it is convenient to use another approach complementing the analysis of dominant wavelengths. This has been done by determining, directly on the road profiles, the wavelength probability density functions. A computer program with a special filter that copies the effect of a field survey (15) was available. The road profiles, both for the right and left wheelpath were again sampled every 0.82 feet. The program compares the heights of the samples, considers as "high points" those which are at least above 8 of the adjacent samples, and measures the horizontal distance between the high points. Next, the program groups these peak-to-peak distances (that can be taken as wavelengths) into 3-foot intervals and prints-out the results. With this information for each roadway segment, its probability density functions of wavelength both for the right and left wheelpath can be plotted. They are included in Appendix V. An as example, one of these graphs is presented in Figure 11. The probability of occurrence has been calculated for each 3-foot interval and plotted in the center of this interval.

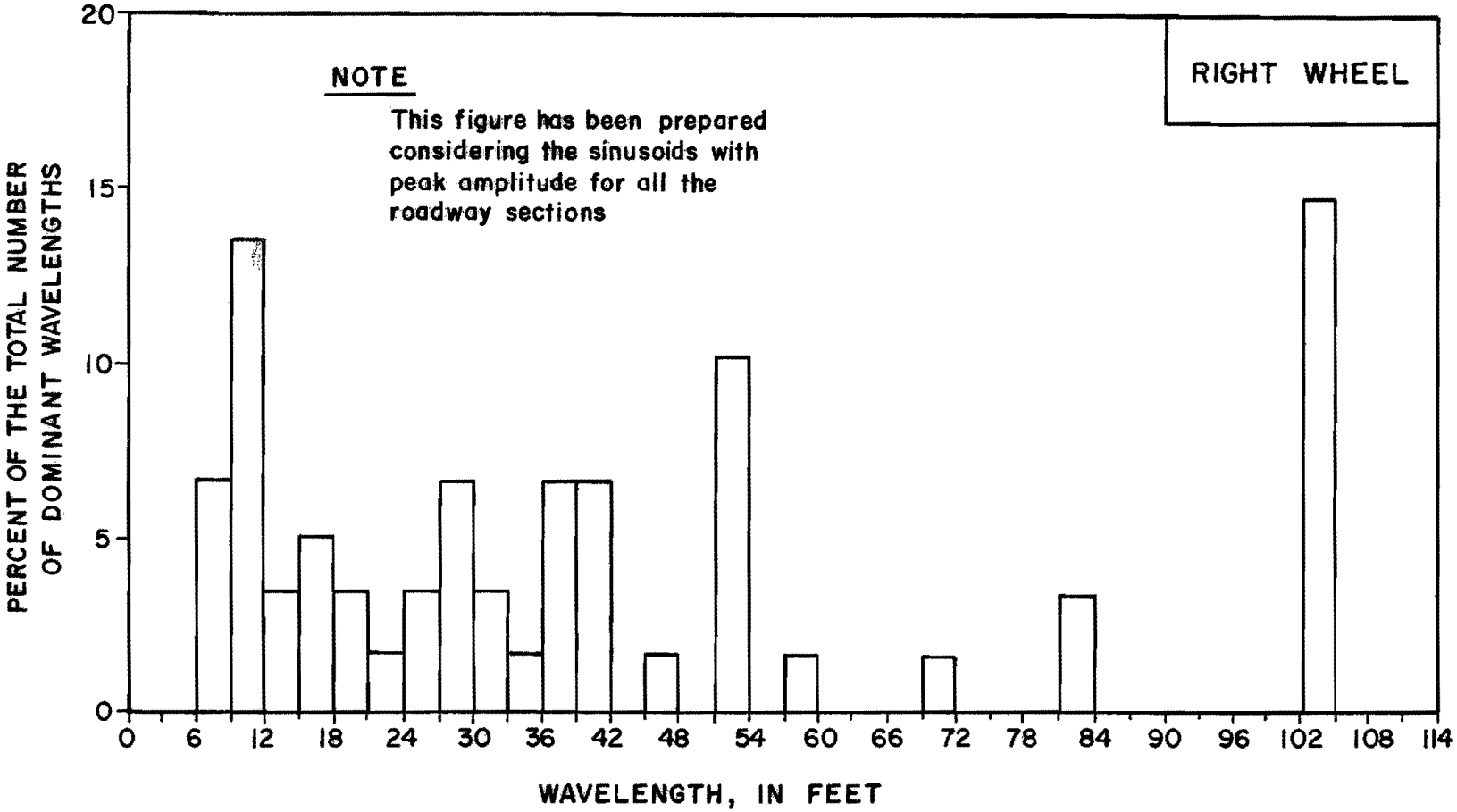

FIGURE 10. Distribution of Dominant Wavelengths (From FFT analysis)

It is assumed that dominant wavelengths will appear as relative maximums in the probability density functions. In other words, this second approach is focused on the relative abundance of waves with specific lengths, instead of the amplitude of the waves, as does the FFT analysis.

The values of the most noticable maximums in the probability density functions for the right wheelpaths are presented in Table 12. Again, it seems that some of these values are the same for a significant number of roadway sections. To enhance this point, a bar graph was prepared considering all the values presented in Table 12 and calculating the percentage of dominant wavelengths in each 3-foot interval with respect to the total number of values (See Figure 12). It appears that dominant wavelengths are most probable between 9-12, 21-24, 30-33, and 45-48 feet.

The comparison between the results obtained from the two techniques used to distinguish dominant wavelengths is shown in Table 13.

TABLE 13. Comparison of Results

Technique (1)	Dominant Wavelengths, in feet (2)
Sinusoids with peak amplitude in frequency domains	9-12 -- 27-30 36-42 51-54 102-105
Relative maximums in probability density functions	9-12 21-24 30-33 -- 45-48 --

A general conclusion might be drawn from the results presented in Table 13: pavement roughness on expansive soils in Central Texas seems to have dominant wavelengths around 10 feet. Furthermore, these 10 foot waves also seem to combine (probably as a function of the pavement characteristics)

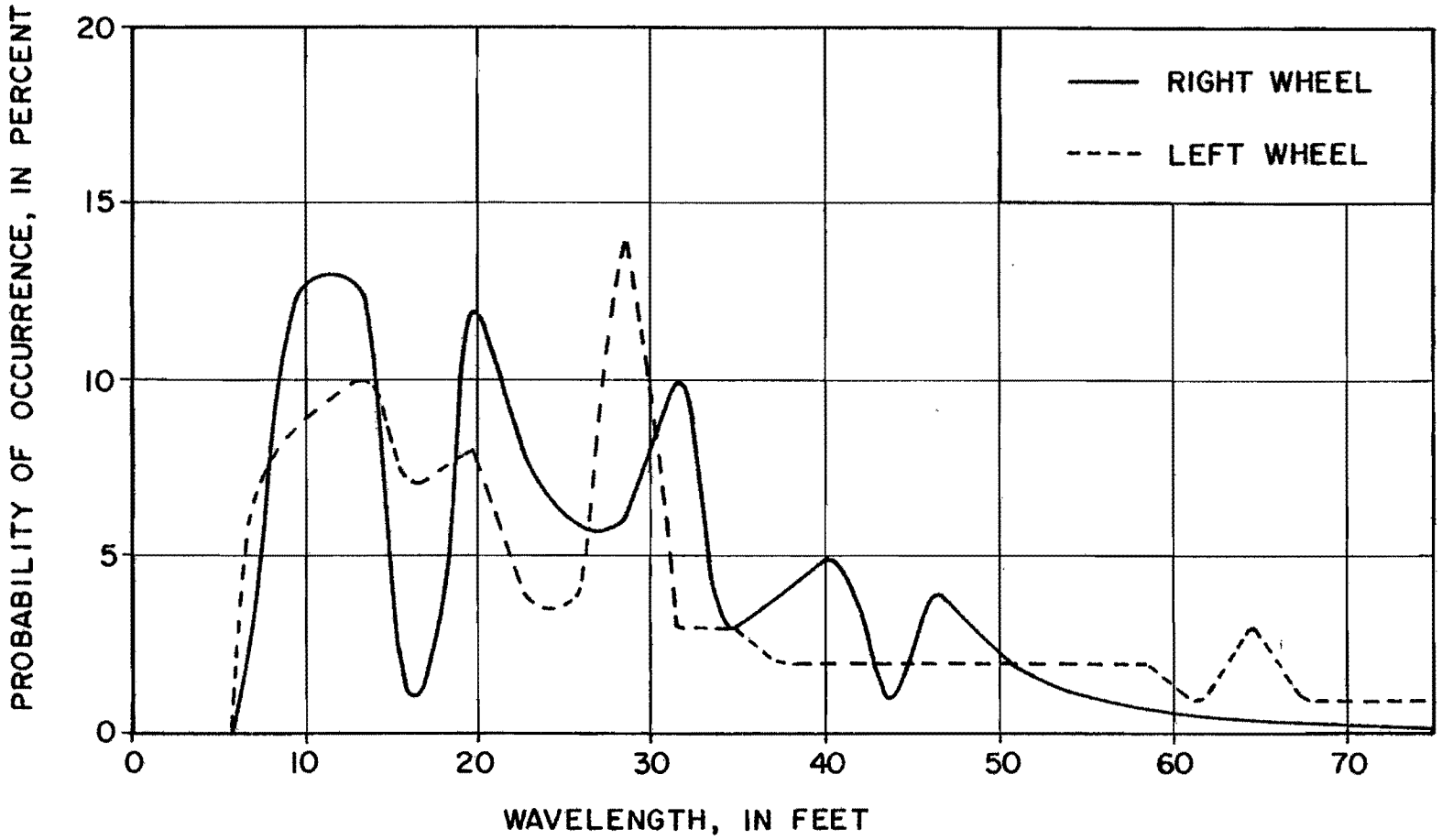

FIGURE 11. Probability Density Function of Wavelength (OSR 2)

TABLE 12. Most Probable Wavelengths (Right Wheelpath)

Section (1)	Dominant Wavelengths[a], in feet (2)				
Huntsville 1	10.5	16.5	22.5	----	----
Huntsville 2	10.5	----	22.5	31.5	----
Ben Arnold 1	10.5	----	22.5	----	46.5
Ben Arnold 2	10.5	----	22.5	----	49.5
Ben Arnold 3	10.5	16.5	28.5	----	----
Buckholts 1	10.5	----	22.5	----	46.5
Buckholts 2	10.5	----	----	31.5	37.5
Fairfield 1	10.5	19.5	----	----	49.5
Fairfield 2	----	13.5	----	40.5	70.5
Smithville 1A	10.5	19.5	----	37.5	----
Smithville 1B	10.5	----	----	34.5	46.5
Snook 1	10.5	19.5	----	----	----
OSR 1	10.5	----	22.5	31.5	46.5
OSR 2	10.5	19.5	----	31.5	----
OSR 3	10.5	---	22.5	----	----
Thrall 1	----	13.5	28.5	----	46.5
S. Antonio 410-1 (Nov. 79)	9.0	16.5	25.5	34.5	----
S. Antonio 37	10.5	----	----	31.5	58.5
S. Antonio 90-5 (April 78)	10.5	19.5	----	----	52.5
S. Antonio 90-3 (April 78)	10.5	----	28.5	----	55.5

[a]Relative maximums in probability density functions

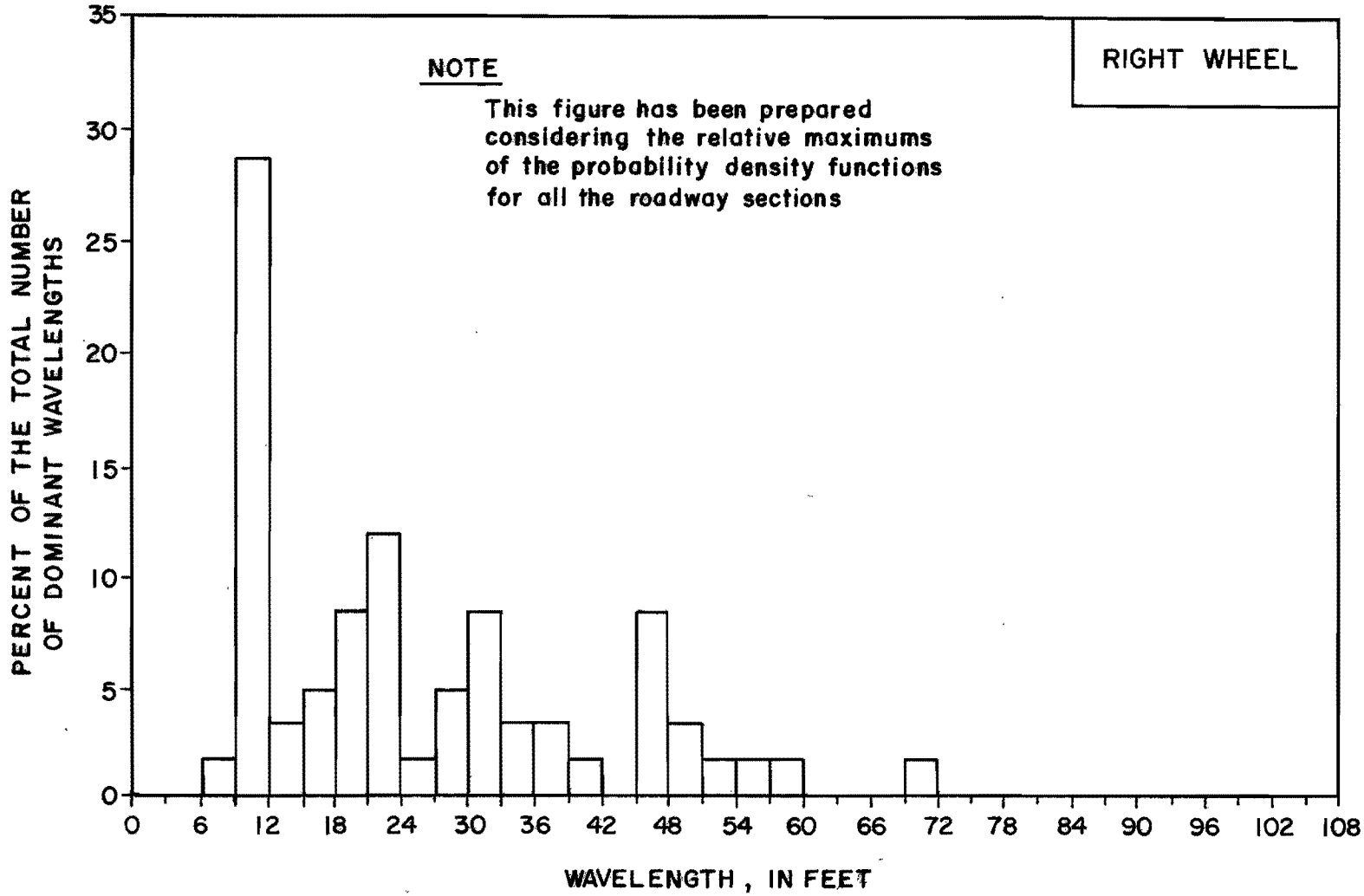

FIGURE 12. Distribution of Dominant Wavelengths (From Probability Density Functions)

giving dominant waves with length multiples of 10 feet, especially around 30 feet and 50 feet.

Finally, to complete the analysis of the roadway profiles, the distributions of wavelengths for the different sections are included in Appendix VI. One of these graphs is presented in Figure 13. These distributions show for a specific wavelength value the percent of waves with lengths less that this value. They are the integral functions of the probability density functions with the upper limit being the wavelength variable.

Table 14 presents the wavelength values which are greater than the lengths of 25%, 50% and 75% of the total number of waves.

Prediction Models

It has been shown in this study that pavement roughness can be described as a function of only two parameters (c and n). Several investigators have also noted this fact (6, 20). Furthermore, the prediction of the parameters values can help to a better understanding of pavement roughness development on expansive soils, and thus improve the design of pavements on these soils.

It is assumed that four principal groups of factors interrelate in the development of roadway roughness: characteristics of the pavement, climate, time, and properties of subgrade soils. Specifically, empirical models to predict c and n (both for right and left wheelpath) have been derived considering 10 possible independent variables, listed in Table 15. To determine the prediction models a regression analysis has been performed, using the SELECT regression program (8). This computer program assumes mathematical models such as:

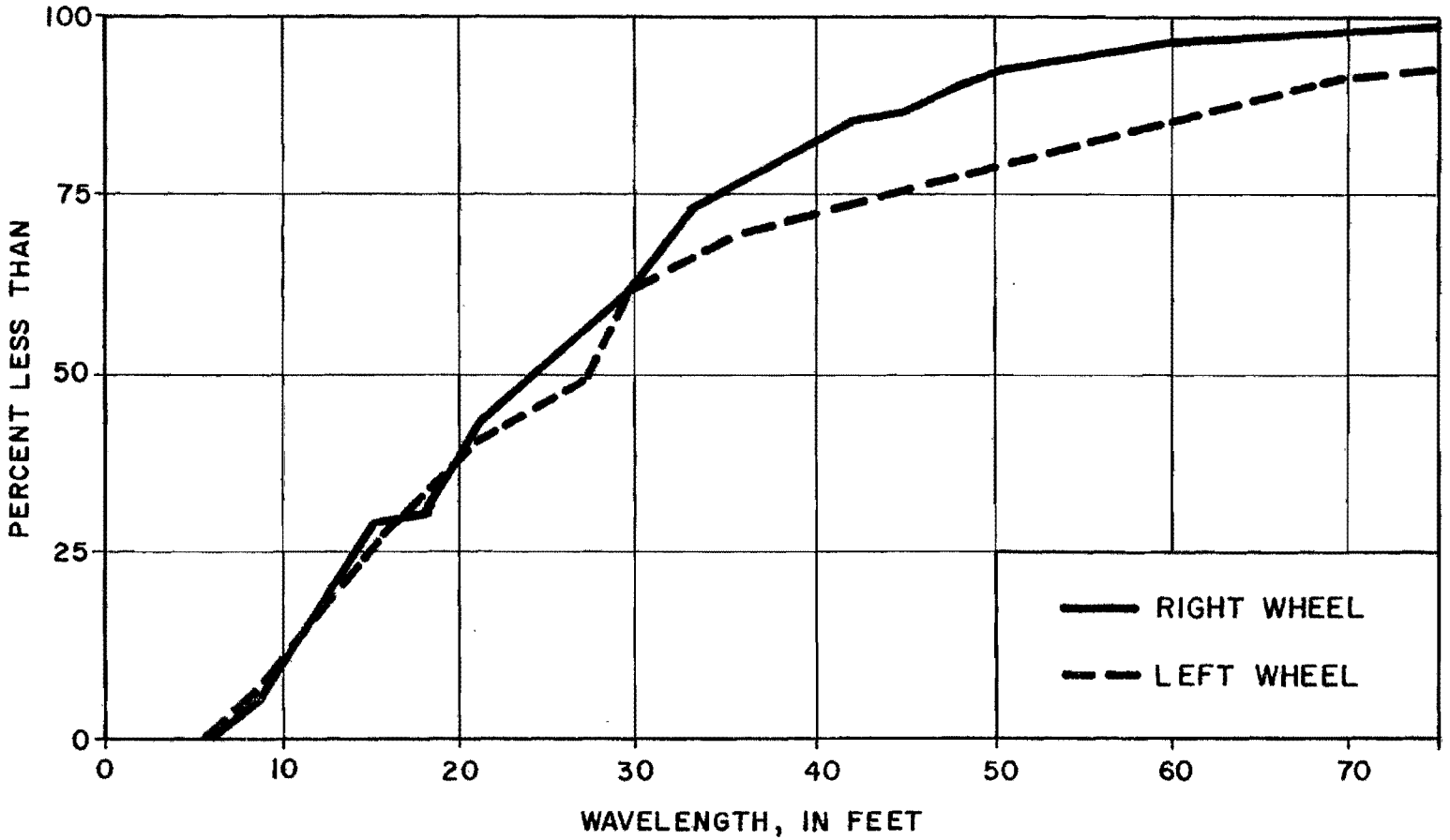

FIGURE 13. Distribution of Wavelengths
(OSR 2)

TABLE 14. Distribution of Wavelengths

Section	Wavelength greater than, in feet					
	Left Wheel			Right Wheel		
	25%	50%	75%	25%	50%	75%
Huntsville 1	15	22	29	14	20	27
Huntsville 2	18	24	32	15	23	32
Ben Arnold 1	23	40	68	15	28	56
Ben Arnold 2	18	29	81	15	30	78
Ben Arnold 3	23	40	71	14	28	46
Buckholts 1	21	48	84	16	24	54
Buckholts 2	12	33	70	14	32	57
Fairfield 1	18	31	56	12	22	48
Fairfield 2	14	29	57	13	27	49
Smithville 1A	12	15	28	13	19	34
Smithville 1B	17	34	45	19	34	48
Snook 1	13	30	51	17	26	49
OSR 1	14	31	68	13	24	47
OSR 2	15	27	45	14	24	35
OSR 3	10	15	24	13	22	39
Thrall 1	11	18	57	14	19	59
S. Antonio 410-1 (Nov. 79)	19	51	82	13	27	84
S. Antonio 37	26	43	69	21	40	69
S. Antonio 90-5 (April 78)	18	31	49	18	36	54
S. Antonio 90-3 (April 78)	15	31	66	15	32	63

$$y = a_o X_1^{a_1} X_2^{a_2} \ldots\ldots\ldots x_n^{a_n} \qquad (9)$$

Then, an equivalent model is:

$$\log y = \log a_o + a_1 \log x_1 + a_2 \log x_2 + \ldots + a_n \log x_n \qquad (10)$$

Given sets of values for the dependent variable y and the independent variables x_1, x_2, ..., x_n, the program uses a linear regression technique to determine the constants in equation (10), and selects the best models using n, n-1, n-2, and so on down to 1 independent variable.

In Table 10, values of log c and n for 20 sections have been presented. The corresponding values of the 10 possible independent variables listed before are included in Tables 1, 3, 5, 8, and 9. Three of these sections have been eliminated from the regressions: San Antonio 410-1, where it was not possible to estimate the effective depth, San Antonio 90-3, which is on fill, and San Antonio 90-5, where the subgrade was ponded prior to construction. The input for the SELECT regression program was 17 sets of values. A summary of the results is presented in Appendix VIII, Tables VIII-2, and VIII-3.

Simplicity, high multiple correlation, and physical meaning have been the criteria followed to choose from those results the best models to predict the parameters c and n. These emprical prediction models are presented in Table 16.

To interpret these equations properly, it should be noted that an increase in the c value represents a proportional increase of amplitude for all of the wavelengths in the roughness spectrum. An increase in the absolute value of n represents a proportionally higher amplitude increase of the long wavelengths than the short wavelengths (See Figures 7 and 8).

TABLE 15. Independent Variables

DEPTH = effective depth of pavement, in inches

TH = mean value of Thornthwaite moisture index for a 20 year period

RANGE = range of values of Thornthwaite moisture index for a 20 year period

TIME = time since construction or last rehabilitation before the roughness was measured, in years

CLAY = percent clay (grain size less than 0.002 mm)

AC = activity, $\left(\frac{\text{Plasticity Index}}{\text{CLAY}}\right)$

CEC = cation exchange capacity, in $\frac{\text{meq}}{100\ \text{gm}}$

CEAC = cation exchange activity, $\left(\frac{\text{CEC}}{\text{CLAY}}\right)$

COLE = coefficient of linear extensibility

ESP = exchange sodium percentage

Besides, it appears that n and c are not truly independent. This point will be explained with more detail in the next pages. With these facts in mind, several observations about the prediction models can be made:

1. The effective depth of the pavement (DEPTH) influences the development of roughness. An increase in DEPTH causes an appreciable decrease in the c values and a minor increase in the absolute values of n. As a result, the stiffer the pavement, the less roughness will develop and this roughness will have longer wavelengths.
2. Roughness increases with time. The TIME variable appears in the equations for the c values, but not in those for the n values.
3. The range of the Thornthwaite moisture index (RANGE) appears in the equations for the n values, but not in those for the c values. RANGE gives a rough indication of the climate variability. As RANGE increases, the absolute values of n decreases. This fact seems to indicate that climate variability enhances the relative importance of the short wavelengths with respect to the long wavelengths.
4. The mean Thornthwaite moisture index (TH) is included only in the model for the parameter n in the left wheelpath, probably indicating that average climate has a greater influence in the roughness developed in the center of the pavement than at the boundaries.
5. The influence of the soil properties in the models is reflected through the variables exchange sodium percentage (ESP), activity (AC), cation exchange capacity (CEC), and percent clay (CLAY). As ESP increases, roughness increases.

TABLE 16. Prediction Models for c and n

Left Wheelpath (1)	Right Wheelpath (2)
$c = 0.0008\ DEPTH^{-1.07}_{TIME}{}^{0.30}_{AC}{}^{-1.04}_{ESP}{}^{0.19}$	$c = 0.0004\ DEPTH^{-0.81}_{TIME}{}^{0.49}_{AC}{}^{-1.20}_{ESP}{}^{0.12}$
($R^2 = 0.78$)	($R^2 = 0.77$)
$n = -1.06\ DEPTH^{0.13}_{CEC}{}^{-0.17}_{CLAY}{}^{0.32}_{(TH+35)}{}^{0.16}_{RANGE}{}^{-0.30}$	$n = -0.79\ DEPTH^{0.09}_{CEC}{}^{-0.16}_{CLAY}{}^{0.40}_{RANGE}{}^{-0.16}$
($R^2 = 0.86$)	($R^2 = 0.83$)

NOTE: Independent variables listed in Table 15.

The other three soil variables, AC, CEC, and CLAY, are not truly independent. Their effects should be considered as a whole. Nevertheless, it seems that a higher CLAY causes high roughness, especially in the long waves. On the other hand, CEC and AC (with minor influence) appear to have the opposite effect. Thus, the models show the complication of the physico-chemical phenomena taking place in the development of expansive soil roughness, which can not be explained only as a function of a single soil property.

6. The values of the parameter n probably are related to the soil cracking spacing.

As it was cited before, c and n not only are complementary parameters of the same phenomenon, but also it seems that they are not completely independent. To analyze this possibility, the log c values have been plotted versus the corresponding n values for all of the roadway sections listed in Table 10. (See Figures 14 and 15). These figures illustrate a general tendency of the absolute value of n to decrease when the log c value increases. Furthermore, in several roadway sections in the San Antonio area, roughness was measured at different dates. The corresponding log c and n values are presented in Appendix VII. These values (for the outside lanes) were also plotted in Figures 14 and 15. The points for each section at different dates are fitted by straight lines with the same slope. The general equation of these straight lines is:

$$\log c = \log c_1 + 2.02\, n \quad \ldots\ldots\ldots\ldots\ldots\ldots\ldots\ldots \quad (11)$$

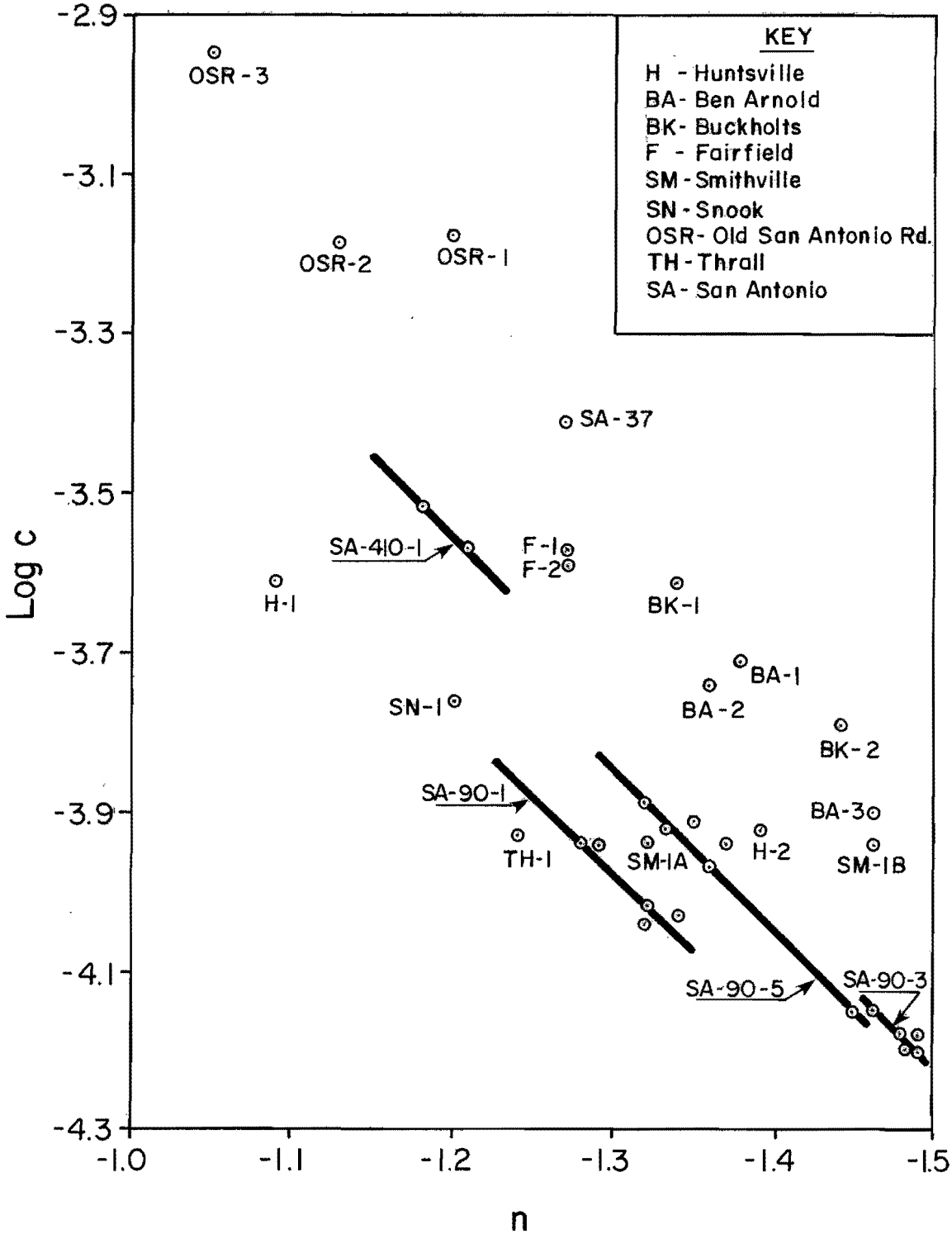

FIGURE 14. Log c versus n (Right Wheelpath)

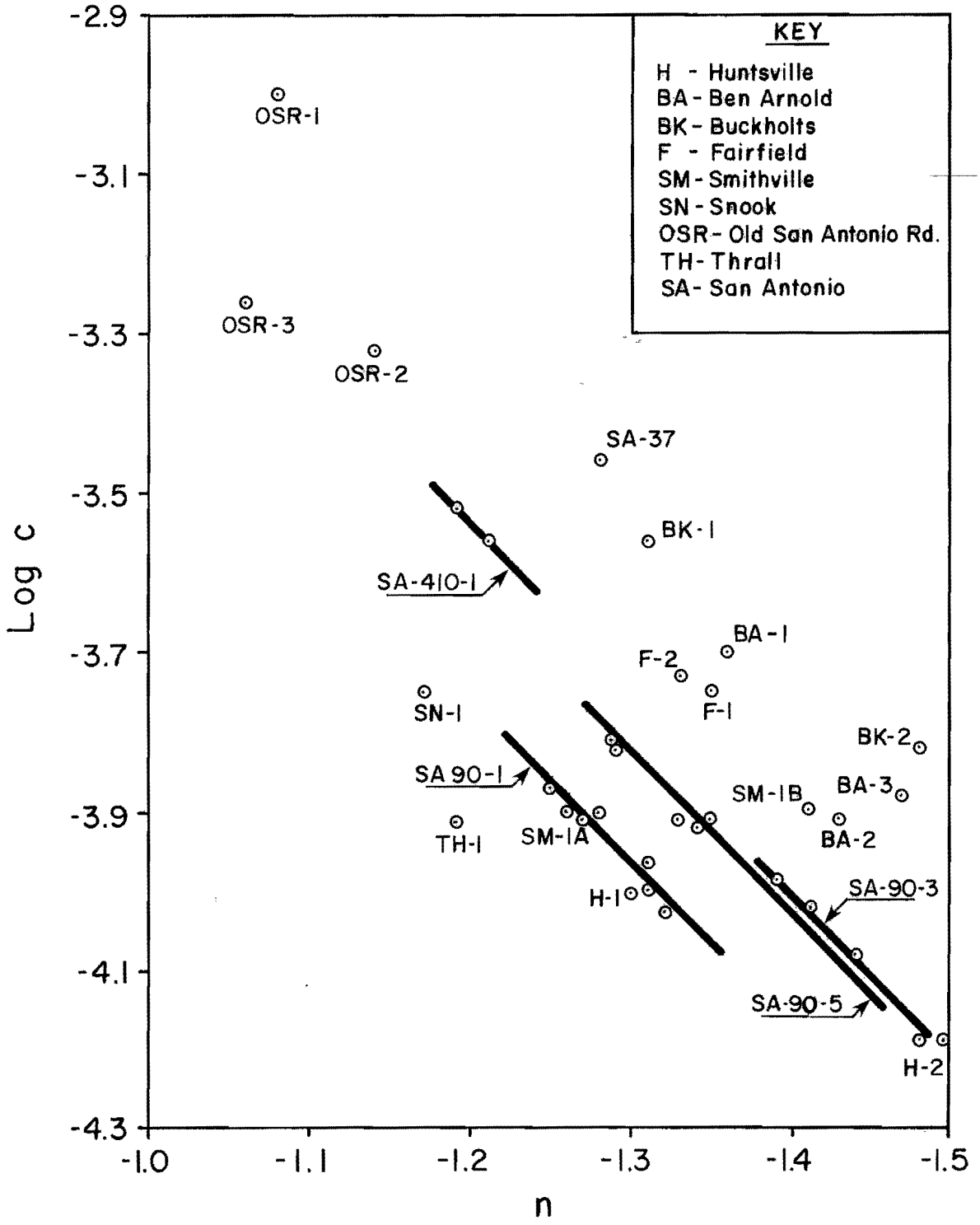

FIGURE 15. Log c versus n (Left Wheelpath)

where

log c, n = parameters characterizing pavement roughness

log c_1 = intercept in the log c versus n plots

If it is assumed that equation (11) holds true for all of the rest of the roadway sections (where roughness measures at different dates are not available), it becomes evident that log c and n are not independent. Moreover, the intercept (log c_1) in equation (11) probably is related to some of the factors causing roughness that do not vary with time, like soil properties.

An increase in the value of c_1 reflects an increase in roughness, but c_1 does not completely characterize the roughness pattern. Nevertheless, its study may complement the understanding of the parameters log c and n. The values of log c_1 for all the roadway segments listed in Table 10 can be calculated with the formula:

$$\log c_1 = \log c - 2.02\, n \quad \ldots\ldots\ldots\ldots\ldots\ldots \quad (12)$$

where

log c_1 = value of the intercept of the straight line log c versus n for a specific section

log c, n = values characterizing the roughness of the section at a specific date.

The log c_1 values are presented in Table 17.

To analyze the factors influencing the value of c_1, a regression analysis was performed with the SELECT regression program and considering again the 10 possible independent variables listed in Table 15. A summary of the results is presented in Appendix VIII, Table VIII-4. The best models (both for the right and left wheelpath) are shown in Table 18.

TABLE 17. Log c_1 Values

Section (1)	Log c_1 Values	
	Left Wheel (2)	Right Wheel (3)
Huntsville 1	-1.37	-1.41
Huntsville 2	-1.14	-1.11
Ben Arnold 1	-0.95	-0.92
Ben Arnold 2	-1.02	-0.99
Ben Arnold 3	-0.91	-0.95
Buckholts 1	-0.91	-0.90
Buckholts 2	-0.83	-0.88
Fairfield 1	-1.02	-1.00
Fairfield 2	-1.04	-1.04
Smithville 1A	-1.34	-1.27
Smithville 1B	-1.05	-0.99
Snook 1	-1.39	-1.34
OSR 1	-0.82	-0.76
OSR 2	-1.02	-0.91
OSR 3	-1.12	-0.83
Thrall 1	-1.51	-1.42
S. Antonio 410-1 (Nov. 79)	-1.12	-1.13
S. Antonio 37	-0.80	-0.86
S. Antonio 90-5 (April 78)	-1.17	-1.22
S. Antonio 90-3 (April 78)	-1.18	-1.19

TABLE 18. Prediction Models for c_1

Wheelpath (1)	Model (2)
Right	$c_1 = 0.82\ ESP^{0.11} COLE^{1.06} AC^{-1.19}$ ($R^2 = 0.45$)
Left	$c_1 = 0.55\ ESP^{0.19} COLE^{0.99} AC^{-1.34}$ ($R^2 = 0.42$)

NOTE Independent variables listed in Table 15

The models for c_1, including only soil properties as independent variables, have poor multiple correlation coefficient values. However, they add information about the appearance of pavement roughness on expansive soils. The models can be interpreted as follows:

1. As the exchange sodium percentage (ESP) increases, roughness increases. This could be expected, as it is known that the higher the proportion of Na cations in the interlayer positions of a clay, the higher the shrink-swell potential. Also, it has been found that dispersive soils have a high ESP.
2. A higher coefficient of linear extensibility (COLE) causes greater roughness.
3. As the activity (AC) decreases, roughness increases, but it should be noted that AC and COLE are not truly independent. It can be expected that if AC decreases, COLE will decrease too. Thus, the models probably are pointing out the relative effects of some of the soils properties. ESP and COLE are

more directly related to the chemical aspects of the swelling phenomenon, while AC in the models may be indicating the influence of some physical aspects, like the permeability of soil clods.

These three observations are consistent with those made for the c and n prediction models.

Correlation with the Serviceability Index

The prediction of the Serviceability Index (SI) decrease with time is a critical aspect in the definition of the optimum strategy to follow in order to minimize the overall cost for the expected life of a pavement. Lu et al. (12) have developed a methodology and presented models to predict serviceability loss of flexible pavements due to fatigue, swelling, shrinkage, and thermal cracking.

A simpler approach to estimate the Serviceability Index reduction (ΔSI) is presented here, based upon the correlation between ΔSI and the parameters c and n, which in turn can be predicted with the models shown in Table 16.

In several roadway sections, the values of the Serviceability Index (calculated by the Center for Transportation Research, University of Texas at Austin) are known. The ΔSI values, along with the correspondent c and n values for the right wheelpath, are presented in Table 19. Multiple regression analysis has been performed with these data to obtain the following equation:

$$\Delta SI = 2675.41\ c^{1.09}\ |n|^{7.62} \quad (R^2 = 0.73) \qquad (13)$$

where

ΔSI = Servicability Index reduction below its initial value

$|n|$ = absolute value of n

c,n = as defined before

As expected, ΔSI increases as c or $|n|$ increases. Moreover, the right wheelpath prediction models for c and n, included in Table 16, can be substituted in Equation (13). The equation obtained is then:

$$\Delta SI = 0.087\ DEPTH^{-0.20} TIME^{0.53} ESP^{0.13} CEC^{-1.22} \times CLAY^{3.05} AC^{-1.31} RANGE^{-1.22} \quad (14)$$

where

ΔSI = Serviceability Index reduction

DEPTH = effective depth of pavement, in inches

TIME = time since construction or last rehabilitation, in years

ESP = exchange sodium percentage

CEC = cation exchange capacity, in meq/100gm

CLAY = percent clay (grain size less than 0.002 mm)

AC = activity $\left(\frac{\text{Plasticity Index}}{\text{CLAY}}\right)$

RANGE = range of values of Thornthwaite moisture index for a 20 year period.

The equation permits approximate prediction of the decrease of Serviceability Index as a function of the characteristics of the pavement, time, subgrade soil properties, and climate. Nevertheless, it should be noted that riding quality (and then Serviceability Index) not only depends on the roughness of the right wheelpath, but also on other factors, such as transverse effects, due to differences between the roughness patterns of the right and left wheelpaths, and the velocity of the vehicle.

TABLE 19. Serviceability Index Reduction

Section (1)	c[a] (2)	n[a] (3)	Serviceability Index Reduction, Δ SI = 5-SI (4)
Snook 1	0.00017	-1.20	0.6
OSR 1	0.00066	-1.20	2.3
OSR 2	0.00065	-1.13	3.3
OSR 3	0.00112	-1.05	2.6
Thrall 1	0.00012	-1.24	0.5
S. Antonio 90-1 (October 75)	0.00011	-1.28	1.0
S. Antonio 90-1 (April 77)	0.00009	-1.34	1.0
S. Antonio 90-5 (April 76)	0.00012	-1.33	1.8
S. Antonio 90-5 (April 77)	0.00011	-1.37	1.9
S. Antonio 90-3 (West, October 75)	0.00006	-1.49	1.5
S. Antonio 90-3 (West, April 77)	0.00007	-1.51	1.4

[a]These values are for the right wheelpath

In Appendix IX, a case study is presented, comparing measured Serviceability Index values in San Antonio 90-5 at different dates and the Serviceability Index reduction prediction with equation (14). Data from this section was not included among the data from which the prediction models for c and n were developed.

In Appendix X, graphs of amplitude versus frequency spectra which were derived directly from the profile using the "bump counter" technique which was mentioned previously in this chapter, are presented. That appendix also presents graphs of the cumulative probability distributions for amplitudes. A correspondence is found between the log c and n values determined by the FFT method and the same values determined directly from the profile. Finally, a method is developed to use the real profile values of c and n to compute the quantity of overlay materials that will be required to level up a rough pavement section and the amount of material that will be removed by heater-planing or roto-milling a rough pavement. All of these equations are expected to be valuable in the determination of the most cost effective combinations of pre-construction and post-construction treatments of pavements on expansive clays.

Summary

In this section, the overall pavement roughness patterns of pavements built on expansive soils in Central Texas have been characterized as a function of only two parameters, c and n. Empirical models to predict the values of c and n have been developed. These models indicate that road roughness depends upon pavement characteristics, time, climate, and subgrade soil properties. Finally, these two parameters have been correlated with the Serviceability Index reduction.

CHAPTER FIVE

CONCLUSIONS AND RECOMMENDATIONS

Conclusions

The study of the roughness patterns developed on Central Texas pavements built on expansive soils, has led to the following conclusions:

1. The Fast Fourier Transform method which was used to study the road profiles in the frequency domain, provides very consistent measures of pavement roughness.
2. Pavement roughness along each wheelpath can be characterized as a function of only two parameters, c and n. This fact has greatly facilitated the quantification of the roughness problem.
3. c and n are not only complementary parameters of the same phenomenon, but also they are correlated.
4. Although the parameters c and n should be considered as a whole, a variation of the c value represents a variation of amplitude proportional for all the wavelengths, while n reflects the relative importance of the long waves respect to the short waves. Probably, the n value is related to the spacing of the major cracks soil cracking fabric.
5. Empirical models to predict c and n have been developed. These models indicate how the stiffness of the pavement, time, climate and several physico-chemical soil properties interrelate in the development of pavement roughness. Eight variables appear in the models, but the four more important are:
    a. effective depth of the pavement
    b. time

c. percent clay

d. exchange sodium percentage

6. The values of the parameters c and n for the right wheelpath have been correlated with the Serviceability Index reduction. With this correlation and the prediction models for c and n, an approximate estimation of the Serviceability Index reduction is also possible.

7. Besides the study of the overall roughness patterns through the parameters c and n, an analysis of the dominant wavelengths present in the patterns has been conducted. In general, the dominant waves in the pavements studied are approximately 10 feet long. Furthermore, these 10 foot waves seem to combine giving other dominant waves with lengths that are multiples of 10 feet, especially around 30 feet and 50 feet.

Recommendations

This study has led to several recommendations presented herein:

1. The values of the parameters c and n used in this study have been obtained through specific procedures to measure pavement roughness and input this measured roughness for the Fast Fourier Transform method. Variations in these procedures will affect the values of c and n. Thus, to apply consistently the methodology presented in this study, the mentioned procedures should be kept the same.

2. The prediction models for c and n can be checked, measuring the pavement roughness and the rest of the variables involved in the models in several road sections. Then, a back-analysis

can be performed, and the models improved, if needed. Also, it would be desirable to collect more data to obtain a better correlation between the Serviceability Index reduction and the parameters c and n.

3. As the effective depth is an important variable in the prediction models, its estimation should be refined.
4. In this study, it has been implicitly assumed that a pavement after resurfacing, (which increases the effective depth) and the same road built originally with that increased effective depth would have the same rate of roughness development. This assumption should be investigated further.
5. The prediction models have been developed from information collected in 9 different areas of Central Texas. Although the ranges of the variables involved are wide, care should be taken with the application of the models using data that is outside those ranges.
6. The methodology presented in this study has practical applications in the design of pavements on expansive soils. A computer program can be designed to calculate the combination of stabilized subgrade, base and surface thicknesses needed to maintain the Serviceability Index above a specific value for a specified length of time after construction.
7. More roughness develops in the right than in the left wheelpath. This fact indicates the effect of horizontal membranes or paved shoulders in reducing expansive clay roughness in the wheelpaths. In this study the empirical model for the reduction

of the Serviceability Index has been developed using the right wheelpath prediction models for c and n, but if the road is built with sealed shoulders or horizontal membranes, a similar model can be developed using in this case the left wheelpath models for c and n.

8. The prediction models have been obtained from data collected on pavements sections in cut and at grade with no protective measures to reduce swelling, except lime stabilitation of the top 6 inches of the subgrade in a few cases. On the other hand, research is now under way in some test sections where ponding prior to construction was conducted or vertical moisture barriers have been implemented. The models can help in the evaluation of these measures, comparing the actual roughness developed with that predicted. Also, the influence of the presence of fill in a roadway should be studied. In the future, with more data available, the models can be improved to account for the effects of protective measures, pretreatments, presence of fill, or the rebound of deep excavations.

APPENDIX I

REFERENCES

APPENDIX I. REFERENCES

1. Anderson J. U., Fadul D. E., and O'Connor G. A., "Factors Affecting the Coefficient of Linear Extensivility in Vertisols", Proceedings, Soil Science Society of America, Vol. 37, 1973, pp. 296-299.

2. Balmer G. G., "Road Roughness Technology, State of the Art", Report No. FHWA-RD-73-75, Federal Highway Administration, Washington, D. C., December, 1973.

3. Bartelli, L. J., and McCormack, D. E., "Morphology and Pedologic Classification of Swelling Soils", Transportation Research Record 568, Transportation Research Board, Washington, D. C., 1976, pp. 1-8.

4. Beckmann, G. G., Hubble G. D., and Thompson, C.H., "Gilgai Forms, Distribution and Soil Relationships in North-Eastern Australia", Proceedings of the Symposium on Soils and Earth Structures in Arid Climates, Institution of Engineers (Australia), Adelaide, May, 1970, pp. 88-93.

5. Bower, C. A., Reitemeir, R. F., and Fireman M., "Exchangeable Cation Analysis of Saline and Alkali Soils", Soil Science, Vol. 73, No. 4, April 1952, pp. 251-261.

6. Brickman, A. D., Wambold, J. C., and Zimmerman, J. R., "An Amplitude-Frequency Description of Road Roughness", Special Report No. 116, Highway Research Board, Washington, D. C., 1971.

7. Brigham, E. O., The Fast Fourier Transform, 1st ed., Prentice-Hall, Inc., Englewood Cliffs, N. J., 1974.

8. Debuse, D. A., "Variable Selection Procedure, Implementing the Hocking-LaMotte-Leslie Method," Institute of Statistics, Texas A&M University, 1970

9. Edelman, C. H., and Brinkman R., "Physiography of Gilgai Soils", Soil Science, Vol. 94, 1962, pp. 366-370.

10. Gromko, G. J., "Review of Expansive Soils", Journal of the Geotechnical Engineering Division, ASCE, Vol. 100, No. GT6, June 1974, pp. 667-687.

11. Hallsworth, E. G., and Beckmann, G. G., "Gilgai in the Quaternary", Soil Science, Vol. 107, No. 6, 1969, pp. 409-420.

12. Lu, D. Y., Lytton, R. L., and Moore, W. M., "Forecasting Serviceability Loss of Flexible Pavements", Research Report No. 57-1F, Texas Transportation Institute, Texas A&M University, College Station, Texas, November 1974.

13. Lytton, R. L., "Expansive Clay Roughness in the Highway Design System", Proceedings of Workshop on Expansive Clays and Shales in Highway Design and Construction, Federal Highway Administration, Vol. 2, May 1973, pp. 123-149.

14. Lytton R. L., "The Characterization of Expansive Soils in Engineering", presented at the December 1977, American Geophysical Union Symposium on Water Movement and Equilibrium in Swelling Soils, held at San Francisco, California.

15. Lytton R. L., Bogges R. L., and Spotts J. W., "Characteristics of Expansive Clay Roughness of Pavements", Transportation Research Record 568, Transportation Research Board, Washington D. C., 1976, pp. 9-23.

16. McKeen R. G., "Field Studies of Airport Pavements on Expansive Clay", Proceedings of the Fourth International Conference on Expansive Soils, American Society of Civil Engineers, Volume 1, June 1980, pp. 242-261.

17. McKeen R. G., and Mielsen J. P., "Characterization of Expansive Soils for Airport Pavement Design", Report No. FAA-RD-78-59, Federal Aviation Administration, Washington, D. C., August 1978.

18. Oetking P. F., "Geological Highway Map of Texas", Dallas Geological Society, 1959.

19. Patrick D. M., and Snethen D. R., "An Occurrence and Distribution Survey of Expansive Materials in the United States by Physiographic Areas," Report No. FHWA-RD-76-82, Federal Highway Administration, Washington D. C., January 1976.

20. Quinn B. E., and Sattaripour S. A., "Measurement and Prediction of the Dynamic Tire Forces of a Passenger Vehicle on a Highway", Report No. FHWA-RD-72-26, Federal Highway Administration, Washington, D. C., August 1972.

21. Roberts F. L., and Hudson W. R., "Pavement Serviceability Equations Using the Surface Dynamics Profilometer", Research Report 73-3, Center for Highway Research, The University of Texas at Austin, April 1970.

22. Snethen D. R., Johnson L. D., and Patrick D. M., "An Investigation of the Natural Microscale Mechanisms That Cause Volume Change in Expansive Clays", Report No. FHWA-RD-77-75, Federal Highway Administration, Washington, D. C., January 1977.

23. Snethen D. R., Johnson L. D., and Patrick D. M., "An Evaluation of Expedient Methodology for Identification of Poetentially Expansive Soils", Report No. FHWA-RD-77-94, Federal Highway Administration, Washington, D. C., June 1977.

24. Snethen D. R., Townsend F. C., Johnson L. D., Patrick D. M., and Vedros P. J., "A Review of Engineering Experiences with Expansive Soils in Highway Subgrades", Report No. FHWA-RD-75-48, Federal Highway Administration, Washington D. C., June 1975.

25. "Soil Survey of Bastrop County, Texas", Soil Survey, Soil Conservation Service, J. S. Department of Agriculture, March 1979.

26. "Soil Survey of Bell County, Texas", Soil Survey, Soil Conservation Service, U. S. Department of Agriculture, March 1977.

27. "Soil Survey of Bexar County, Texas", Soil Survey, Soil Conservation Service, U. S. Department of Agriculture, August 1978.

28. "Soil Survey of Falls County, Texas", Soil Survey, Soil Conservation Service, U. S. Department of Agriculture, August 1978.

29. "Soil Survey of Freestone County, Texas", Soil Survey, Bureau of Soils, U. S. Department of Agriculture, 1921.

30. "Soil Survey of Navarro County, Texas", Soil Survey, Soil Conservation Service, U. S. Department of Agriculture, December 1974.

31. "Soil Survey of Walker County, Texas", Soil Survey, Soil Conservation Service, U. S. Department of Agriculture, May 1979.

32. "Soil Survey of Williamson County, Texas", Soil Survey, Bureau of Chemistry and Soils, U. S. Department of Agriculture, November 1938.

33. Steinberg M. L., "Continuing Measurements of a Swelling Clay in a Ponded Cut", Research Report 118-8, Center for Highway Research, The University of Texas at Austin, August 1973.

34. Thornthwaite C. W., "An approach Toward a Rational Classification of Climate", The Geographical Review, Vol. 38, No. 1, 1948, pp. 55-94.

35. Walker R. S., and Hudson W. R., "The Use of Spectral Estimates for Pavement Characterization", Research Report 156-2, Center for Highway Research, The University of Texas at Austin, August 1973.

36. Watt W. G., and Steinberg M. L., "Measurements of a Swelling Clay in a Ponded Cut", Research Report 118-6, Center for Highway Research, The University of Texas at Austin, June 1972.

37. Williamson H. J., and Hudson W. R., "A Study of the Relationships between Various Classes of Road-Roughness and Human Ratings of Riding Quality", Research Report 156-5F, Center for Highway Research, The University of Texas at Austin, August 1975.

38. Wise J. R., and Hudson W. R., "An Examination of Expansive Clay Problems in Texas", Research Report 118-5, Center for Highway Research, The University of Texas at Austin, July 1971.

39. Zable J., "Design of a Linear Vibrating System to Measure Low Frequency Random Excitation", Ph.D. Thesis, Purdue University LaFayette, Indiana, 1969.

40. Stone, R.O. and Dugundji, J., "A Study of Microrelief-Its Mapping, Classification, and Quantification by Means of a Fourier Analysis," Engineering Geology, Vol. 1, No. 2, 1965-66, pp. 91-187.

APPENDIX II

NOTATION

APPENDIX II - NOTATION

a = surface depth

A = mean amplitude

AC = activity of the soil

b = base depth

c = parameter characterizing paveement roughness

c_1 = parameter

CEAC = cation exchange activity

CEC = cation exchange capacity

CLAY = percent clay (grain size less than 0.002 mm)

COLE = coefficient of linear extensibility

$C(\ell)$ = autocovariance function

d = deficit of water

DEPTH = effective depth of pavement

E_b = modulus of elasticity for base course

E_o = modulus of elasticity for asphalt concrete

E_s = modulus of elasticity for surface materials

E_p = potential evapo-transpiration

ESP = exchange sodium percentage

f = frequency

h_f = final value of suction

h_i = initial value of suction

HMAC = hot mix asphalt concrete

I = momentum of inertia for the equivalent configuration

Im = Thornthwaite moisture index

ℓ = lag of the variable x

L = length

n = parameter characterizing pavement roughness

N = number of samples in road profile

P(f) = power spectrum of the road profile

PI = plasticity index

RANGE = range of values of Thornthwaite moisture index for a 20 year period

S = surplus of water

SI = serviceability index

ΔSI = serviceability index reduction

TH = mean value of Thornthwaite moisture index for a 20 year period

TIME = time since construction or last rehabilitation

V_i = initial volume

ΔV = volume change

x = distance along the road

y(x) = a function which describes the road profile elevation

γ_h = suction compression index

APPENDIX III

DEFINITION OF SOME PEDOLOGIC TERMS

APPENDIX III - DEFINITION OF SOME PEDOLOGIC TERMS

The Soil Conservation Service has defined a system* to group soils into classes based on observable and measurable properties. In this system, 6 levels are considered in the nomenclature order, suborder, great group, subgroup, family, and series. Orders reflect in a general way geographic distribution of soils similar in degree and kind of horizon development. Suborders group soils with uniform effects of the soil forming factors. The great groups are defined basically on the presence or absence of diagnostic horizons and the arrangement of these horizons. The next level of classification, subgroup, is reflected in the nomenclature modifying the names of the great groups by one or more adjectives. Soils similar in texture below the surface layer and similar in clay mineralogy, temperature, and other properties are grouped in the same family. Finally, soils essentially uniform in kind, thickness, and sequence of horizons and very similar physically, chemically, and minerlogically are called a soil series.

In Table 7, "Soil Type", it is shown that the soils in the 23 roadway sections that are the subject of this study belong to the Alfisol and Vertisol orders. Furthermore, the Alfisols are classified into the Vertic Ochraqualfs, Vertic Paleudalfs, Aquic Paleustalfs, and Udertic Paleustalfs subgroups, while the Vertisols are classified in to the Idic Chromusters,

---

* "Soil Taxonomy. A Basic System of Soil Classification for Making and Interpreting Soil Surveys," Soil Conservation Service, U.S. Department of Agriculture, Agriculture Handbook No. 436, Washington, D.C., December 1975.

Udorthentic Chromusters, and Udic Pellusters subgroups. Following, a brief description of these orders and subgroups is presented.

ALFISOLS: soils mainly light colored in the A horizon with B horizons more clayey and higher in bases than the A horizon. They are moderately leached in the upper horizons but commonly become more basic with depth. The A horizons are thin and loamy over very clayey slowly permeable B horizons. The water is held at <15-bars during at least 3 months each year.

Vertic Ochraqualfs

Cracks at some period in most years that are 1 cm or more wide at a depth of 50 cm and at least 30 cm long in some part and that expent upward to the surface or to the base of an Ap or an albic horizon.

Vertic Paleudalfs

Clayey argillic horizon that contains expanding clays; deep wide cracks at some time in most years, but at other times these soils may be quite wet. They formed mostly in materials that are rich in montmorillonite.

Aquic Paleustalfs

Freely drained soils that have a thin or loamy epidedon. They have an argillic horizon; they do not have deep wide cracks in most years and do not have a high COLE. They have, within 75 cm of the surface mottles that have chroma of 2 or less, and the mottled horizon is saturated

Udic Pellusters

Soils gray to black in the surface 12 inches. They are nearly level except for their gilgai micro-relief. Their cracks are open from 90 to 150 days in most years or the mean annual soil temperature is lower than 15° C, or both.

APPENDIX IV

FREQUENCY DOMAIN PLOTS

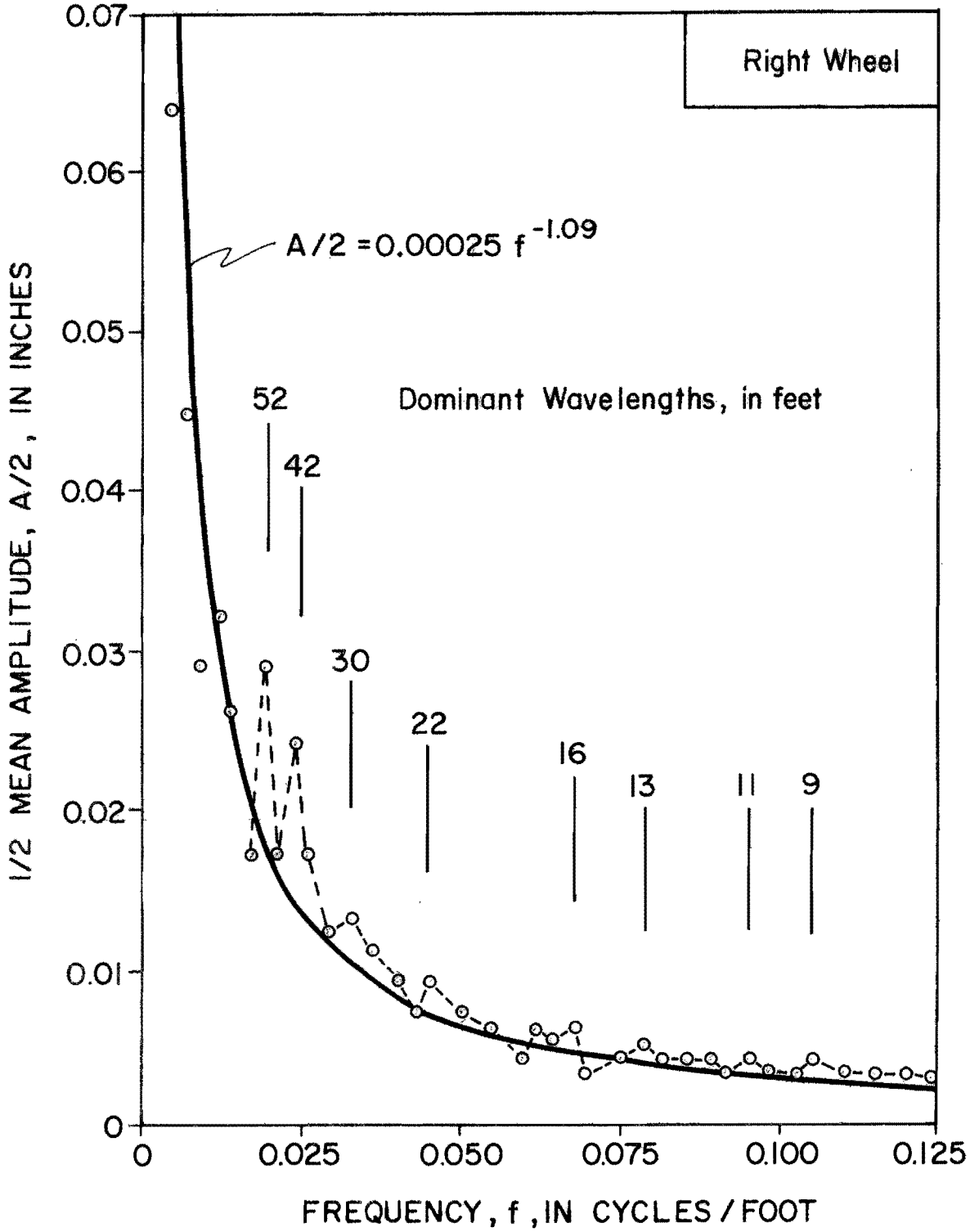

FIGURE IV-1. Frequency Domain Plot
(Huntsville 1)

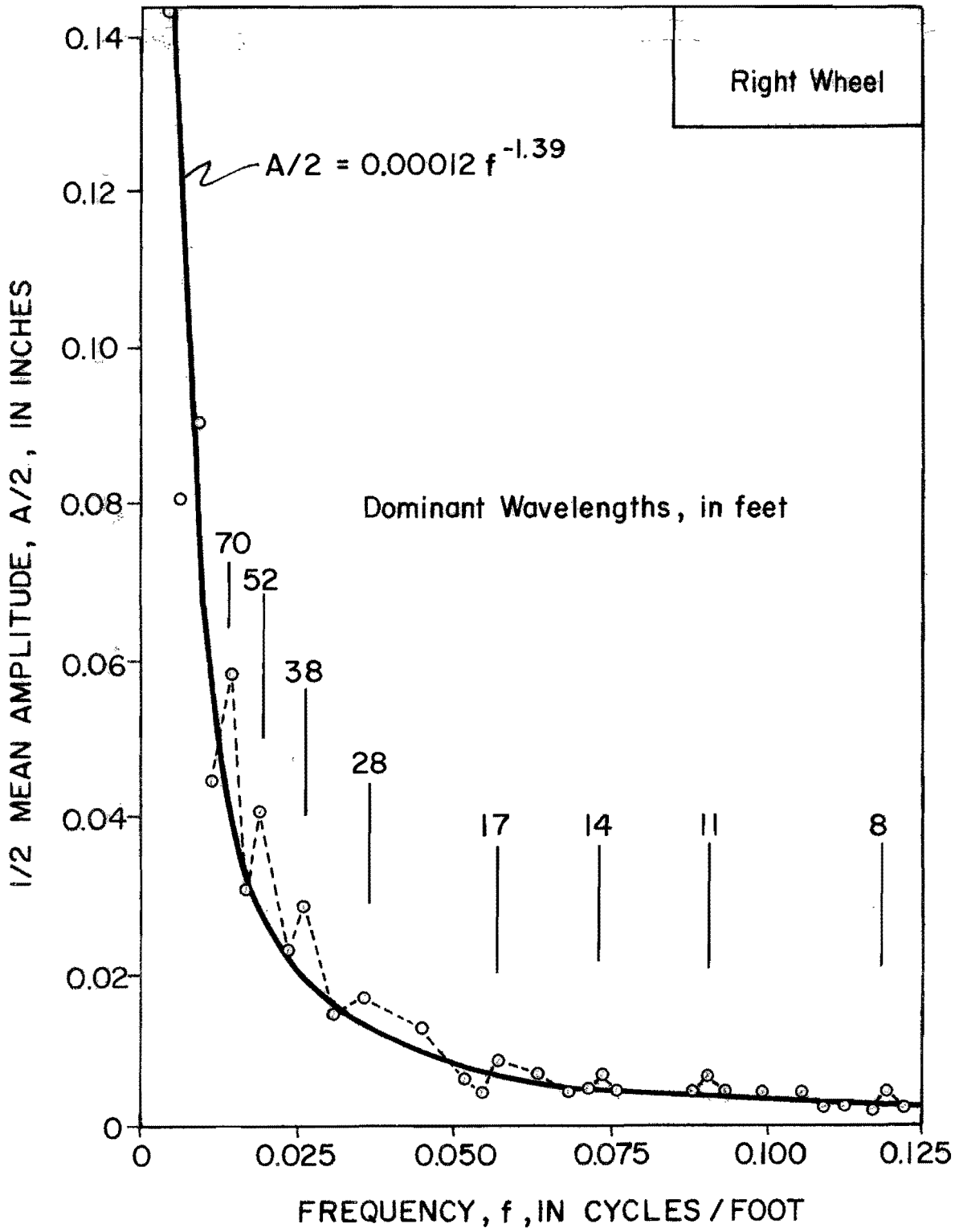

FIGURE IV-2. Frequency Domain Plot
(Huntsville 2)

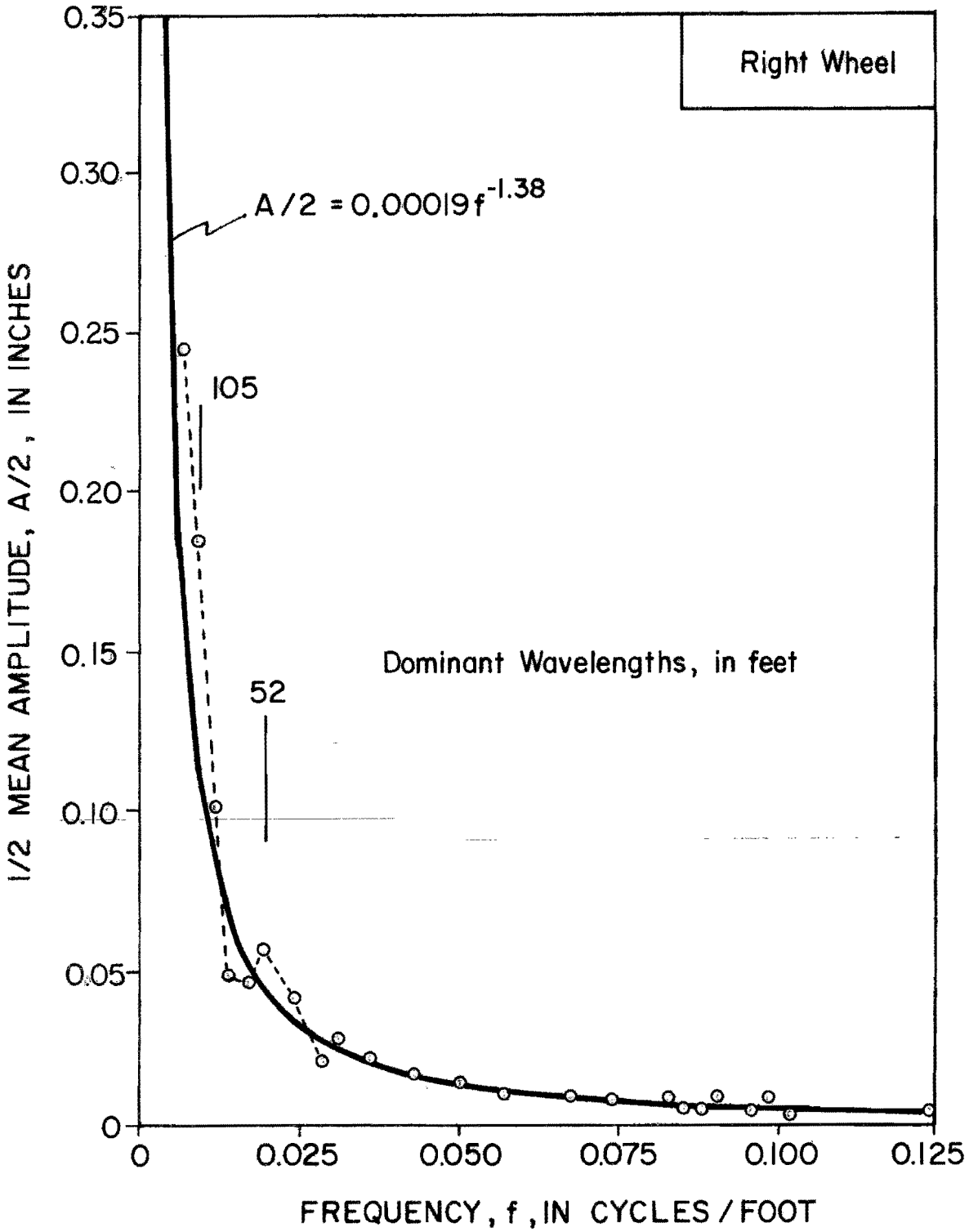

FIGURE IV-3. Frequency Domain Plot
(Ben Arnold 1)

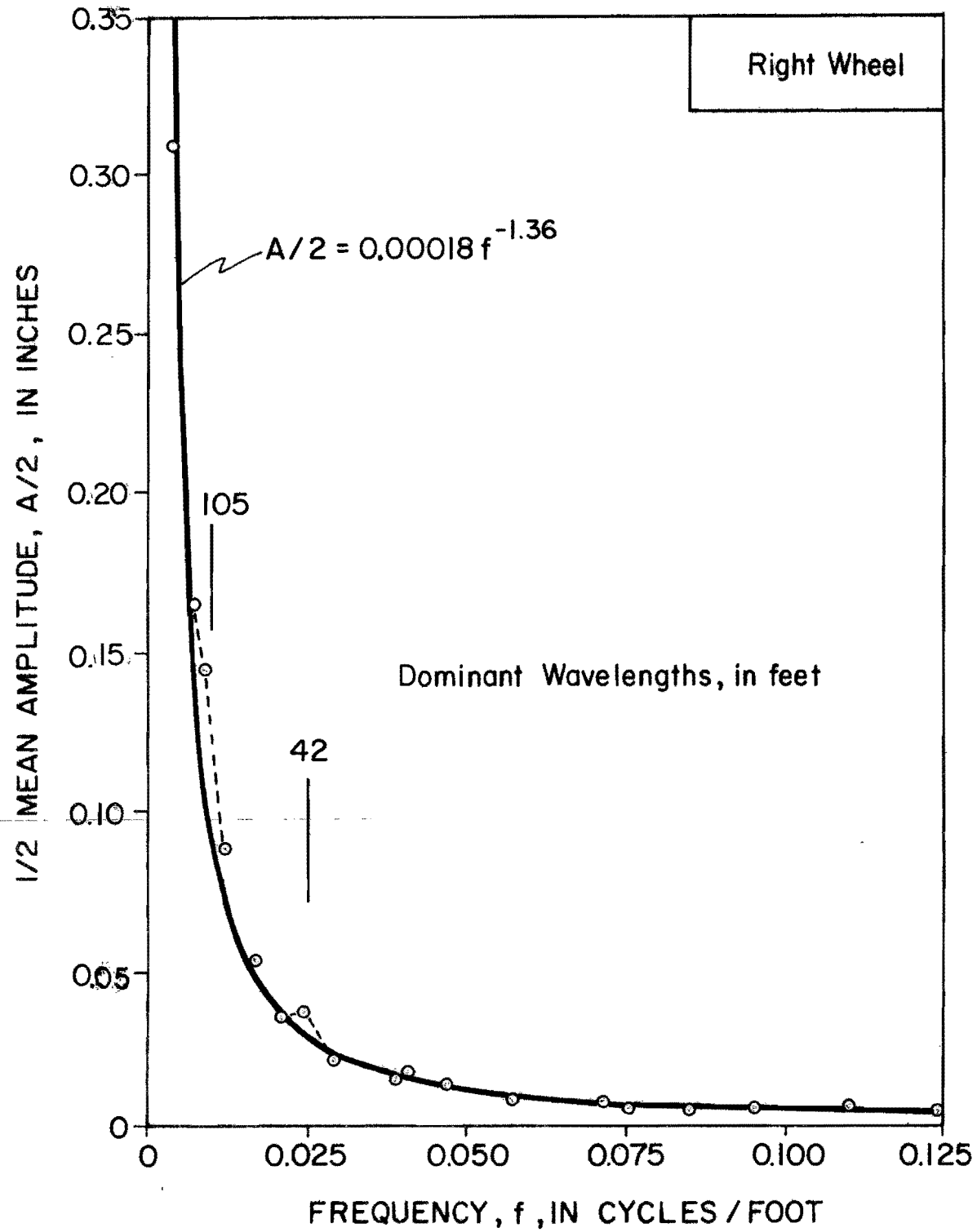

FIGURE IV-4. Frequency Domain Plot
(Ben Arnold 2)

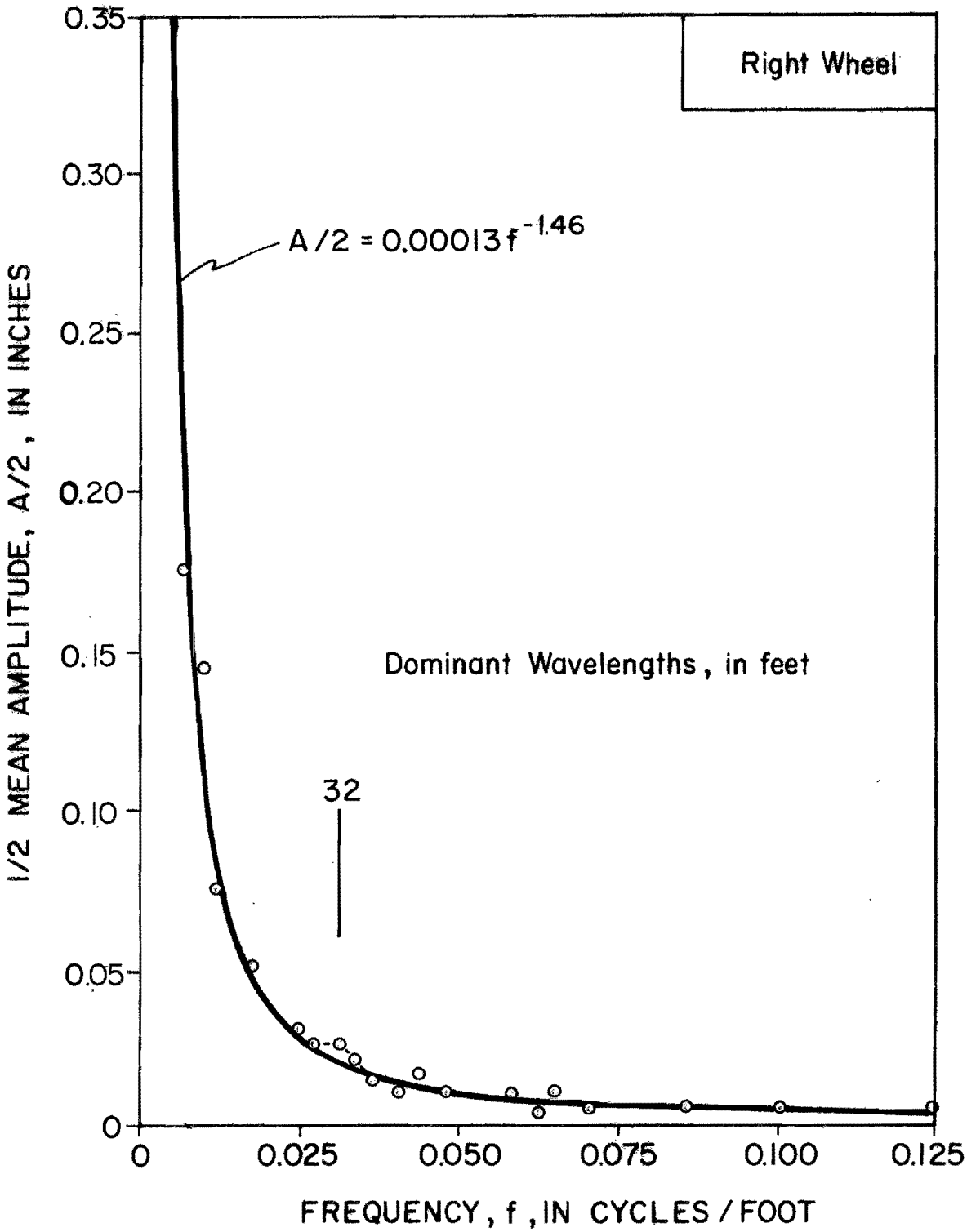

FIGURE IV-5. Frequency Domain Plot
(Ben Arnold 3)

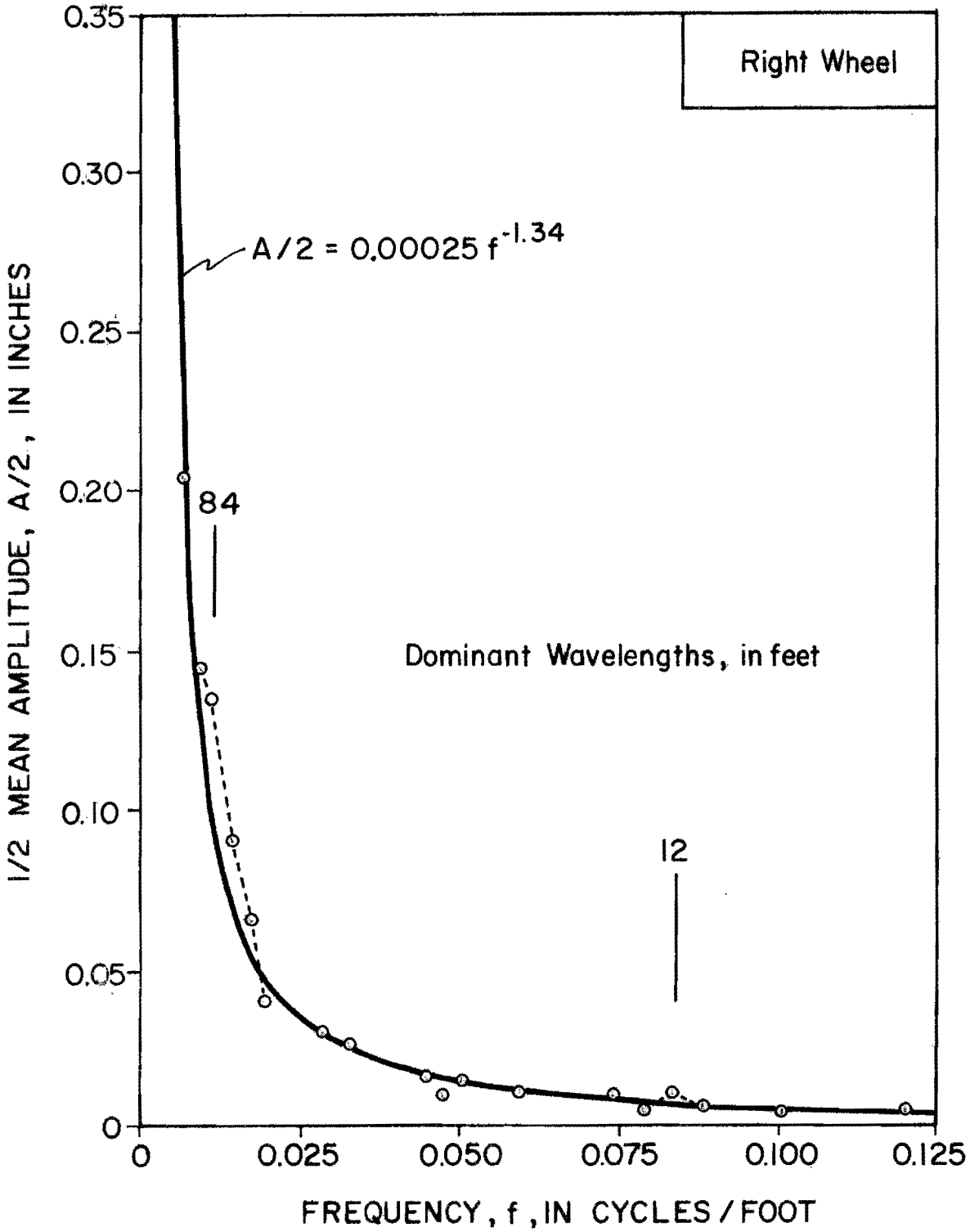

FIGURE IV-6. Frequency Domain Plot
(Buckholts 1)

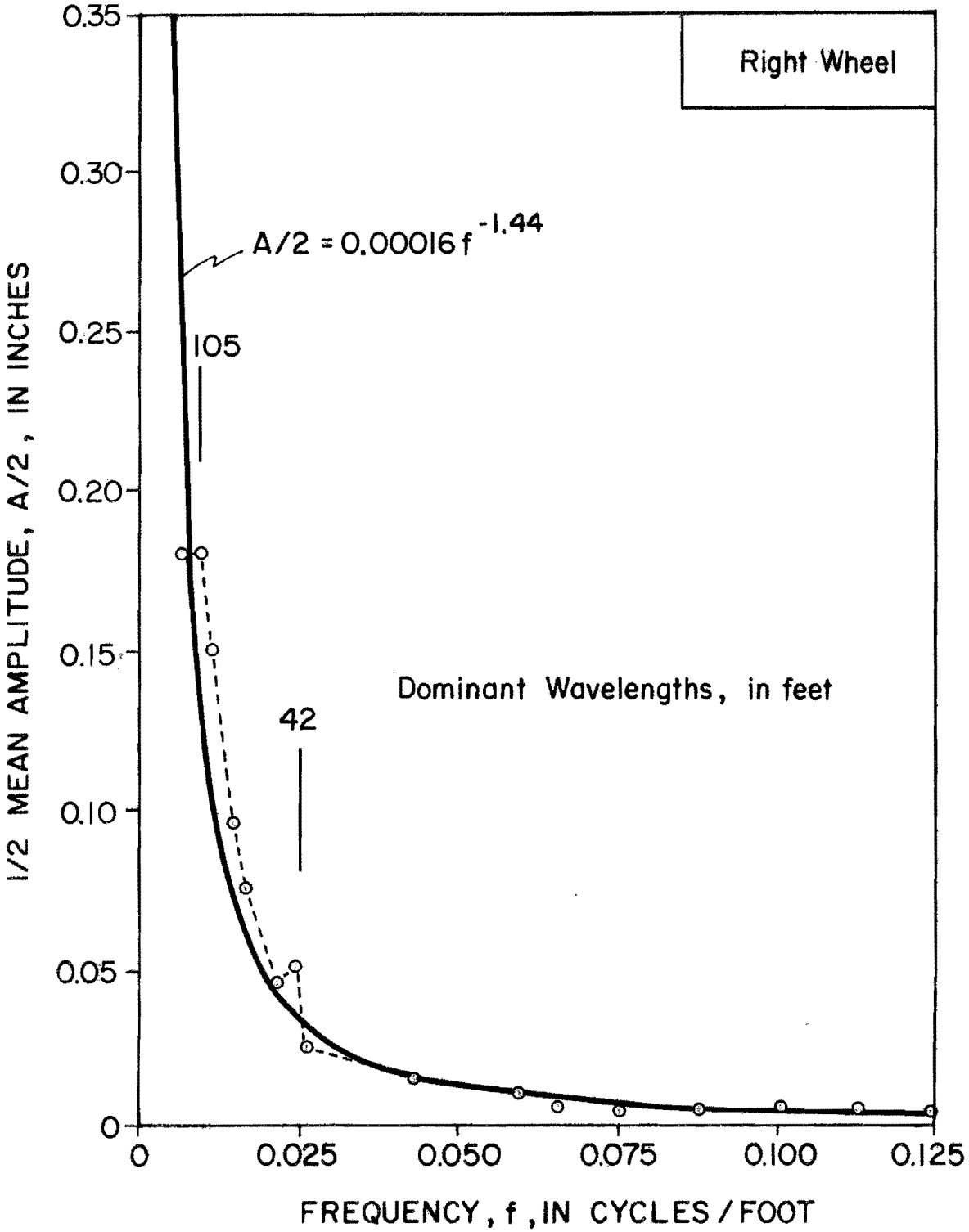

FIGURE IV-7. Frequency Domain Plot
(Buckholts 2)

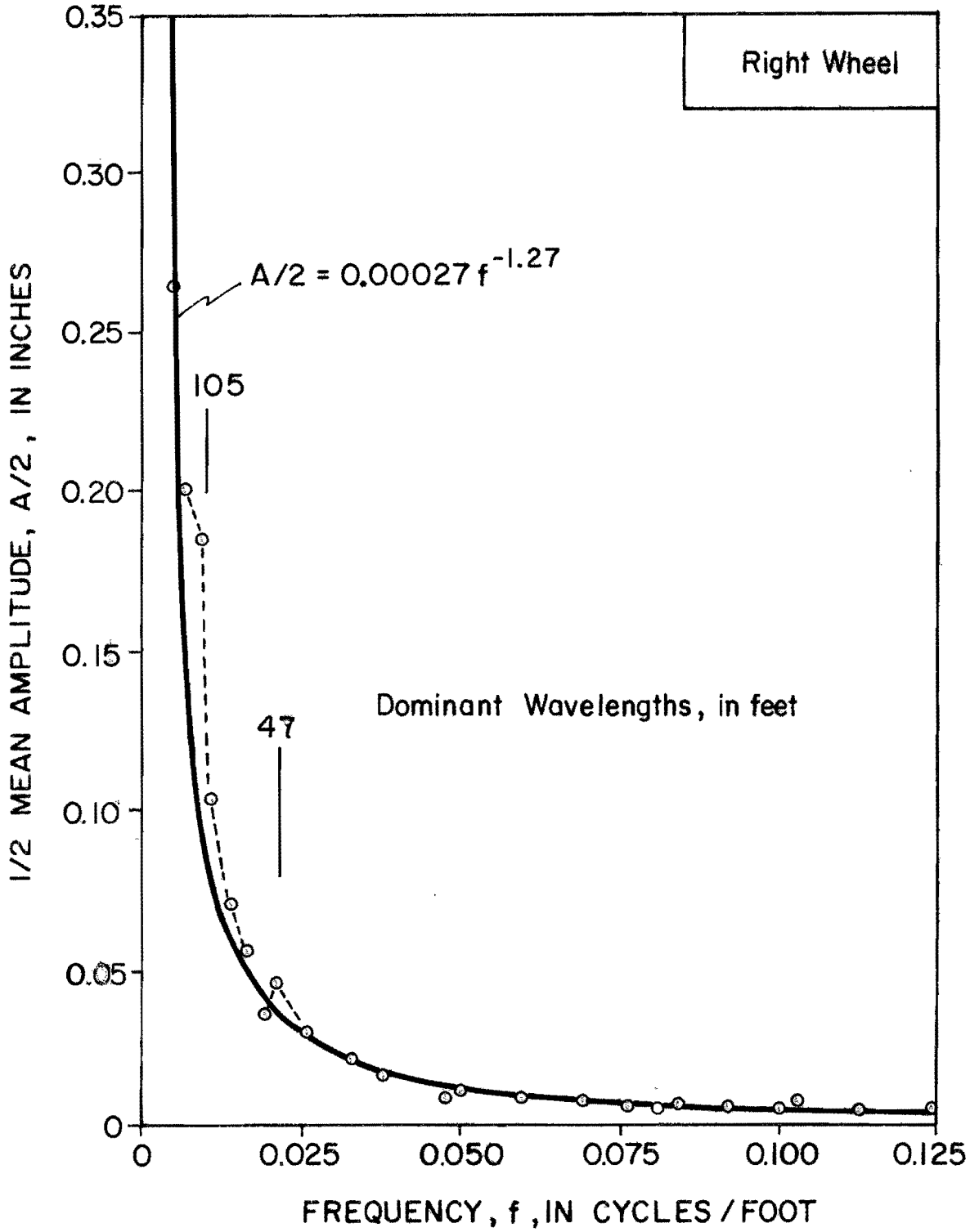

FIGURE IV-8. Frequency Domain Plot
(Fairfield 1)

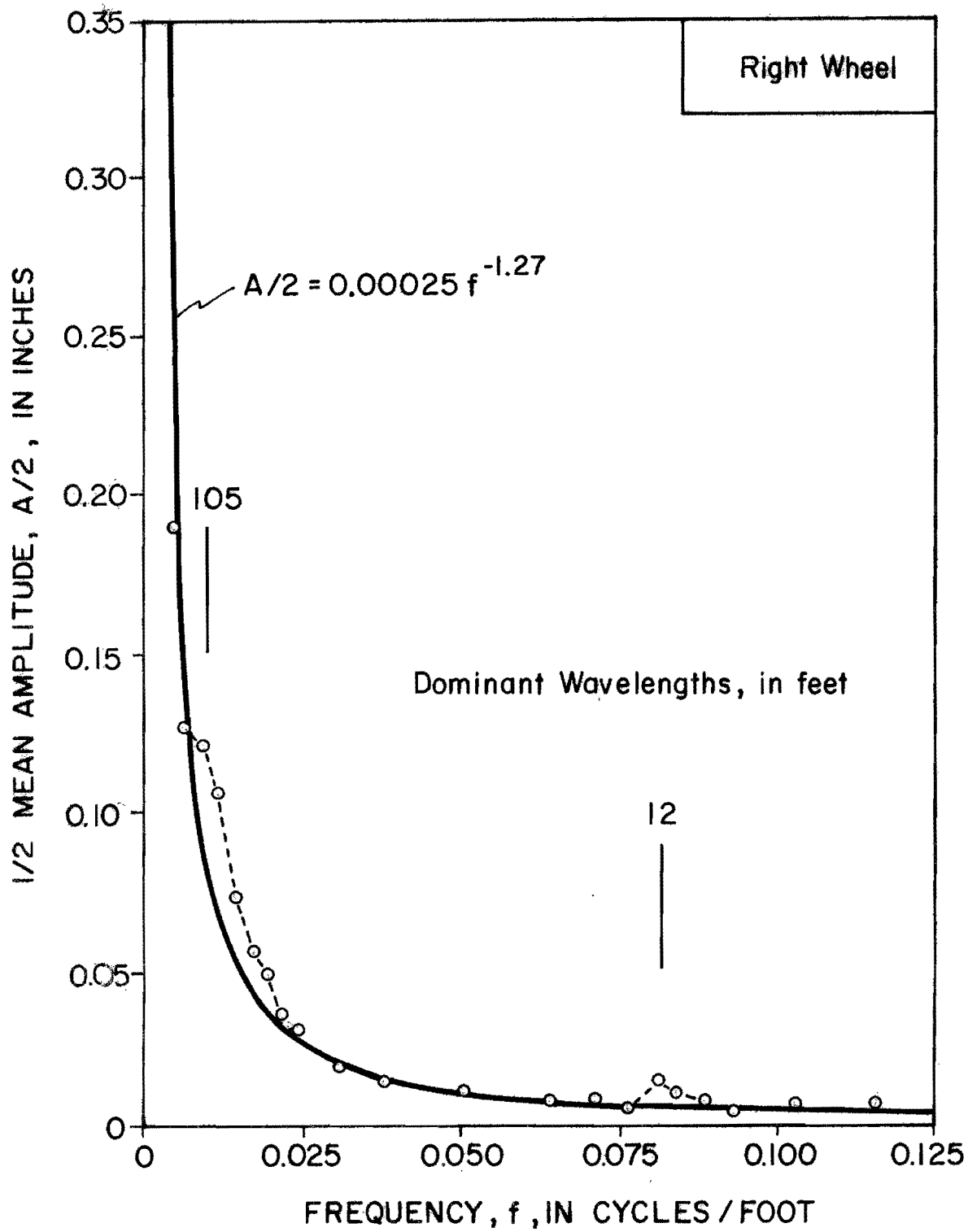

FIGURE IV-9. Frequency Domain Plot
(Fairfield 2)

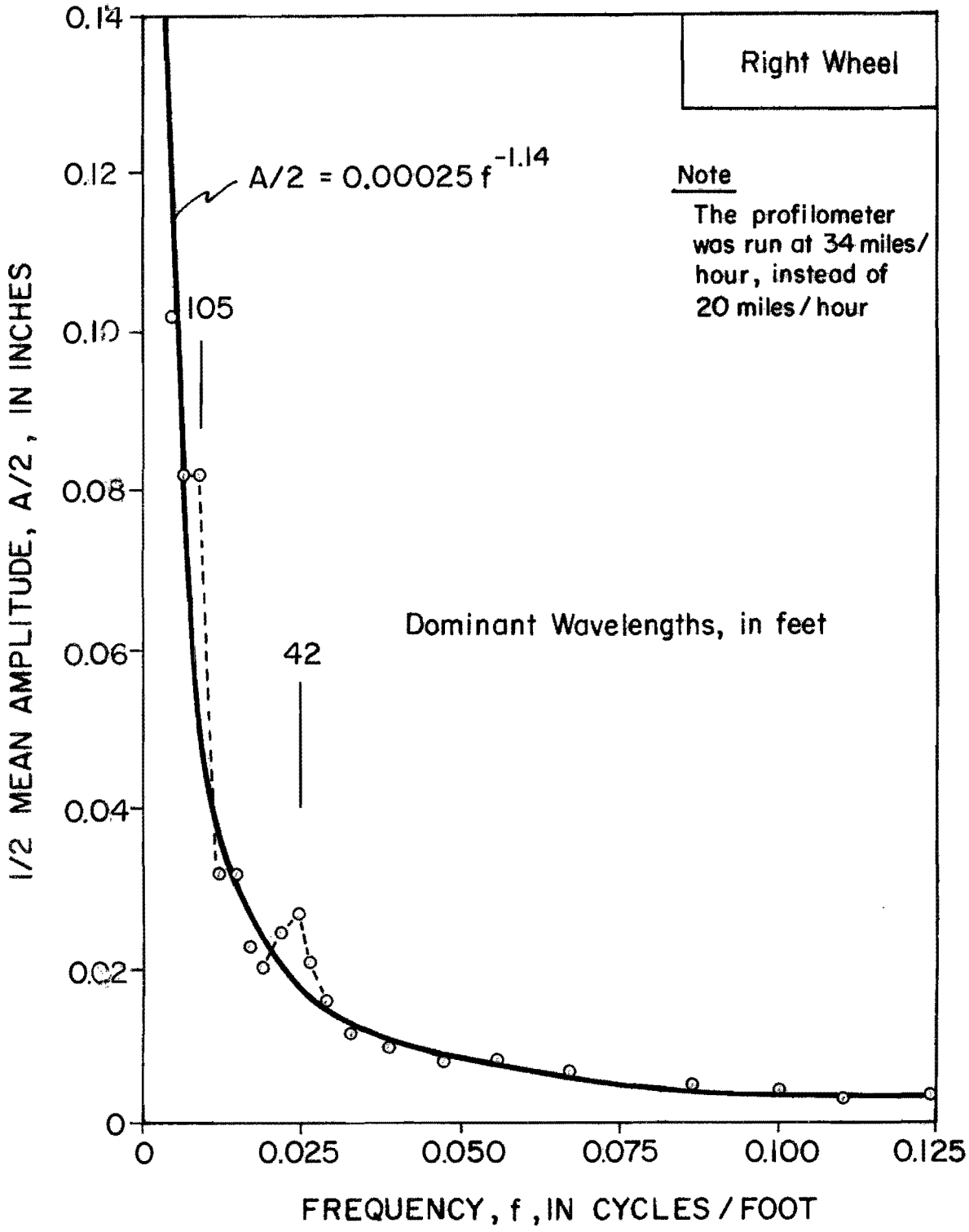

FIGURE IV-10. Frequency Domain Plot
(Smithville 1A)

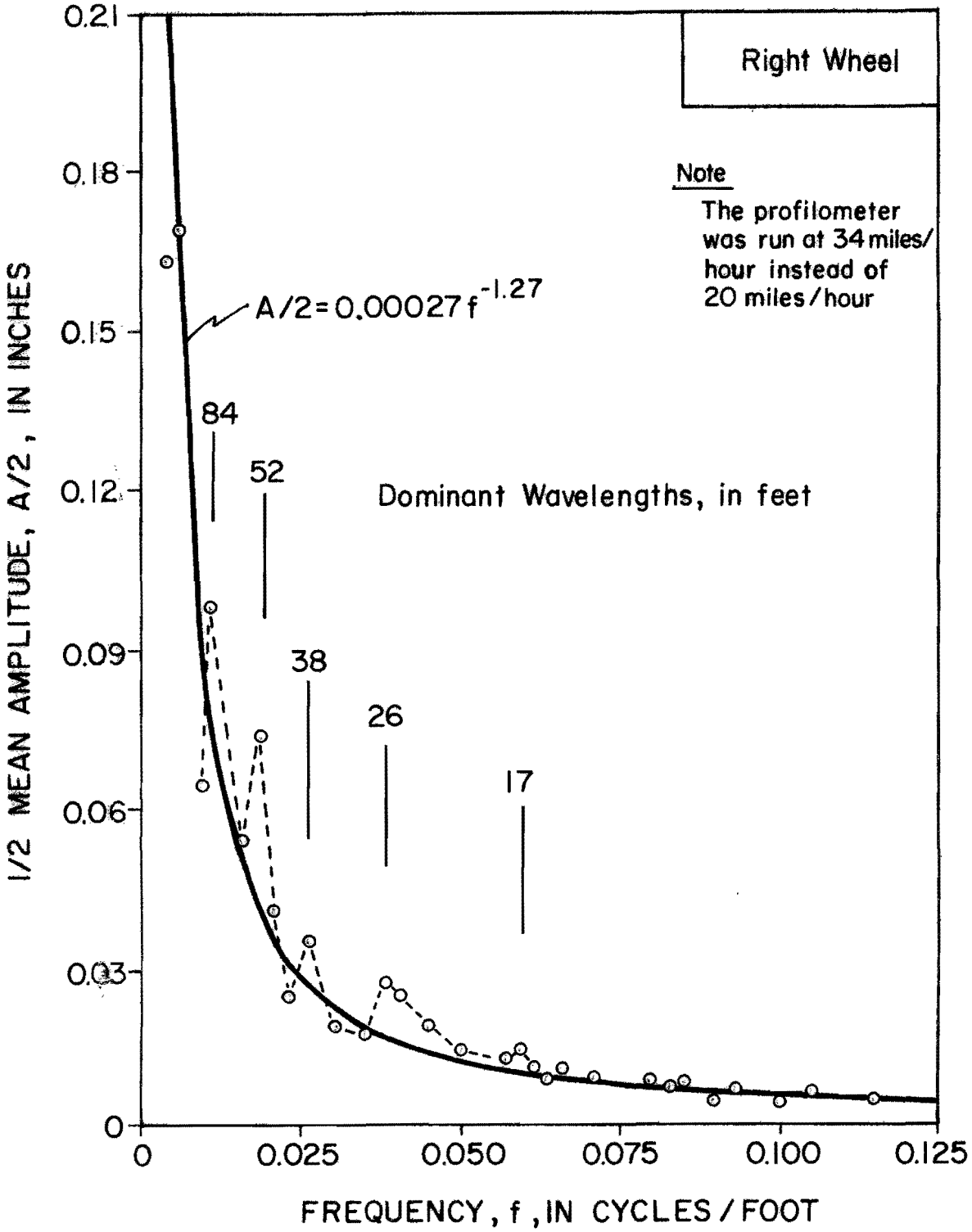

FIGURE IV-11. Frequency Domain Plot (Smithville 1B)

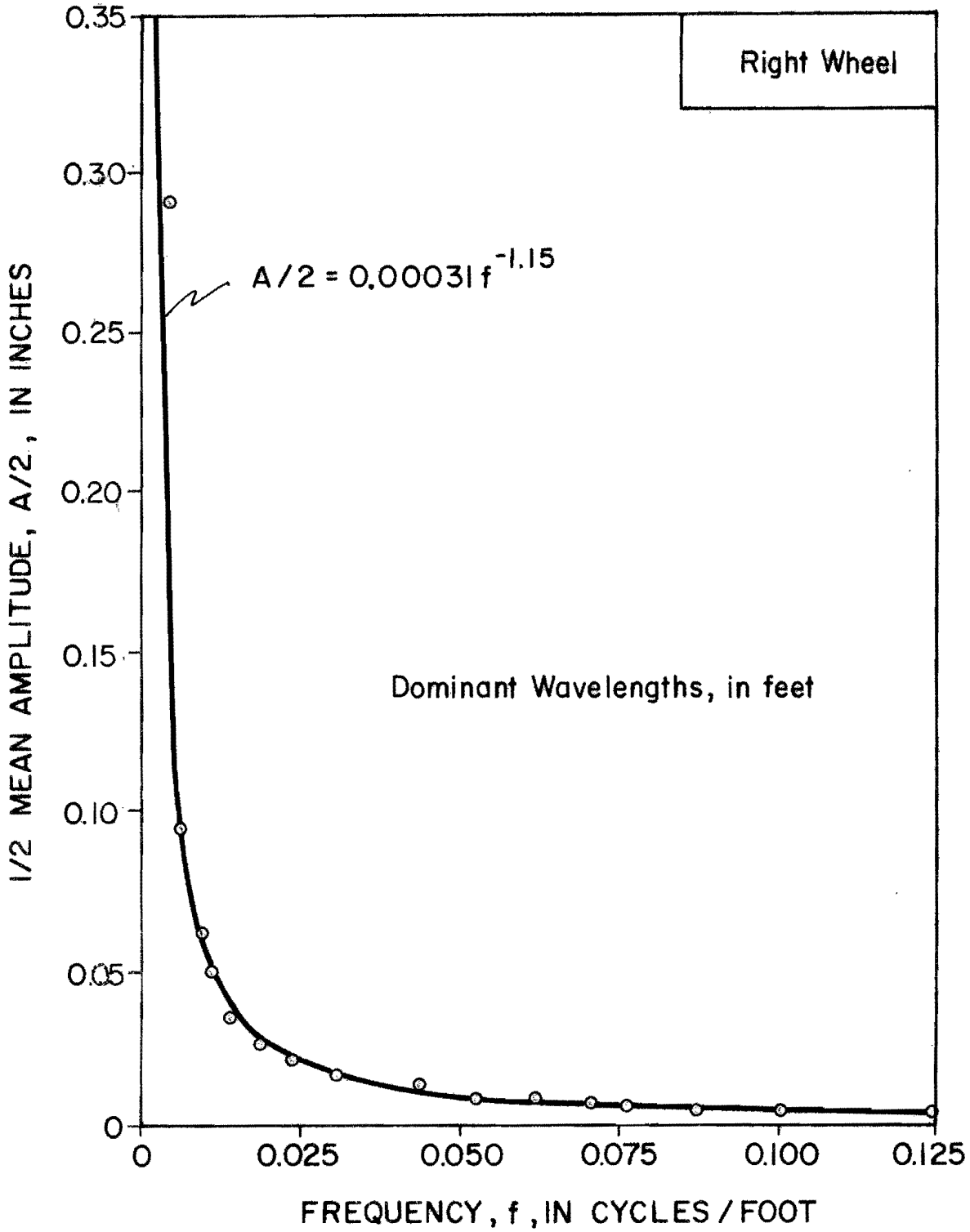

FIGURE IV-12. Frequency Domain Plot
(Snook 1)

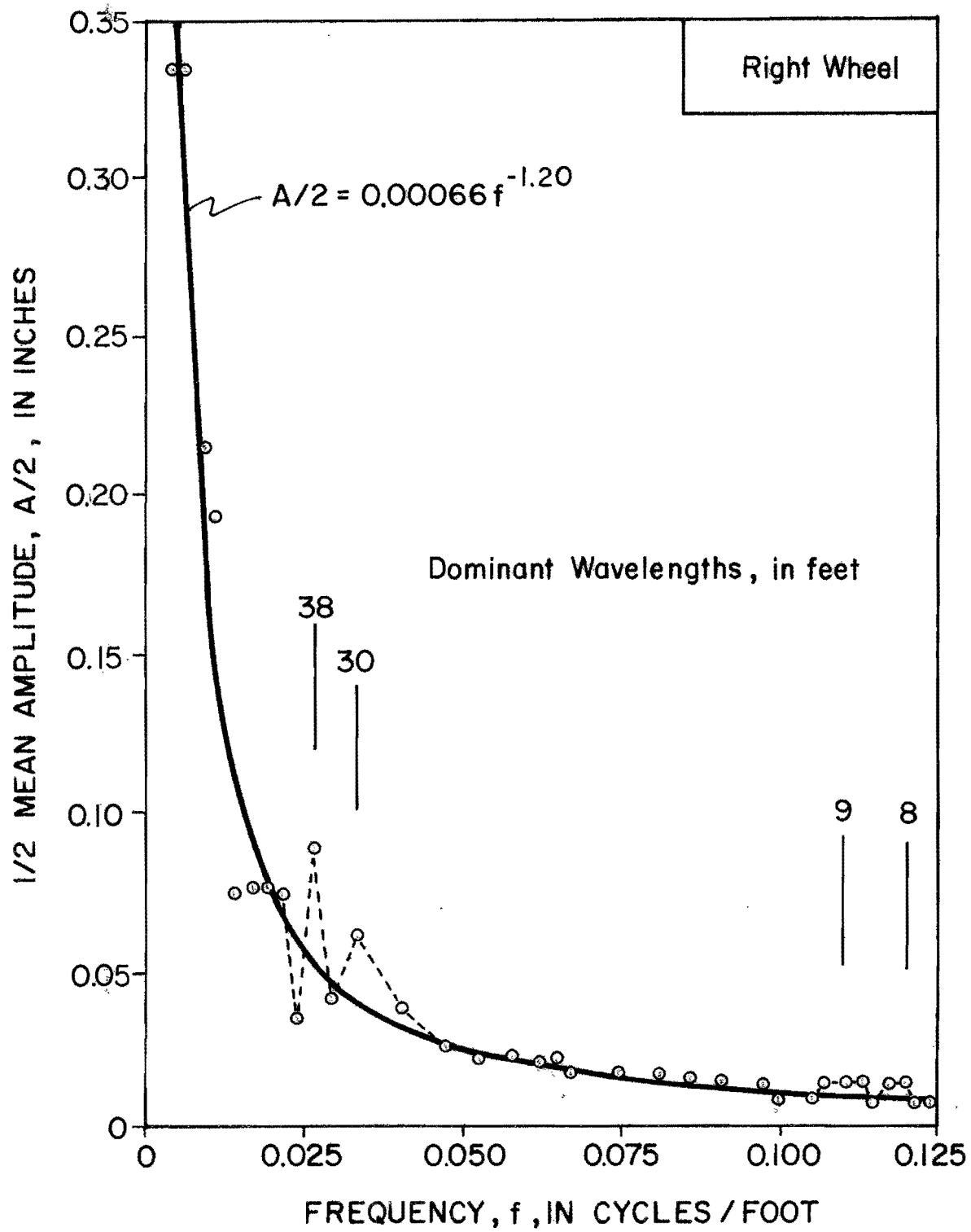

FIGURE IV-13. Frequency Domain Plot (OSR 1)

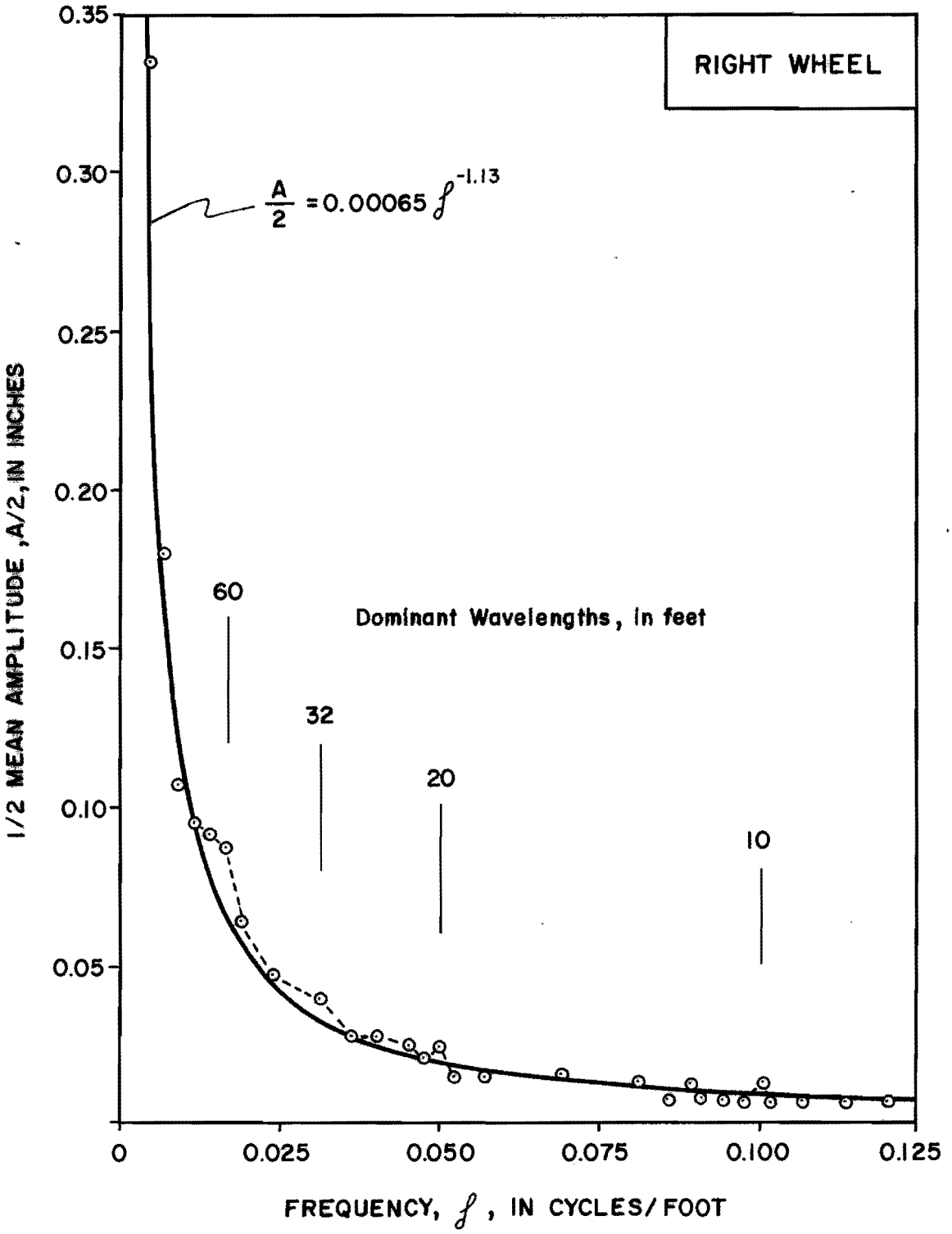

Figure IV-14. Frequency Domain Plot (OSR 2)

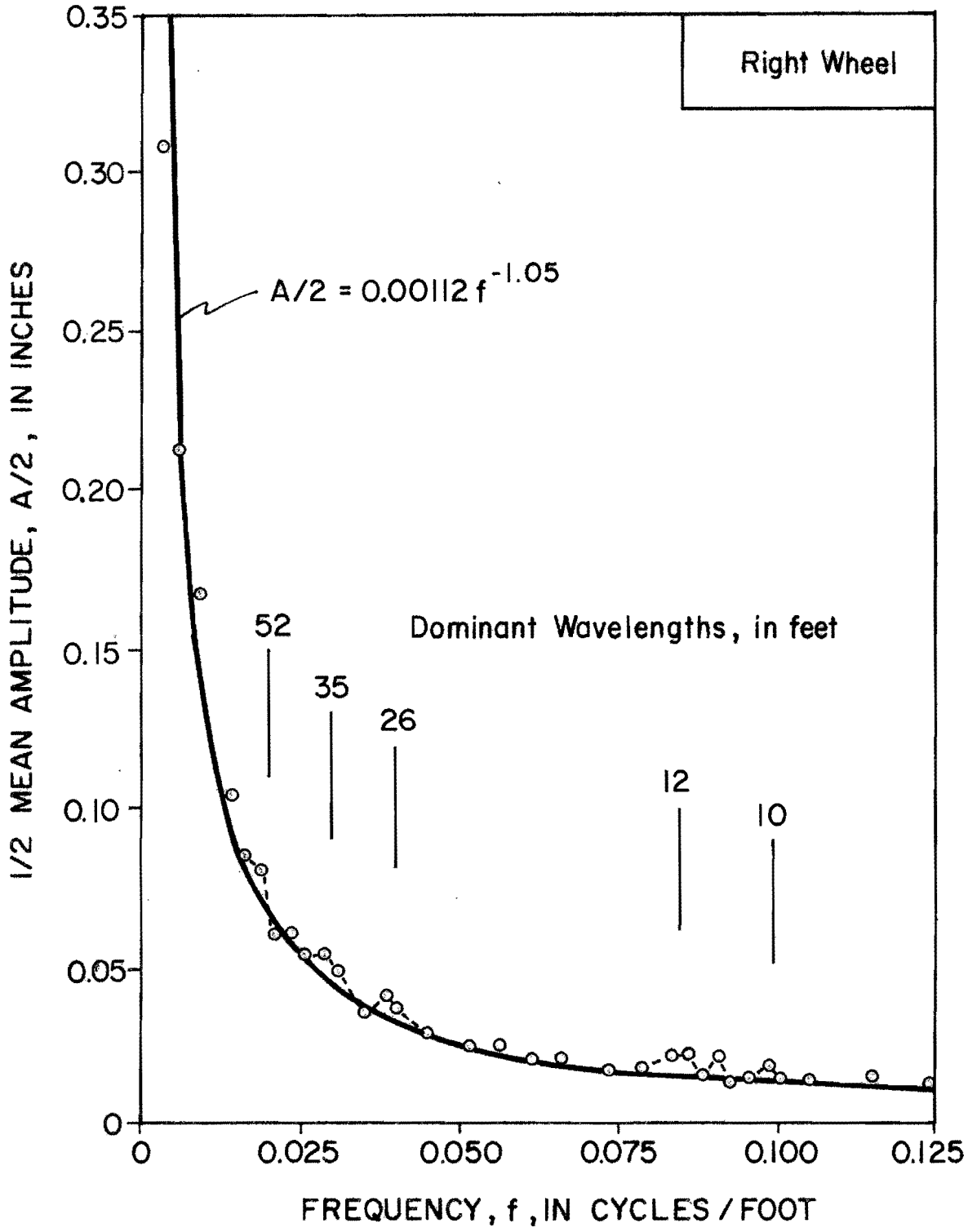

FIGURE IV-15. Frequency Domain Plot (OSR 3)

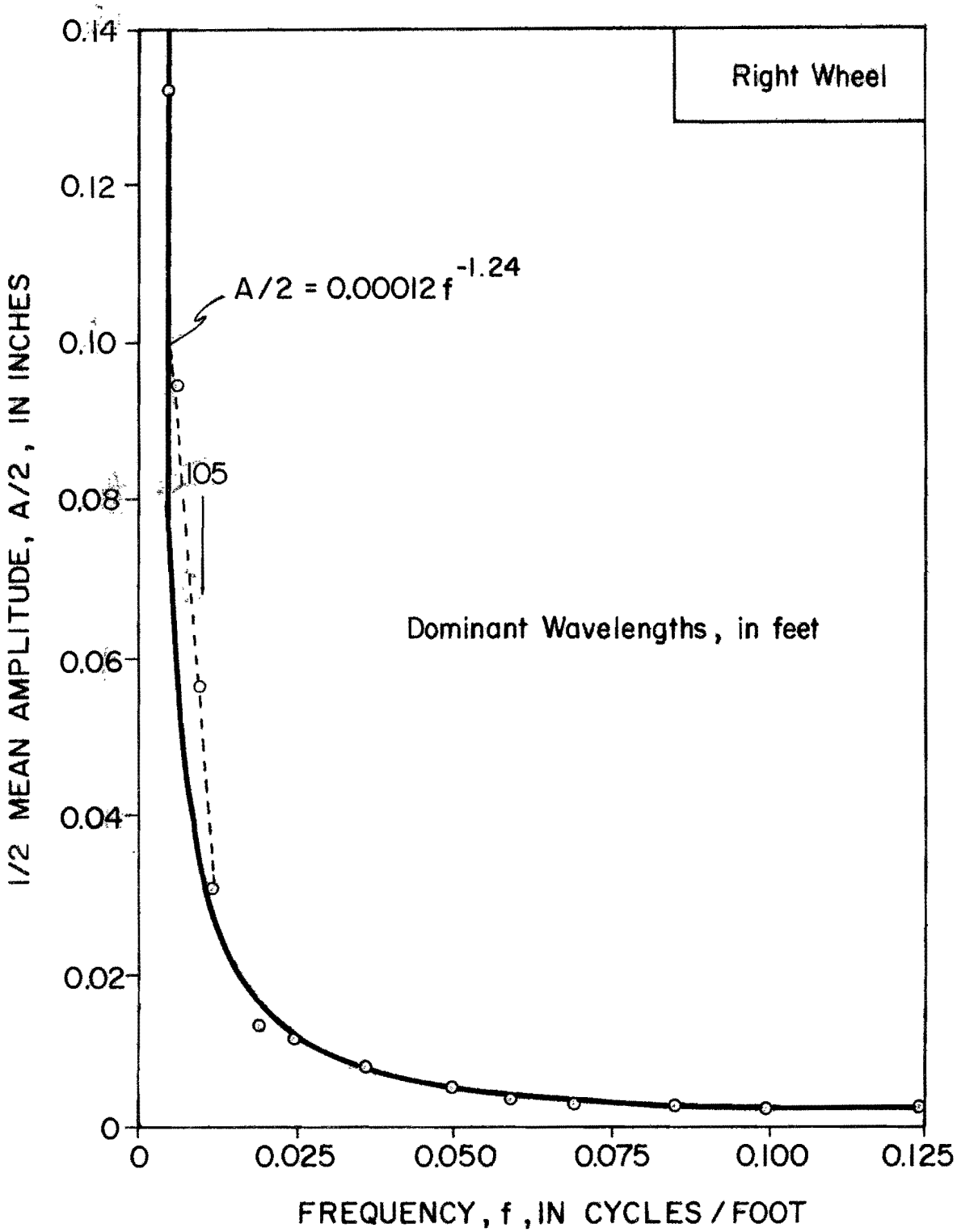

FIGURE IV-16. Frequency Domain Plot
(Thrall 1)

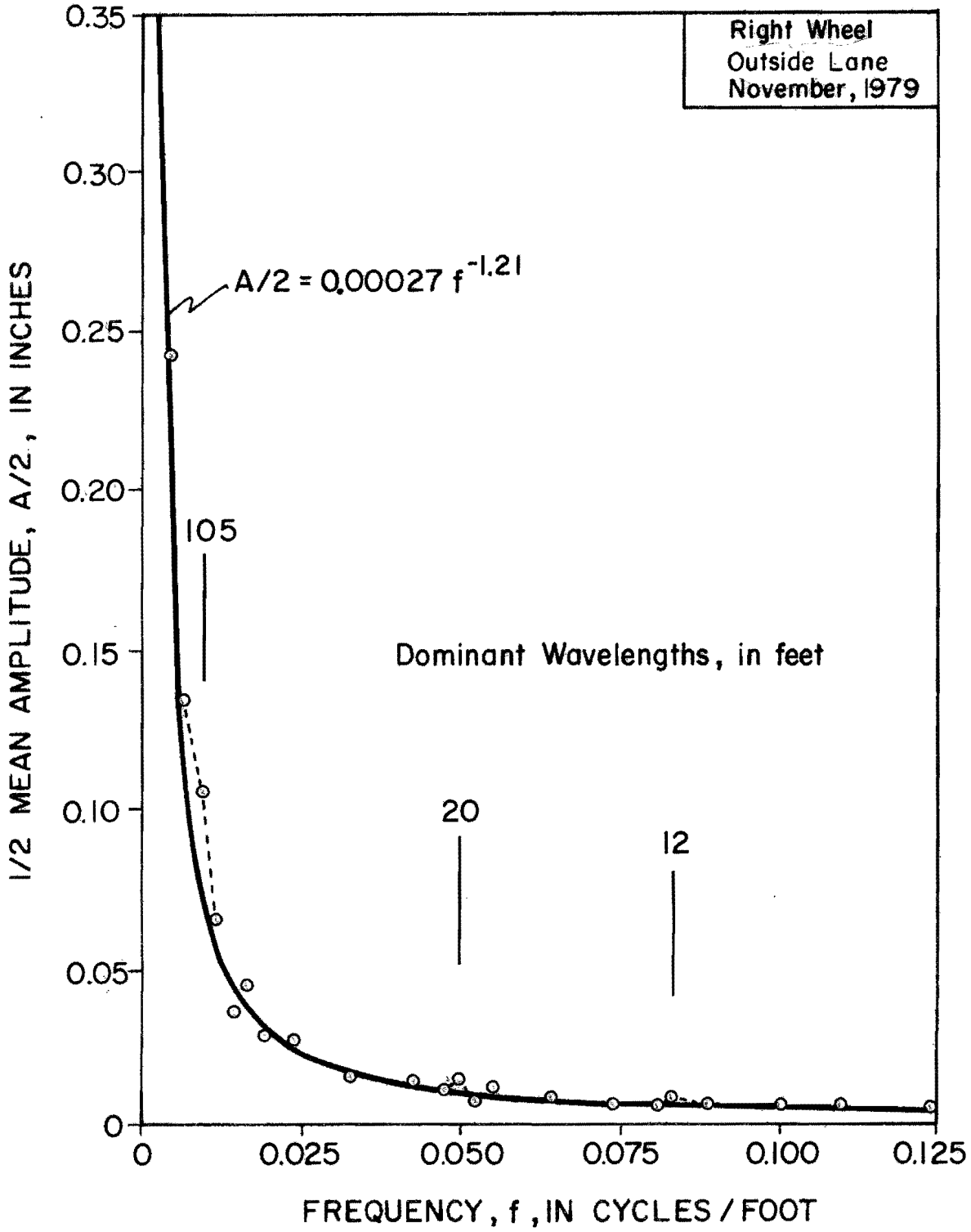

FIGURE IV-17. Frequency Domain Plot
(San Antonio 410-1)

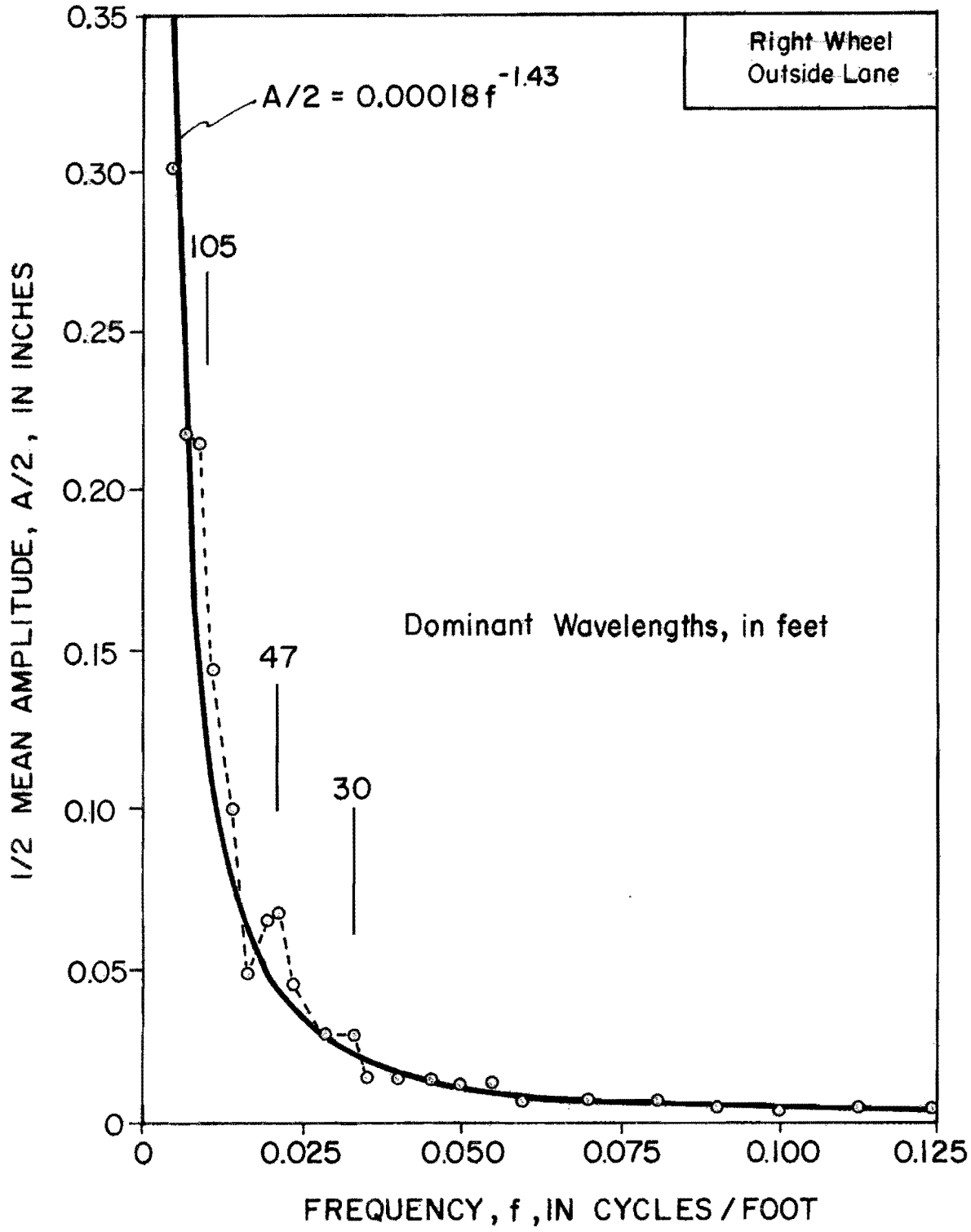

FIGURE IV-18. Frequency Domain Plot
(San Antonio 37)

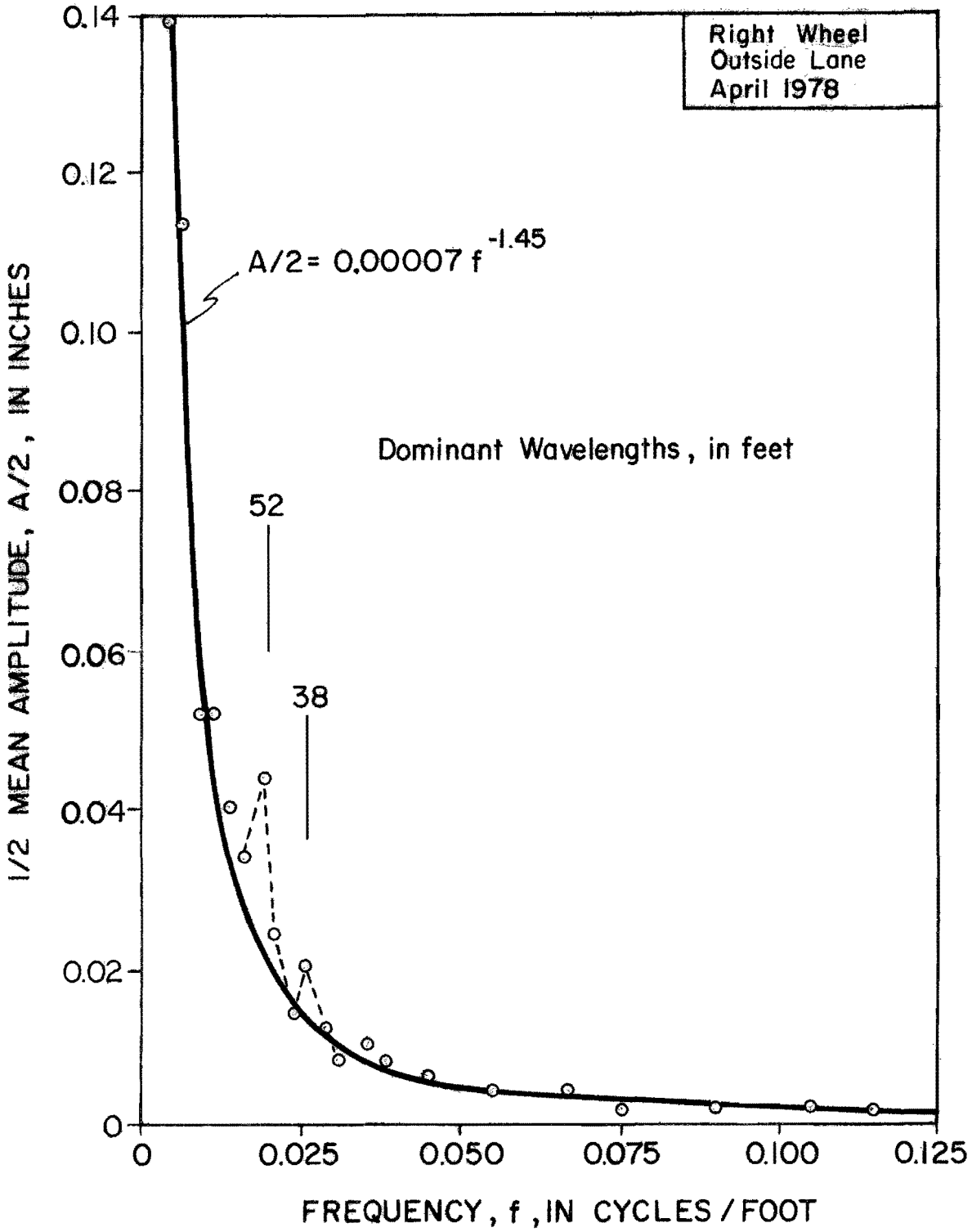

FIGURE IV-19. Frequency Domain Plot
(San Antonio 90-5)

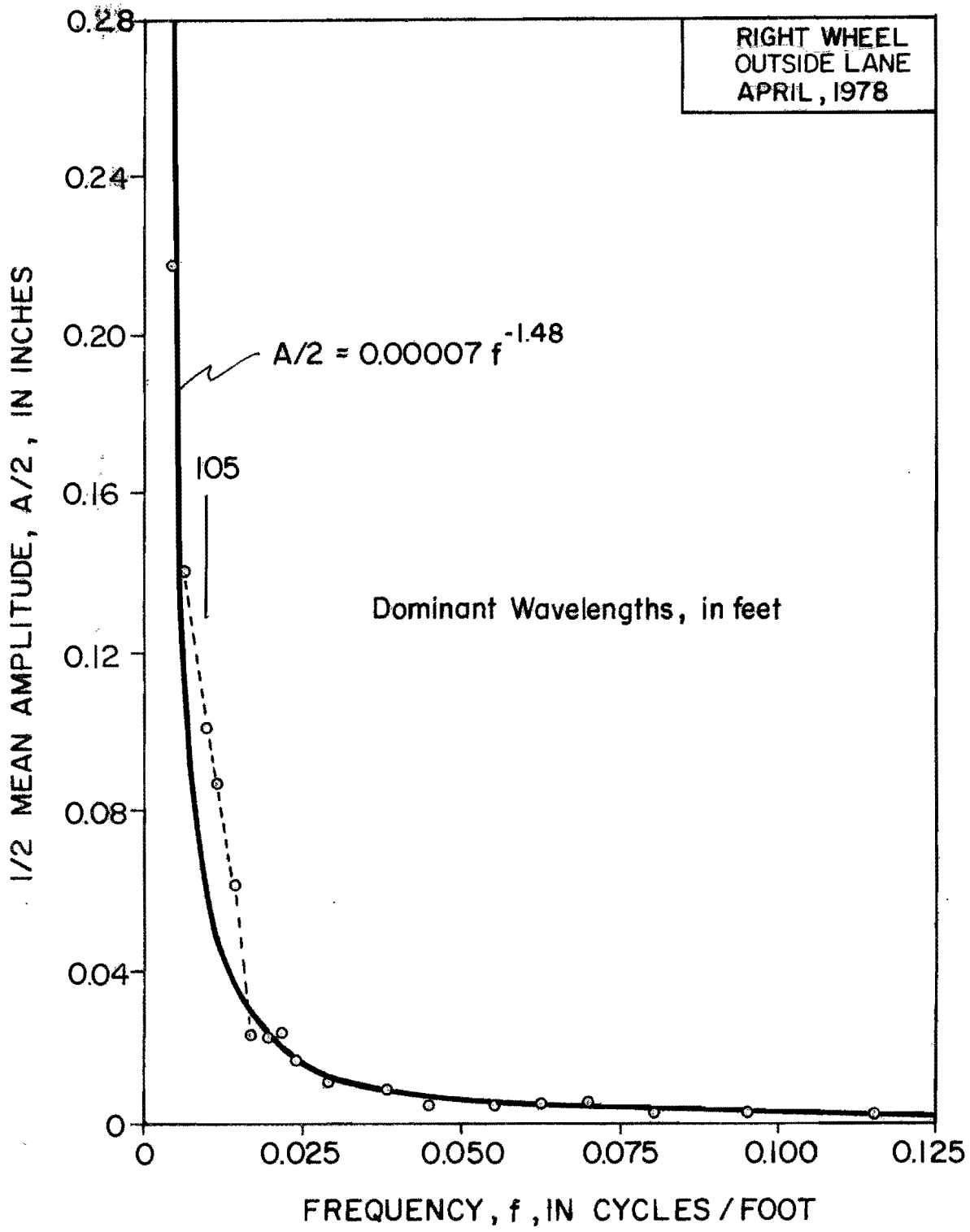

FIGURE IV-20. Frequency Domain Plot
(San Antonio 90-3 West)

APPENDIX V

PROBABILITY DENSITY FUNCTIONS OF WAVELENGTH

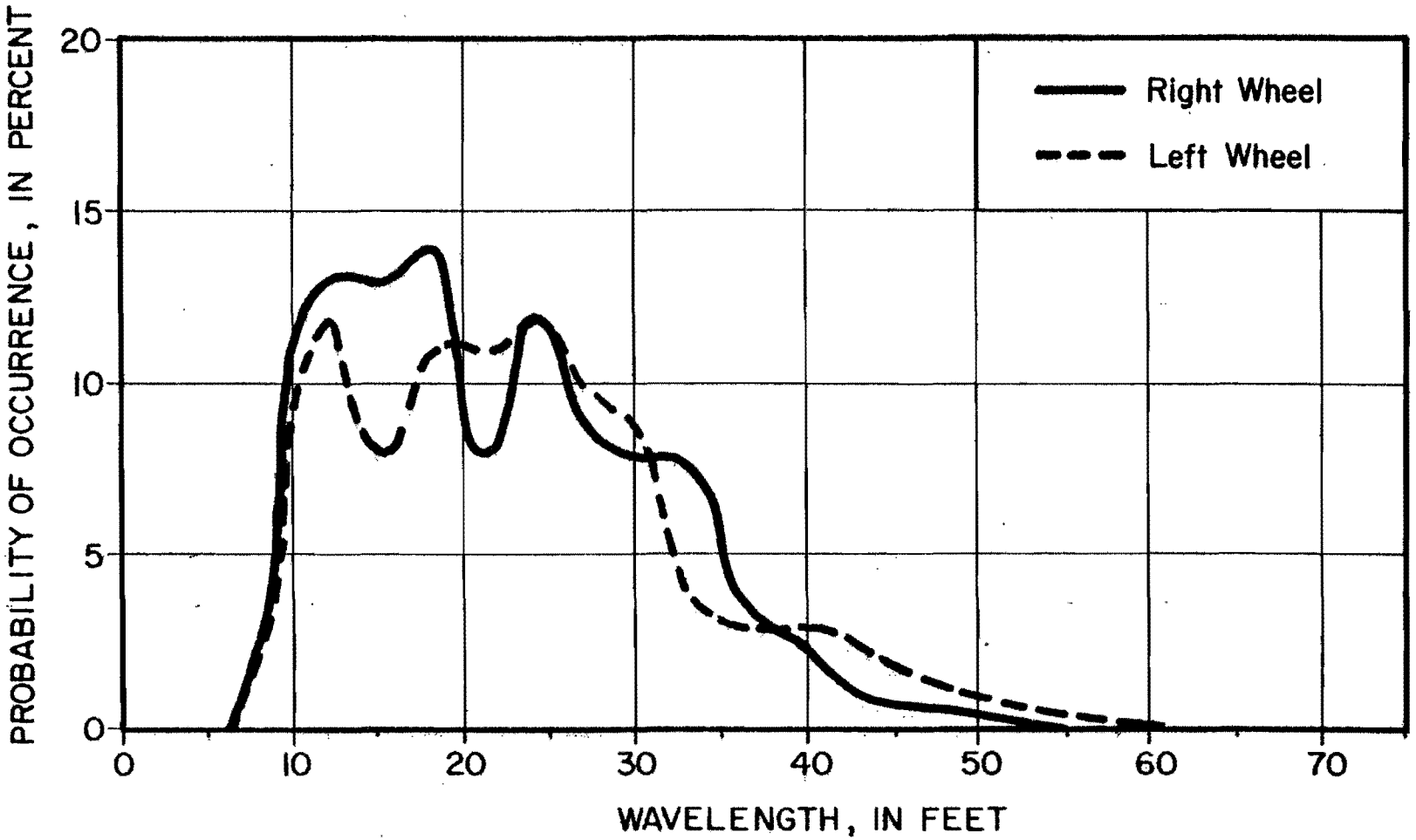

FIGURE V-1. Probability Density Function of Wavelength (Huntsville 1)

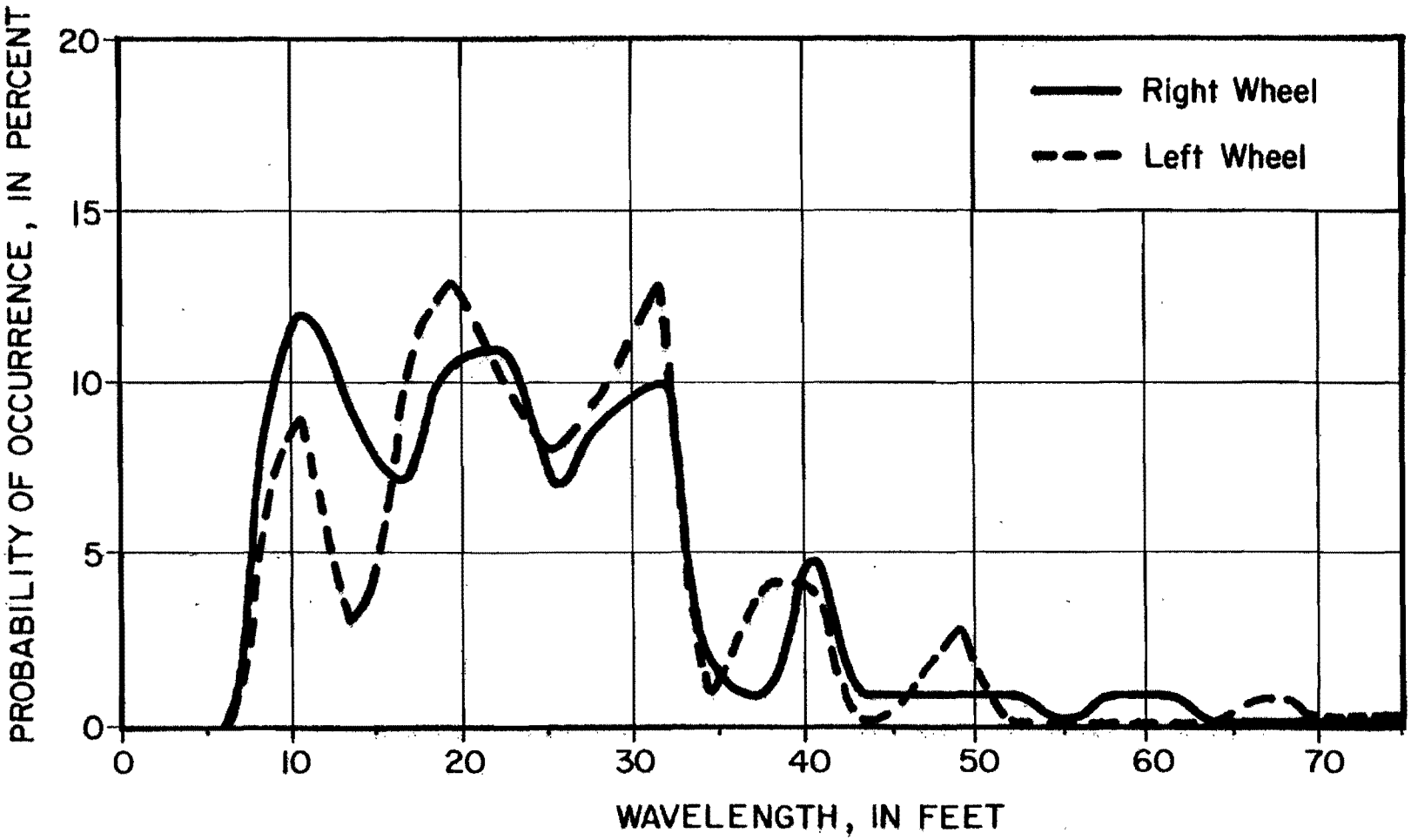

FIGURE V-2. Probability Density Function of Wavelength (Huntsville 2)

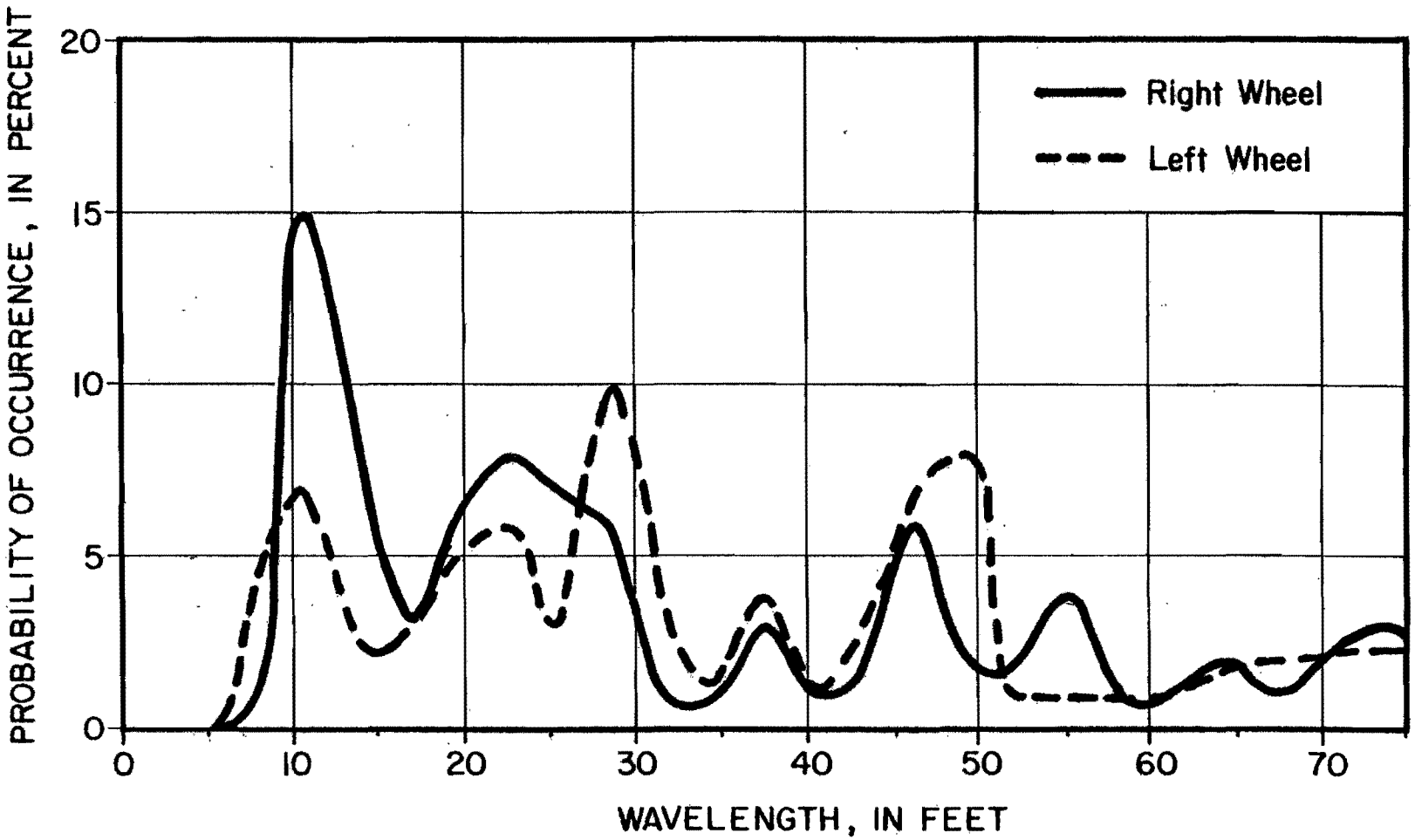

FIGURE V-3. Probability Density Function of Wavelength
(Ben Arnold 1)

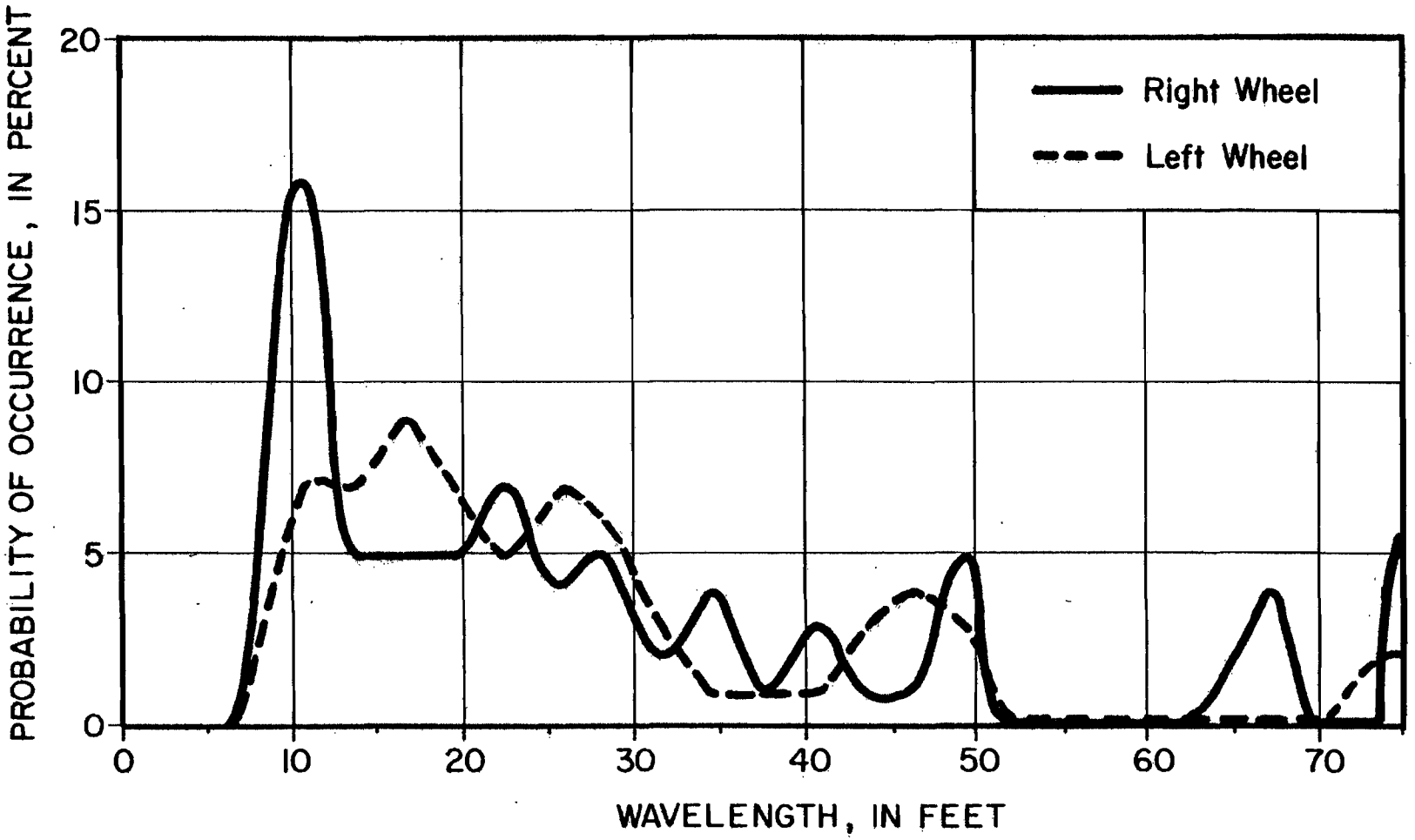

FIGURE V-4. Probability Density Function of Wavelength
(Ben Arnold 2)

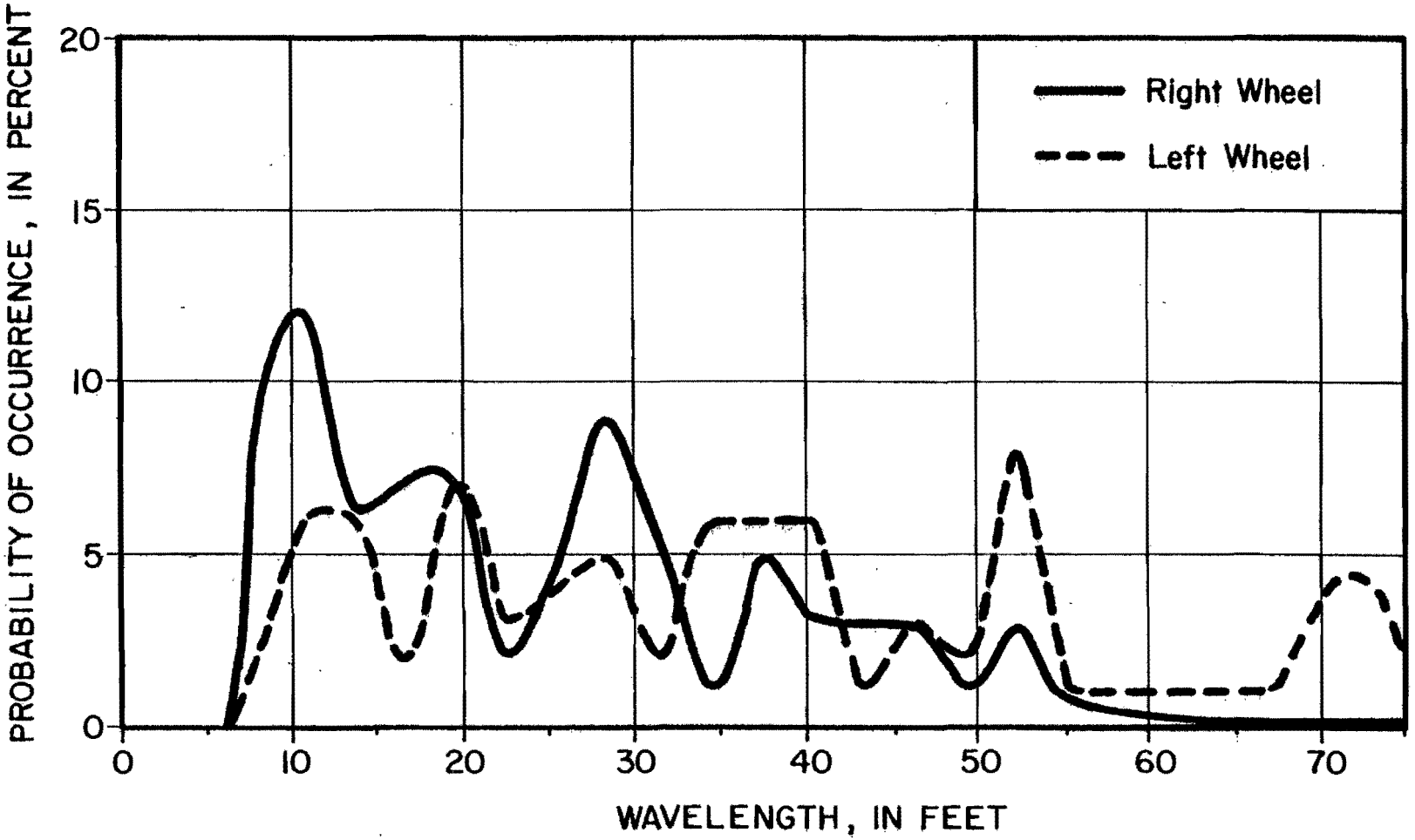

FIGURE V-5. Probability Density Function of Wavelength
(Ben Arnold 3)

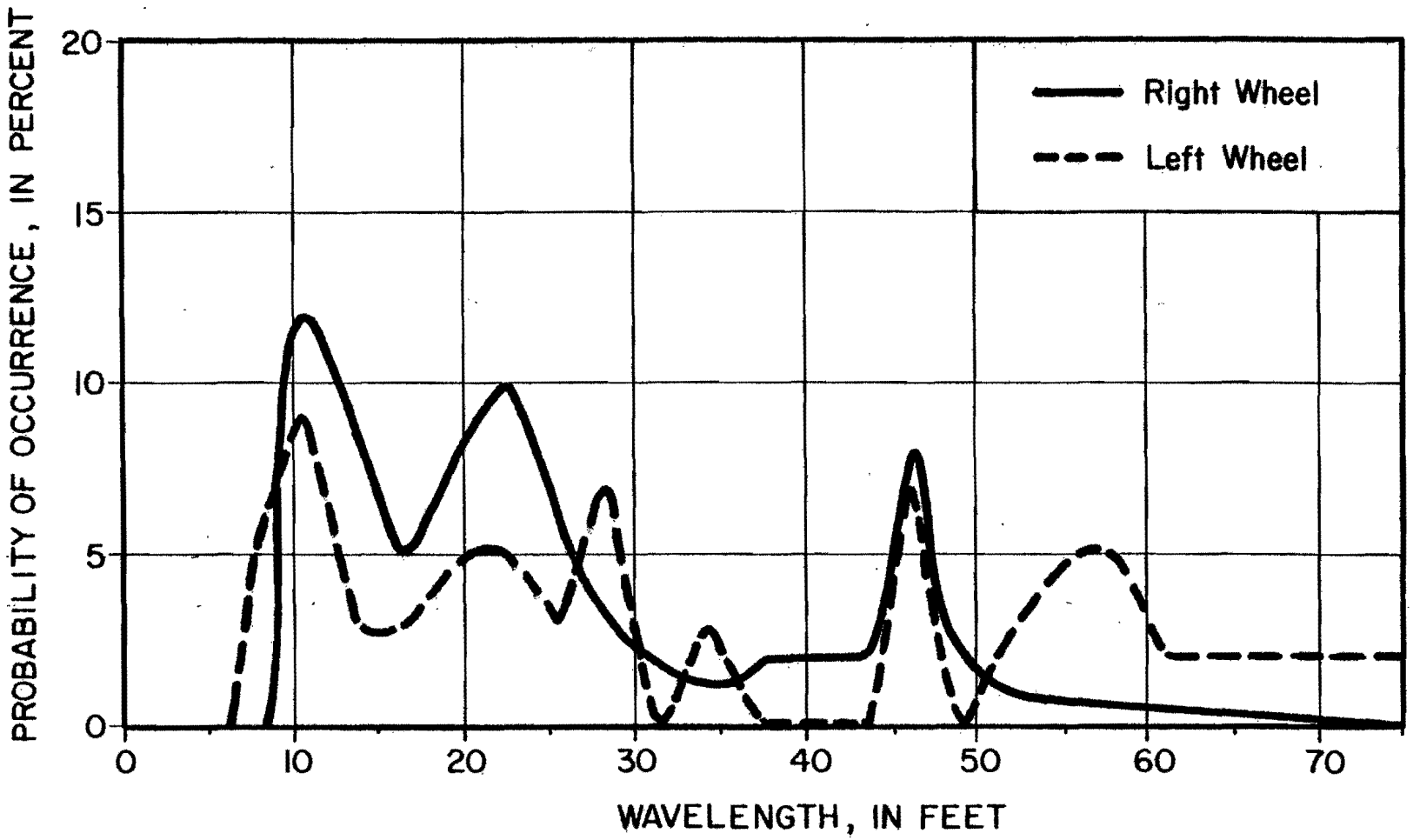

FIGURE V-6. Probability Density Function of Wavelength (Buckholts 1)

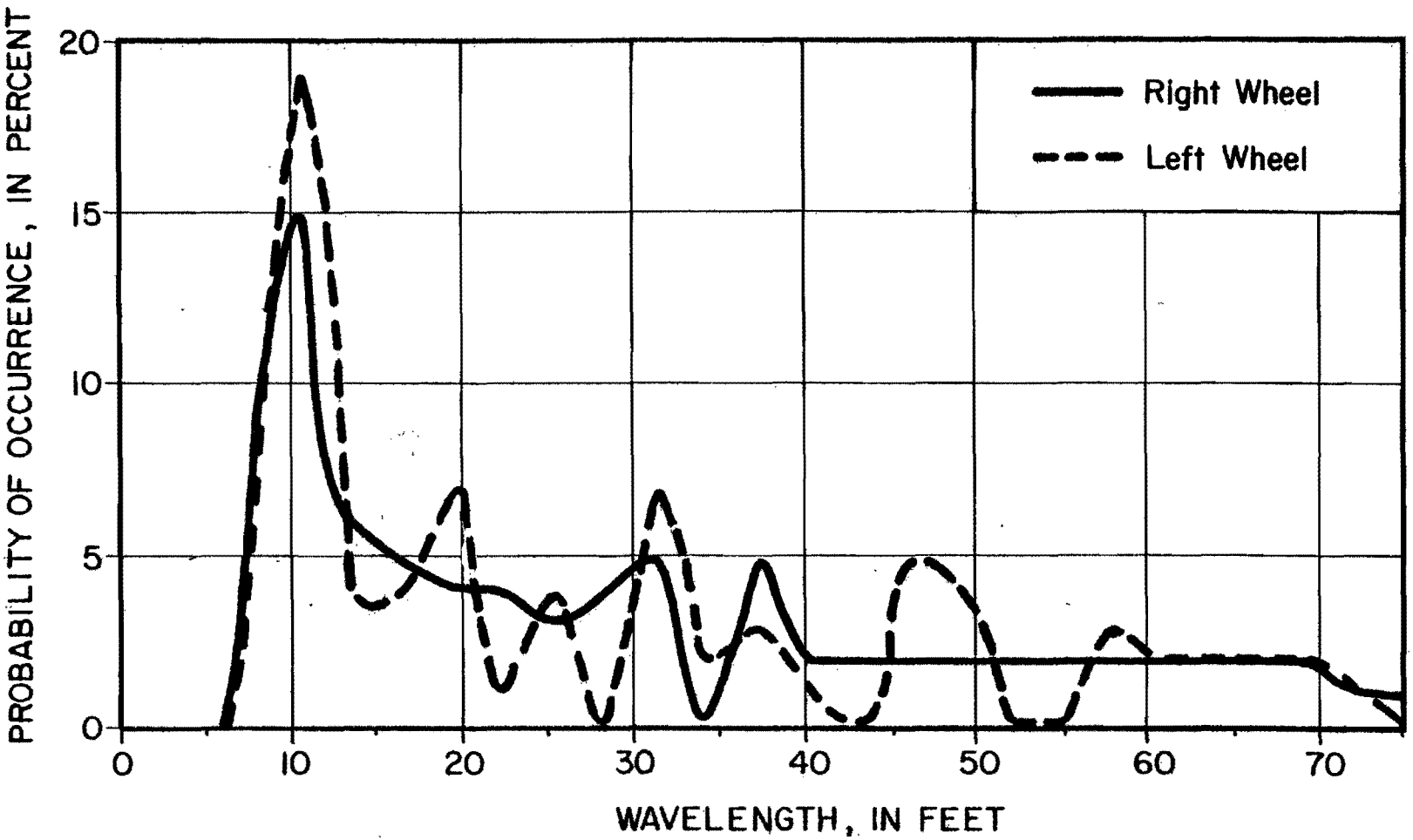

FIGURE V-7. Probability Density Function of Wavelength (Buckholts 2)

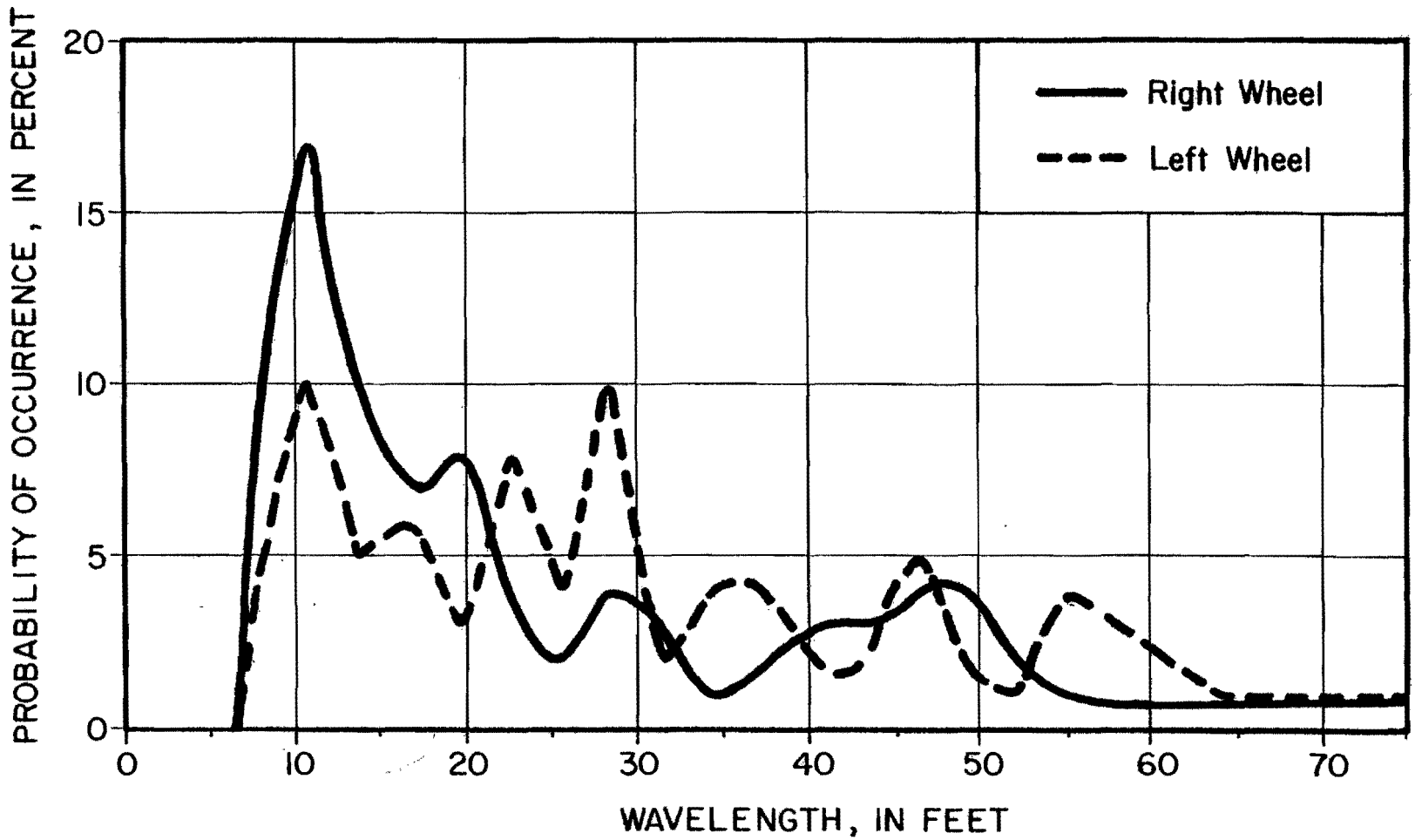

FIGURE V-8. Probability Density Function of Wavelength (Fairfield 1)

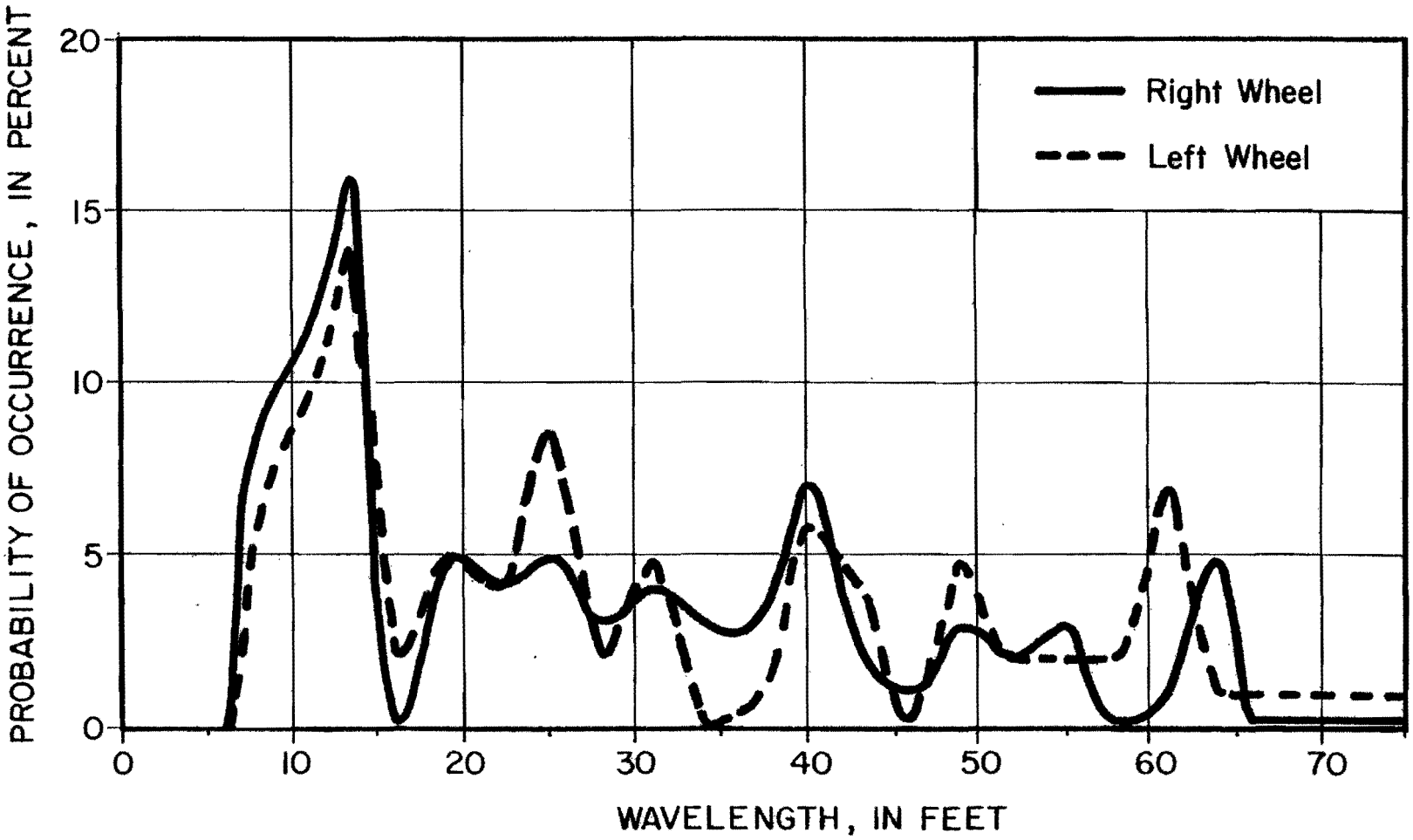

FIGURE V-9. Probability Density Function of Wavelength (Fairfield 2)

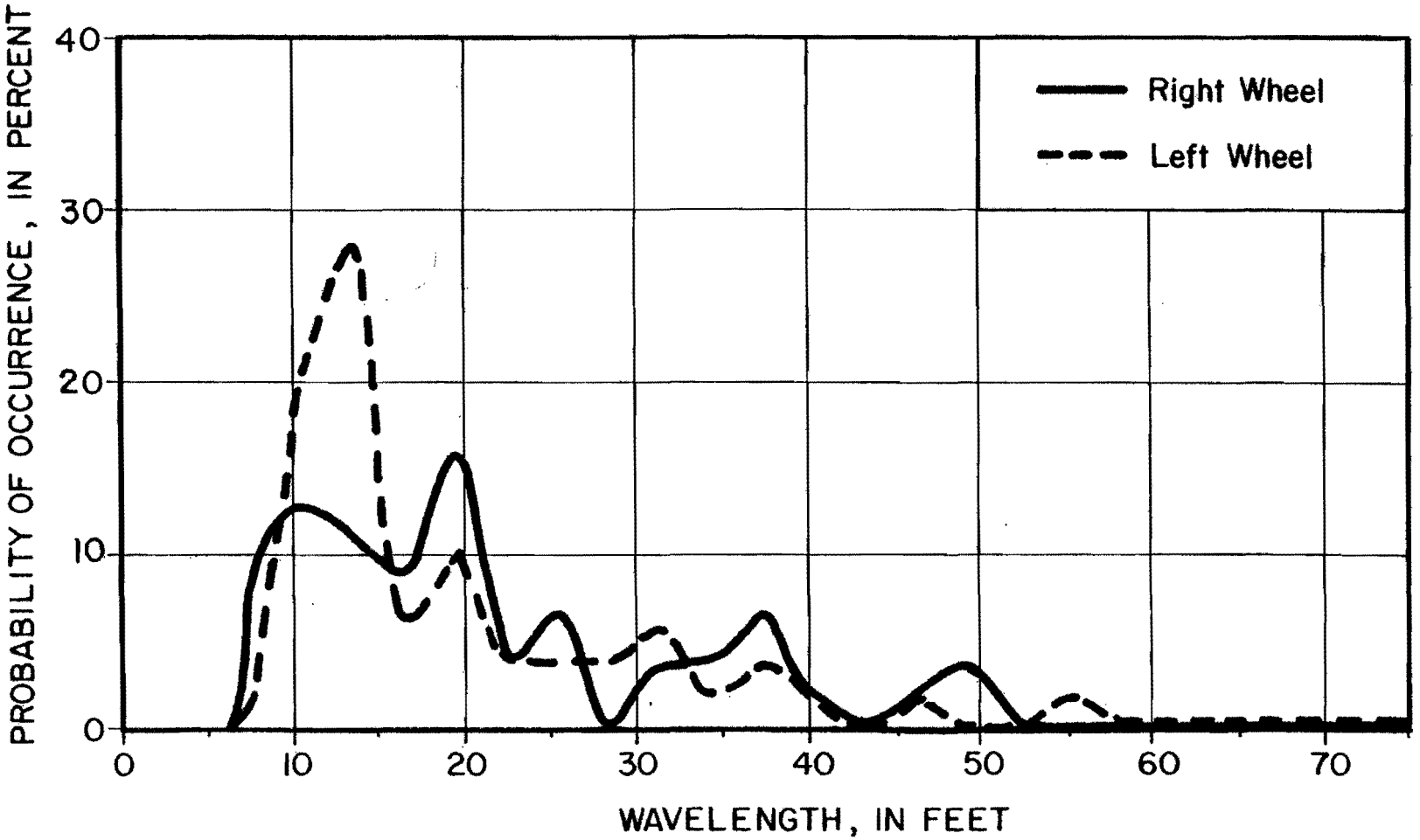

FIGURE V-10. Probability Density Function of Wavelength (Smithville 1A)

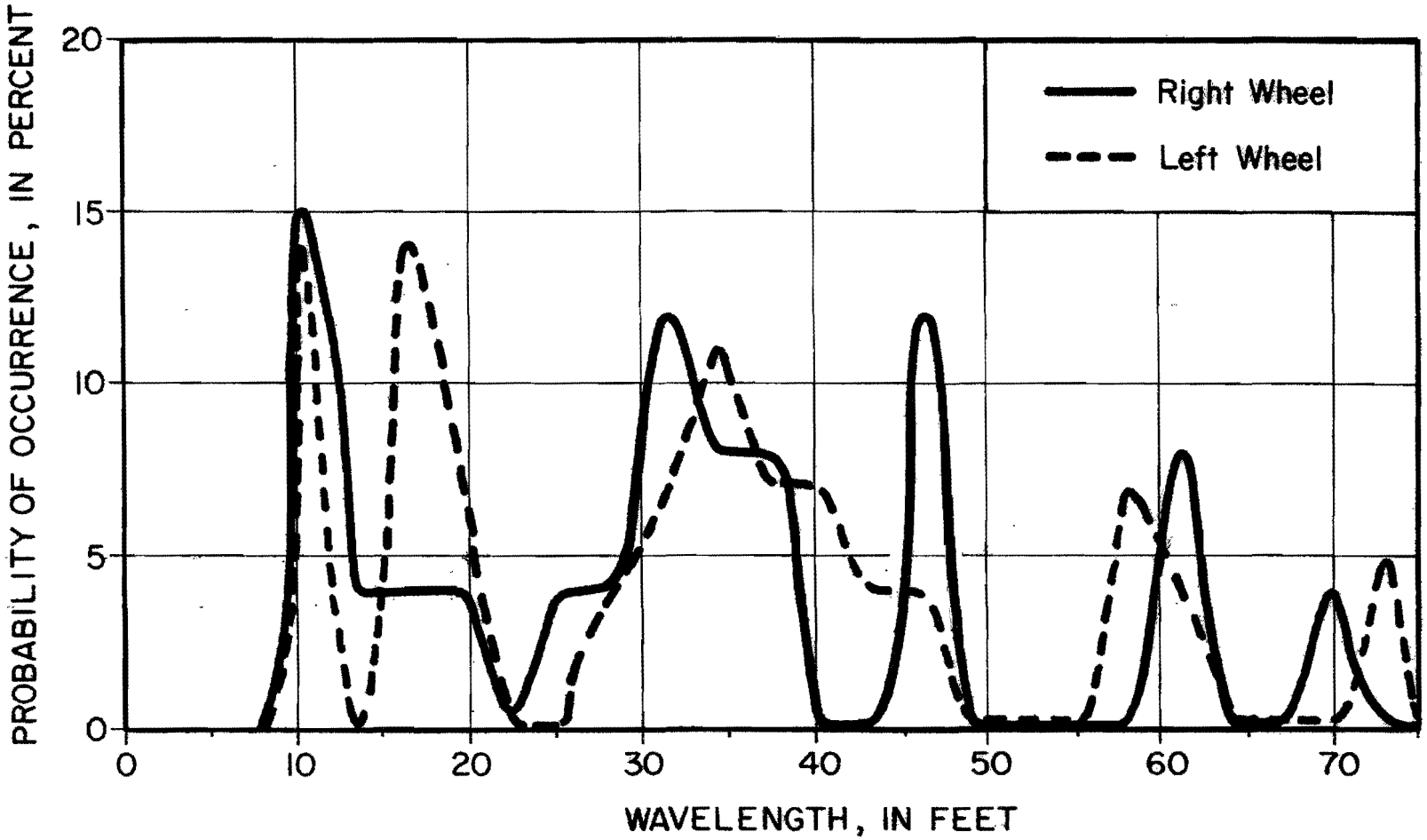

FIGURE V-11. Probability Density Function of Wavelength (Smithville 1B)

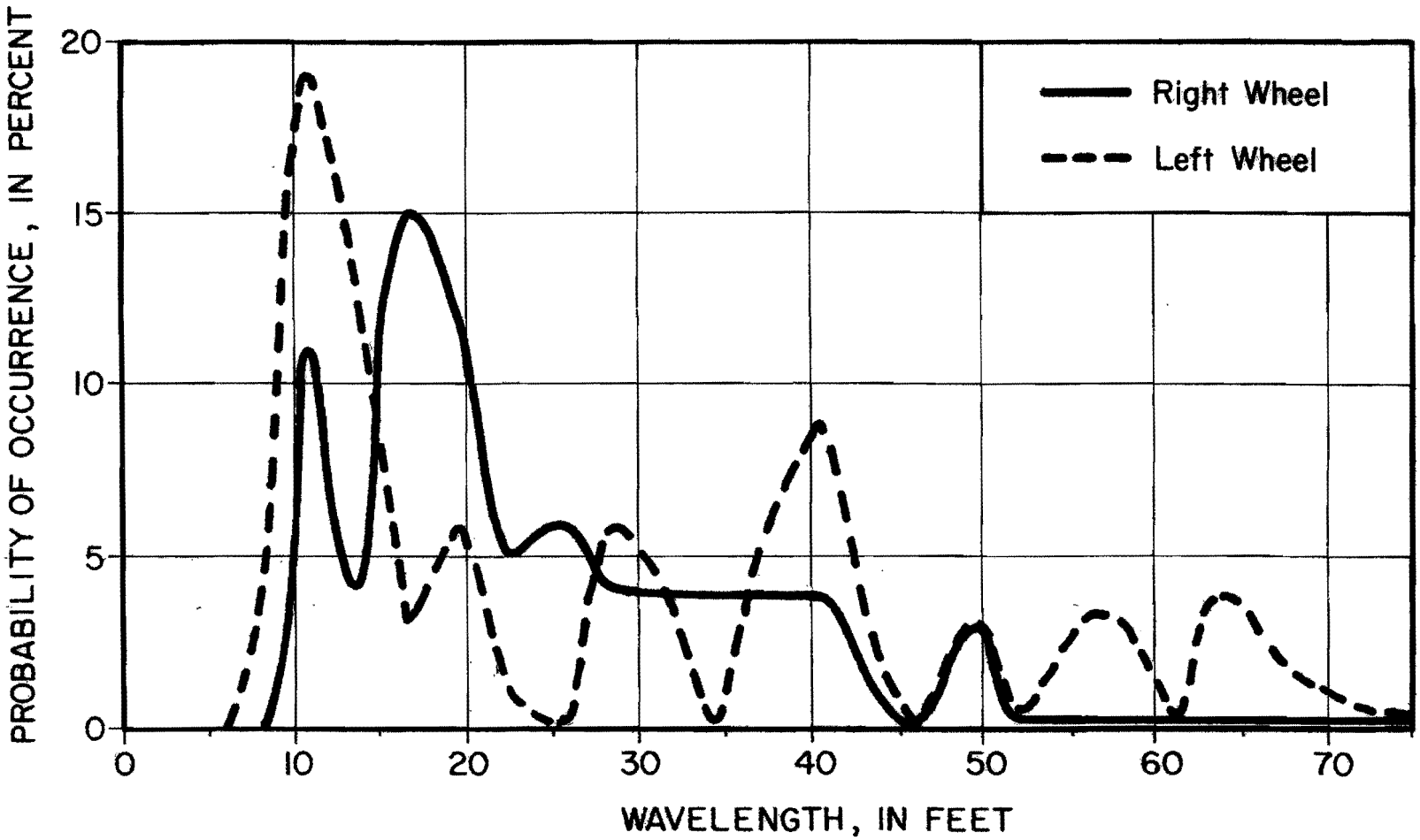

FIGURE V-12. Probability Density Function of Wavelength (Snook 1)

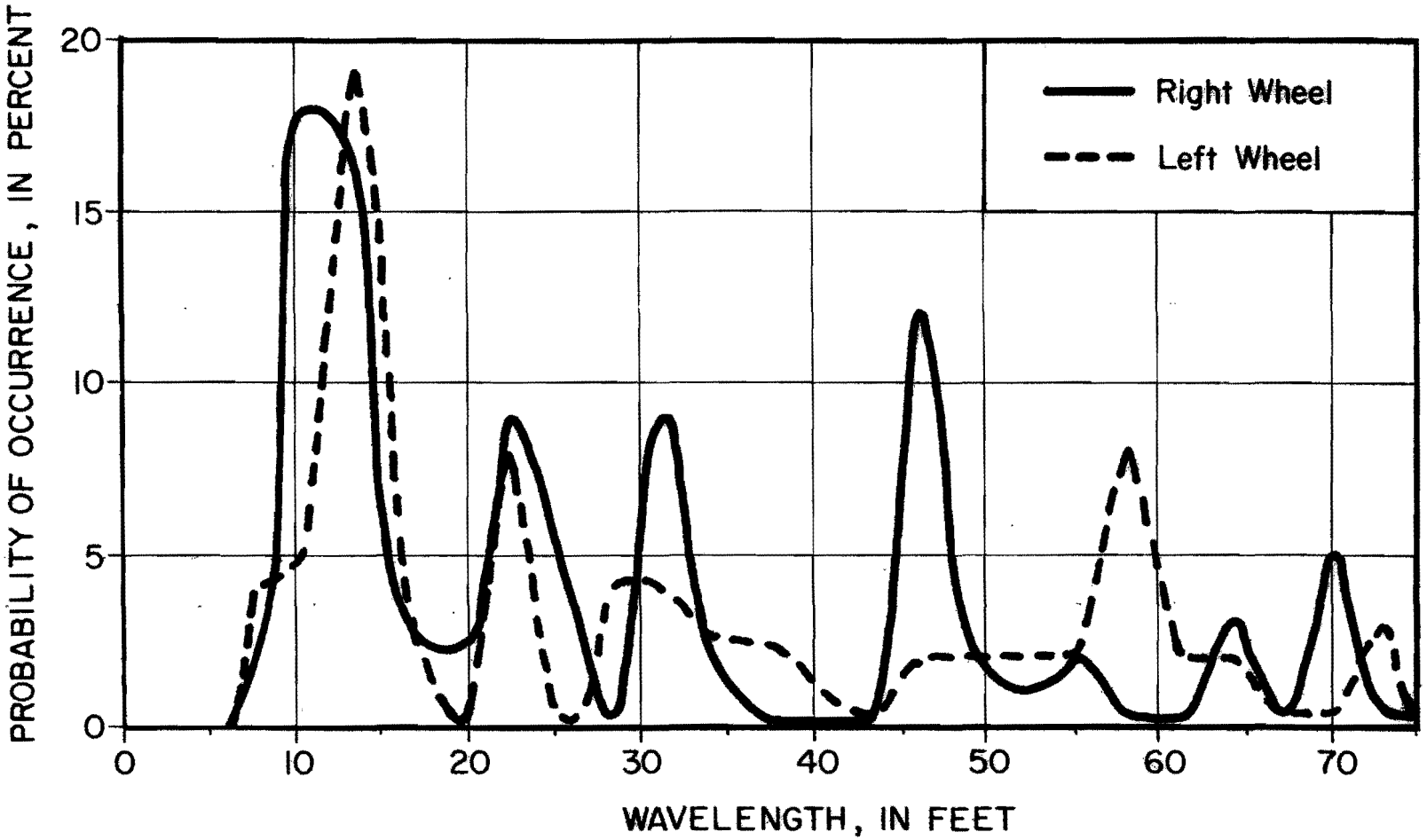

FIGURE V-13. Probability Density Function of Wavelength (OSR 1)

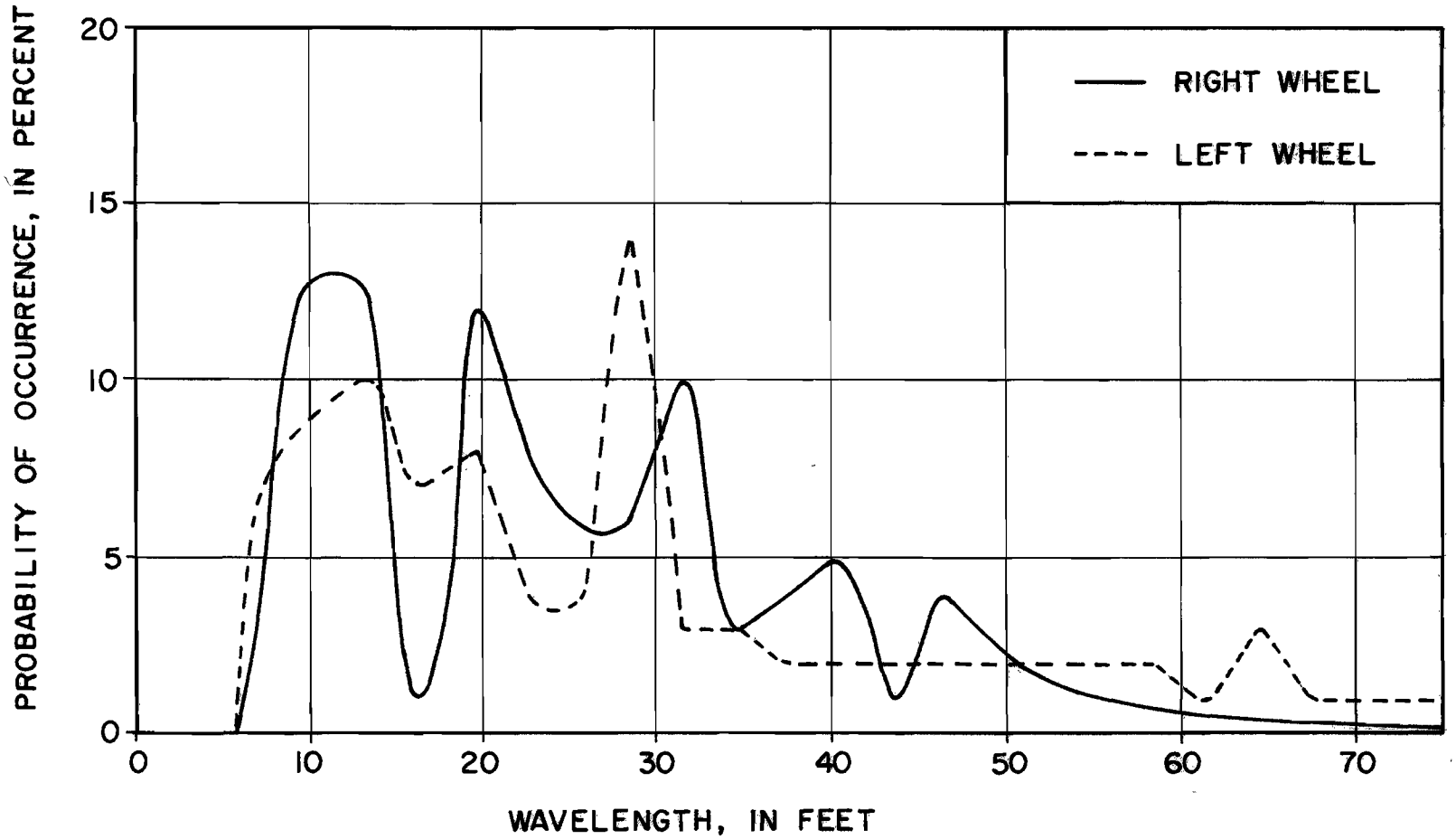

Figure V-14. Probability Density Function of Wavelength (OSR 2)

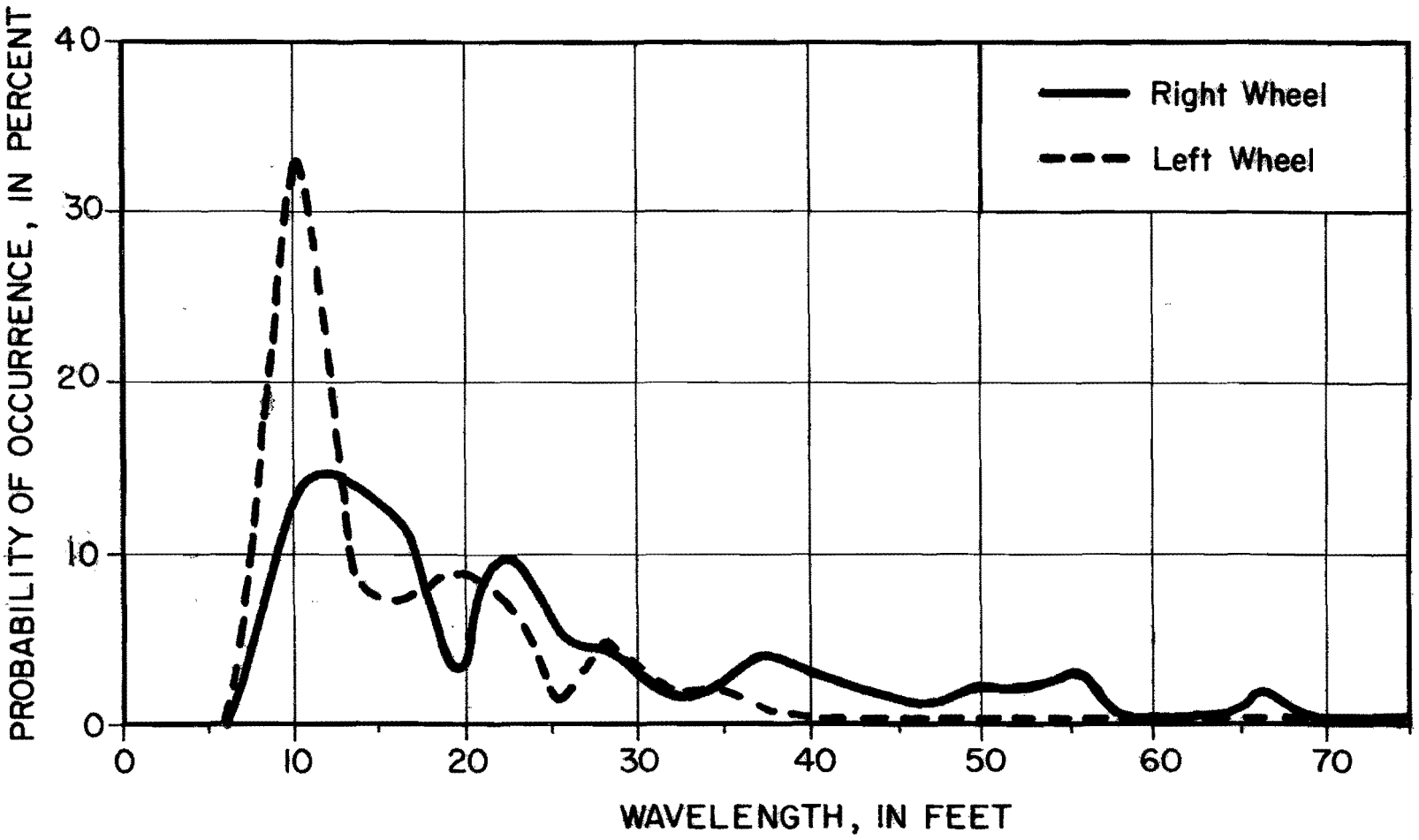

FIGURE V-15. Probability Density Function of Wavelength (OSR 3)

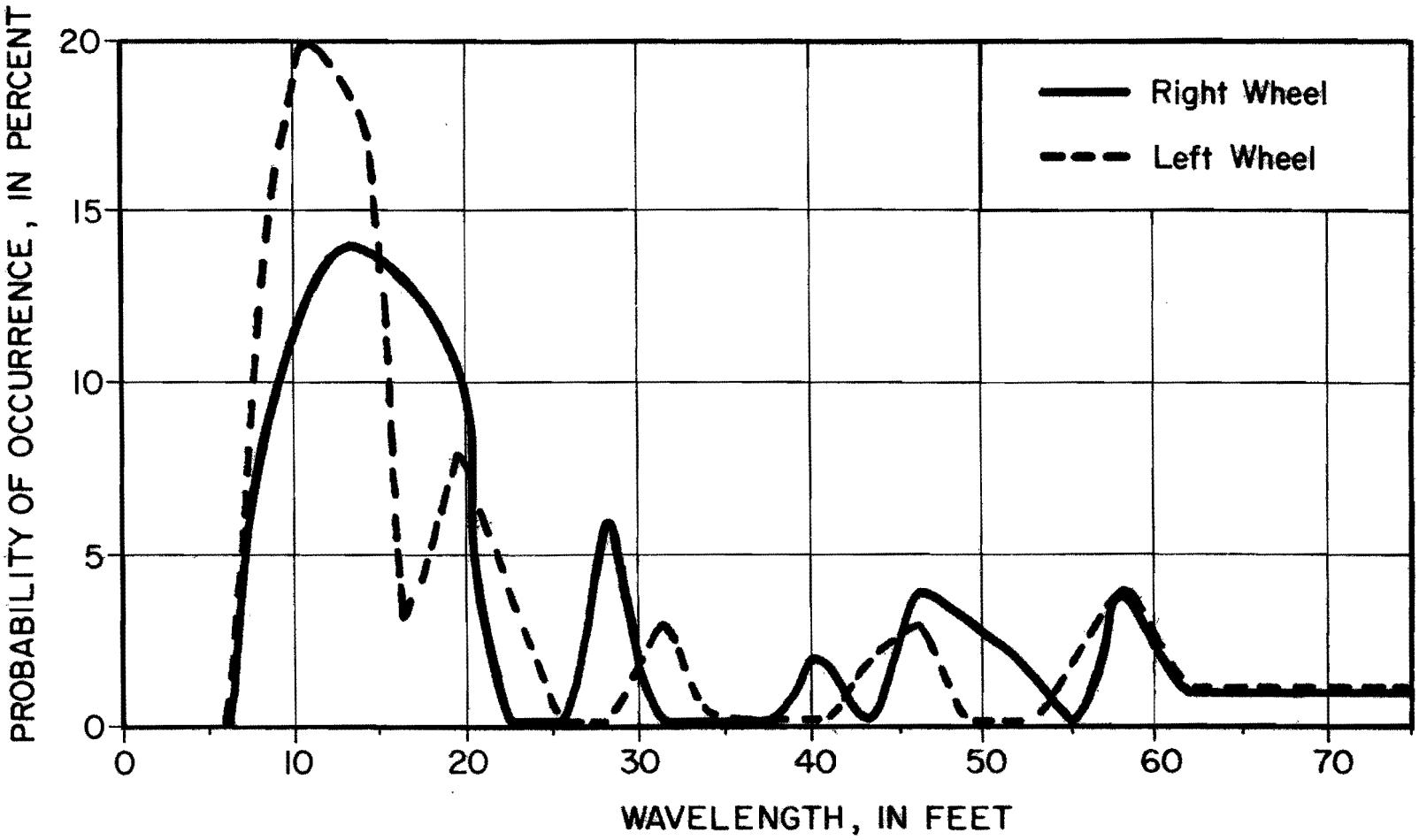

FIGURE V-16. Probability Density Function of Wavelength
(Thrall 1)

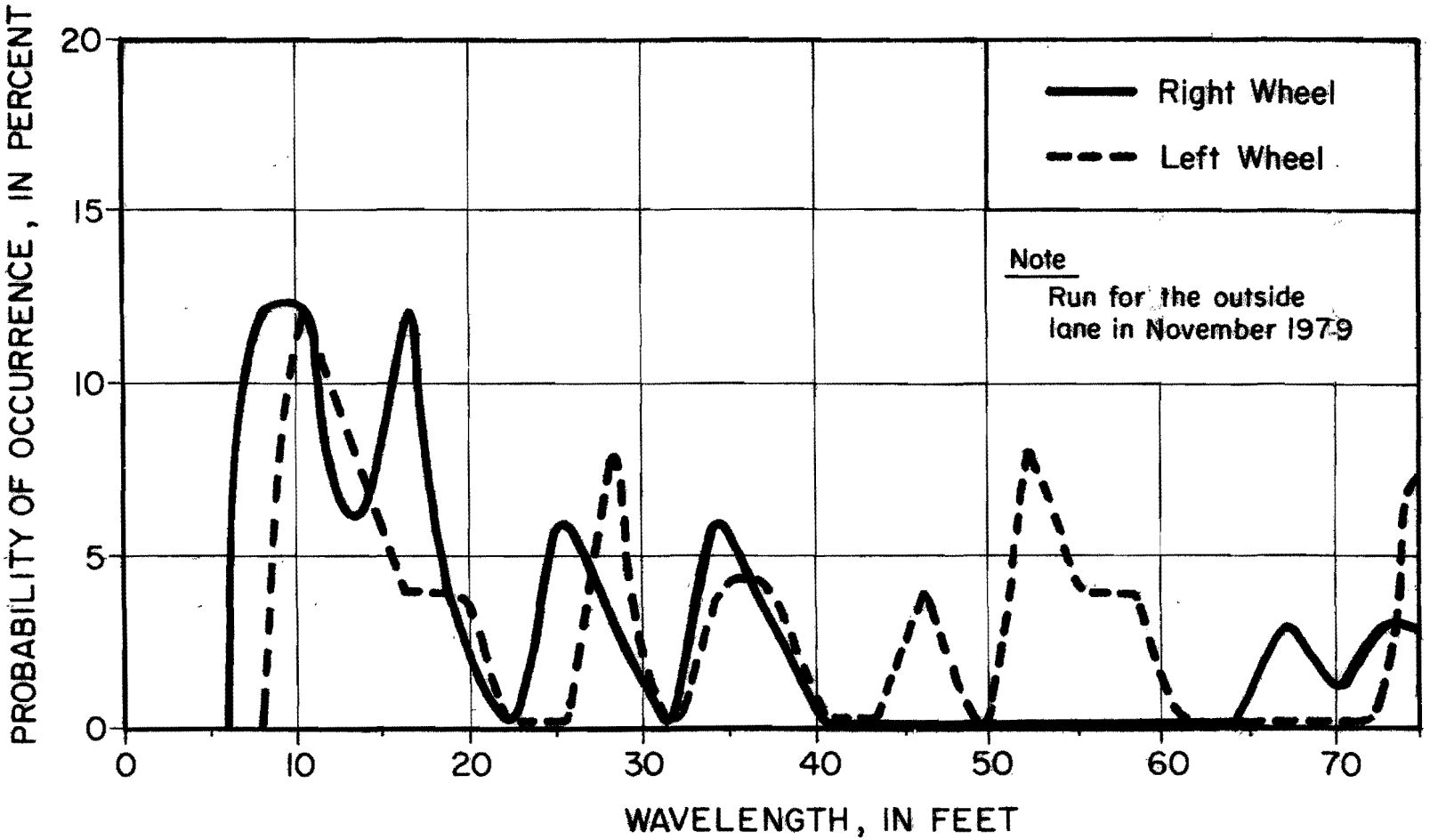

FIGURE V-17. Probability Density Function of Wavelength (San Antonio 410-1)

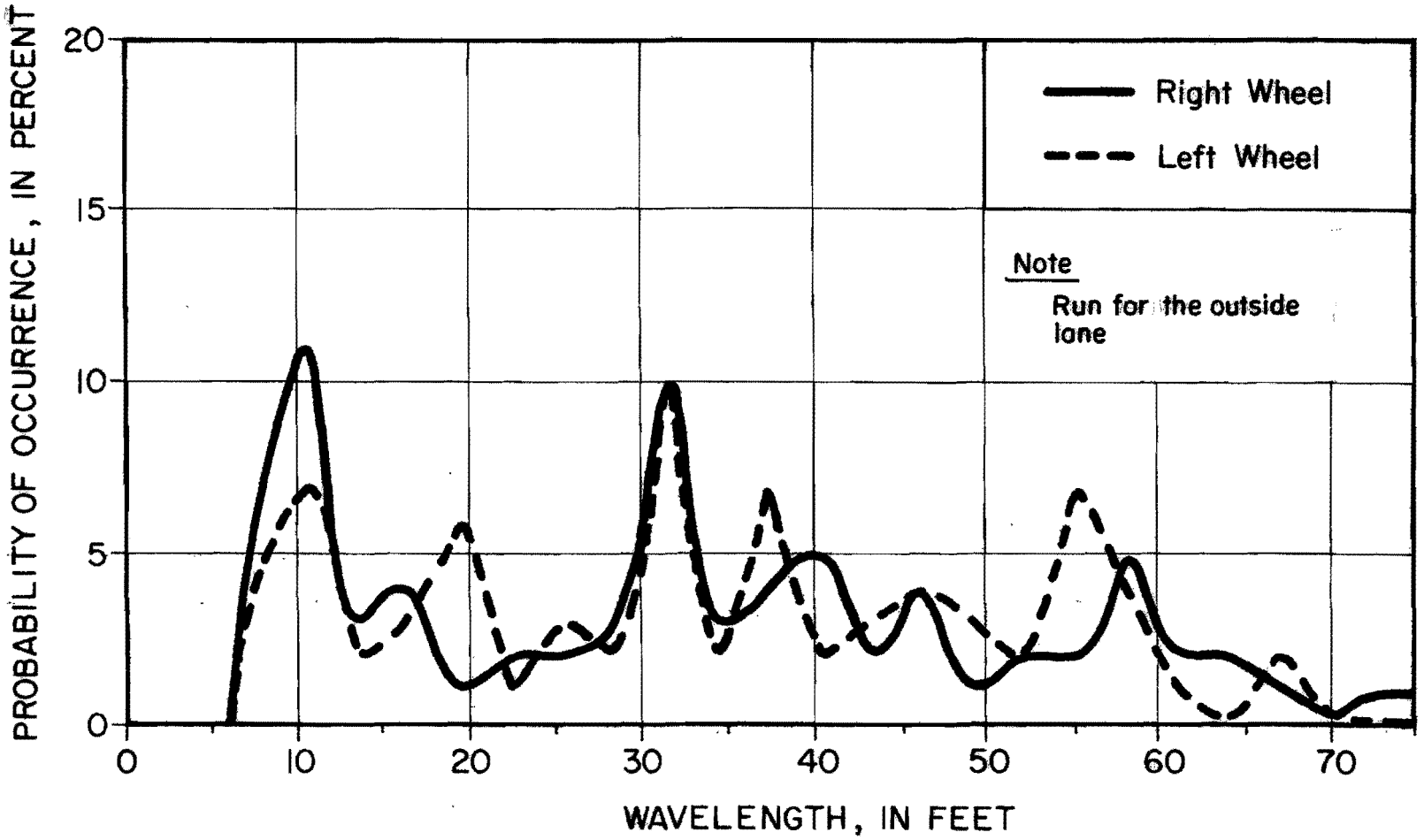

FIGURE V-18. Probability Density Function of Wavelength (San Antonio 37)

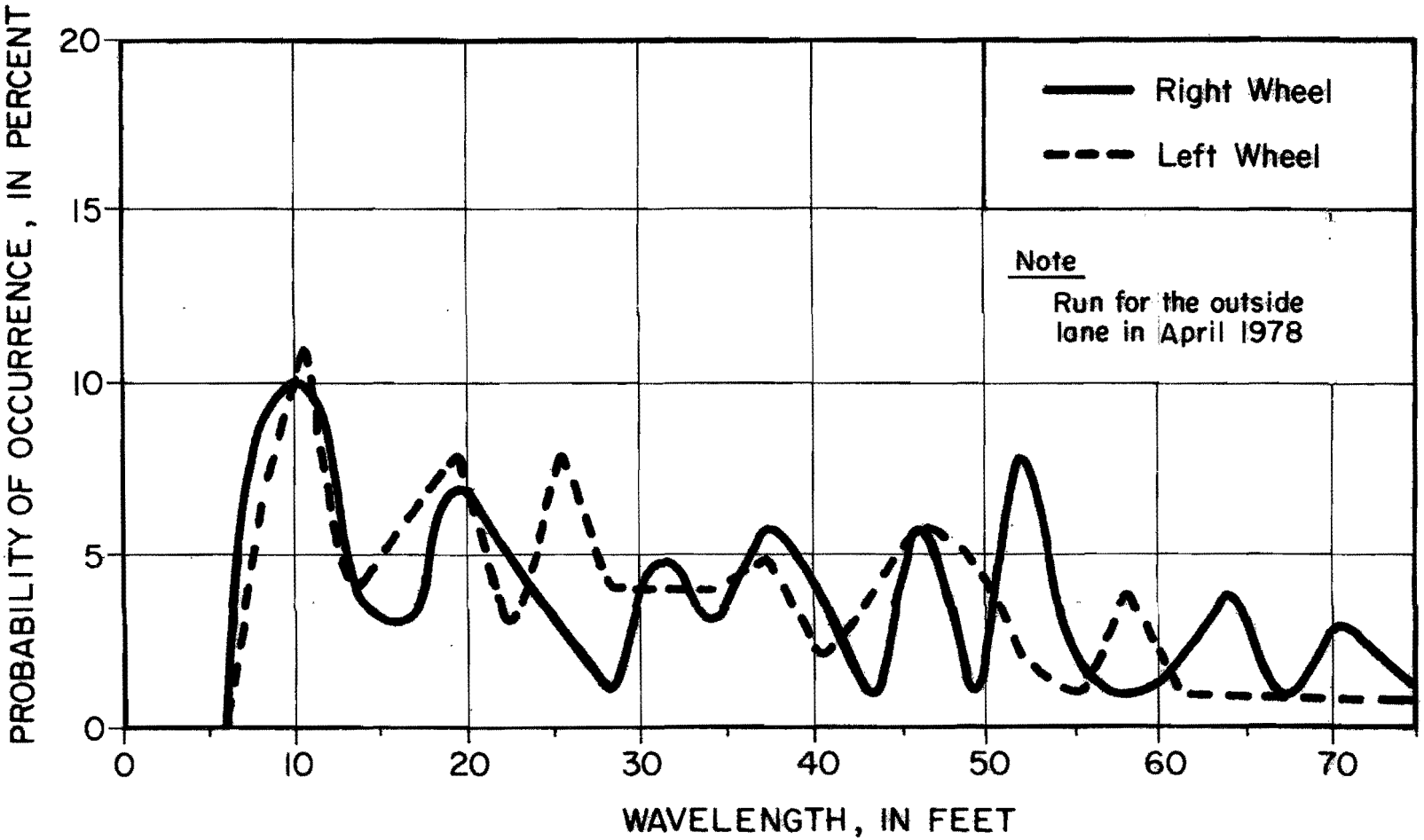

FIGURE V-19. Probability Density Function of Wavelength (San Antonio 90-5)

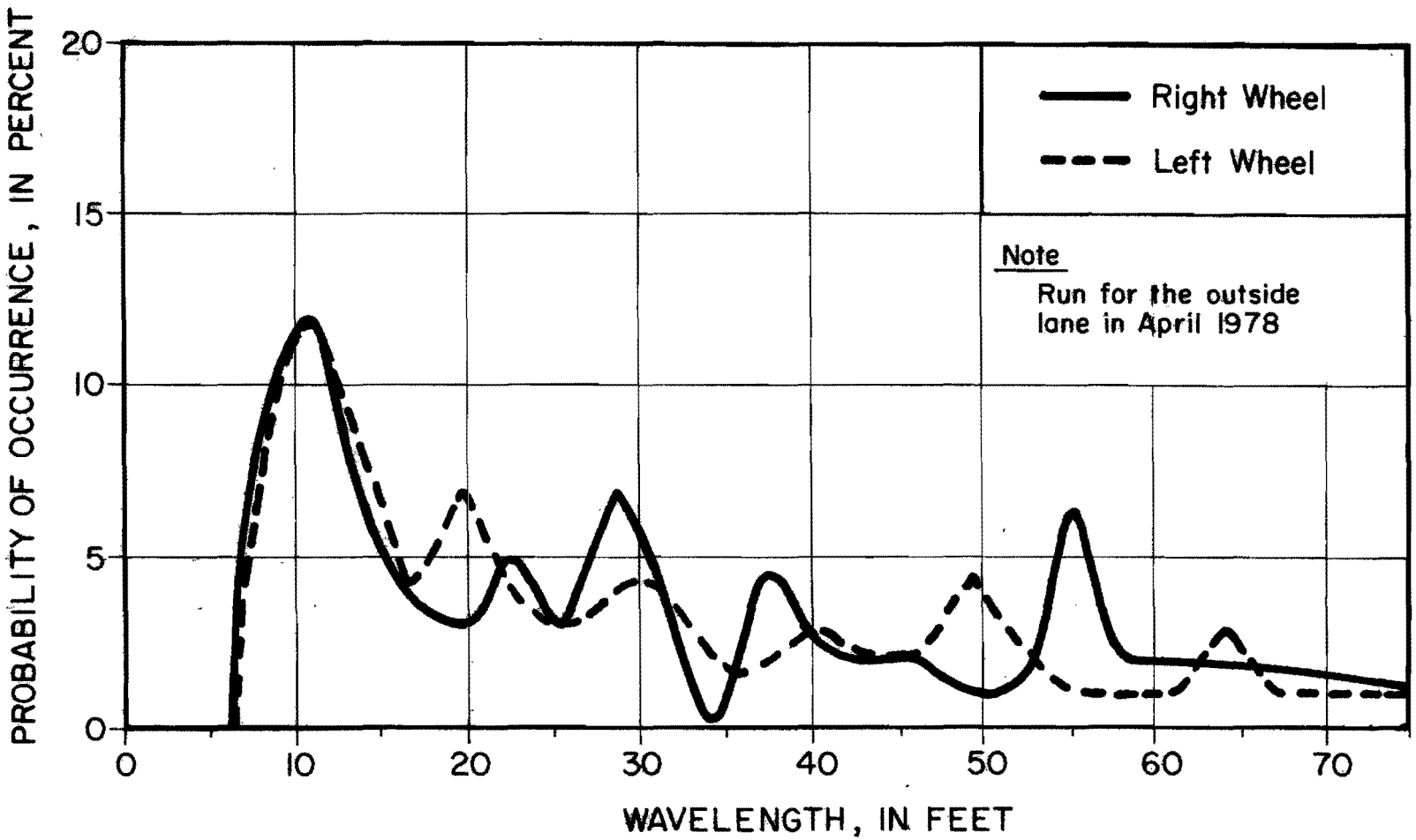

FIGURE V-20. Probability Density Function of Wavelength (San Antonio 90-3 West)

APPENDIX VI

DISTRIBUTIONS OF WAVELENGTHS

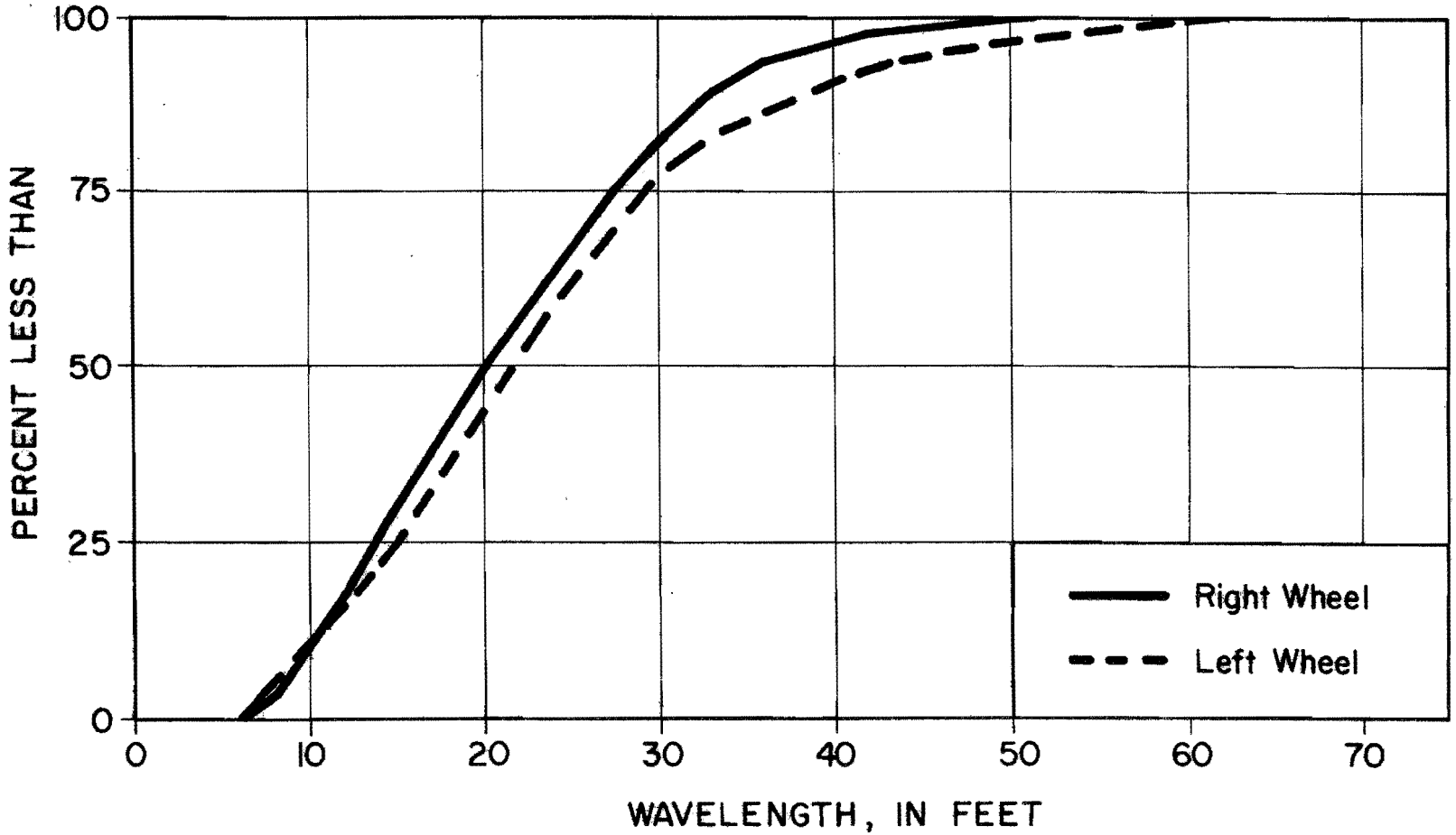

FIGURE VI-1. Distribution of Wavelengths (Huntsville 1)

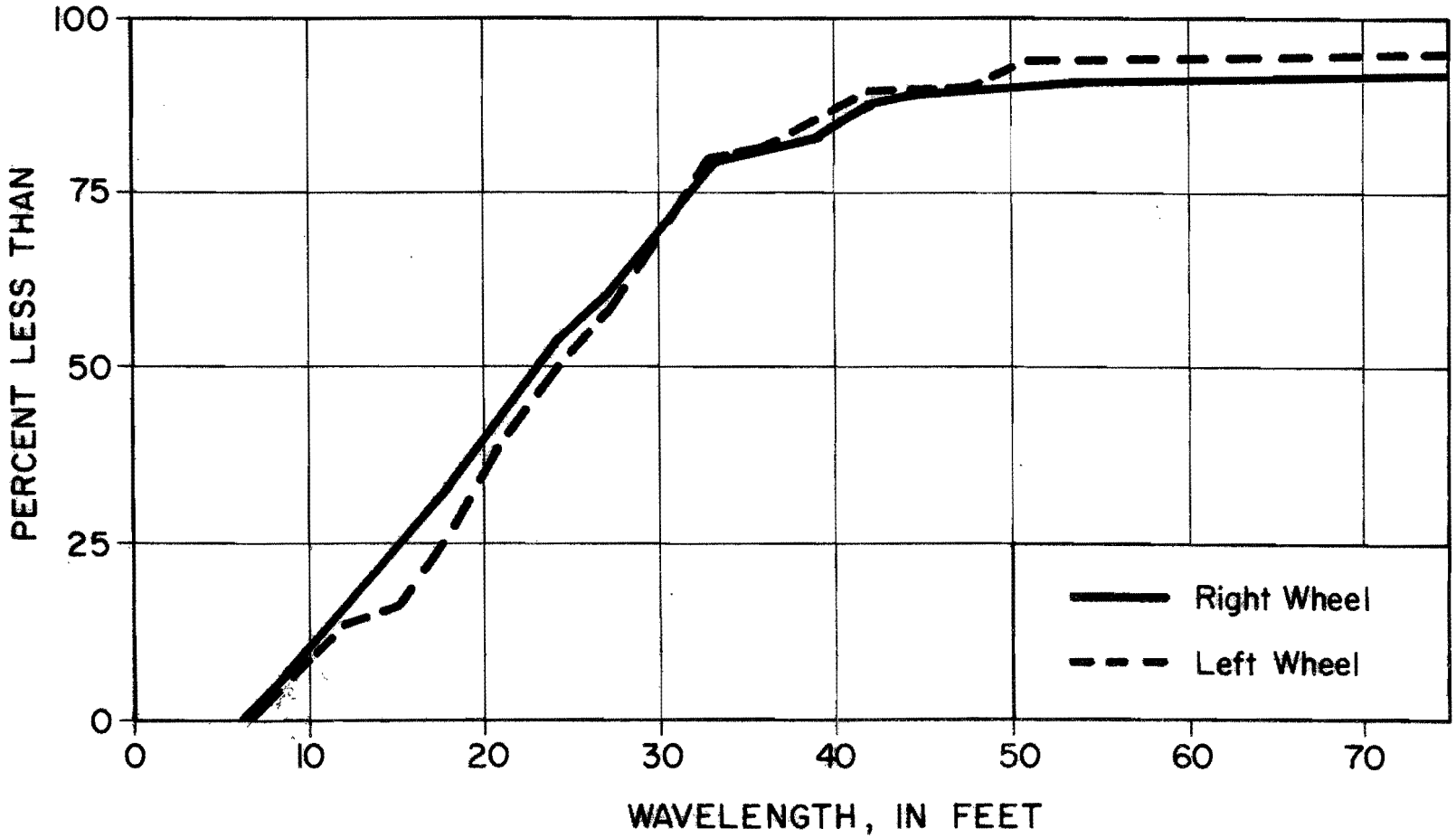

FIGURE VI-2. Distribution of Wavelengths (Huntsville 2)

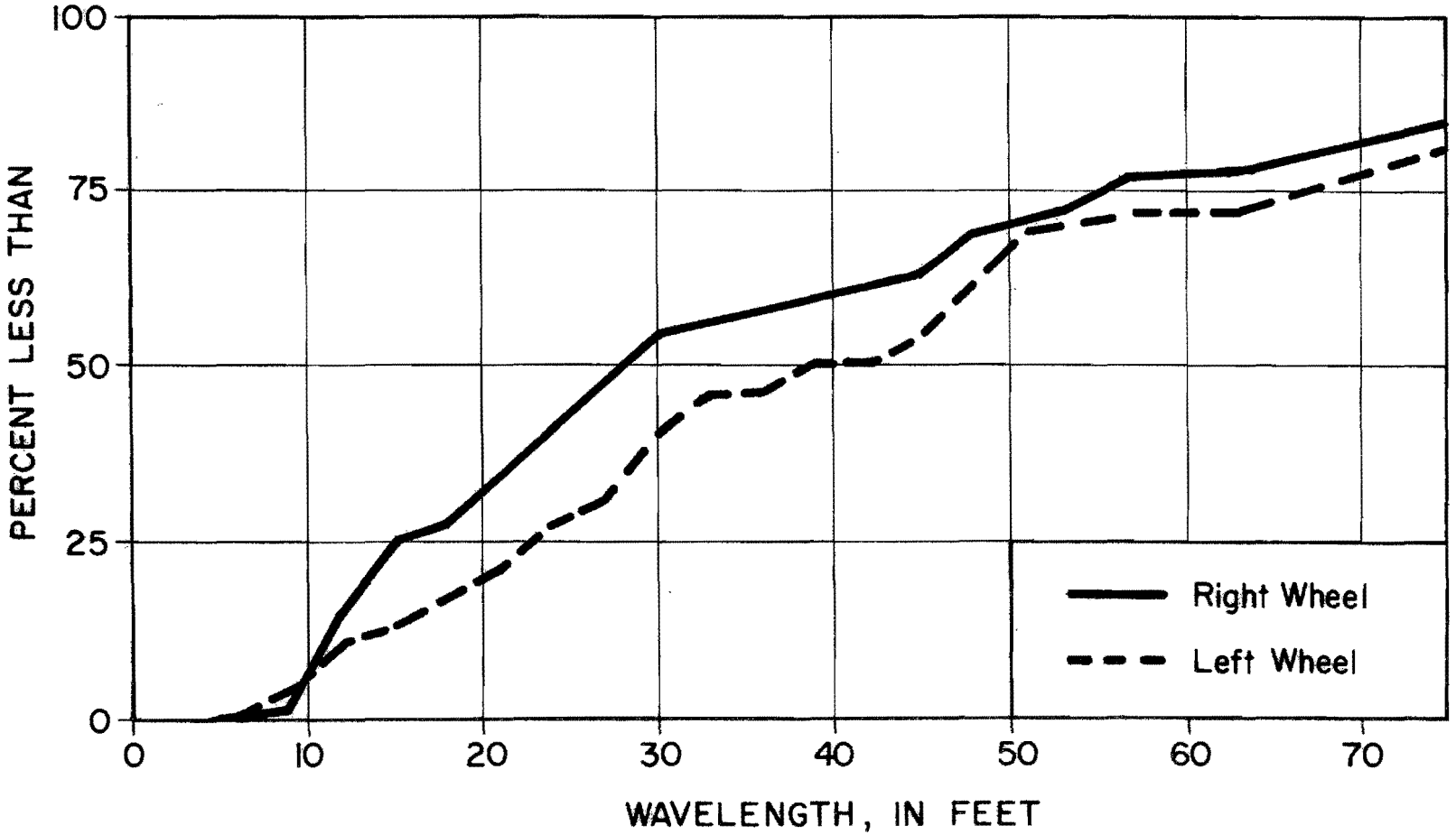

FIGURE VI-3. Distribution of Wavelengths
(Ben Arnold 1)

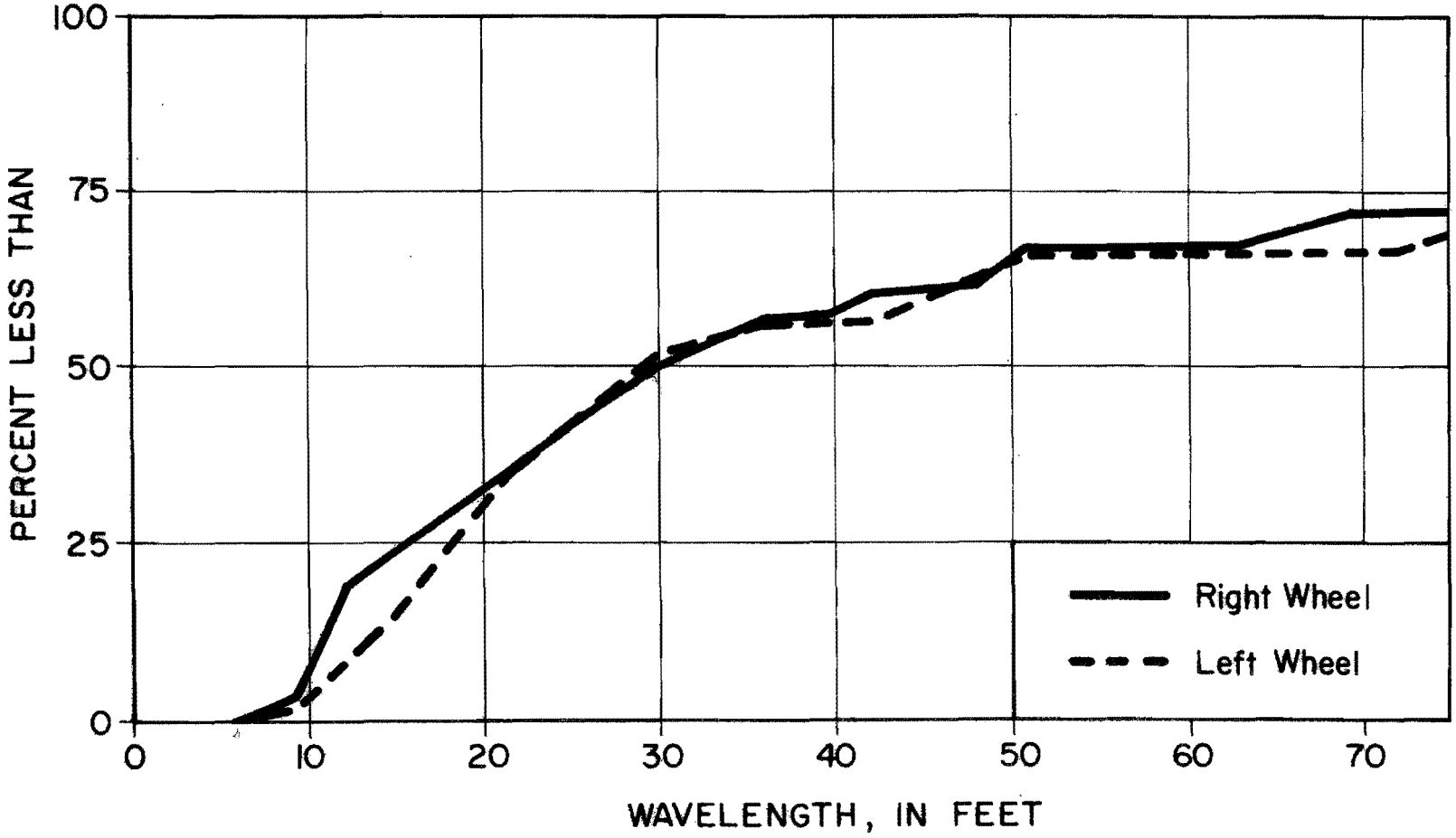

FIGURE VI-4. Distribution of Wavelengths
(Ben Arnold 2)

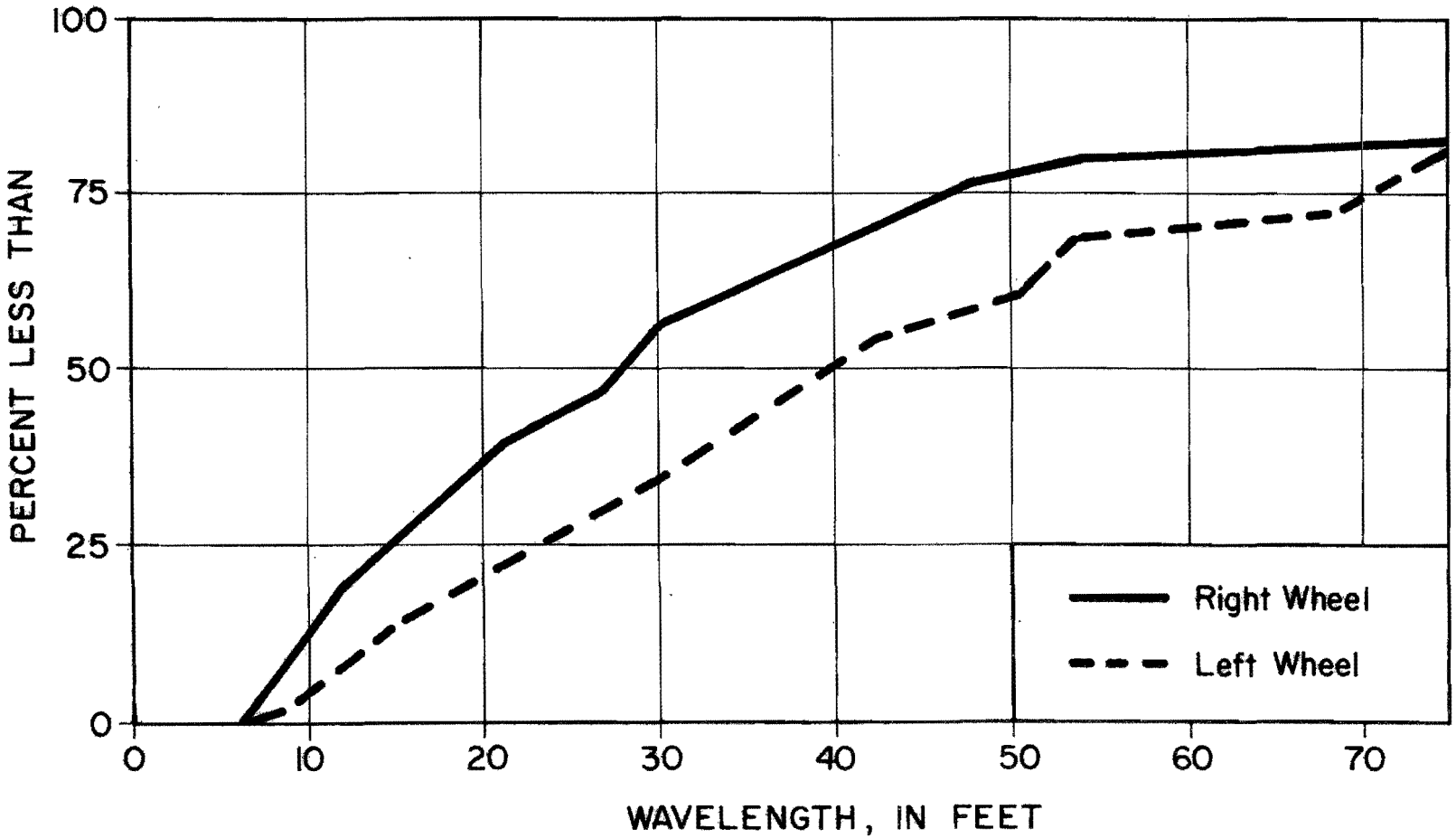

FIGURE VI-5. Distribution of Wavelengths (Ben Arnold 3)

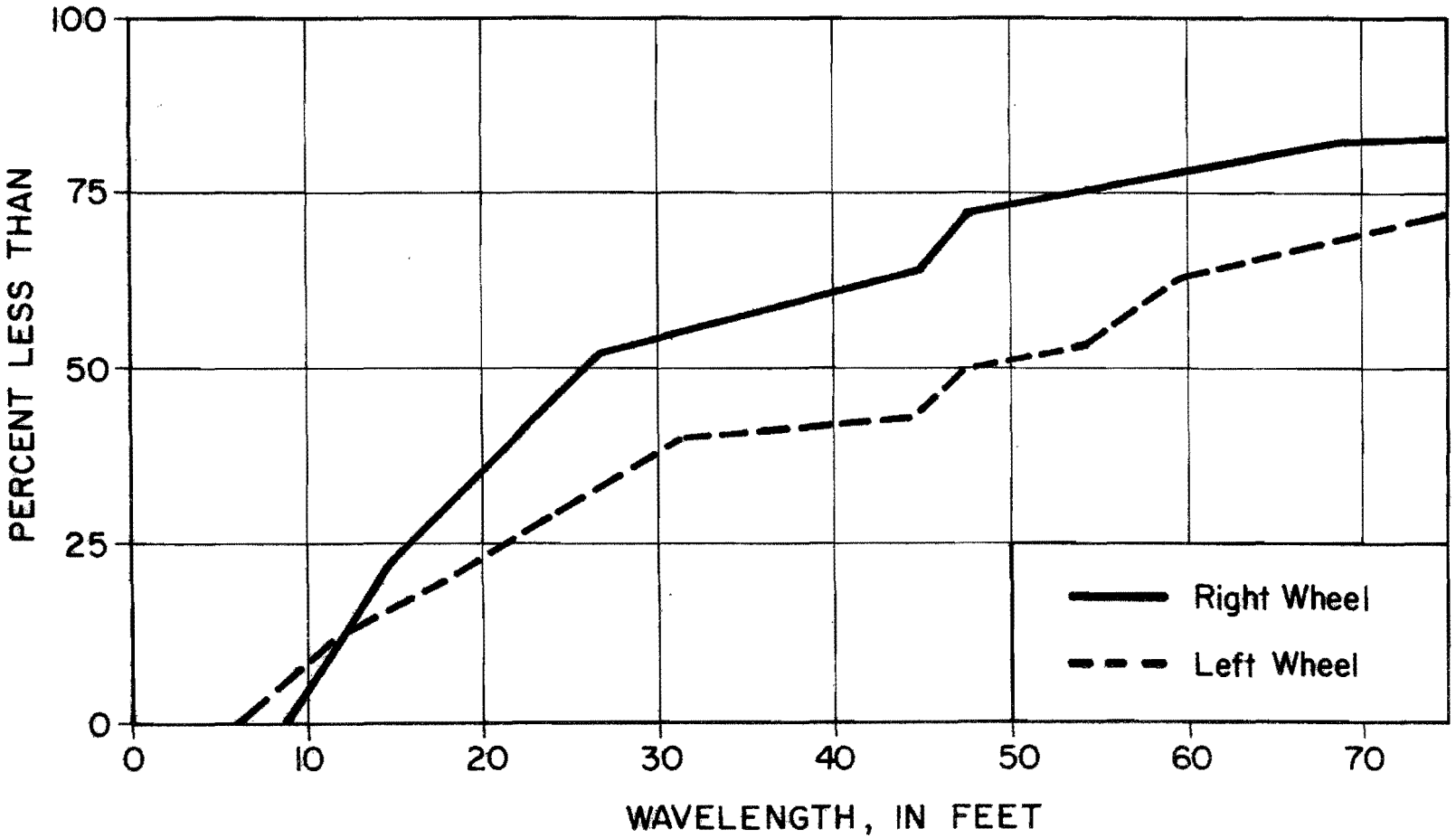

FIGURE VI-6. Distribution of Wavelengths
(Buckholts 1)

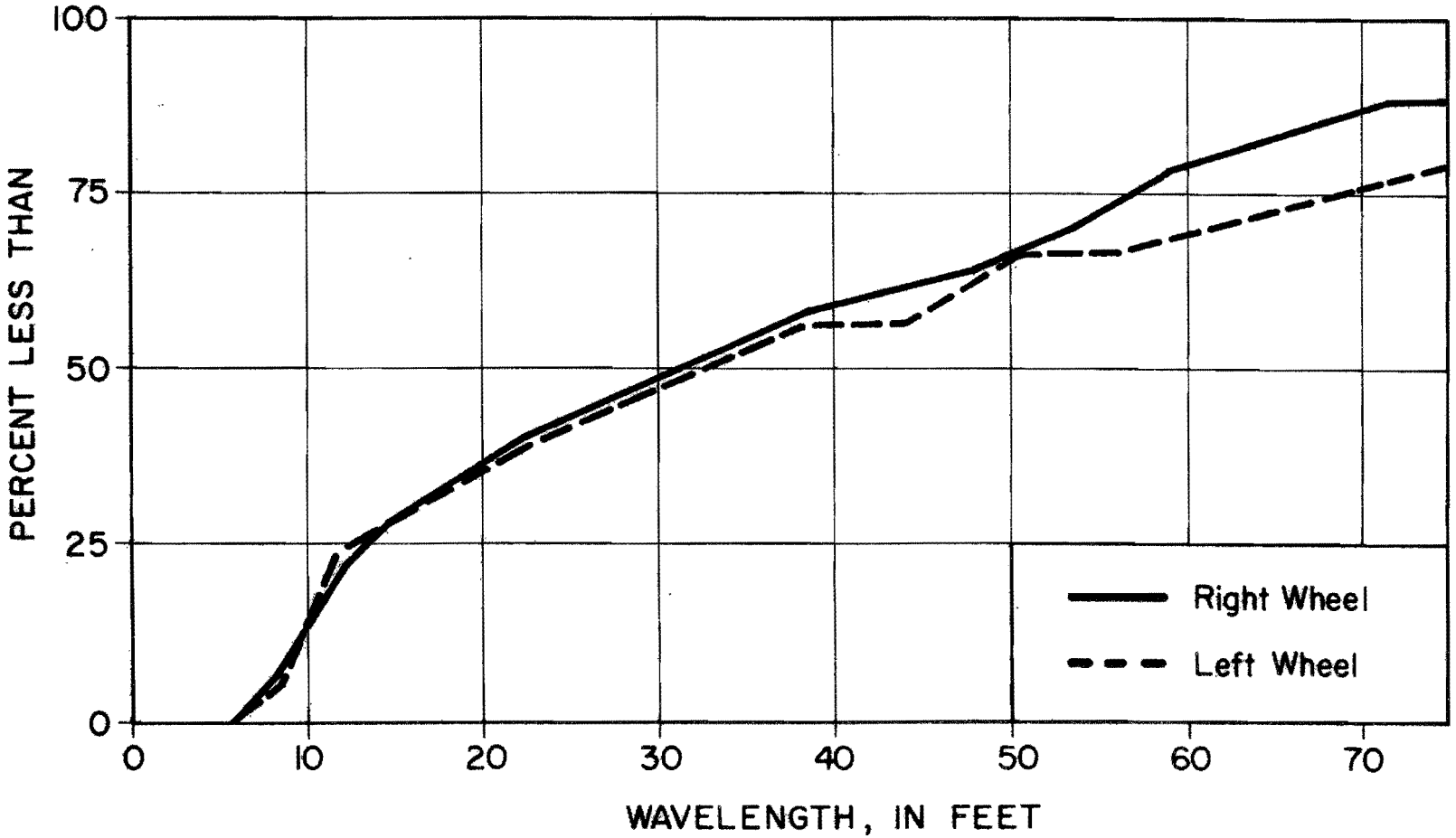

FIGURE VI-7. Distribution of Wavelengths
(Buckholts 2)

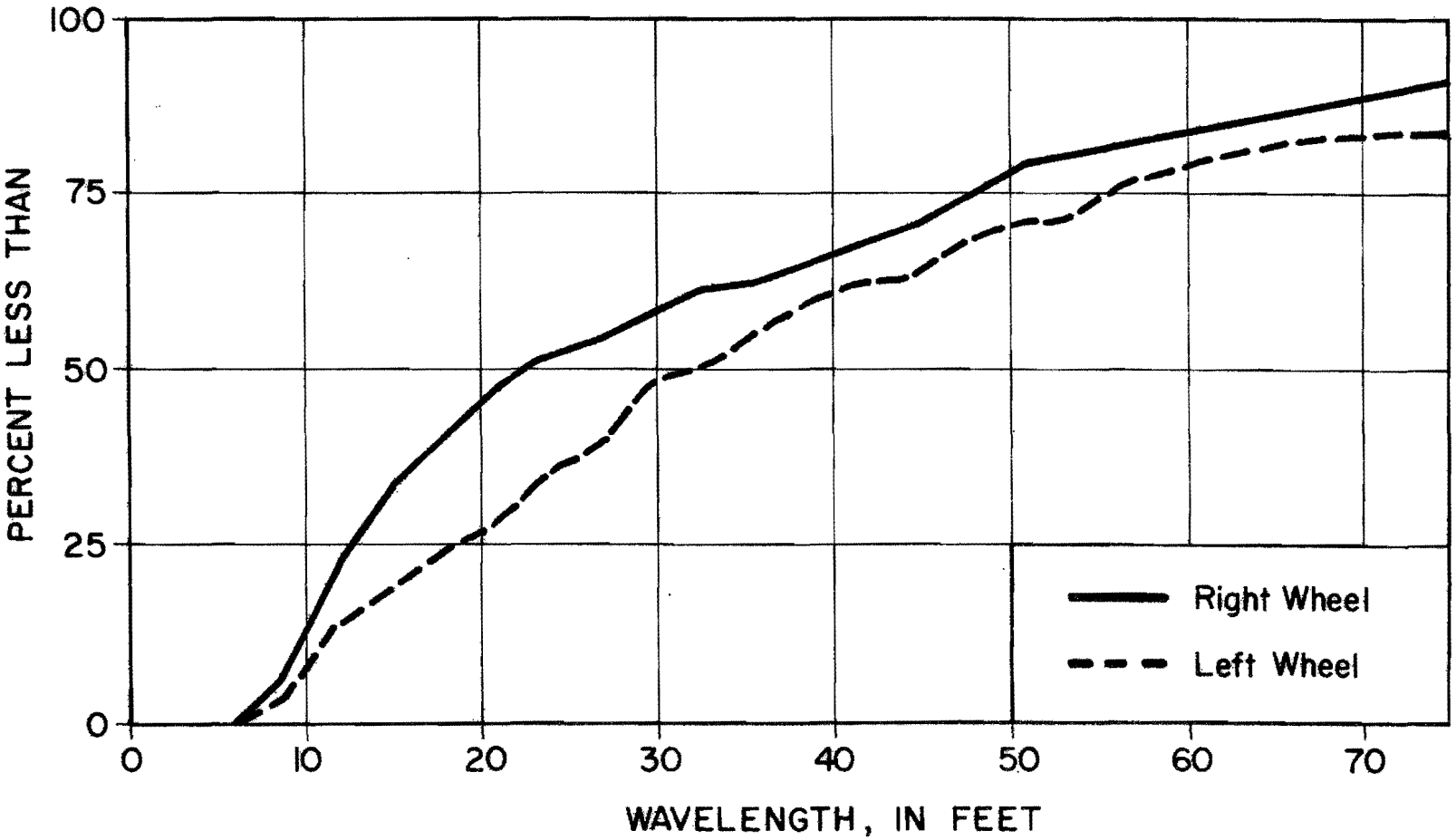

FIGURE VI-8. Distribution of Wavelengths
(Fairfield 1)

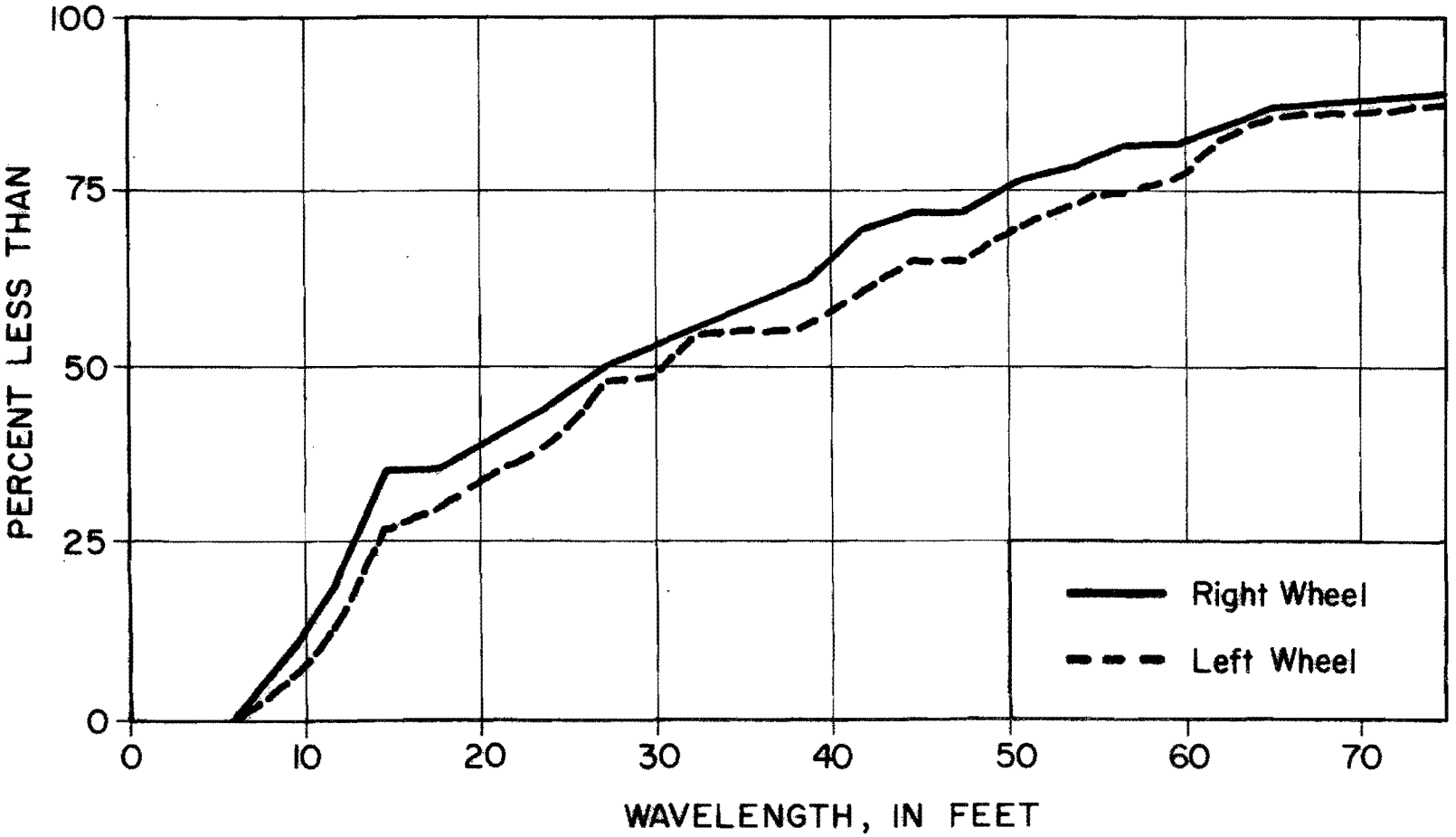

FIGURE VI-9. Distribution of Wavelengths (Fairfield 2)

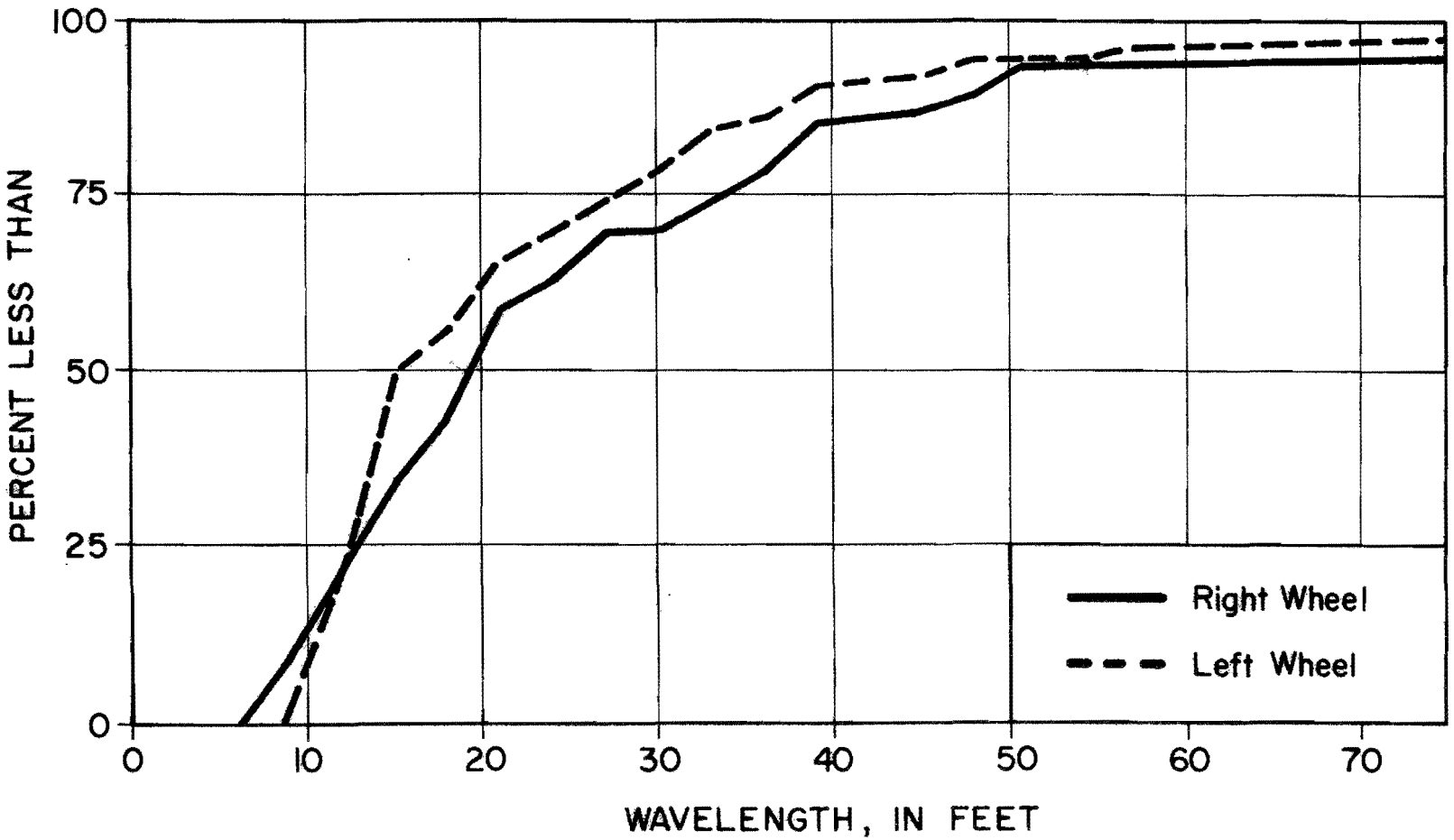

FIGURE VI-10. Distribution of Wavelengths
(Smithville 1A)

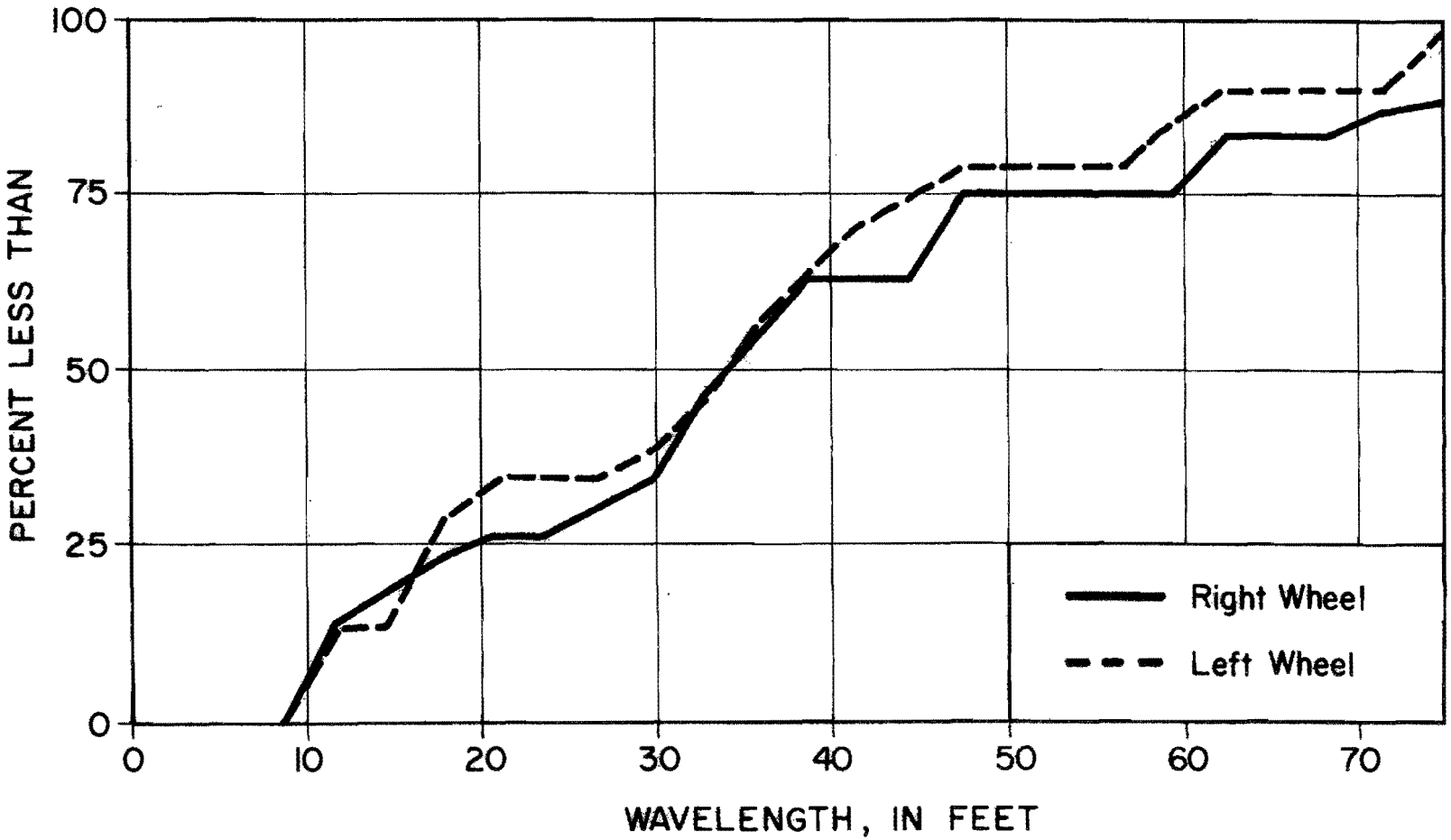

FIGURE VI-11. Distribution of Wavelengths
(Smithville 1B)

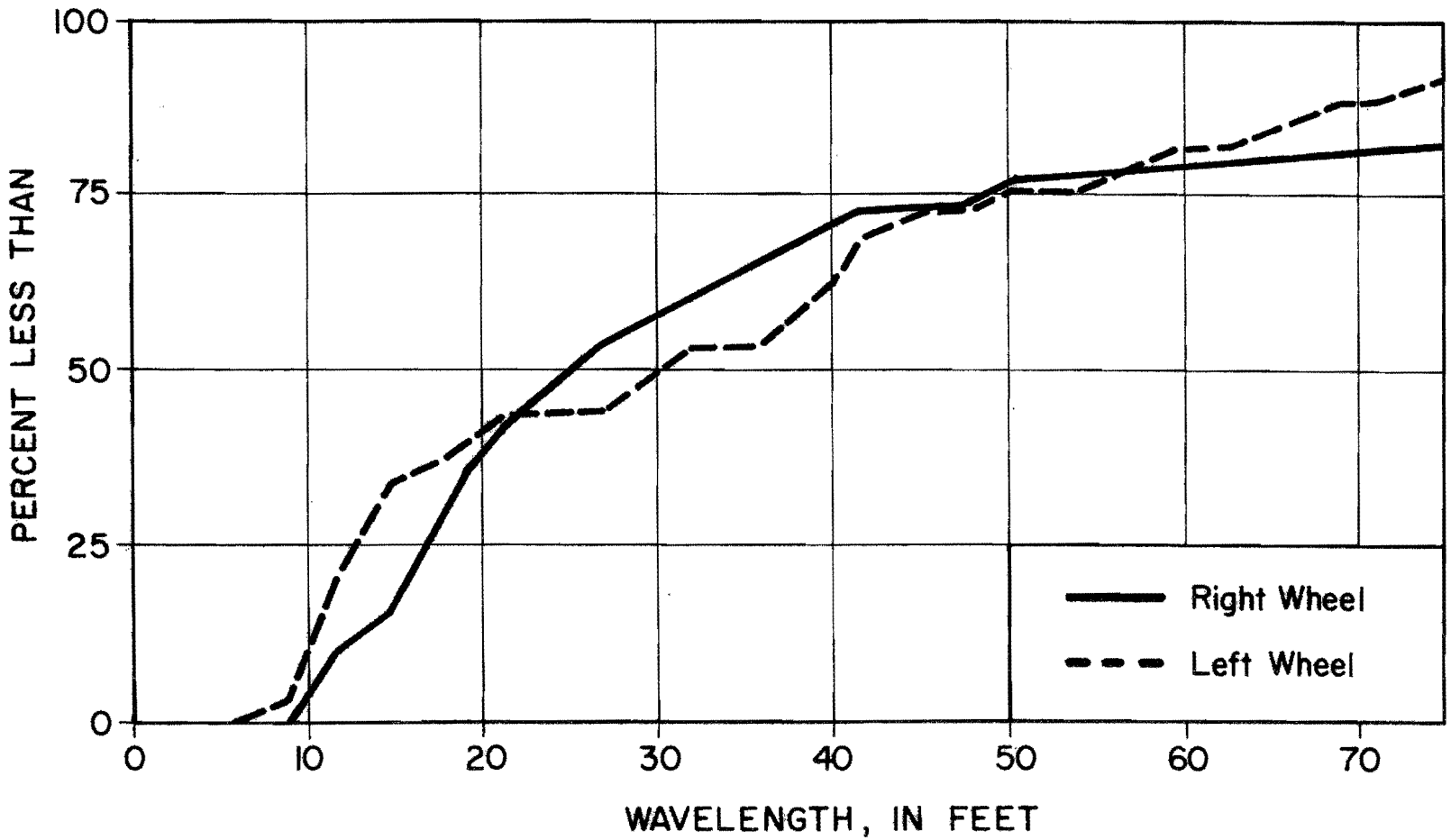

FIGURE VI-12. Distribution of Wavelengths
(Snook 1)

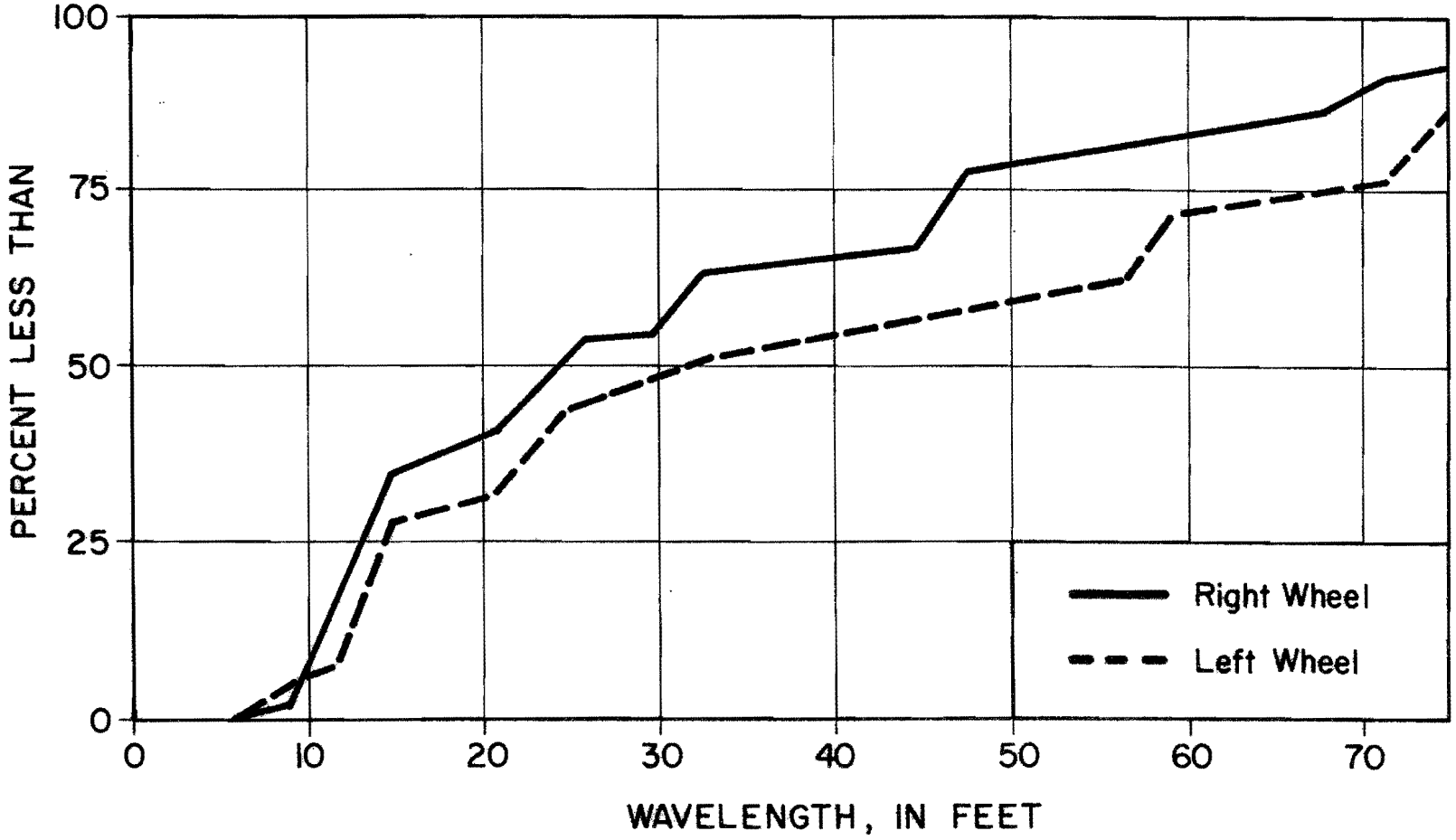

FIGURE VI-13. Distribution of Wavelengths (OSR 1)

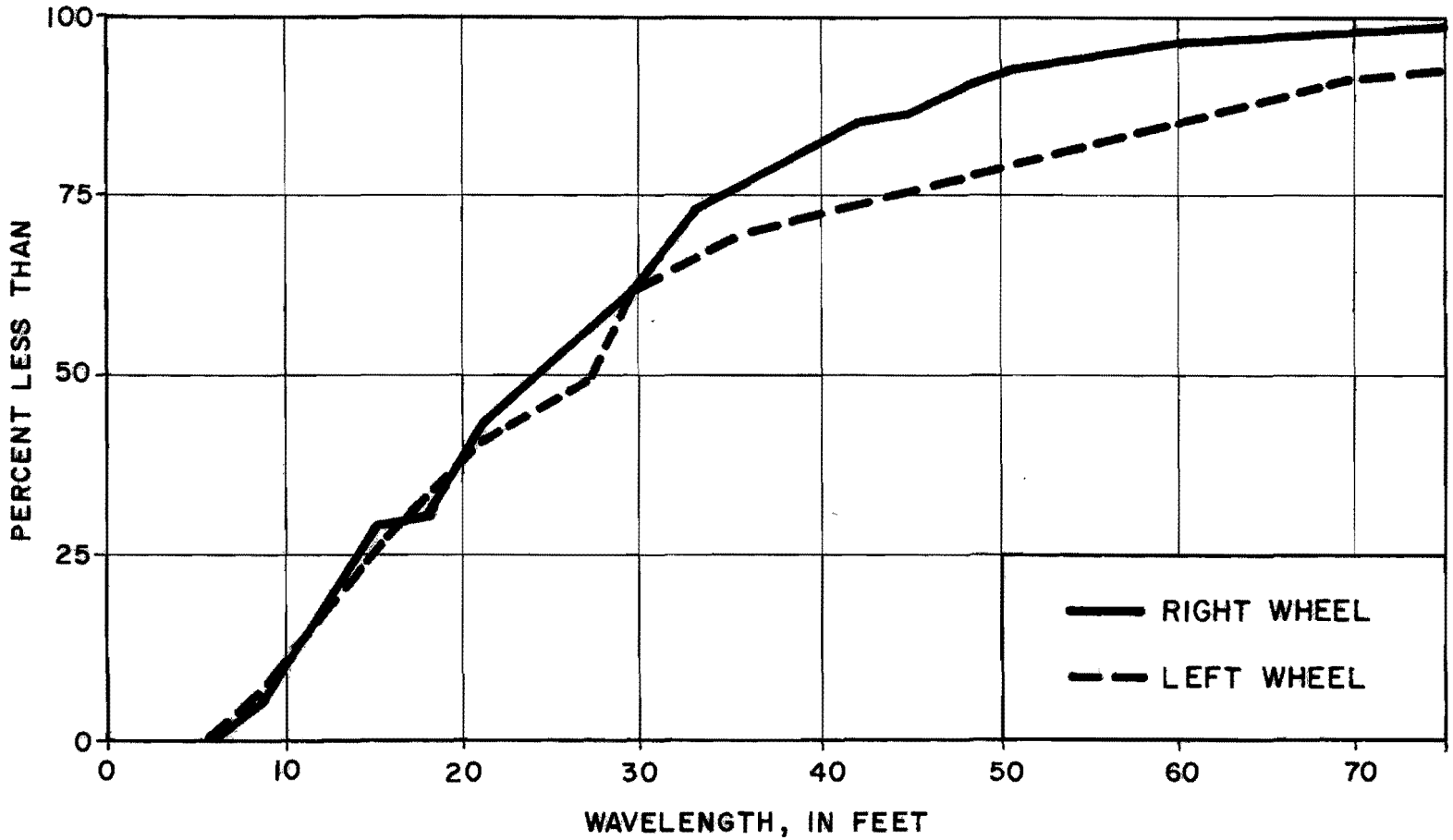

Figure VI-14. Distribution of Wavelengths (OSR 2)

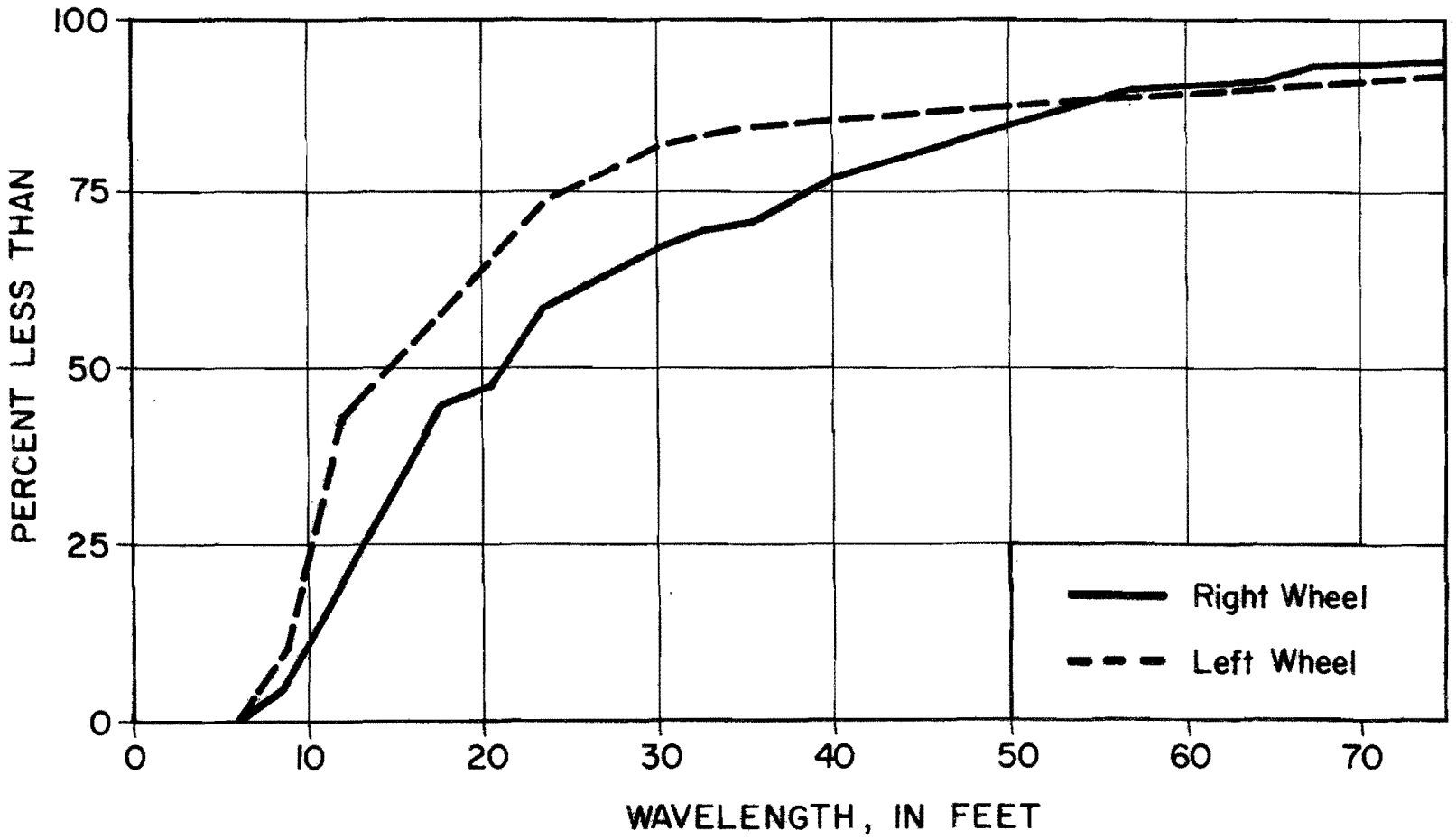

FIGURE VI-15. Distribution of Wavelengths
(OSR 3)

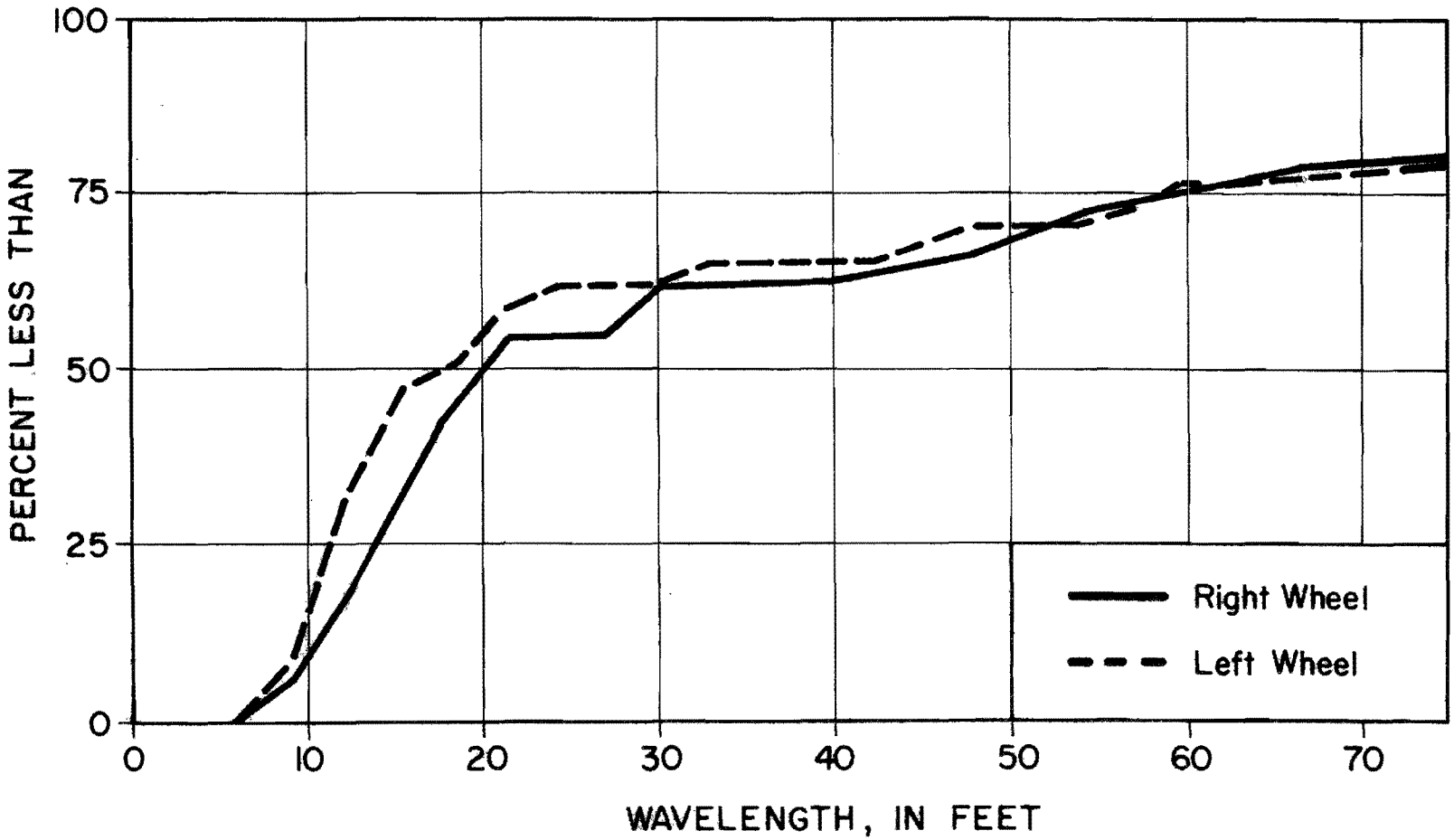

FIGURE VI-16. Distribution of Wavelengths
(Thrall 1)

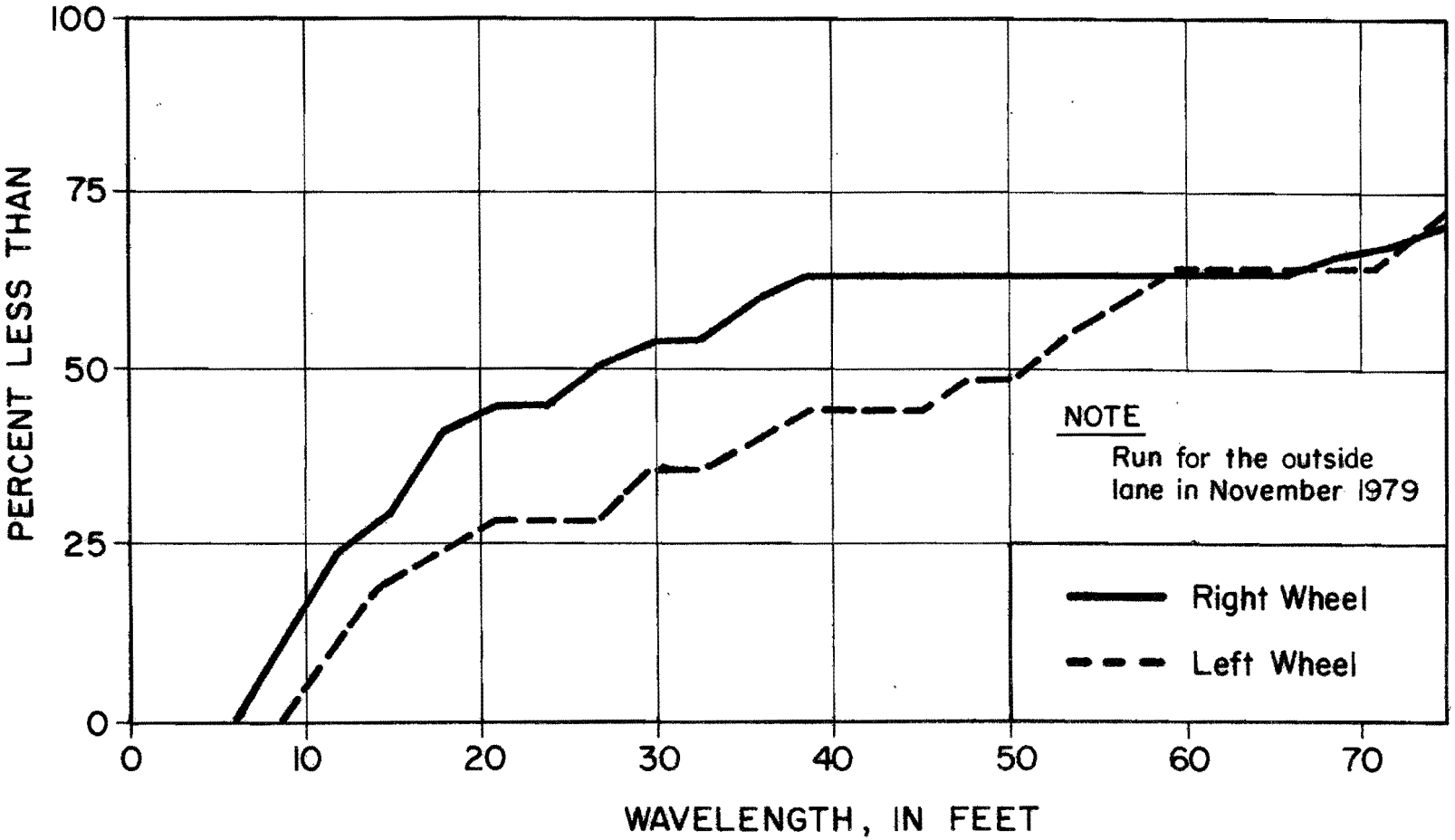

FIGURE VI-17. Distribution of Wavelengths
(San Antonio 410-1)

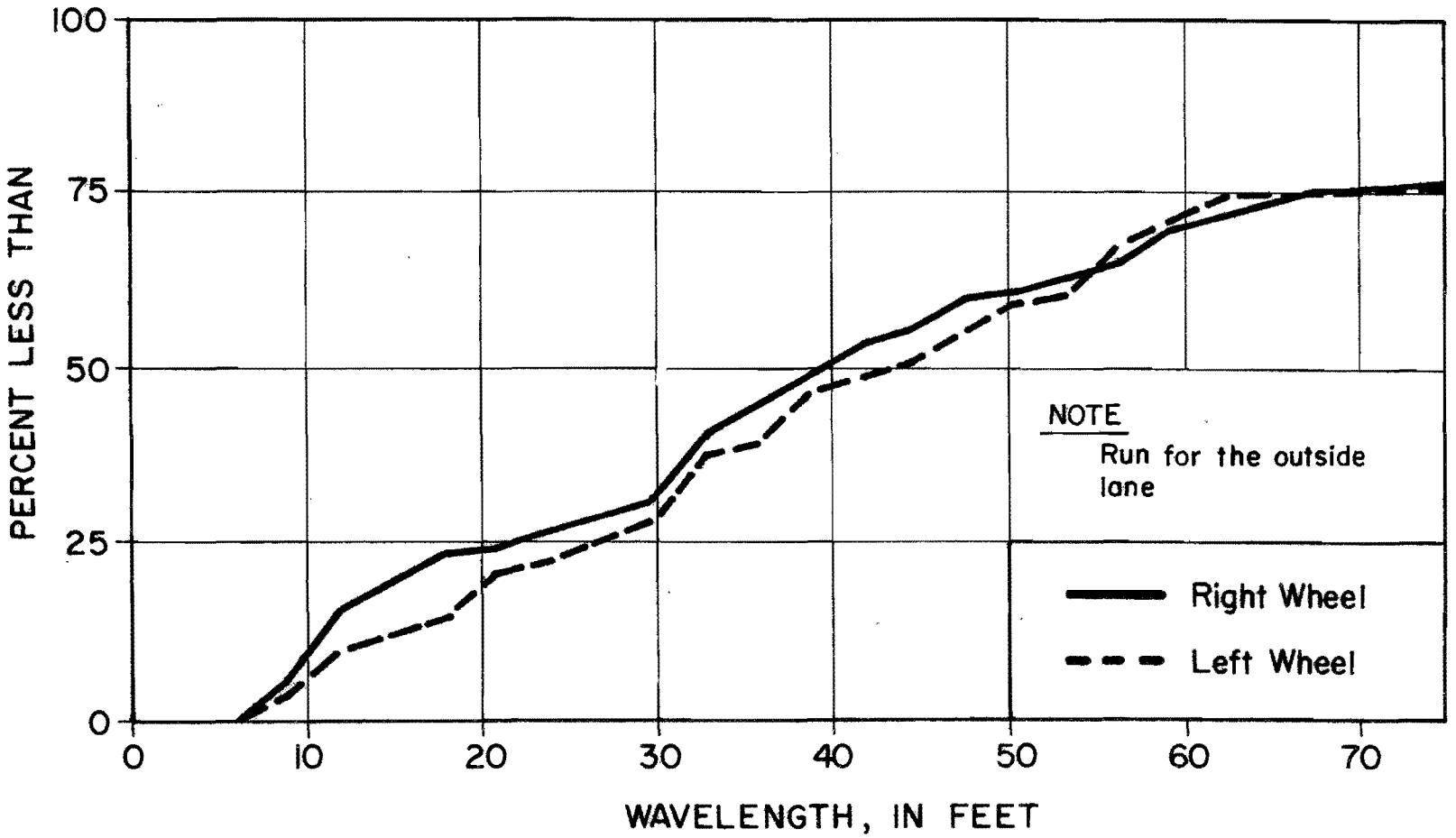

FIGURE VI-18. Distribution of Wavelengths
(San Antonio 37)

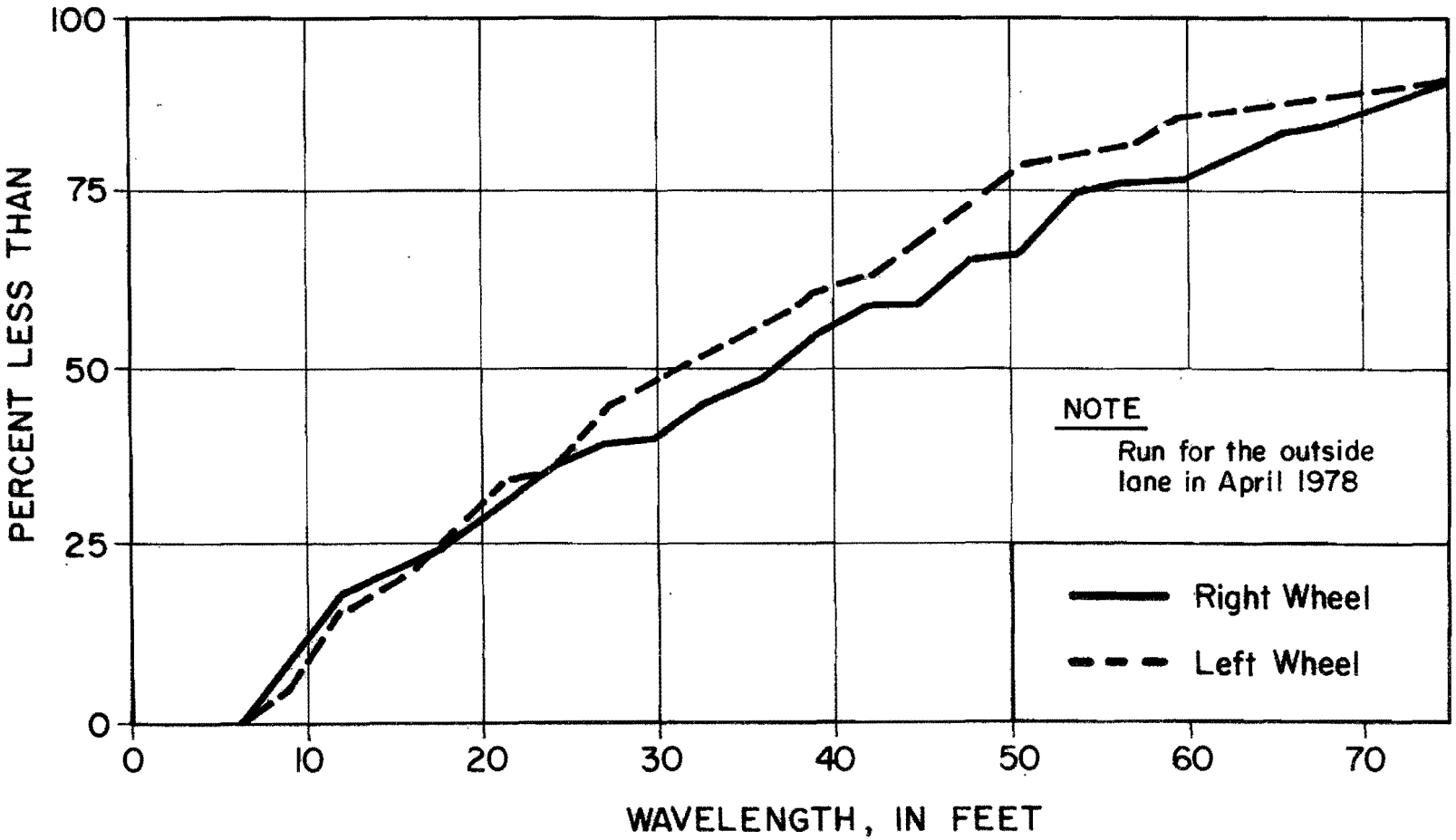

FIGURE VI-19. Distribution of Wavelengths (San Antonio 90-5)

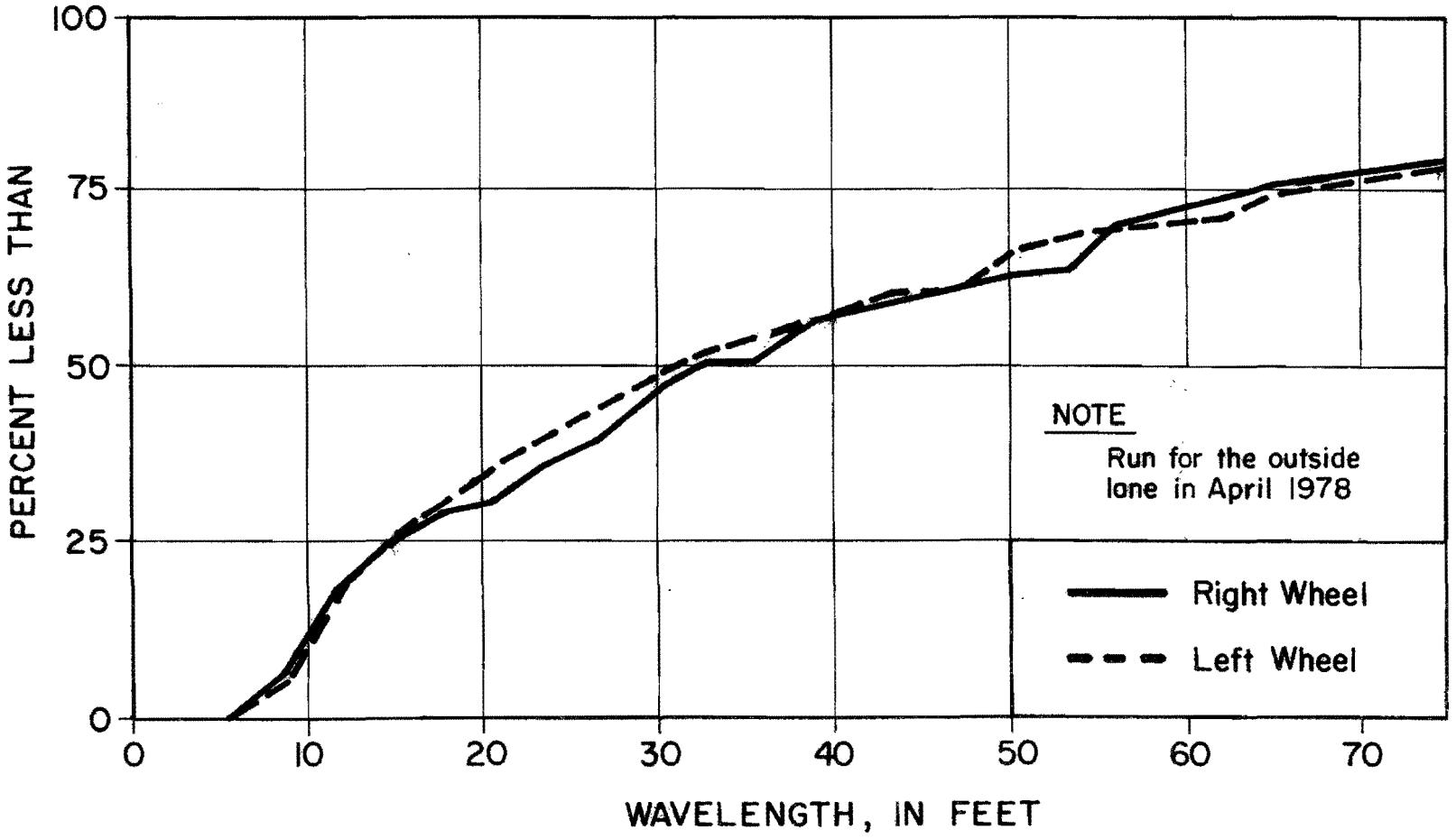

FIGURE VI-20. Distribution of Wavelengths
(San Antonio 90-3 West)

APPENDIX VII

PARAMETER VALUES IN SAN ANTONIO 410 AND SAN ANTONIO 90

TABLE VII-1. Log c and n Values in San Antonio 410-1

Date	Inside Lane				Outside Lane			
	Left Wheel		Right Wheel		Left Wheel		Right Wheel	
(1)	Log c (2)	n (3)	Log c (4)	n (5)	Log c (6)	n (7)	Log c (8)	n (9)
June 79	-3.58	-1.20	-3.58	-1.20	-3.52	-1.19	-3.52	-1.18
November 79	-3.59	-1.22	-3.55	-1.21	-3.56	-1.21	-3.57	-1.21

TABLE VII-3. Log c and n Values in San Antonio 90-1

Date	Inside Lane				Outside Lane			
	Left Wheel		Right Wheel		Left Wheel		Right Wheel	
(1)	Log c (2)	n (3)	Log c (4)	n (5)	Log c (6)	n (7)	Log c (8)	n (9)
October 75	-4.16	-1.37	-4.20	-1.37	-4.00	-1.31	-3.94	-1.28
April 76	-4.17	-1.38	-4.11	-1.34	-4.03	-1.32	-4.04	-1.32
October 76	-4.14	-1.38	-4.08	-1.34	-3.96	-1.31	-3.94	-1.29
April 77	-4.18	-1.44	-4.13	-1.40	-3.90	-1.26	-4.03	-1.34
October 77	-4.10	-1.39	-4.13	-1.38	-3.87	-1.25	-4.02	-1.32
April 78	-4.13	-1.41	-4.17	-1.38	-3.90	-1.28	-4.02	-1.32

TABLE VII-4. Log c and n Values in San Antonio 90-5

Date	Inside Lane				Outside Lane			
	Left Wheel		Right Wheel		Left Wheel		Right Wheel	
(1)	Log c (2)	n (3)	Log c (4)	n (5)	Log c (6)	n (7)	Log c (8)	n (9)
October 75	-3.99	-1.35	-3.98	-1.34	-3.91	-1.33	-3.89	-1.32
April 76	-3.96	-1.33	-3.95	-1.32	-3.92	-1.34	-3.92	-1.33
October 76	-3.94	-1.34	-3.94	-1.34	-3.91	-1.35	-3.91	-1.35
April 77	-4.02	-1.39	-3.97	-1.36	-3.81	-1.29	-3.94	-1.37
October 77	-3.95	-1.37	-4.02	-1.37	-3.82	-1.29	-3.97	-1.36
April 78	-3.93	-1.36	-3.94	-1.33	-4.08	-1.44	-4.15	-1.45

TABLE VII-5. Log c and n Values in San Antonio 90-3 (East)

Date	Inside Lane				Outside Lane			
	Left Wheel		Right Wheel		Left Wheel		Right Wheel	
(1)	Log c (2)	n (3)	Log c (4)	n (5)	Log c (6)	n (7)	Log c (8)	n (9)
October 75	-4.07	-1.37	-4.09	-1.35	-4.04	-1.32	-4.03	-1.31
April 76	-4.15	-1.40	-4.11	-1.38	-4.19	-1.36	-4.18	-1.35
October 76	-4.21	-1.44	-4.16	-1.40	-4.20	-1.39	-4.13	-1.34
April 77	-3.85	-1.31	-4.05	-1.38	-4.15	-1.38	-4.14	-1.38
October 77	-4.02	-1.38	-4.19	-1.41	-4.24	-1.42	-4.27	-1.40
April 78	-4.03	-1.38	-4.25	-1.43	-4.19	-1.41	-4.29	-1.42

TABLE VII-6. Log c and n Values in San Antonio 90-3 (West)

Date	Inside Lane				Outside Lane			
	Left Wheel		Right Wheel		Left Wheel		Right Wheel	
(1)	Log c (2)	n (3)	Log c (4)	n (5)	Log c (6)	n (7)	Log c (8)	n (9)
October 75	-4.04	-1.42	-4.03	-1.41	-4.19	-1.48	-4.20	-1.49
April 76	-4.30	-1.54	-4.21	-1.50	-4.23	-1.51	-4.20	-1.48
October 76	-4.24	-1.52	-4.17	-1.48	-4.18	-1.50	-4.18	-1.49
April 77	-3.91	-1.38	-4.07	-1.45	-4.02	-1.41	-4.17	-1.51
October 77	-4.07	-1.44	-4.32	-1.54	-3.99	-1.38	-4.15	-1.46
April 78	-4.05	-1.44	-4.31	-1.54	-3.99	-1.39	-4.18	-1.48

APPENDIX VIII

REGRESSION ANALYSIS SUMMARY

TABLE VIII-1. List of Independent Variables
Used in Regression Analyses

DEPTH = effective depth of pavement, in inches

TIME = time since construction or last rehabilitation, in years

CEC = cation exchange capacity, in $\frac{\text{meq}}{100\ \text{gm}}$

ESP = exchange sodium percentage, in percent

CLAY = percent clay (grain size less than 0.002 mm)

AC = activity $(\frac{\text{Plasticity Index}}{\text{CLAY}})$

CEAC = cation exchange activity $(\frac{\text{CEC}}{\text{CLAY}})$

COLE = coefficient of linear extensibility

TH = Thornthwaite moisture index

RANGE = range of Thornthwaite moisture index

TABLE VIII-2. Summary of Regression Models for Log c

Model Number (1)	Dependent Variable Transformation (2)	Independent Variables (3)	Left Wheel			Right Wheel		
			Regression Coefficients (4)	Intercept (5)	R^2 (6)	Regression Coefficients (7)	Intercept (8)	R^2 (9)
1	log	DEPTH	-0.892	-3.381	0.67	-0.745	-2.728	0.73
		TIME	0.433			0.586		
		CEC	1.011			1.228		
		ESP	0.190			0.160		
		CLAY	-0.902			-1.606		
2	log	DEPTH	----	----	---	-0.728	-5.620	0.70
		TIME				0.634		
		CEC				0.835		
		ESP				0.147		
		COLE				-0.666		

TABLE VIII-2. (Continuation)

Model Number (1)	Dependent Variable Transformation (2)	Independent Variables (3)	Left Wheel			Right Wheel		
			Regression Coefficients (4)	Intercept (5)	R^2 (6)	Regression Coefficients (7)	Intercept (8)	R^2 (9)
3	log	DEPTH	-1.067	-3.085	0.78	-0.805	-3.447	0.77
		TIME	0.296			0.493		
		AC	-1.042			-1.197		
		ESP	0.191			0.123		
4	log	DEPTH	----	----	---	-0.773	-3.316	0.72
		TIME				0.518		
		CEAC				0.674		
		ESP				0.126		
5	log	DEPTH	----	----	---	-0.524	-3.135	0.69
		TIME				0.599		
		CEC				0.933		
		CLAY				-1.183		

TABLE VIII-2. (Continuation)

Model Number (1)	Dependent Variable Transformation (2)	Indepent Variables (3)	Left Wheel			Right Wheel		
			Regression Coefficients (4)	Intercept (5)	R^2 (6)	Regression Coefficients (7)	Intercept (8)	R^2 (9)
6	log	DEPTH	----	----	---	-0.523	-5.172	0.67
		TIME				0.628		
		CEC				0.614		
		COLE				-0.463		
7	log	DEPTH	-0.809	-3.264	0.73	-0.638	-3.563	0.75
		TIME	0.320			0.508		
		AC	-0.797			-1.039		
8	log	DEPTH	-1.012	-2.954	0.73	----	----	---
		TIME	0.272					
		ESP	0.150					

TABLE VIII-2. (Continuation)

Model Number (1)	Dependent Variable Transformation (2)	Indepent Variables (3)	Left Wheel			Right Wheel		
			Regression Coefficients (4)	Intercept (5)	R^2 (6)	Regression Coefficients (7)	Intercept (8)	R^2 (9)
9	log	DEPTH	-1.175	-2.712	0.70	----	----	---
		AC	-0.899					
		ESP	0.214					
10	log	DEPTH	-0.742	-2.551	0.64	----	----	---
		TIME	0.453					
		TH	-0.513					
11	log	DEPTH	-1.152	-1.628	0.56	----	----	---
		ESP	0.190					
		CLAY	-0.549					
12	log	DEPTH	----	----	---	-0.634	-2.498	0.66
		TIME				0.473		
		CLAY				-0.501		

TABLE VIII-2. (Continuation)

Model Number (1)	Dependent Variable Transformation (2)	Independent Variables (3)	Left Wheel			Right Wheel		
			Regression Coefficients (4)	Intercept (5)	R^2 (6)	Regression Coefficients (7)	Intercept (8)	R^2 (9)
13	log	DEPTH	----	----	---	-0.615	-3.691	0.65
		TIME				0.511		
		COLE				-0.248		
14	log	DEPTH	-0.810	-3.128	0.70	-0.639	-3.384	0.69
		TIME	0.296			0.477		
15	log	DEPTH	-0.889	-2.797	0.61	-0.768	-2.851	0.46

TABLE VIII-3. Summary of Regression Models for Log (-n)

Model Number (1)	Dependent Variable Transformation (2)	Independent Variables (3)	Left Wheel			Right Wheel		
			Regression Coefficients (4)	Intercept (5)	R^2 (6)	Regression Coefficients (7)	Intercept (8)	R^2 (8)
1	log	DEPTH	0.128	0.332	0.85	0.099	0.010	0.87
		TIME	-0.020			-0.022		
		CEC	-0.324			-0.255		
		ESP	-0.025			-0.020		
		CLAY	0.368			0.462		
		RANGE	-0.222			-0.185		
2	log	DEPTH	0.153	0.137	0.89	----	----	---
		CEC	-0.240					
		ESP	-0.026					
		CLAY	0.382					
		TH	0.152					
		RANGE	-0.352					

TABLE VIII-3. (Continuation)

Model Number (1)	Dependent Variable Transformation (2)	Independent Variables (3)	Left Wheel			Right Wheel		
			Regression Coefficients (4)	Intercept (5)	R^2 (6)	Regression Coefficients (7)	Intercept (8)	R^2 (9)
3	log	DEPTH	0.120	0.069	0.87	----	----	---
		TIME	-0.022					
		CEC	-0.204					
		CLAY	0.333					
		TH	0.152					
		RANGE	-0.279					
4	log	DEPTH	0.122	0.675	0.85	----	----	---
		TIME	-0.038					
		CEC	-0.144					
		COLE	0.155					
		TH	0.130					
		RANGE	-0.234					

TABLE VIII-3. (Continuation)

Model Number (1)	Dependent Variable Transformation (2)	Independent Variables (3)	Left Wheel			Right Wheel		
			Regression Coefficients (4)	Intercept (5)	R^2 (6)	Regression Coefficients (7)	Intercept (8)	R^2 (9)
5	log	DEPTH	0.156	0.730	0.84	----	----	---
		CEC	-0.125					
		ESP	-0.022					
		COLE	0.157					
		TH	0.133					
		RANGE	-0.316					
6	log	DEPTH	----	----	---	0.081	0.161	0.86
		TIME				-0.036		
		CEC				-0.201		
		CLAY				0.308		
		COLE				0.066		
		RANGE				-0.122		

TABLE VIII-3. (Continuation)

Model Number (1)	Dependent Variable Transformation (2)	Independent Variables (3)	Left Wheel			Right Wheel		
			Regression Coefficients (4)	Intercept (5)	R^2 (6)	Regression Coefficients (7)	Intercept (8)	R^2 (9)
7	log	DEPTH	----	----	---	0.078	-0.60	0.85
		TIME				-0.029		
		CEC				-0.210		
		CLAY				0.418		
		RANGE				-0.137		
8	log	DEPTH	----	----	---	0.098	0.011	0.82
		TIME				-0.052		
		CEC				-0.178		
		CLAY				0.265		
		COLE				0.105		

TABLE VIII-3. (Continuation)

Model Number (1)	Dependent Variable Transformation (2)	Independent Variables (3)	Left Wheel			Right Wheel		
			Regression Coefficients (4)	Intercept (5)	R^2 (6)	Regression Coefficients (7)	Intercept (8)	R^2 (9)
9	log	DEPTH	----	----	---	0.080	-0.177	0.82
		TIME				-0.040		
		CEC				-0.229		
		CLAY				0.424		
		TH				-0.073		
10	log	DEPTH	0.130	0.027	0.86	----	----	---
		CEC	-0.166					
		CLAY	0.322					
		TH	0.160					
		RANGE	-0.304					

TABLE VIII-3. (Continuation)

Model Number (1)	Dependent Variable Transformation (2)	Independent Variables (3)	Left Wheel			Right Wheel		
			Regression Coefficients (4)	Intercept (5)	R^2 (6)	Regression Coefficients (7)	Intercept (8)	R^2 (9)
11	log	DEPTH	0.140	0.317	0.84	0.112	-0.007	0.86
		CEC	-0.302			-0.231		
		ESP	-0.029			-0.024		
		CLAY	0.365			0.459		
		RANGE	-0.246			-0.212		
12	log	DEPTH	0.136	0.552	0.82	----	----	---
		CEC	-0.075					
		COLE	0.133					
		TH	0.143					
		RANGE	-0.280					

TABLE VIII-3. (Continuation)

Model Number (1)	Dependent Variable Transformation (2)	Independent Variables (3)	Left Wheel			Right Wheel		
			Regression Coefficients (4)	Intercept (5)	R^2 (6)	Regression Coefficients (7)	Intercept (8)	R^2 (9)
13	log	DEPTH	0.106	0.806	0.81	-0.084	0.679	0.81
		TIME	-0.043			-0.048		
		CEC	-0.207			-0.125		
		COLE	0.152			0.198		
		RANGE	-0.134			0.101		
14	log	DEPTH	0.102	0.435	0.83	0.045	0.526	0.71
		CEAC	-0.182			-0.202		
		AC	0.127			0.151		
		TH	0 .109			-0.078		
		RANGE	-0.311			-0.179		

TABLE VIII-3. (Continuation)

Model Number (1)	Dependent Variable Transformation (2)	Independent Variables (3)	Left Wheel			Right Wheel		
			Regression Coefficients (4)	Intercept (5)	R^2 (6)	Regression Coefficients (7)	Intercept (8)	R^2 (9)
15	log	DEPTH	0.113	0.205	0.81	0.090	-0.102	0.83
		CEC	-0.223			-0.164		
		CLAY	0.297			0.401		
		RANGE	-0.186			-0.162		
16	log	DEPTH	0.150	-0.164	0.81	----	----	---
		CLAY	0.213					
		TH	0.209					
		RANGE	-0.303					
17	log	DEPTH	0.148	0.345	0.81	----	----	---
		COLE	0.115					
		TH	0.177					
		RANGE	-0.283					

TABLE VIII-3. (Continuation)

Model Number (1)	Dependent Variable Transformation (2)	Independent Variables (3)	Left Wheel			Right Wheel		
			Regression Coefficients (4)	Intercept (5)	R^2 (6)	Regression Coefficients (7)	Intercept (8)	R^2 (9)
18	log	DEPTH	0.099	0.437	0.80	0.042	0.530	0.66
		CEAC	-0.210			-0.235		
		TH	0.094			-0.096		
		RANGE	-0.309			-0.177		
19	log	DEPTH	0.136	-0.0002	0.70	0.106	-0.253	0.77
		CLAY	0.122			0.272		
		RANGE	-0.129			-0.120		
20	log	DEPTH	0.159	-0.370	0.65	0.128	-0.596	0.71
		CLAY	0.183			0.329		
21	log	DEPTH	0.163	0.070	0.67	0.130	0.181	0.68
		COLE	0.116			0.191		

TABLE VIII-3. (Continuation)

Model Number (1)	Dependent Variable Transformation (2)	Independent Variables (3)	Left Wheel			Right Wheel		
			Regression Coefficients (4)	Intercept (5)	R^2 (6)	Regression Coefficients (7)	Intercept (8)	R^2 (9)
22	log	DEPTH	0.130	-0.024	0.52	0.076	0.028	0.21

TABLE VIII-4. Summary of Regression Models for Log c_1

Model Number (1)	Dependent Variable Transformation (2)	Independent Variables (3)	Left Wheel			Right Wheel		
			Regression Coefficients (4)	Intercept (5)	R^2 (6)	Regression Coefficients (7)	Intercept (8)	R^2 (9)
1	log	TIME	0.327	0.858	0.55	----	----	---
		ESP	0.085					
		COLE	0.590					
		TH	0.447					
		RANGE	-1.221					
2	log	TIME	0.323	-0.367	0.60	0.388	-0.219	0.73
		ESP	0.222			0.149		
		COLE	1.237			1.361		
		AC	-2.042			-2.044		
3	log	TIME	0.267	2.791	0.56	----	----	---
		CEC	-0.721					
		COLE	0.798					
		RANGE	-1.070					

TABLE VIII-4. (Continuation)

Model Number (1)	Dependent Variable Transformation (2)	Independent Variables (3)	Left Wheel			Right Wheel		
			Regression Coefficients (4)	Intercept (5)	R^2 (6)	Regression Coefficients (7)	Intercept (8)	R^2 (9)
4	log	TIME	0.350	0.722	0.52	----	----	---
		ESP	0.084					
		COLE	0.522					
		RANGE	-0.838					
5	log	TIME	0.436	-0.626	0.49	0.489	-1.959	0.60
		CLAY	0.876			1.244		
		TH	0.515			0.422		
		RANGE	-1.674			-1.223		
6	log	TIME	0.226	-0.614	0.44	0.291	-0.465	0.56
		ESP	0.161			0.088		
		COLE	0.647			0.770		
7	log	TIME	0.389	1.193	0.49	0.409	0.713	0.59
		COLE	0.466			0.658		
		RANGE	-1.126			-0.738		

TABLE VIII-4. (Continuation)

Model Number (1)	Dependent Variable Transformation (2)	Independent Variables (3)	Left Wheel			Right Wheel		
			Regression Coefficients (4)	Intercept (5)	R^2 (6)	Regression Coefficients (7)	Intercept (8)	R^2 (9)
8	log	TIME	----	----	---	0.345	-0.258	0.62
		AC				-1.469		
		COLE				1.163		
9	log	TIME	----	----	---	0.379	-3.669	0.53
		ESP				0.105		
		CLAY				1.315		
10	log	ESP	0.188	-0.256	0.42	0.108	-0.086	0.45
		COLE	0.986			1.059		
		AC	-1.336			-1.195		
11	log	TIME	0.206	-0.577	0.30	0.280	-0.445	0.52
		COLE	0.608			0.749		
12	log	ESP	0.151	-0.461	0.34	0.075	-0.268	0.38
		COLE	0.610			0.723		

TABLE VIII-4. (Continuation)

Model Number (1)	Dependent Variable Transformation (2)	Independent Variables (3)	Left Wheel			Right Wheel		
			Regression Coefficients (4)	Intercept (5)	R^2 (6)	Regression Coefficients (7)	Intercept (8)	R^2 (9)
13	log	TIME	----	----	---	0.360	-3.471	0.47
		CLAY				1.234		
14	log	COLE	0.577	-0.444	0.23	0.706	-0.256	0.35

APPENDIX IX

A CASE STUDY: SAN ANTONIO 90-5

APPENDIX IX. A CASE STUDY: SAN ANTONIO 90-5

Background

The location of the San Antonio 90-5 roadway segment was presented in Table 2. The segment starts at station 250+02 of US Highway 90 and ends at station 268+98. It is included within a longer test section where the technique of ponding was studied in a research project carried out by personnel of District 15 of the Texas Department of Highways and Public Transportation and the Center for Transportation Research at the University of Texas at Austin. Complete information about the development of this project and the results obtained have been reported by Steinberg and Watt (33, 36). The ponded section starts at station 242+00 and ends at station 271+00, approximately. It was constructed in a cut. The excavation, which reached a maximum of 27 feet deep, cuts into the Taylor formation, which in this area is a greenish-gray calcareous nodular clay. After the excavation was completed, the site was divided into six areas that were ponded during periods from 30 to 45 days in the spring of 1970 and the first months of 1971. Deep bench marks were set at 2, 3.3, 4.5, 10.5, and 19 feet, to record vertical movements before, during, and after ponding. Dry density and moisture content of the soil were also measured in the field. From the data collected, Watt and Steinberg (36) concluded that water penetrated only the upper 3 feet of soil during ponding but some wetting at depth was indicated after the area had been drained. These authors also reported that about 50 percent of the potential vertical rise was achieved by the ponding.

After the end of construction (November 1971), vertical movements were still being recorded. These data, analyzed by Steinberg (33), show that, even though a sustantial part of the potential vertical rise took place before November 1971, in July 1973 the subgrade was still heaving. Steinberg pointed out that movement was measured initially on the shallowest bench marks, while later the rods at 10.5 feet deep began to indicate vertical movement.

Also, as part of research project 1-10-76-224, being developed by the Texas Department of Highways and Public Transportation, pavement roughness has been measured periodically and the Serviceability Index on different segments of the test section obtained. In Table IX-1, the Serviceability Indexes for two of these segments, that approximately coincide with San Antonio 90-5, are presented.

Prediction of Serviceability Index Reduction

In the section of this study entitled "Methods of Analysis and Results," an equation for the prediction of the Serviceability Index reduction has been presented. The equation is:

$$\Delta SI = 0.087\ DEPTH^{-0.20} TIME^{0.53} ESP^{0.13} CEC^{-1.22}$$

$$\times\ CLAY^{3.05} AC^{-1.31} RANGE^{-1.22} \qquad \text{(IX-1)}$$

where

ΔSI = Serviceability Index reduction

DEPTH = effective depth of pavement, in inches

TIME = time since construction or last rehabilitation, in years.

TABLE IX-1. Serviceability Indexes in US-90

Segment	Serviceability Index								
	Feb. 72	July 72	Aug. 72	Jan. 74	May 75	Oct. 75	Apr. 76	Oct. 76	Apr. 77
252+70 to 264+40	3.5	3.5	3.8	3.2	2.9	2.7	3.3	2.8	3.0
264+40 to 276+20	---	3.8	4.0	---	3.7	3.3	3.4	3.5	3.8

NOTES 1. San Antonio 90-5 from Station 250+02 to 268+98

2. End of construction in November 1971

ESP = exchange sodium percentage

CEC = cation exchange capacity, in meq/100 gm

CLAY = percent clay (grain size less than 0.002 mm)

AC = activity $\left(\frac{\text{Plasticity Index}}{\text{CLAY}}\right)$

RANGE = range of values of the Thornthwaite moisture index for a 20 year period.

The pavement structure within San Antonio 90-5 roadway segment has the following characteristics:

HMAC	3 inches
Type A Grade 1 Base	8 inches
Type A Grade 4 Base	6 inches
Clay Gravel Grade 4	18 inches

The effective depth of this pavement was calculated according to the procedure outlined in Chapter 3, "Data Collection", assuming the following values of the modulus of elasticity for the different materials:

HMAC	200,000 psi
Type A Grade 1 Base	30,000 psi
Type A Grade 4 Base	30,000 psi
Clay Gravel Grade 4	20,000 psi

The calculated effective depth of asphalt concrete is equal to 20.9 inches.

The range of values of the Thornthwaite moisture index for a 20 year period in Bexar County is 62.6.

Also, a soil sample was taken from the slope of the excavation, approximately at the middle of San Antonio 90-5 (≈ station 260+00).

The percent clay, plasticity index, cation exchange capacity, and exchange sodium percentage of the soil sample were determined. They have been presented in Table 8.

Thus the values of the independent variables (except TIME) in equation (IX-1) are:

DEPTH = 20.9 inches

ESP = 16.3%

CEC = 68 meq/100 gm

CLAY = 48%

AC = 1.04

RANGE = 62.6

Substituting these values in equation (IX-1), it becomes:

$$\Delta SI = 0.3294\ TIME^{0.53} \quad \ldots\ldots\ldots\ldots\ldots\ldots\ldots \quad (IX\text{-}2)$$

Thus, this equation allows the estimation of the values of the Serviceability Index (SI) with time in San Antonio 90-5 if the Serviceability Index value at the end of construction is known. Ideally, this value could be as high as 5 but in practice most roadways have a Serviceability Index value between 4.0 and 4.5 at the end of construction. Then, two prediction curves have been calculated, using equation IX-2 and two different hypotheses:

Hypothesis 1: SI = 5.00 at TIME = 0

Hypothesis 2: SI = 4.25 at TIME = 0

These two curves are presented in Figure IX-1. Also in this figure,

the measured values of the Serviceability Index (SI) shown in Table IX-1 are plotted. Several observations can be made:

1. The measured SI values from station 264+40 to 276+20 are higher than those from station 252+72 to 264+40. Maybe this is due to the fact that the first roadway segment (264+40 to 276+20) lies at one of the ends of the excavation where the subgrade soil is less active and even has some portion of fill.
2. The prediction curves have been calculated using data from a soil sample taken at station 260+00, approximately. Thus, they can be compared with the measured SI values from station 252+72 to 264+40. It seems that the prediction model (Equation IX-2) accounts for the measured trend in the Serviceability Index reduction.
3. Even with the hypothesis of SI = 4.25 at the end of construction, the predicted values of SI with time are higher than those measured, but it should be noticed that, within the first year after the end of construction, SI values as low as 3.5 were measured, indicating that the actual SI value at the end of construction may have been less than 4.25.
4. The prediction model can help in the evaluation of the ponding technique used US Highway 90.

Finally, to show the sensitivity of the Serviceability Index reduction model to the values of the effective depth (DEPTH) and percent clay (CLAY) variables, three curves are presented in Figure IX-2. One of the curves has been calculated with the actual values of all the variables (thus, this curve is the same as the one presented in Figure IX-1). The second curve has been determined varying only the value of

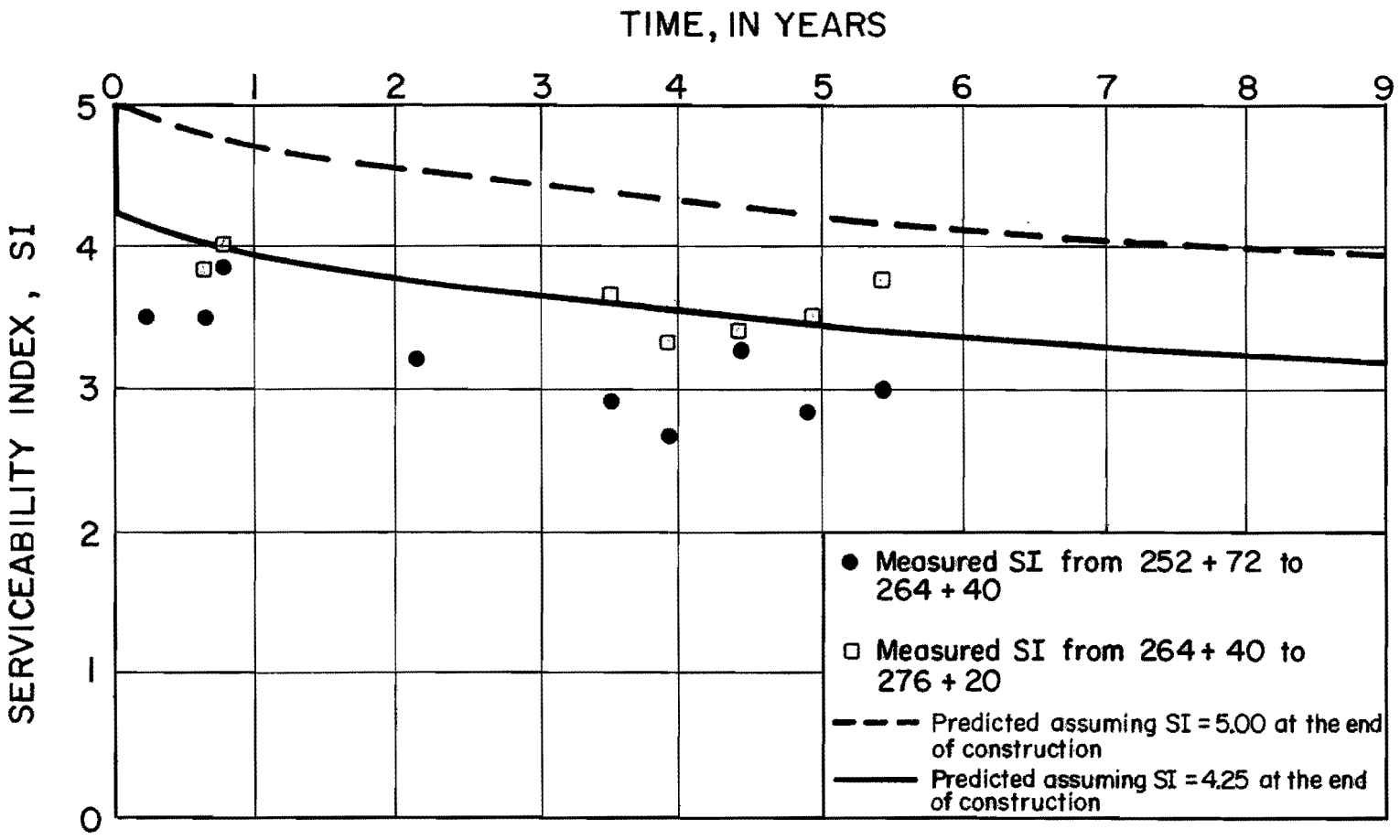

FIGURE IX-1. Prediction of Serviceability Index Reduction
(San Antonio 90-5)

the variable CLAY (CLAY = 60%, instead of CLAY = 48%), and the third curve changing also the value of the variable DEPTH (CLAY = 60% and DEPTH = 15 inches, instead of DEPTH = 20.9 inches).

It can be observed in Figure IX-2 that the percent clay (CLAY) has an appreciable effect in the reduction of the Serviceability Index. On the other hand, the variable DEPTH only alters the result slightly.

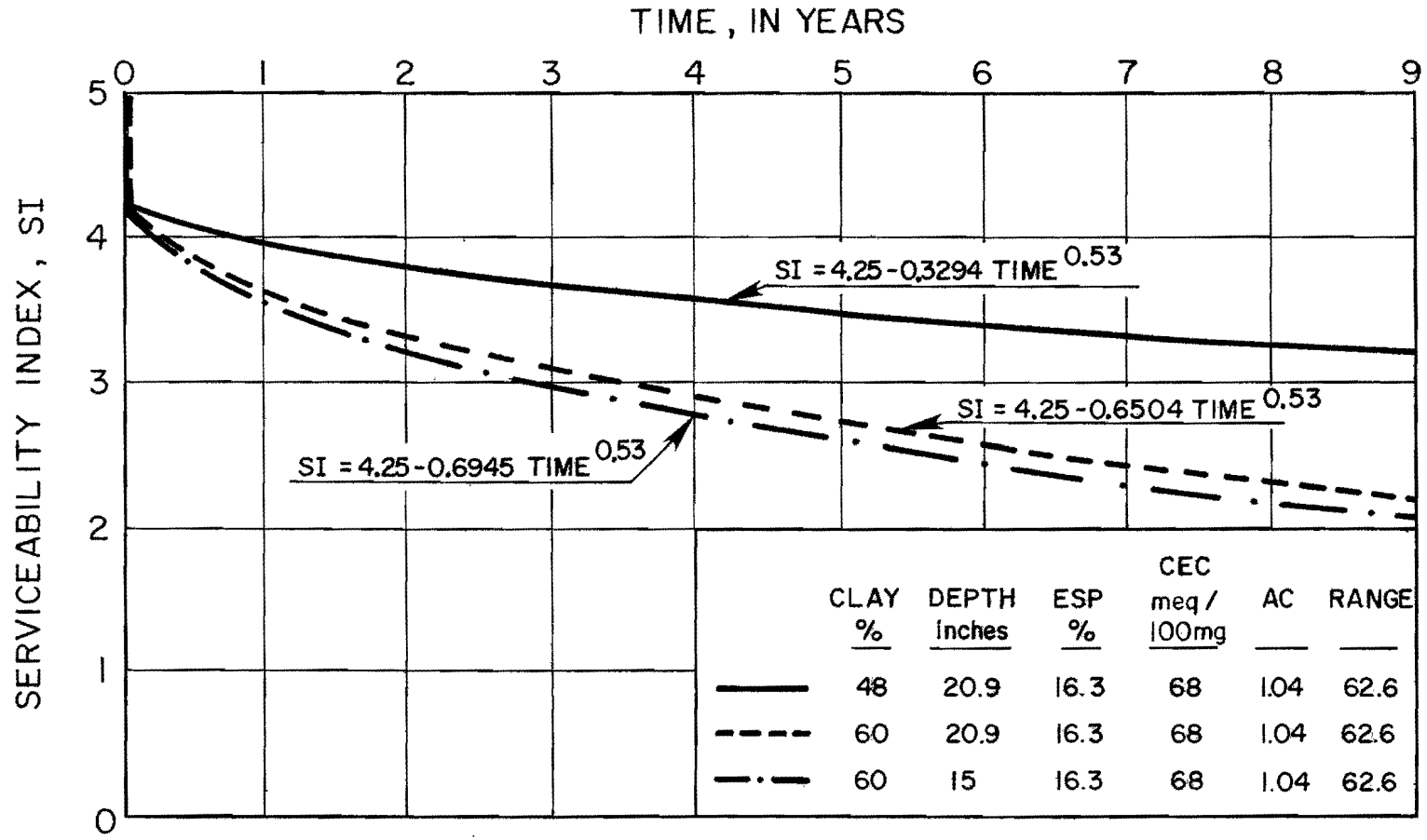

FIGURE IX-2. Sensitivity of the Serviceability Index Reduction Model to the CLAY and DEPTH Variables (San Antonio 90-5)

APPENDIX X

CHARACTERISTICS OF THE REAL PROFILE:

BUMP HEIGHT AND SPACING

APPENDIX X: CHARACTERISTICS OF THE REAL PROFILE: BUMP HEIGHT AND SPACING

The body of this report presented a determination of the two roughness spectrum constants log c and n for each pavement section on which profile data had been collected. The method used for determining the characteristic amplitude for each wave length employed Fast Fourier Transforms (FFT) which assumes that a pavement profile is made up of the sum of sine or cosine waves with different wavelengths and amplitudes. A further study was made on the actual sizes and spacing of bumps in the profile to see how they compare with the spectrum measures determined using the Fourier transforms. It was not expected that the two spectra would be the same because the FFT approach assumes that each bump is actually made up of the sum of several component amplitudes. In fact, it was determined by Stone and Dugundji' (40) that the most probable height of a bump on a profile is

$$h = \sqrt{\sum_{i=1}^{n} a_i^2}$$

where

a_i = the amplitude of the ith wavelength determined by the FFT.

The additional study of the pavement profiles was made with a special computer routine called the "bump counter" which measures the distance between two adjacent high points, called spacing, s, and also measures the average change of elevation in the dip between the two high points, calling that distance twice the bump amplitude, a. Graphs of the bump frequency, f(=1/s bumps per foot) versus the corresponding half amplitude are shown in Figures X-1 through X-16. As can be seen from these

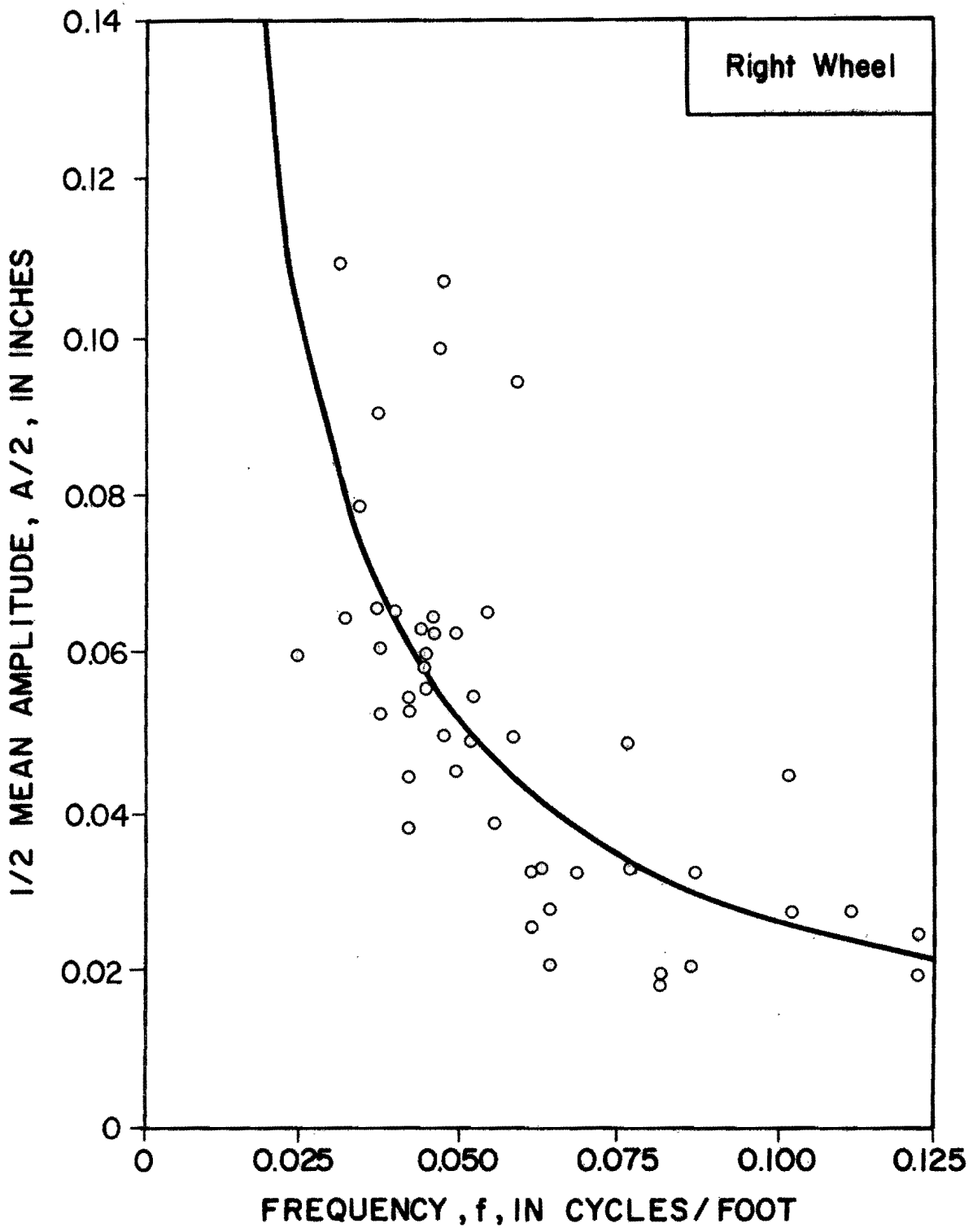

Figure X-1. Half Amplitude versus Bump Frequency in Cycles/Foot For Huntsville, Section 1

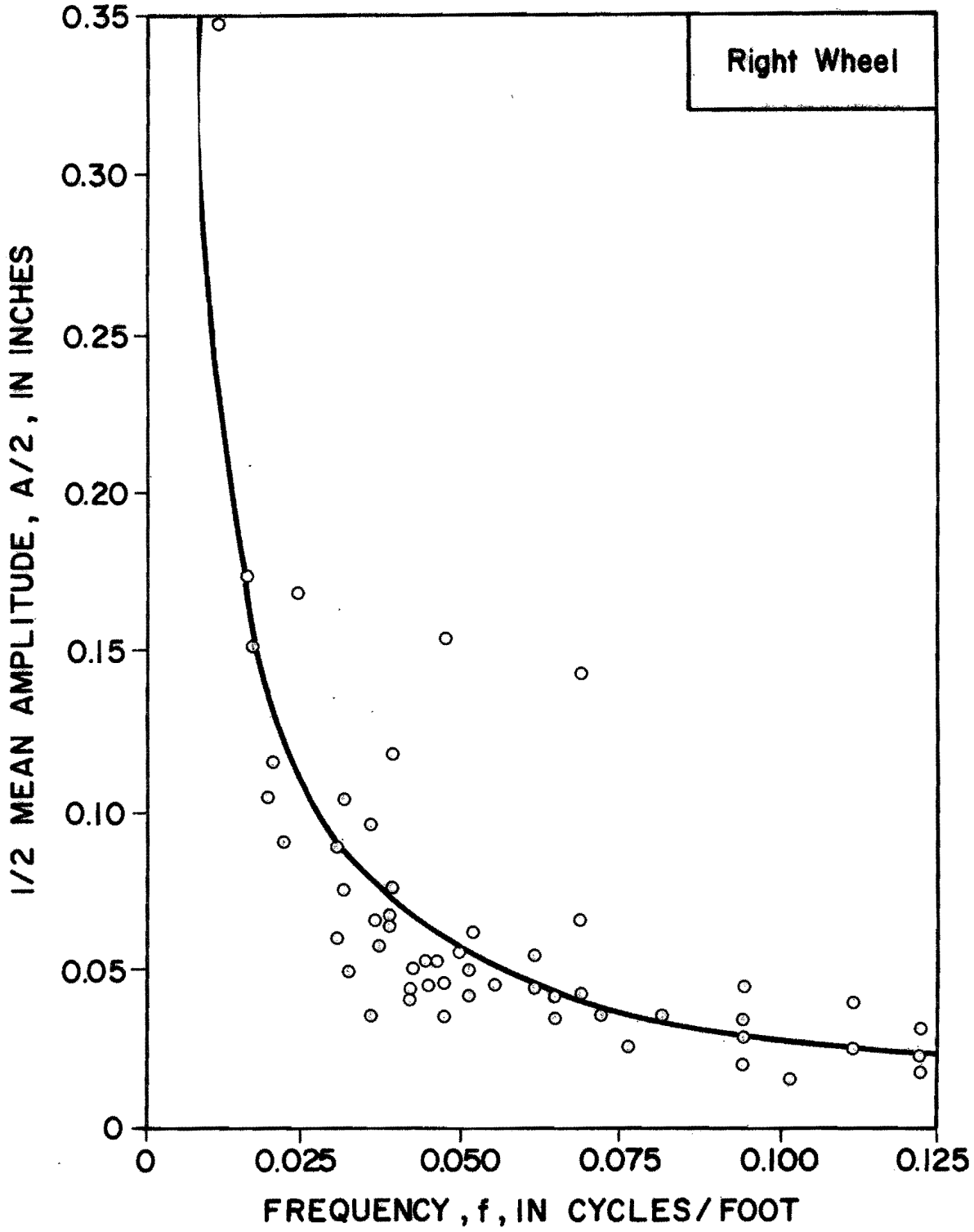

Figure X-2. Half Amplitude versus Bump Frequency in Cycles/Foot for Huntsville Section 2

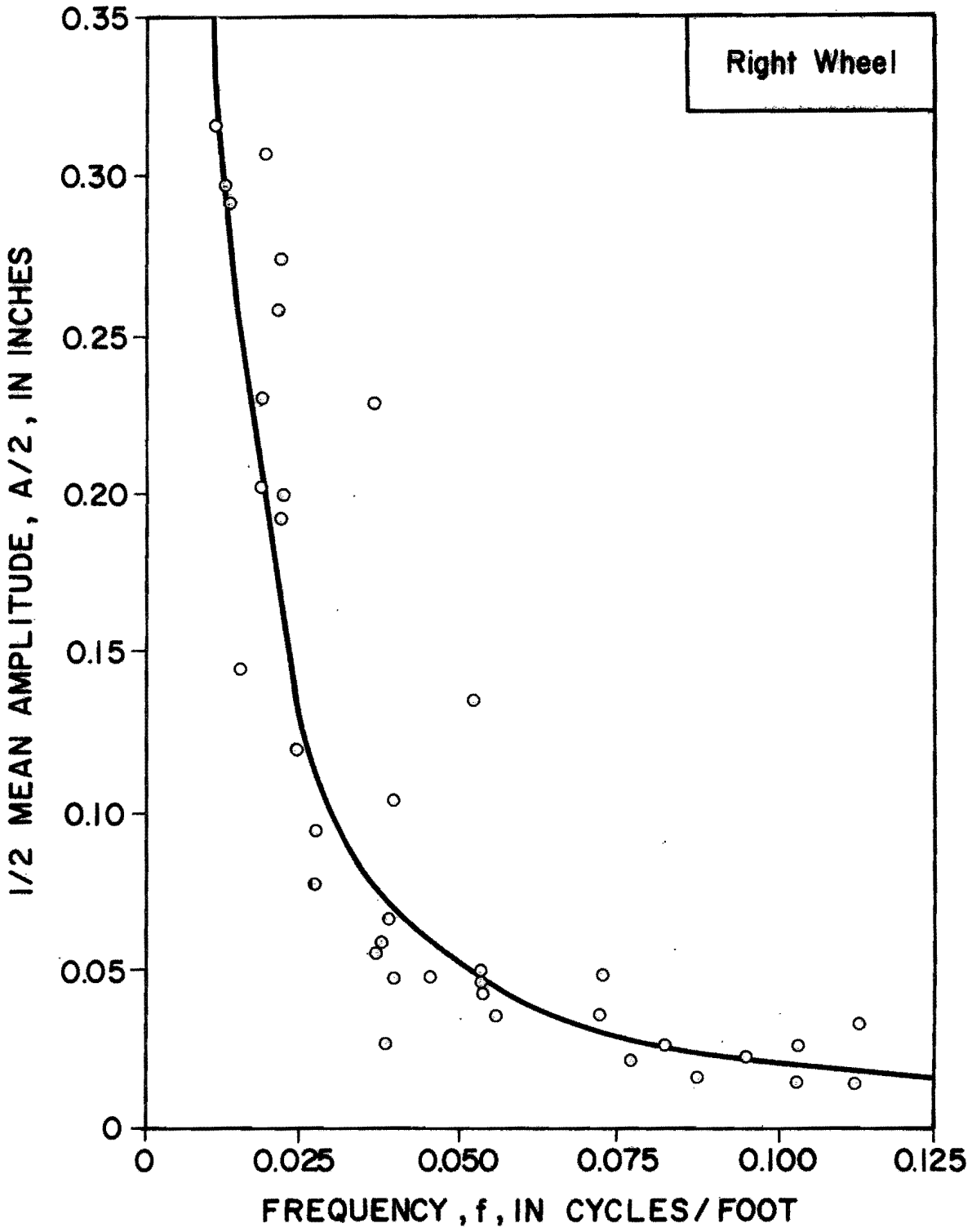

Figure X-3. Half Amplitude versus Bump Frequency in Cycles/Foot for Ben Arnold 1

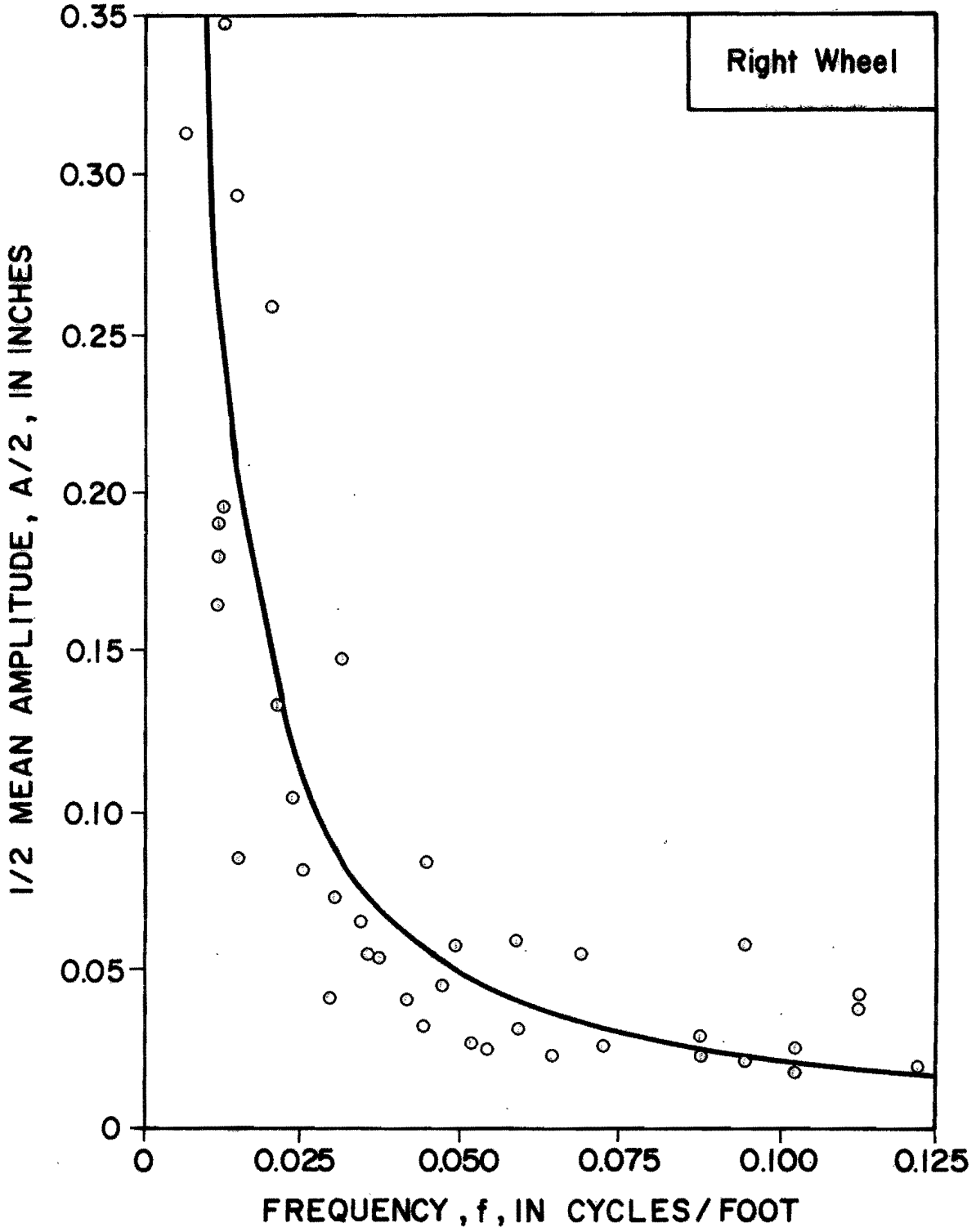

Figure X-4. Half Amplitude versus Bump Frequency is Cycles/Foot for Ben Arnold 2

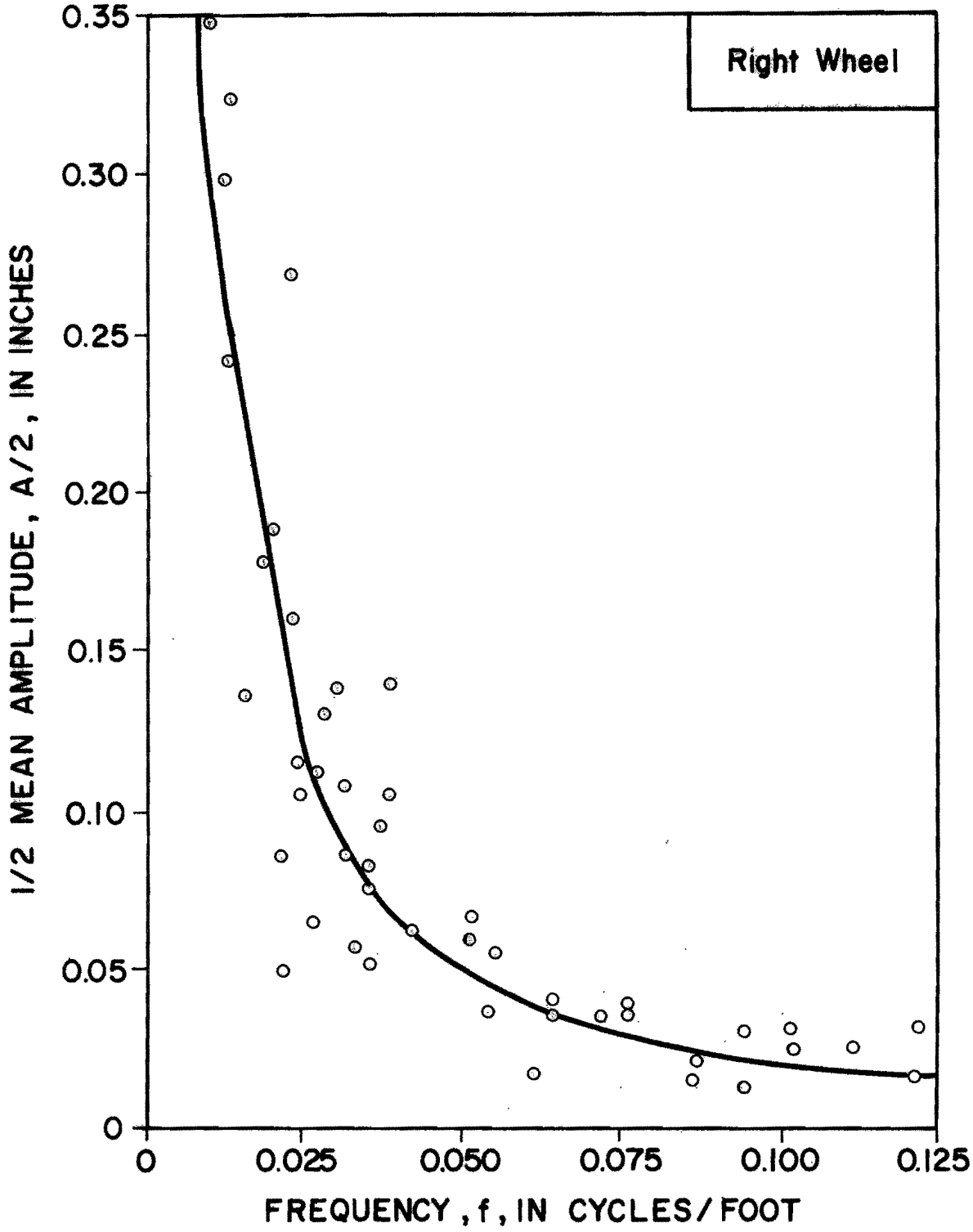

Figure X-5. Half Amplitude versus Bump Frequency in Cycles/Foot for Ben Arnold 3

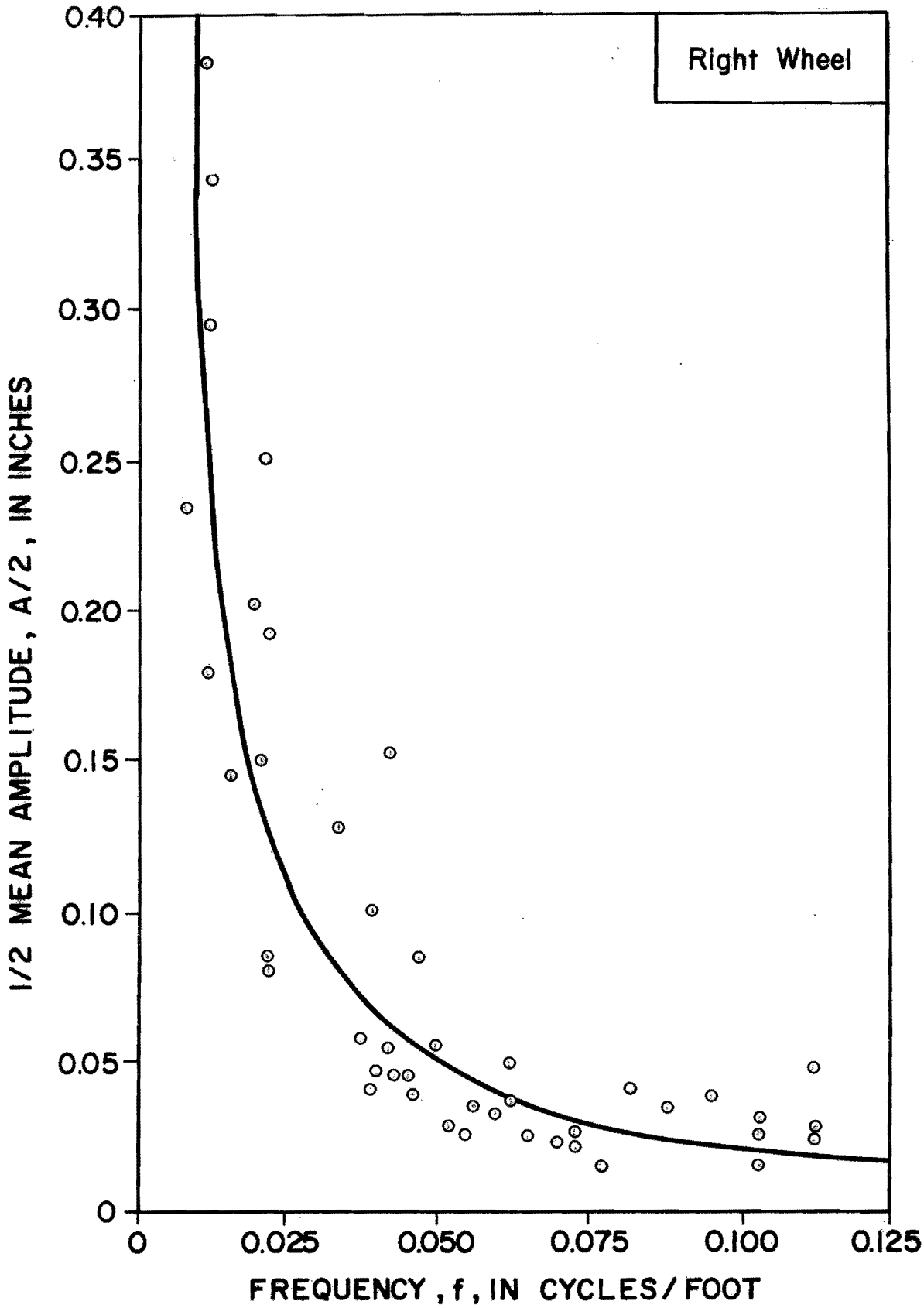

Figure X-6. Half Amplitude versus Bump Frequency in Cycles/Foot for Buckholts 1

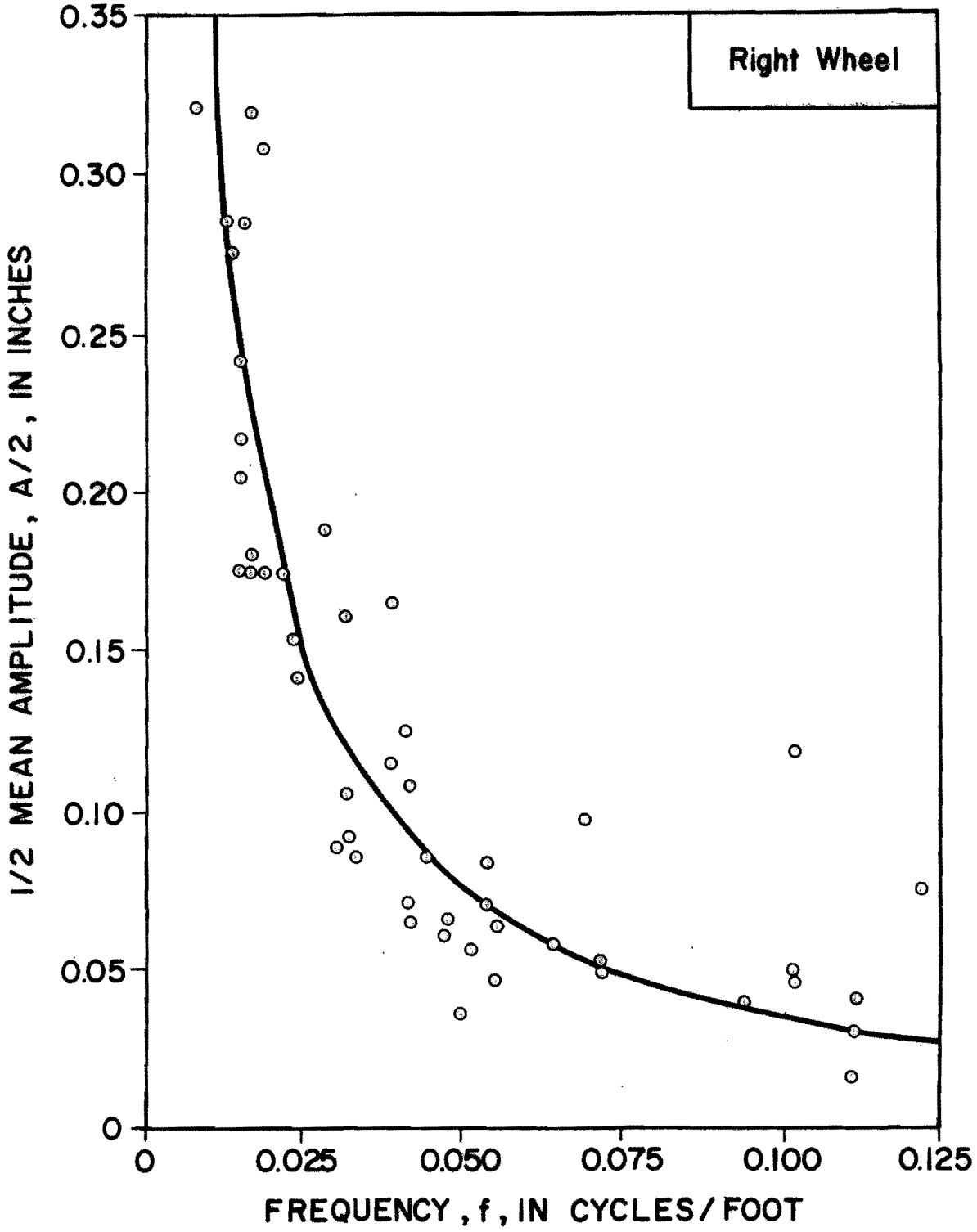

Figure X-7. Half Amplitude versus Bump Frequency in Cycles/Feet for Buckholtd 2

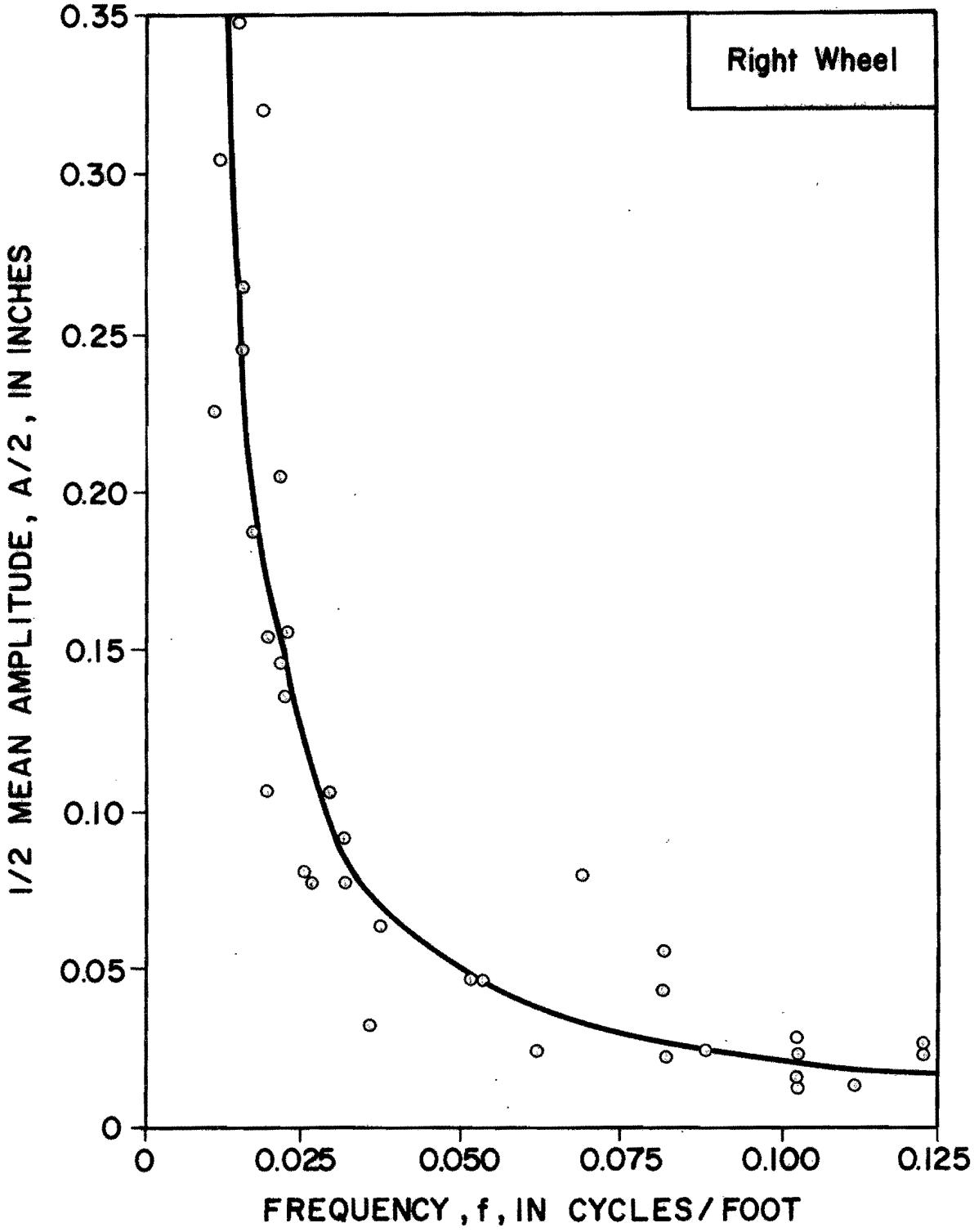

Figure X-8. Half Amplitude versus Bump Frequency in Cycles/Foot for Fairfield 1

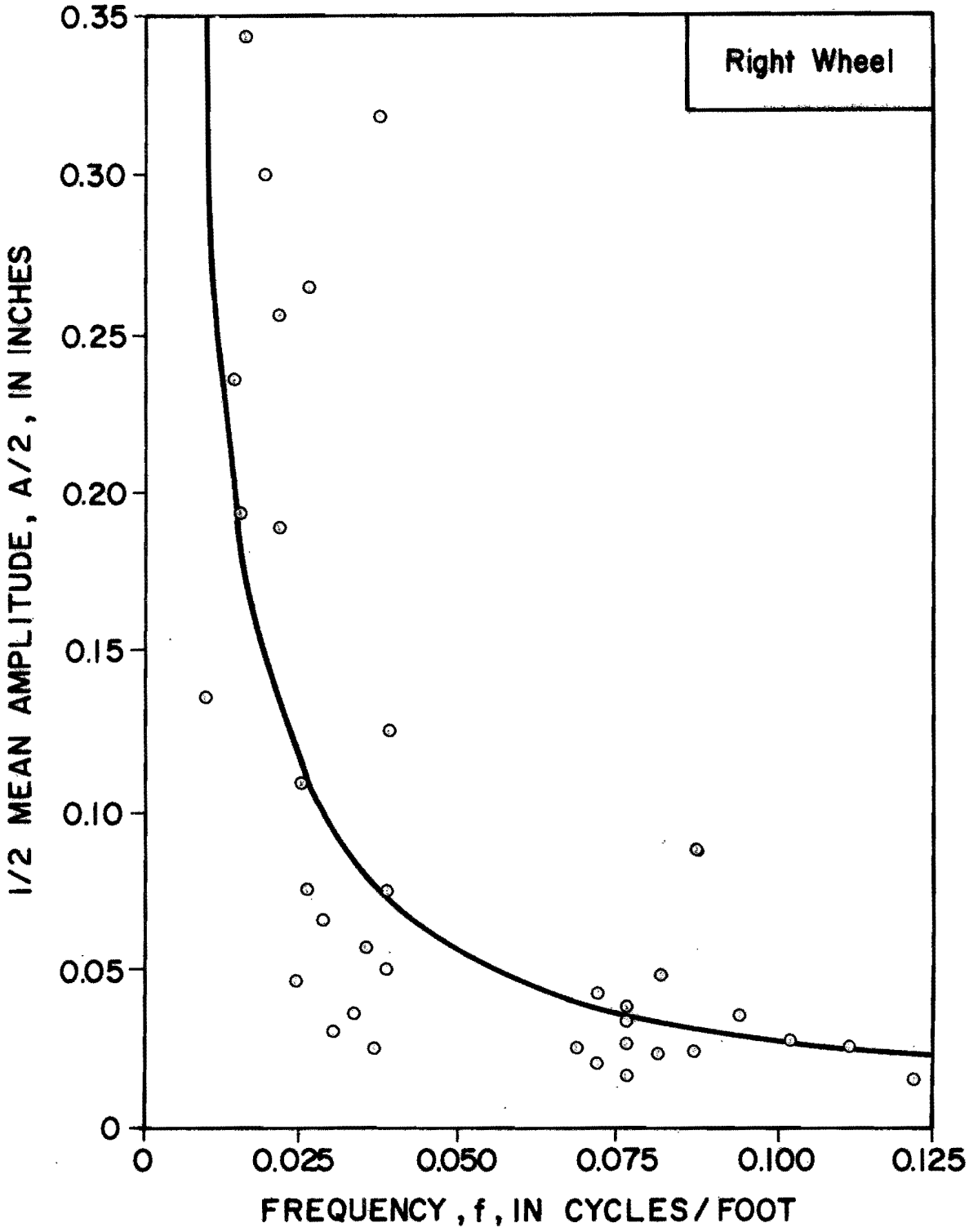

Figure X-9. Half Amplitude versus Bump Frequency in Cycles/Foot for Fairfield 2

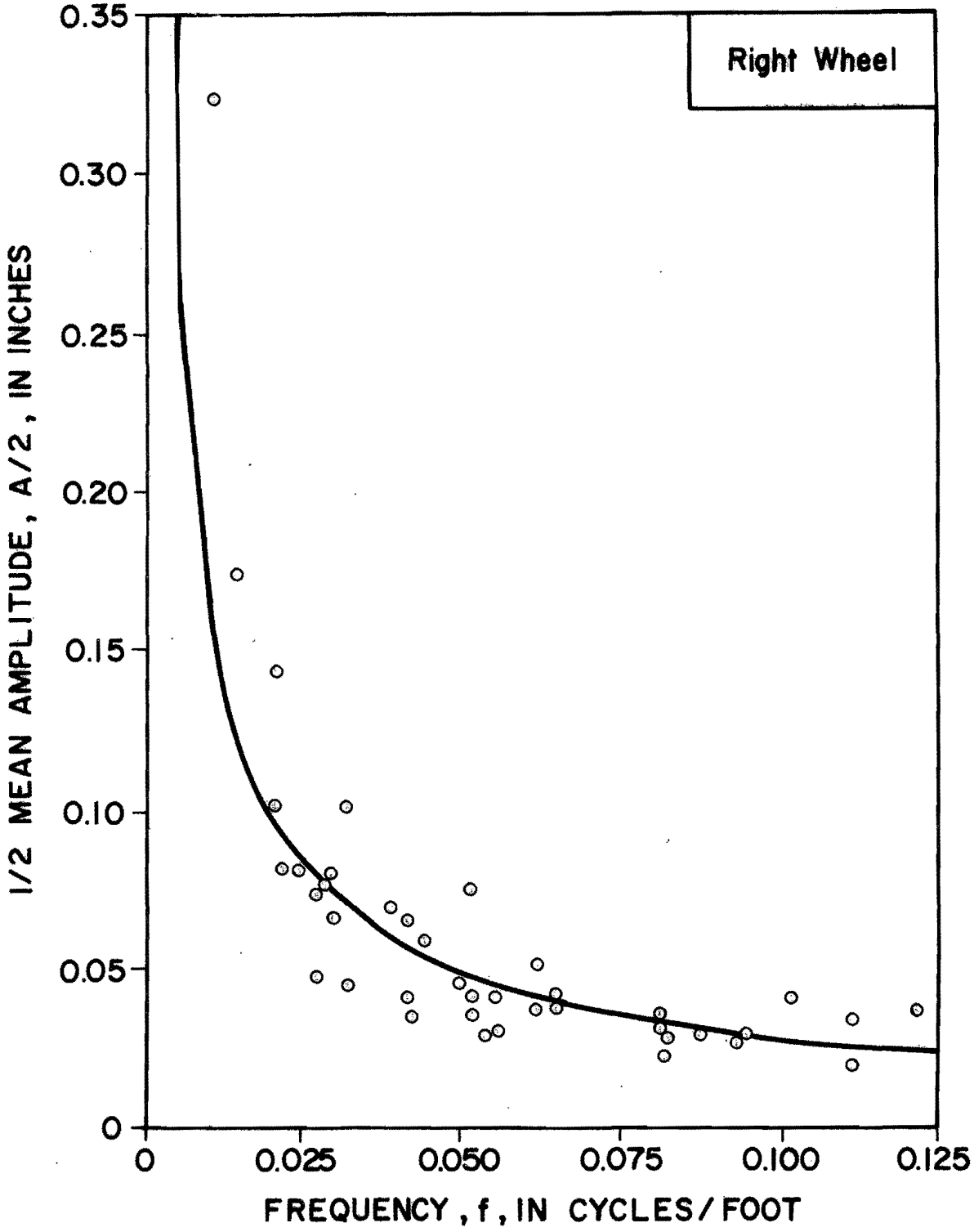

Figure X-10. Half Amplitude versus Bump Frequency in Cycles/Foot for Smithville 1A

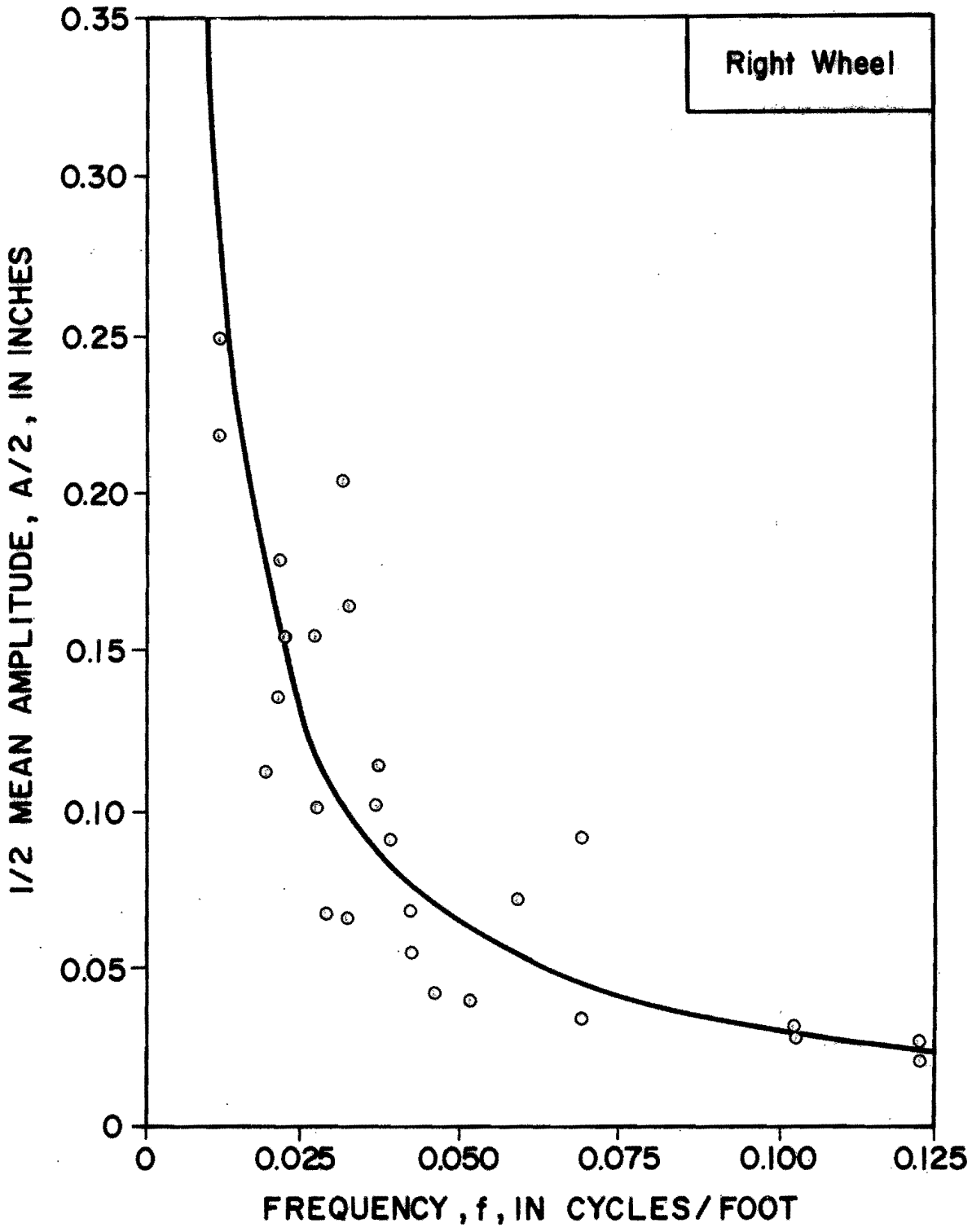

Figure X-11. Half Amplitude versus Bump Frequency in Cycles/Foot for Smithville 1B

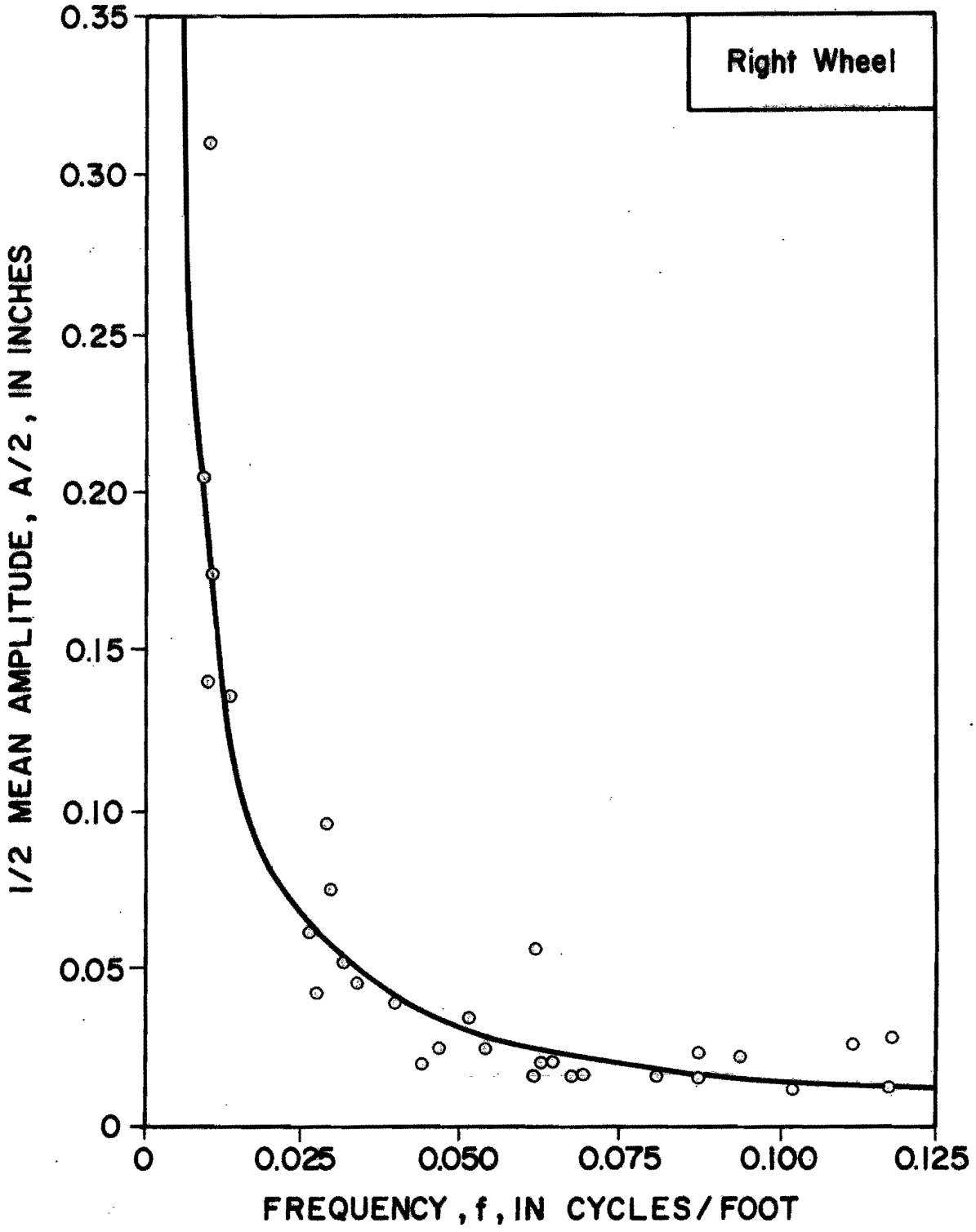

Figure X-12. Half Amplitude versus Bump Frequency in Cycles/Foot for Snook 1

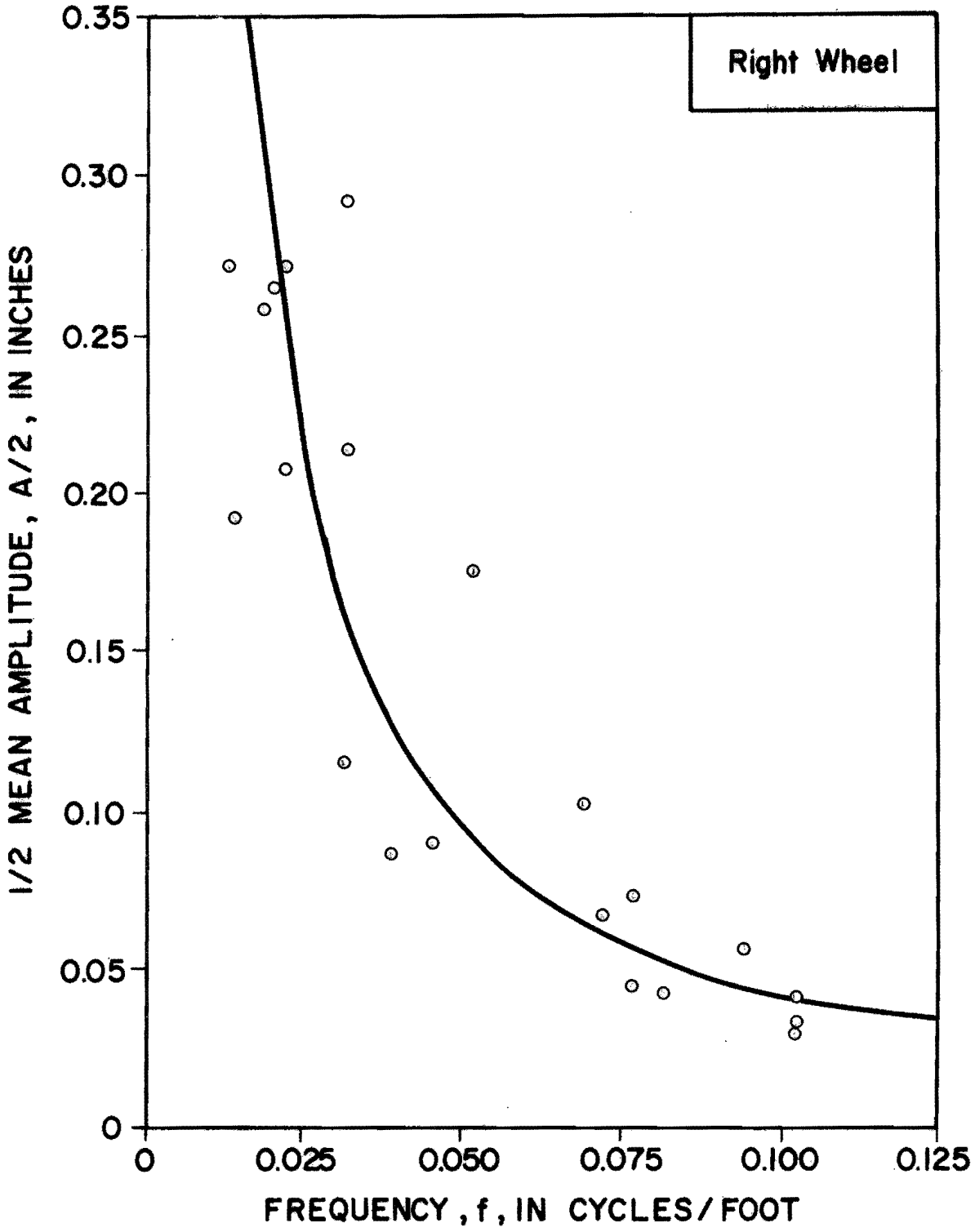

Figure X-13. Half Amplitude versus Bump Frequency in Cycles/Foot for OSR 1

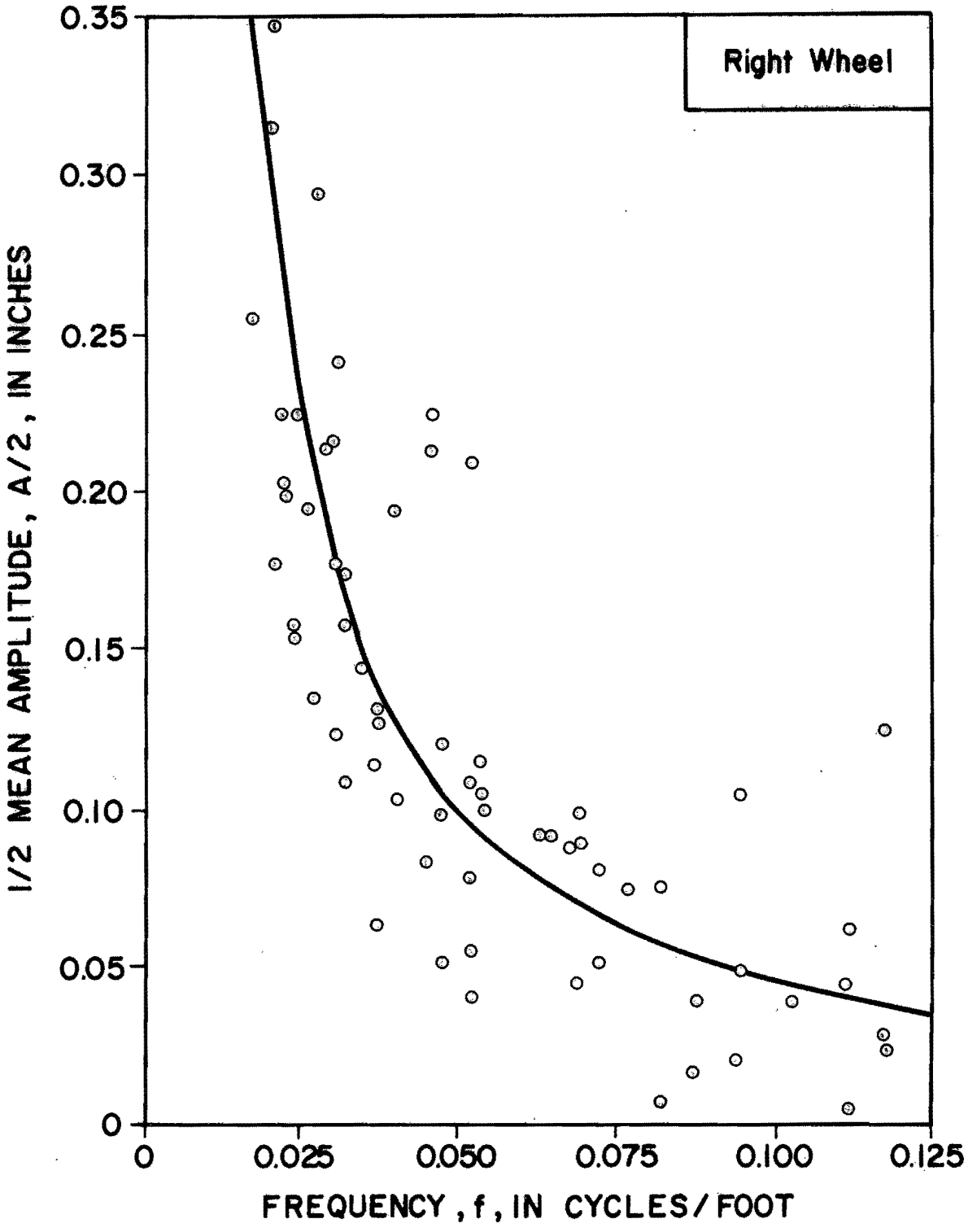

Figure X-14. Half Amplitude versus Bump Frequency in Cycles/Foot for OSR 2

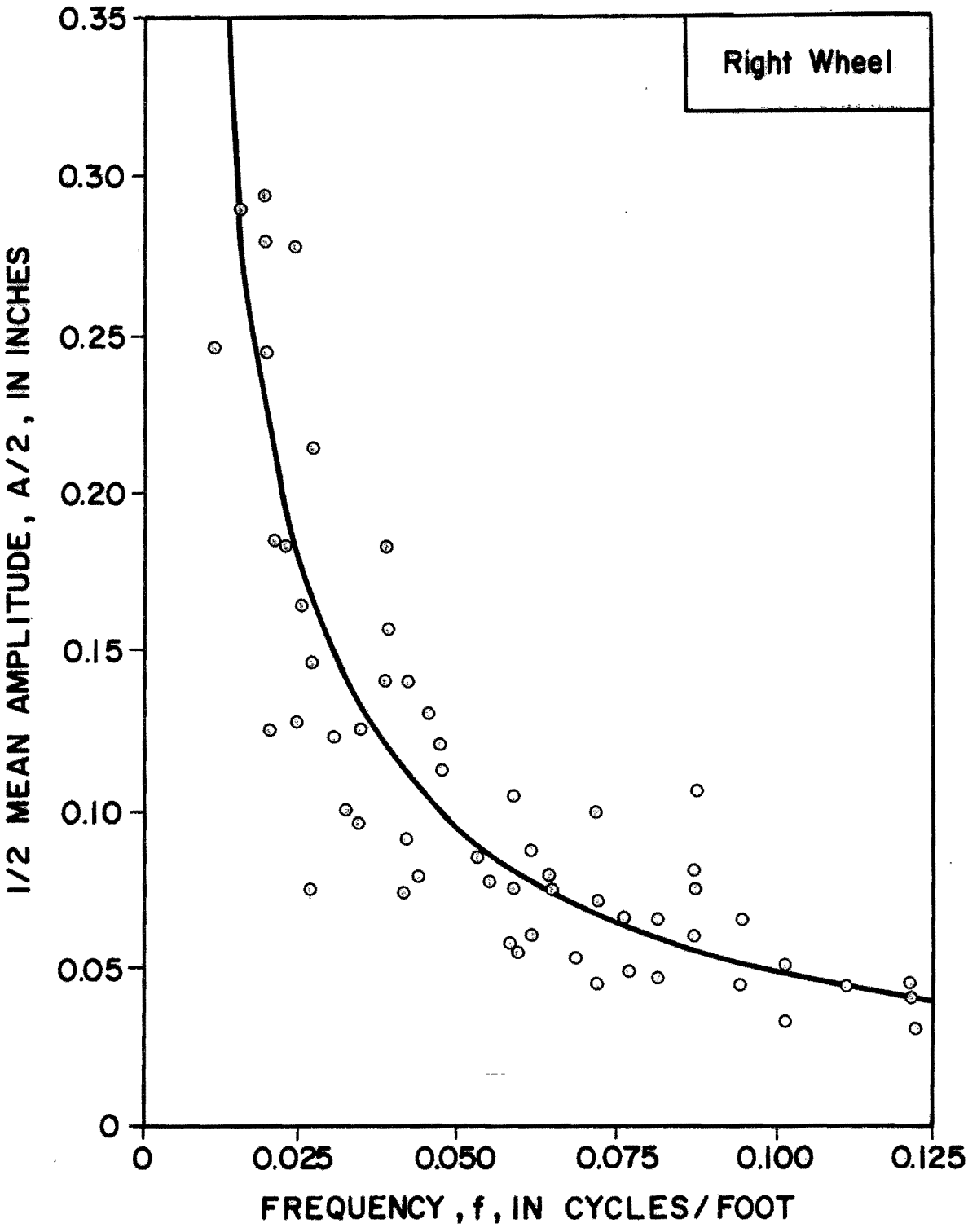

Figure X-15. Half Amplitude versus Bump Frequency in Cycles/Foot for OSR 3

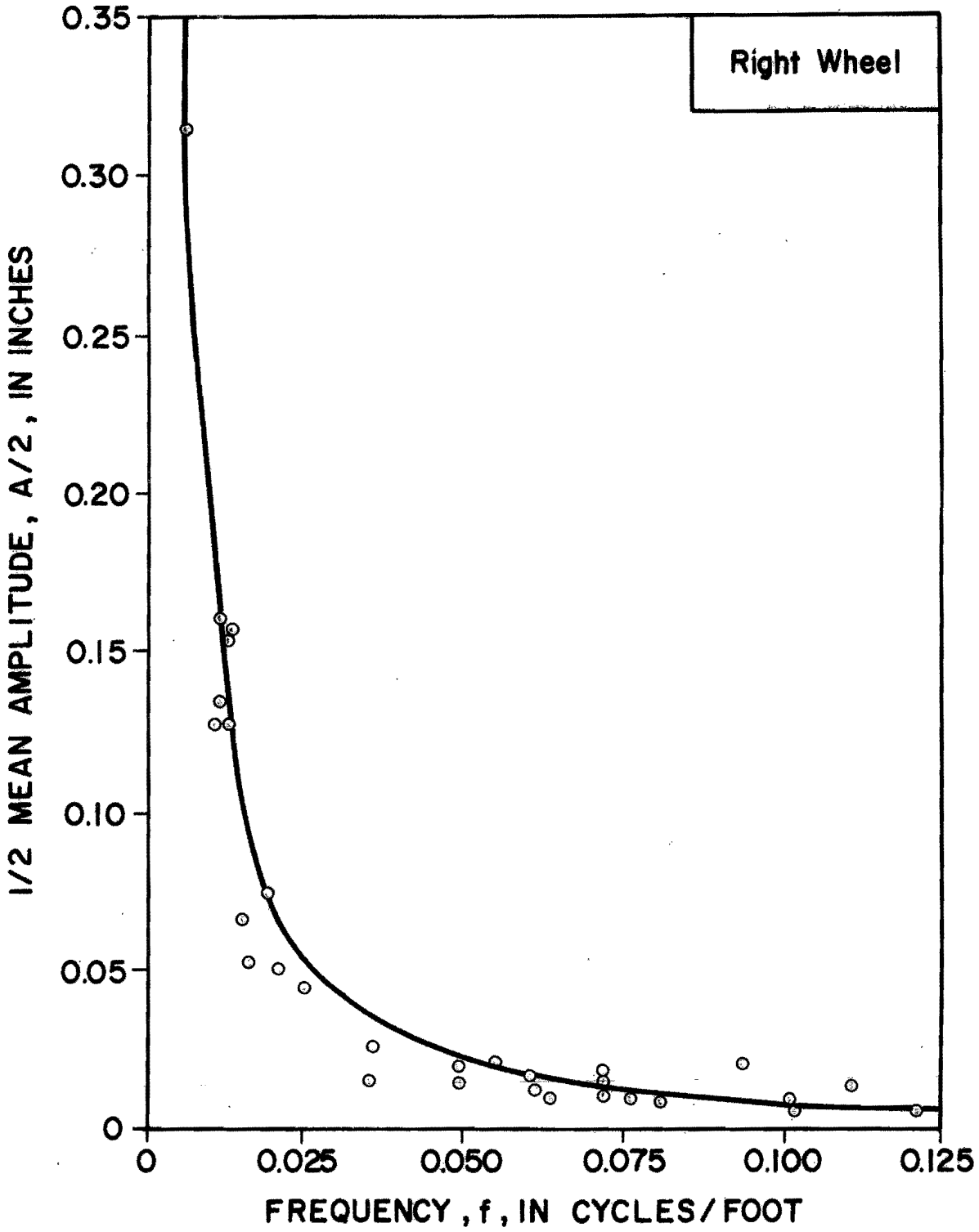

Figure X-16. Half Amplitude versus Bump Frequency in Cycles/Foot for Thrall 1

figures, the scatter of the data around the best fit regression line is considerably greater than was observed with the FFT data. Table X-1 gives the values of log c and n that were found by regression analysis along with the coefficients of determination (R^2) of the equation. Values of R^2 lower than about 0.70 represent a fairly poor fit for these data and these include the Huntsville sections (Figures X-1 and X-2), Fairfield, Section 2 (Figure X-9), Old San Antonio Road, Section 2 (Figure X-14), and Thrall (Figure X-16).

Table X-2 shows a comparison of the values of log c and n determined by both methods, along with the ratios of log c and n which were so determined. The mean ratio for log c is 0.75 and for n is 0.88.

Using these ratios, it is now possible to determine the values of log c and n for the actual sizes of the bumps on the road, and thus to generate the real profile roughness spectrum. The process for doing this is as follows:

1. From the equations in Table 16 in Chapter 4, determine loc c and n for the FFT data.
2. Find the log c for the real profile by the equation:

$$\log c = 0.75 \log c_{FFT}$$

3. Find the n for the real profile by the equation:

$$n = 0.88\ n_{FFT}$$

4. The predicted value of the amplitude of a bump of spacing s is given by

Table X-1. Spectral Constants of The Actual Profile (Right Wheelpath)

Section	Log c	n	R^2
Huntsville 1	-2.53	-0.96	0.97
Huntsville 2	-2.51	-0.96	0.64
Ben Arnold 1	-3.10	-1.38	0.88
Ben Arnold 2	-2.91	-1.22	0.84
Ben Arnold 3	-3.02	-1.31	0.90
Buckholts 1	-2.95	-1.26	0.78
Buckholts 2	-2.51	-1.05	0.86
Fairfield 1	-3.01	-1.30	0.89
Fairfield 2	-2.64	-1.06	0.62
Smithville 1A	-2.33	-0.78	0.75
Smithville 1B	-2.59	-1.06	0.82
Snook 1	-2.96	-1.11	0.87
OSR 1	-2.58	-1.19	0.84
OSR 2	-2.50	-1.15	0.59
OSR 3	-2.24	-0.93	0.84
Thrall 1	-3.31	-1.27	0.70

$$\log \frac{A}{2} = \log c + \log f$$

Table X-2. Right Wheelpath Spectra Constants

Section	FFT Data		Real Profile		Ratios Real/FFT	
	Log c	n	Log c	n	r_c	r_n
Huntsville 1	-3.61	-1.09	-2.53	-0.96	0.70	0.88
Huntsville 2	-3.92	-1.39	-2.51	-0.96	0.64	0.69
Ben Arnold 1	-3.71	-1.38	-3.10	-1.38	0.84	1.00
Ben Arnold 2	-3.74	-1.36	-2.91	-1.22	0.78	0.90
Ben Arnold 3	-3.90	-1.46	-3.02	-1.31	0.77	0.90
Buckholts 1	-3.61	-1.34	-2.95	-1.26	0.82	0.94
Buckholts 2	-3.79	-1.44	-2.51	-1.05	0.66	0.73
Fairfield 1	-3.57	-1.27	-3.01	-1.30	0.84	1.02
Fairfield 2	-3.61	-1.27	-2.64	-1.06	0.73	0.83
Smithville 1A	-3.94	-1.32	-2.33	-0.78	0.59	0.59
Smithville 1B	-3.94	-1.46	-2.59	-1.06	0.66	0.73
Snook 1	-3.76	-1.20	-2.96	-1.11	0.79	0.93
OSR 1	-3.18	-1.20	-2.58	-1.19	0.81	0.99
OSR 2	-3.19	-1.13	-2.50	-1.15	0.78	1.02
OSR 3	-2.95	-1.05	-2.24	-0.93	0.76	0.89
Thrall 1	-3.93	-1.24	-3.31	-1.27	0.84	1.02
				Mean Ratio	0.752	0.879

$$a = 2\ c\ s^n$$

where a = the amplitude of the bump, in inches, and

s = the bump spacing.

These amplitudes can be compared with the actual measured values of bump amplitude that are shown in Figures X-17 through X-32. It is interesting to note that in the majority of the profiles, the left wheelpath has larger bump amplitudes than in the right wheelpath. This is consistent with the other findings since the right wheel path should be expected to have a larger number of small, closely-spaced bumps since it is more susceptible to moisture changes at the edge of the pavement.

The quantity of material that is required to level up a section of pavement can be found by using the following formula:

Total level-up material

$$= \text{Width} \times \sum_{i=1}^{m} \left[s_i \times a_i \times p(s_i) \times \left(\frac{\text{Length}}{s_i} \right) \right]$$

where

s_i = the spacing of the ith bump in the bump spectrum

a_i = the amplitude of the bump with spacing, s_i

$p(s_i)$ = the probability of finding a bump with spacing s_i along the length of the road

$\frac{\text{Length}}{s_i}$ = the number of bumps of spacing s_i that will make up the total length.

The equation simplifies to the following form

Total level-up material =

$$\text{Length} \times \text{Width} \times \sum_{i=1}^{m} 2\ c\ s_i^{\ n} \times p(s_i)$$

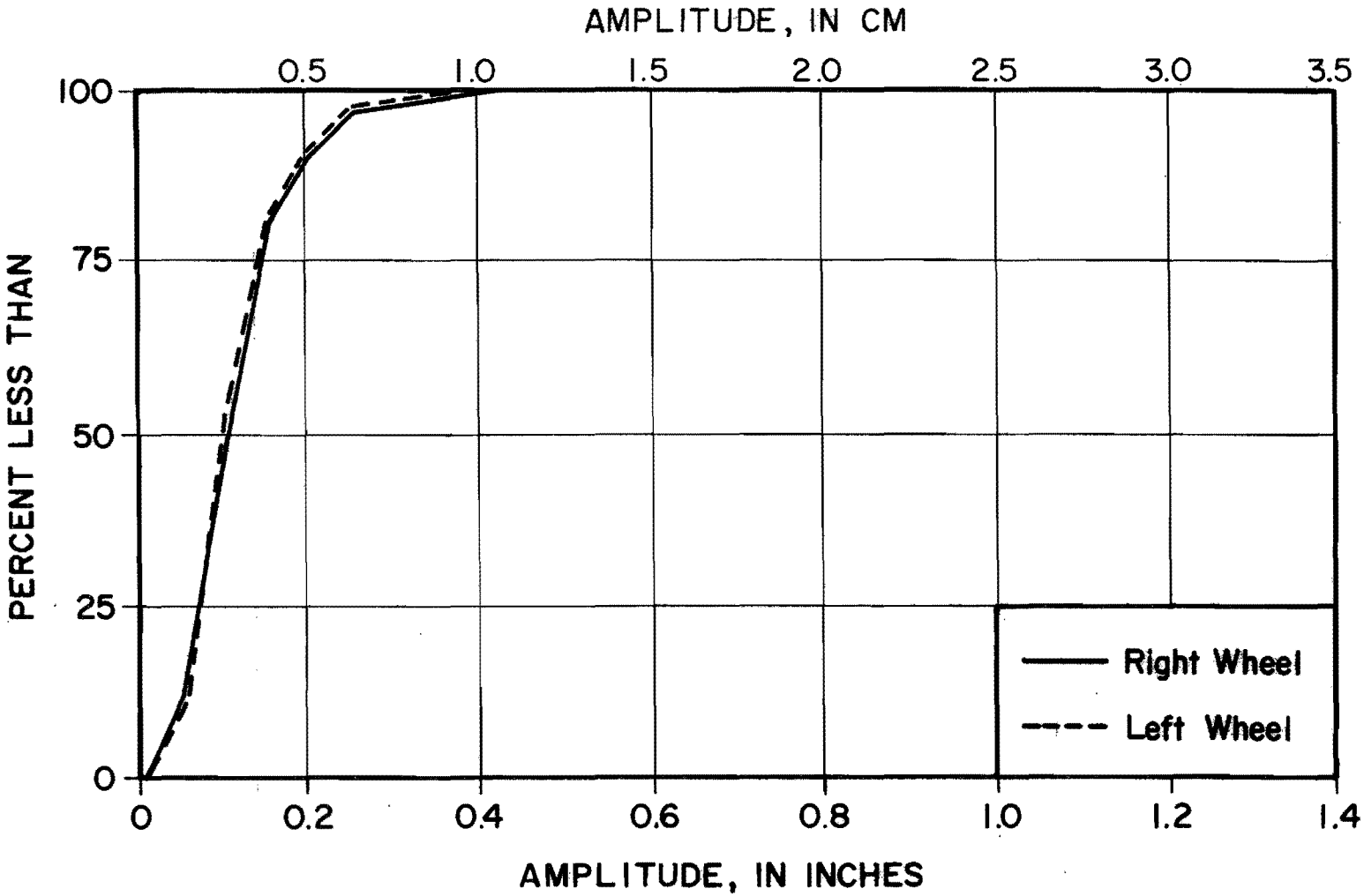

Figure X-17. Distribution of Amplitudes (Huntsville 1)

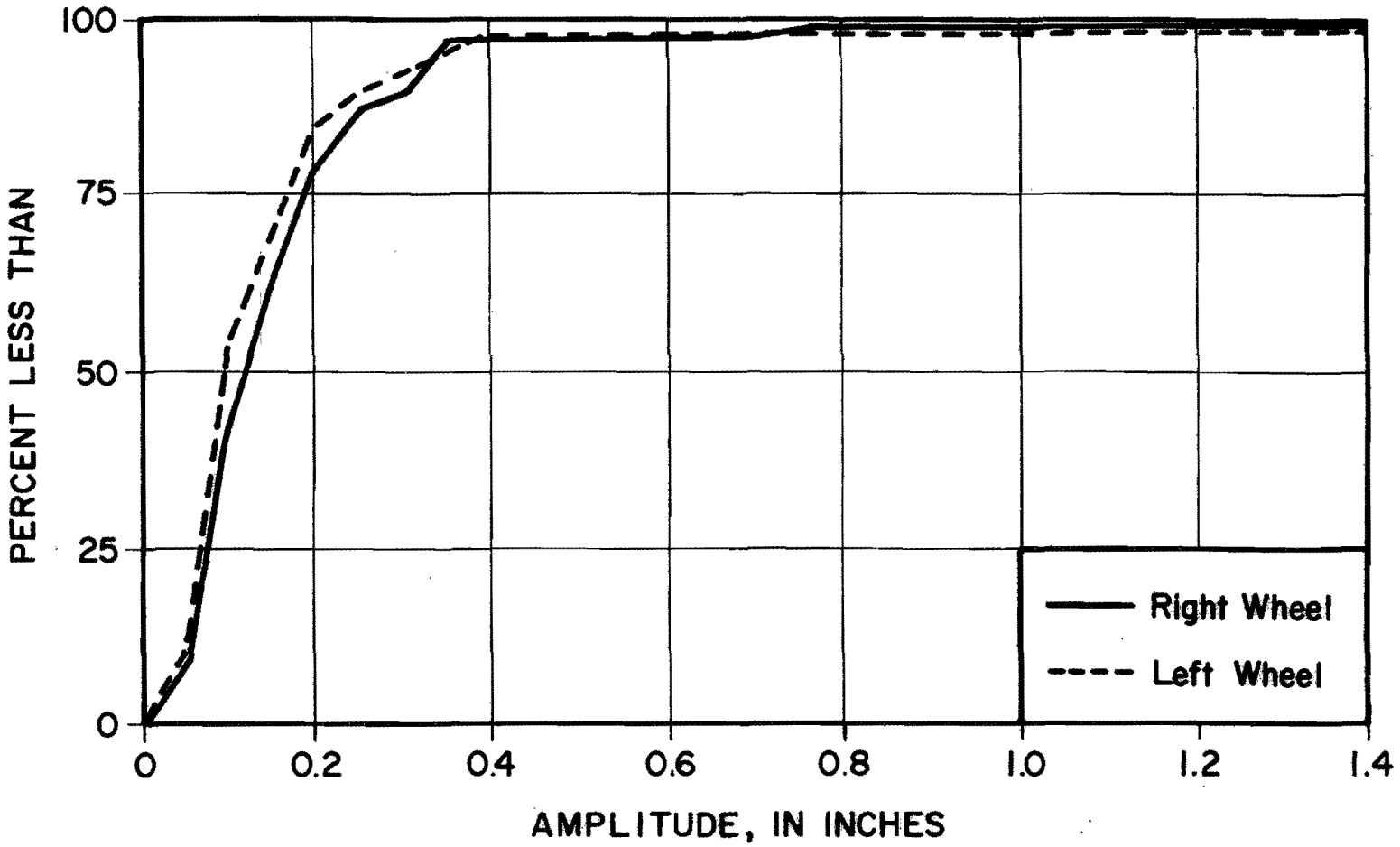

Figure X-18. Distribution of Amplitudes (Huntsville 2)

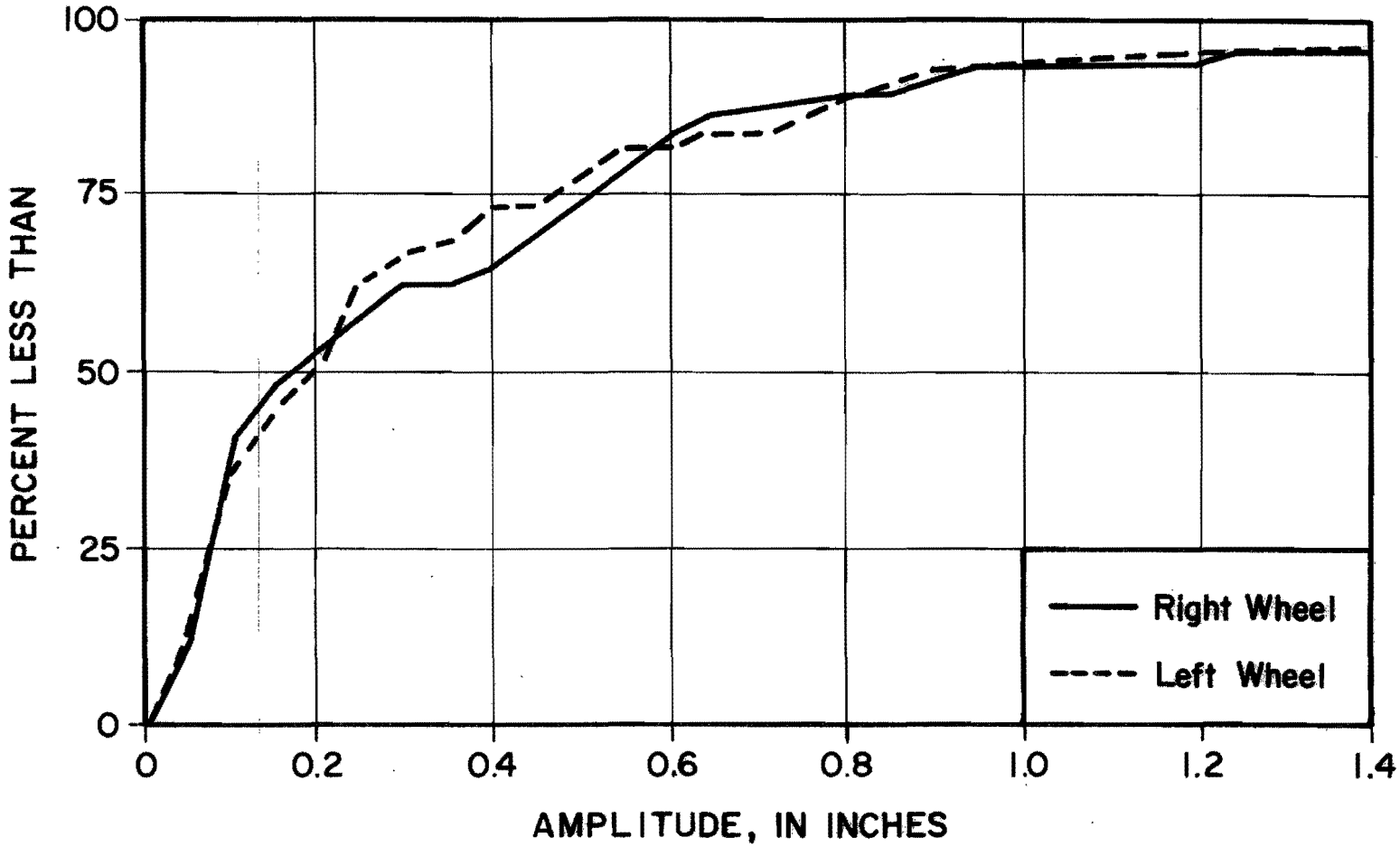

Figure X-19. Distribution of Amplitudes (Ben Arnold 1)

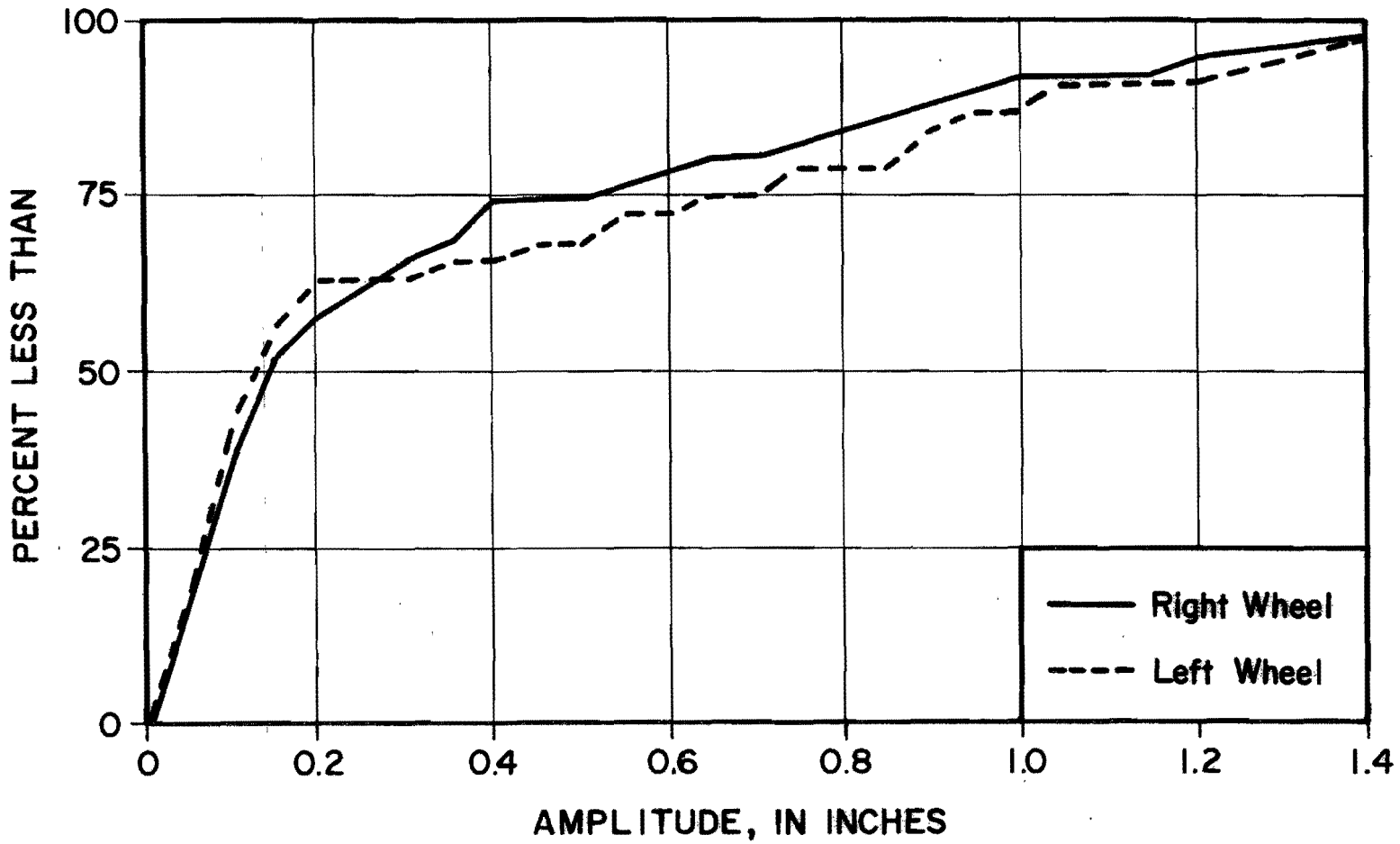

Figure X-20. Distribution of Amplitudes (Ben Arnold 2)

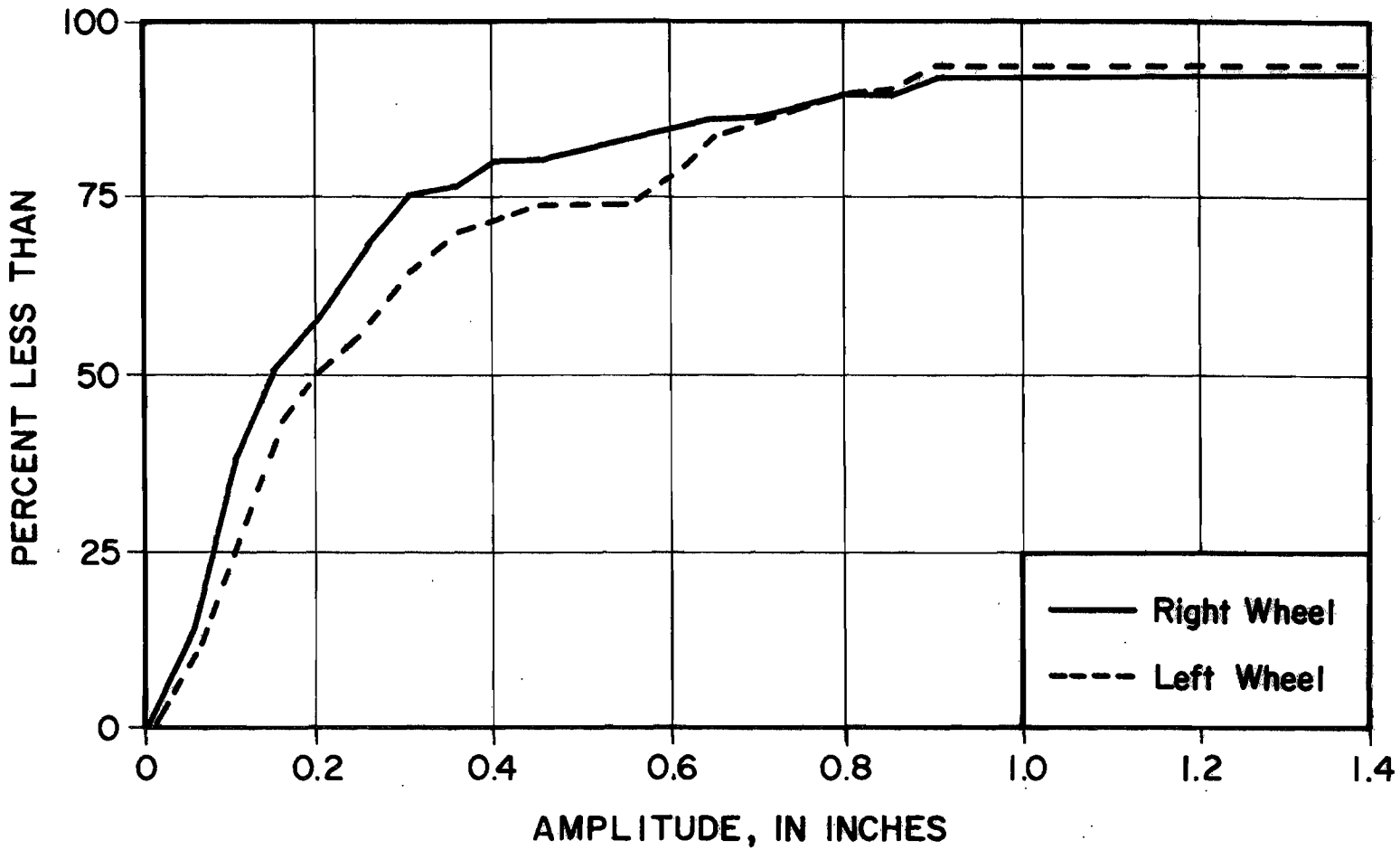

Figure X-21. Distribution of Amplitudes (Ben Arnold 3)

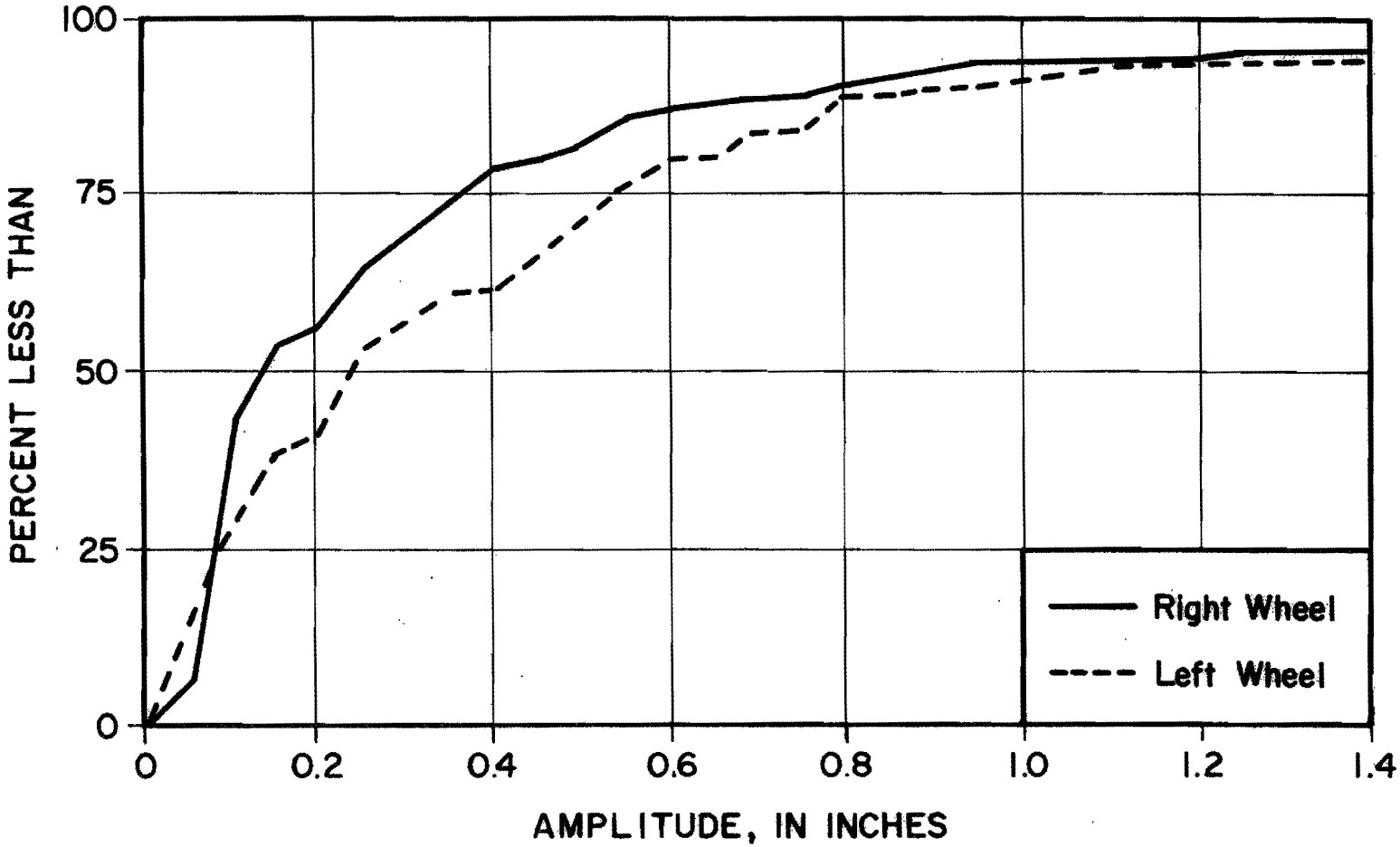

Figure X-22. Distribution of Amplitudes (Buckholts 1)

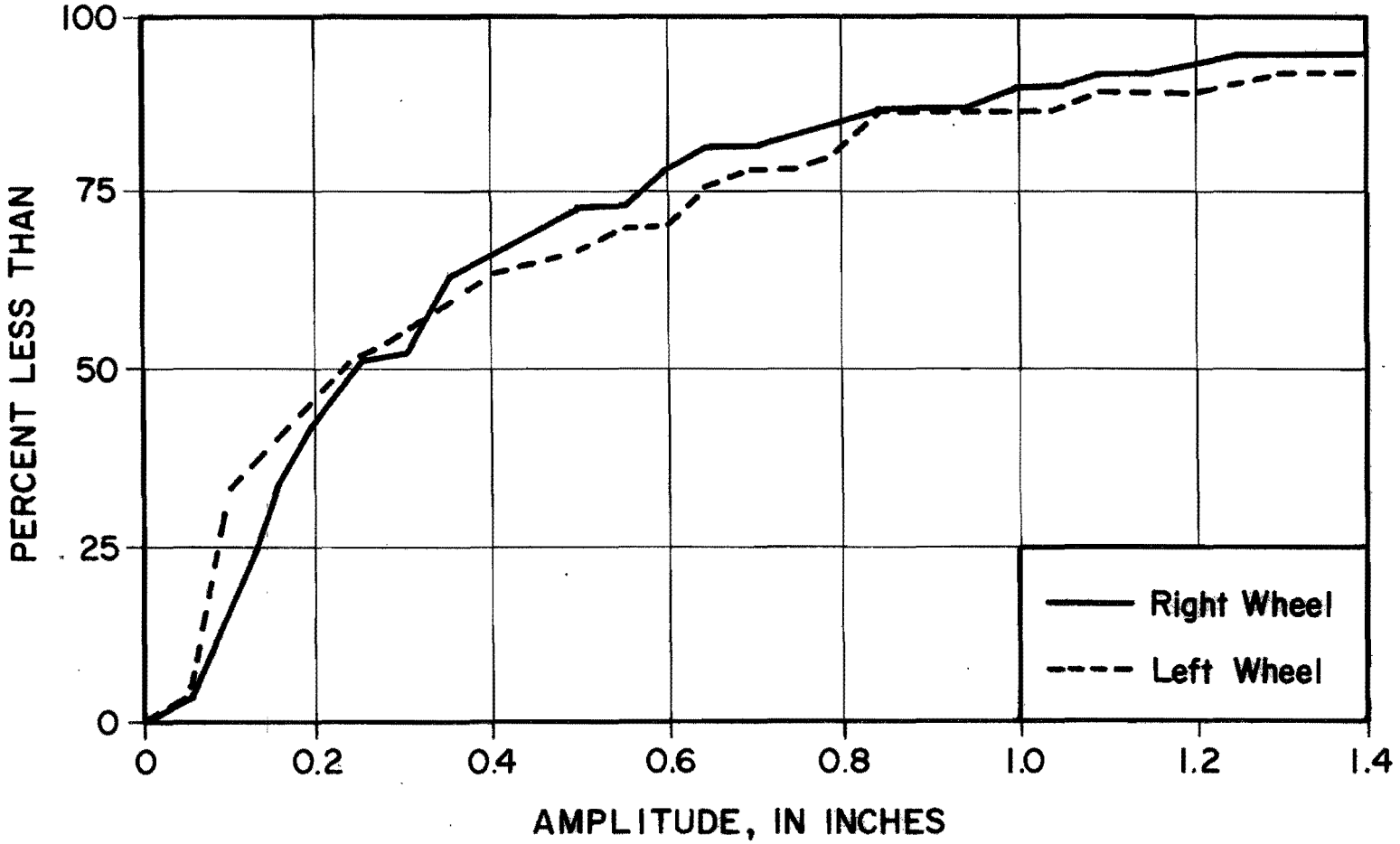

Figure X-23. Distribution of Amplitudes (Buckholts 2)

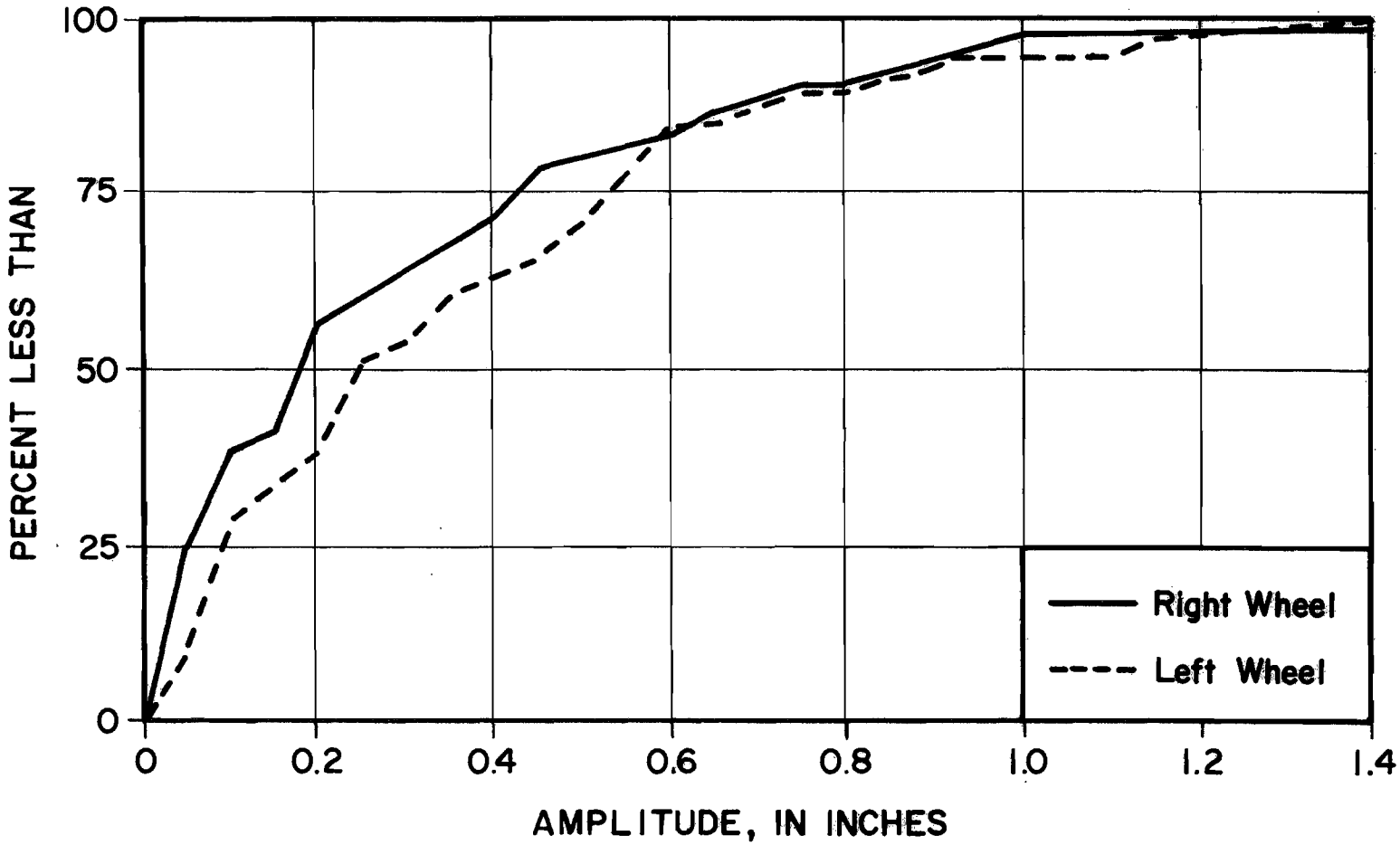

Figure X-24. Distribution of Amplitudes (Fairfield 1)

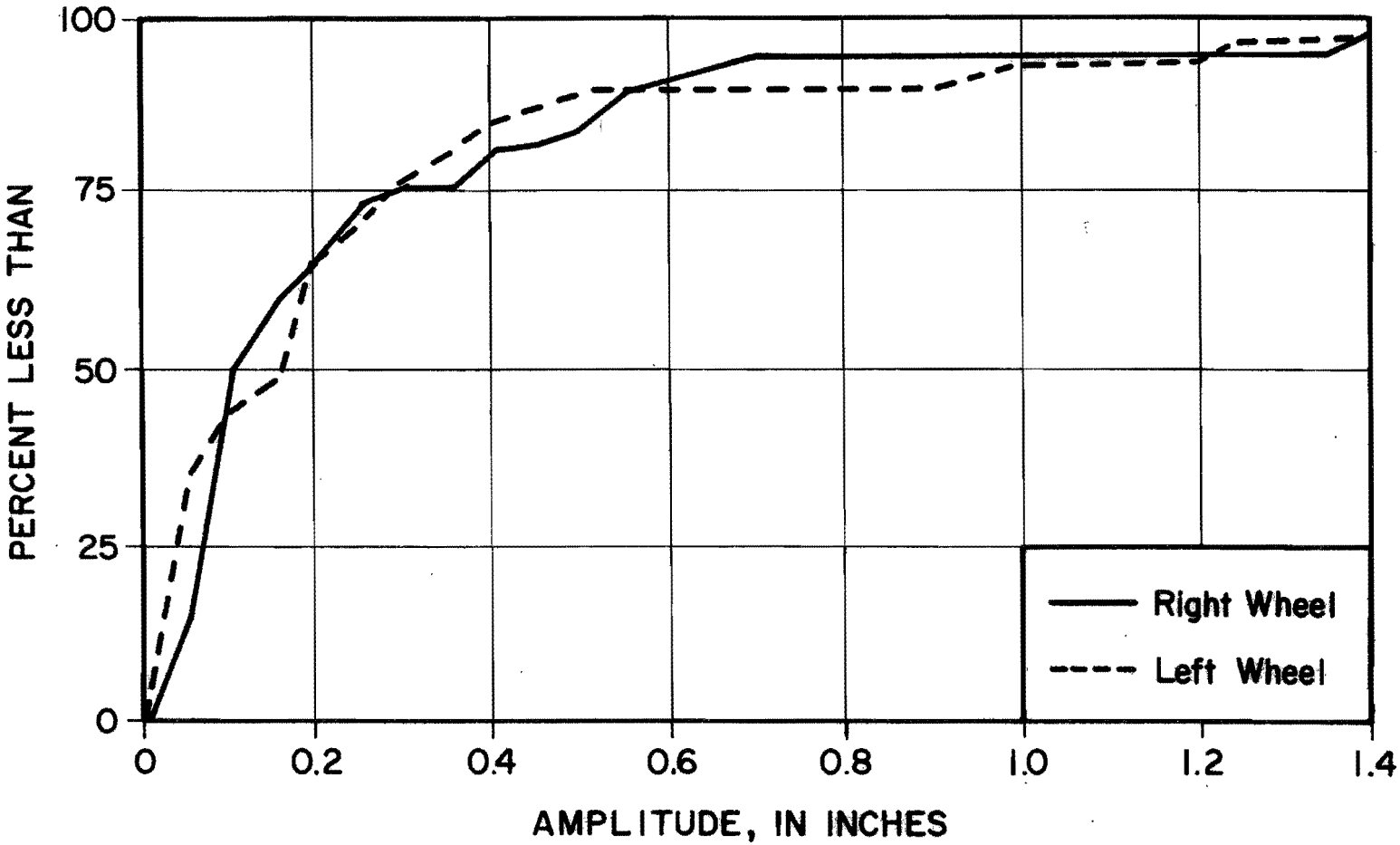

Figure X-25. Distribution of Amplitudes (Fairfield 2)

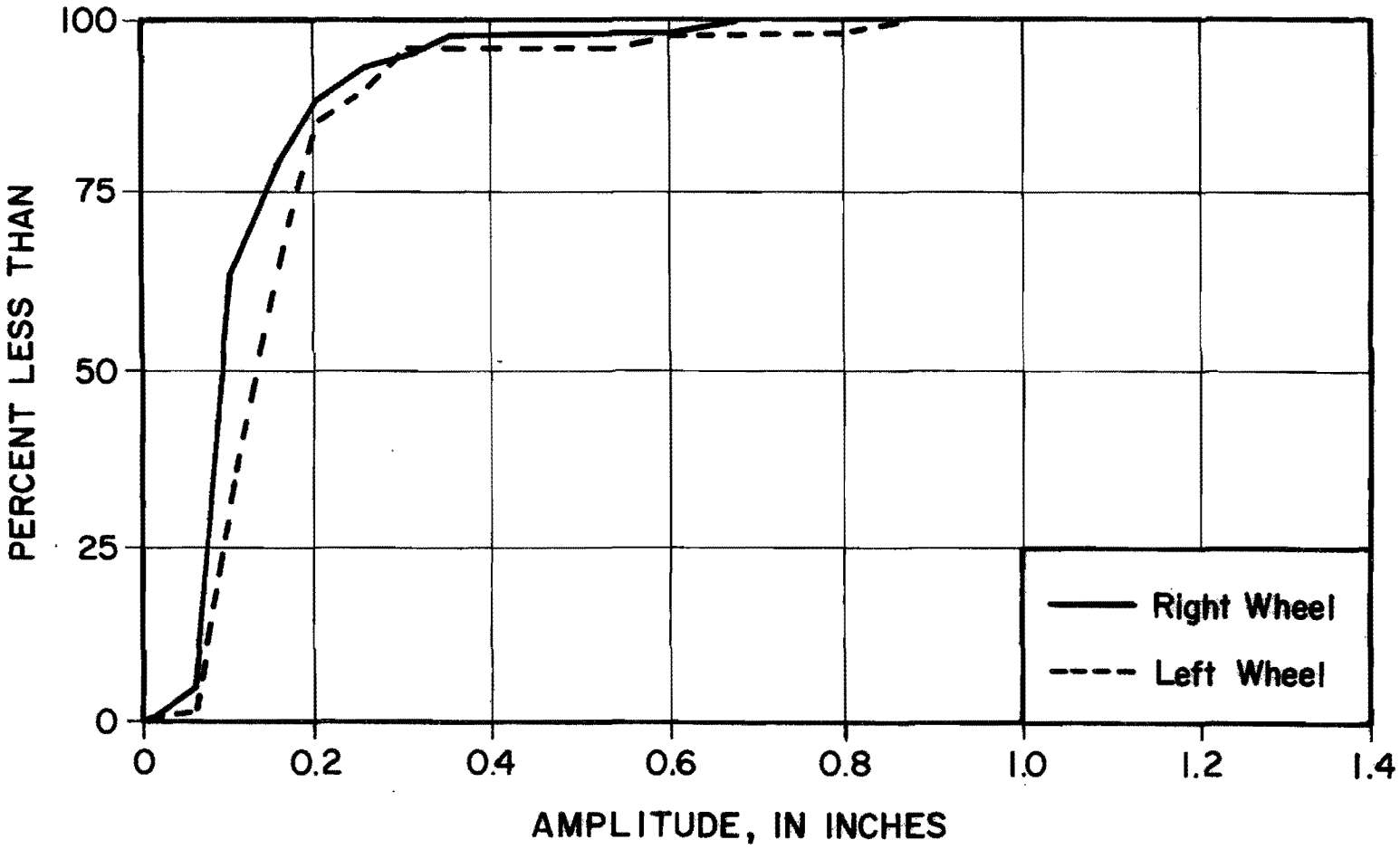

Figure X-26. Distribution of Amplitudes (Smithville 1A)

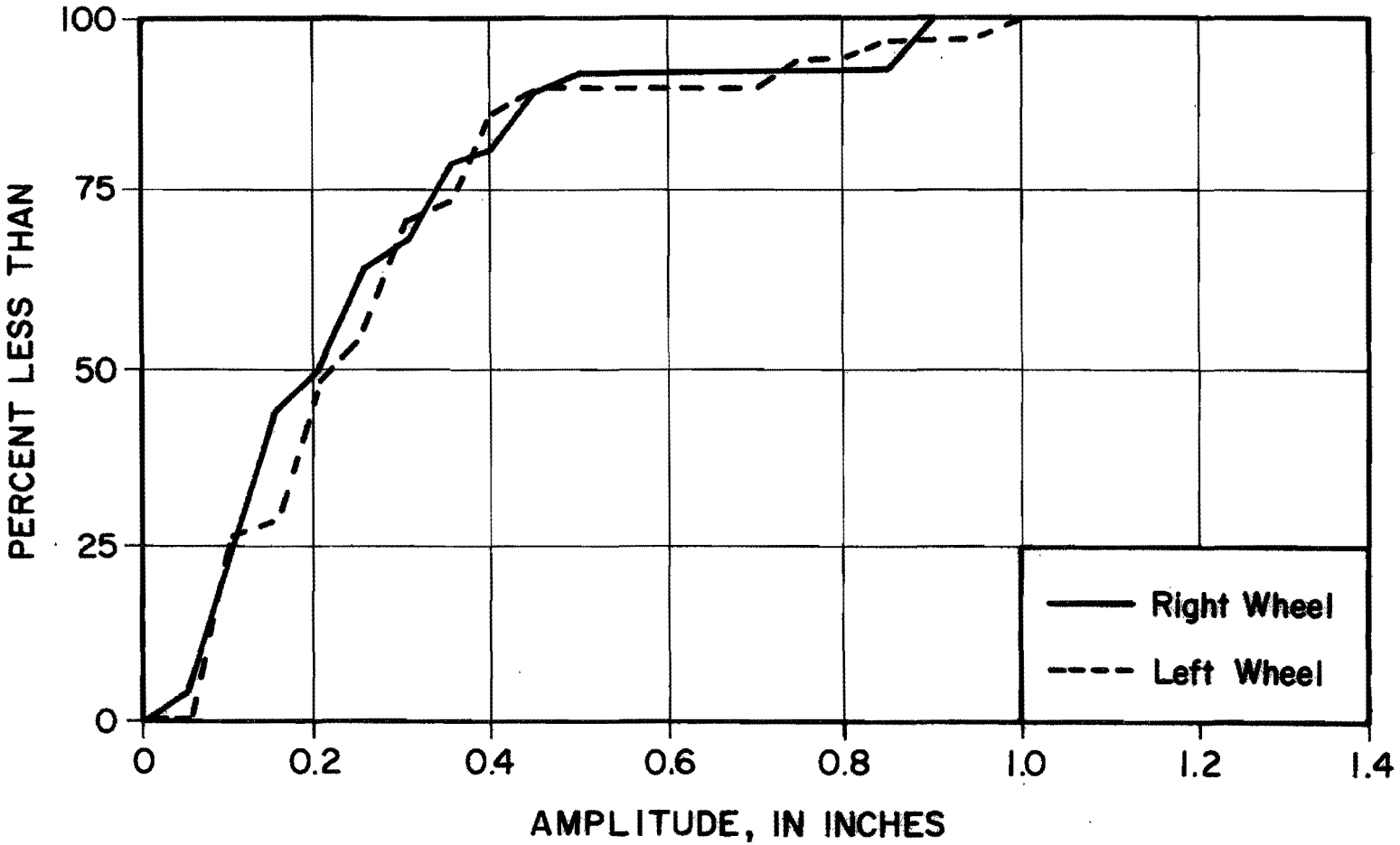

Figure X-27. Distribution of Amplitudes (Smithville 1B)

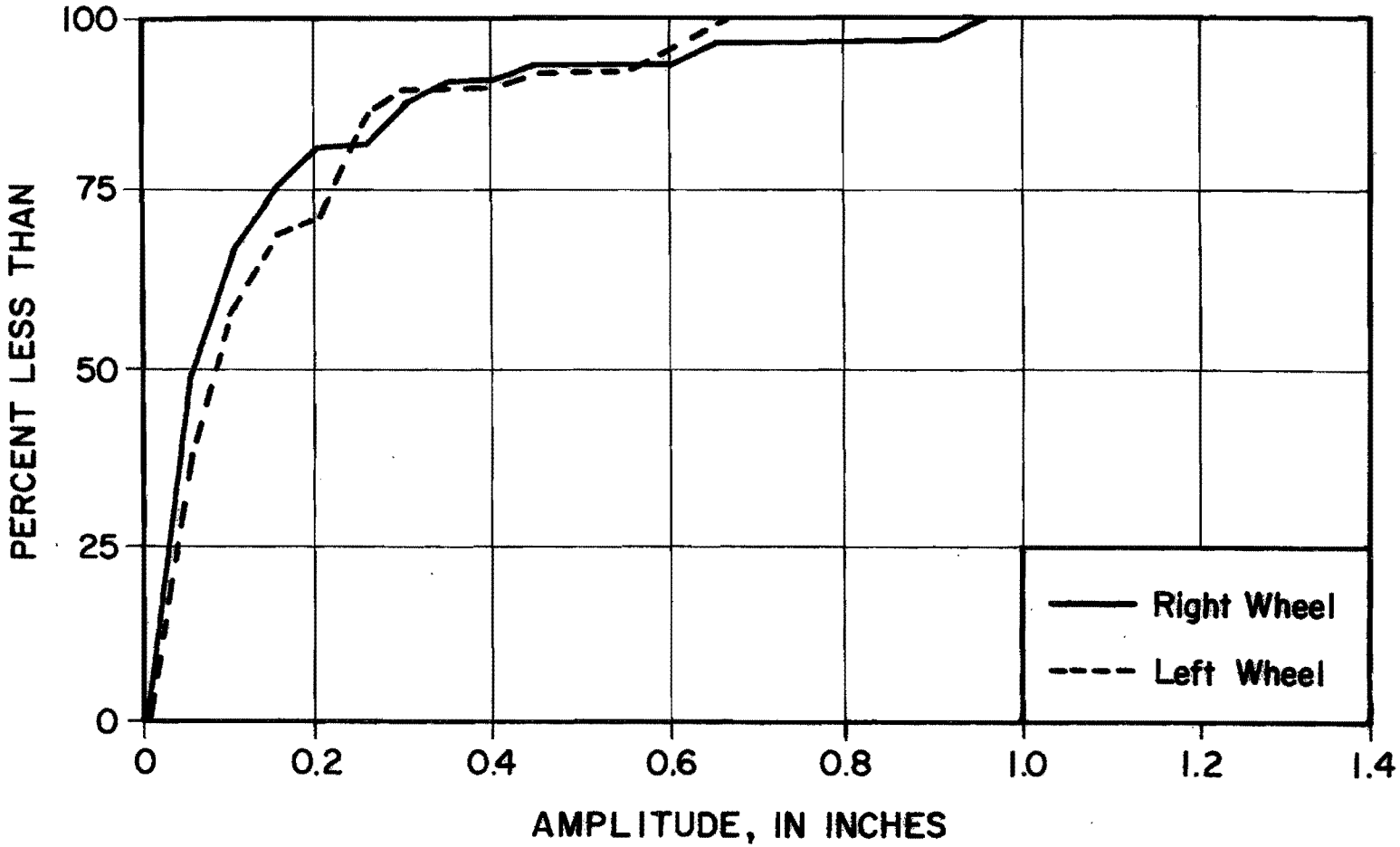

Figure X-28. Distribution of Amplitudes (Snook 1)

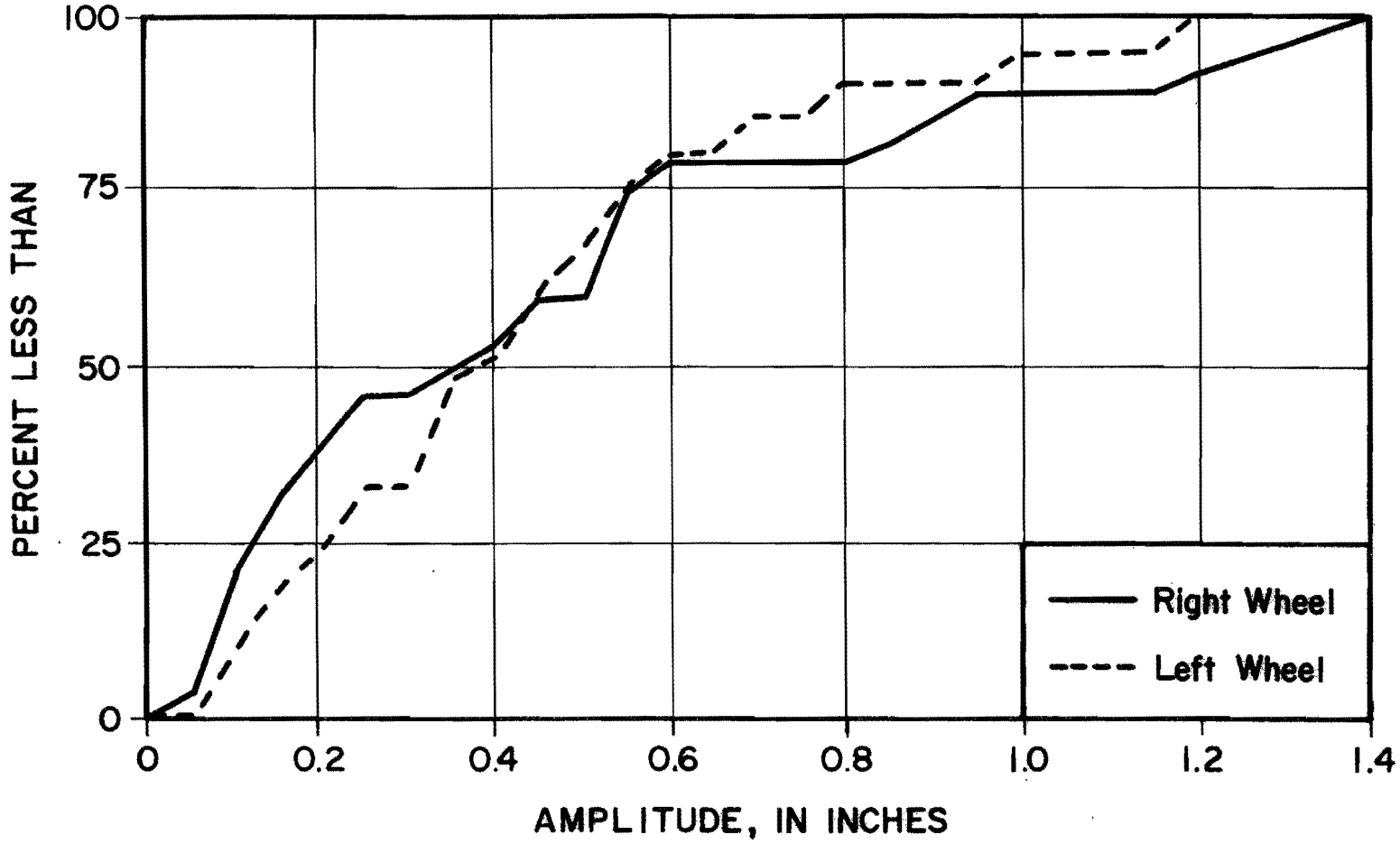

Figure X-29. Distribution of Amplitudes (OSR 1)

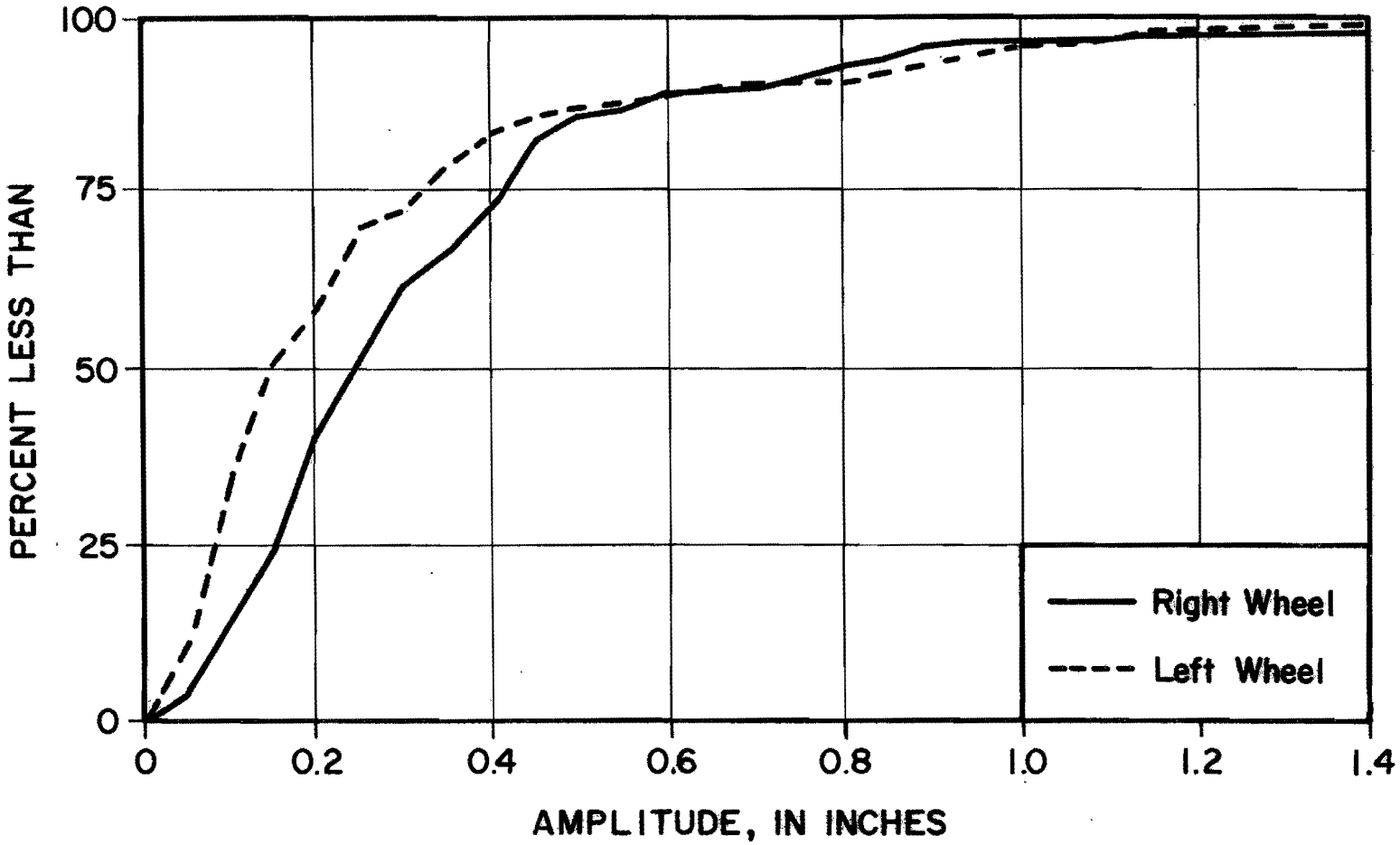

Figure X-30. Distribution of Amplitudes (OSR 2)

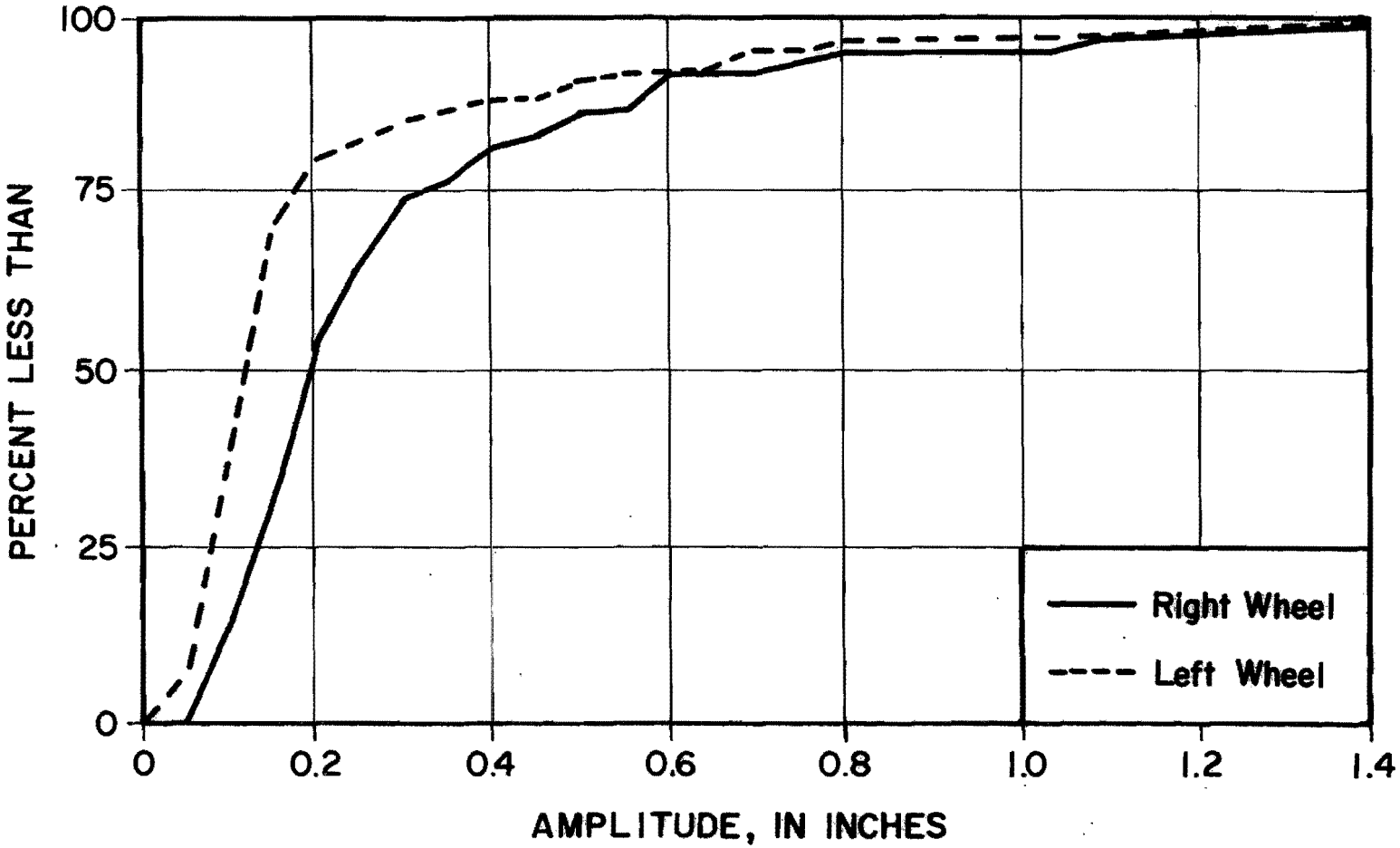

Figure X-31. Distribution of Amplitude (OSR 3)

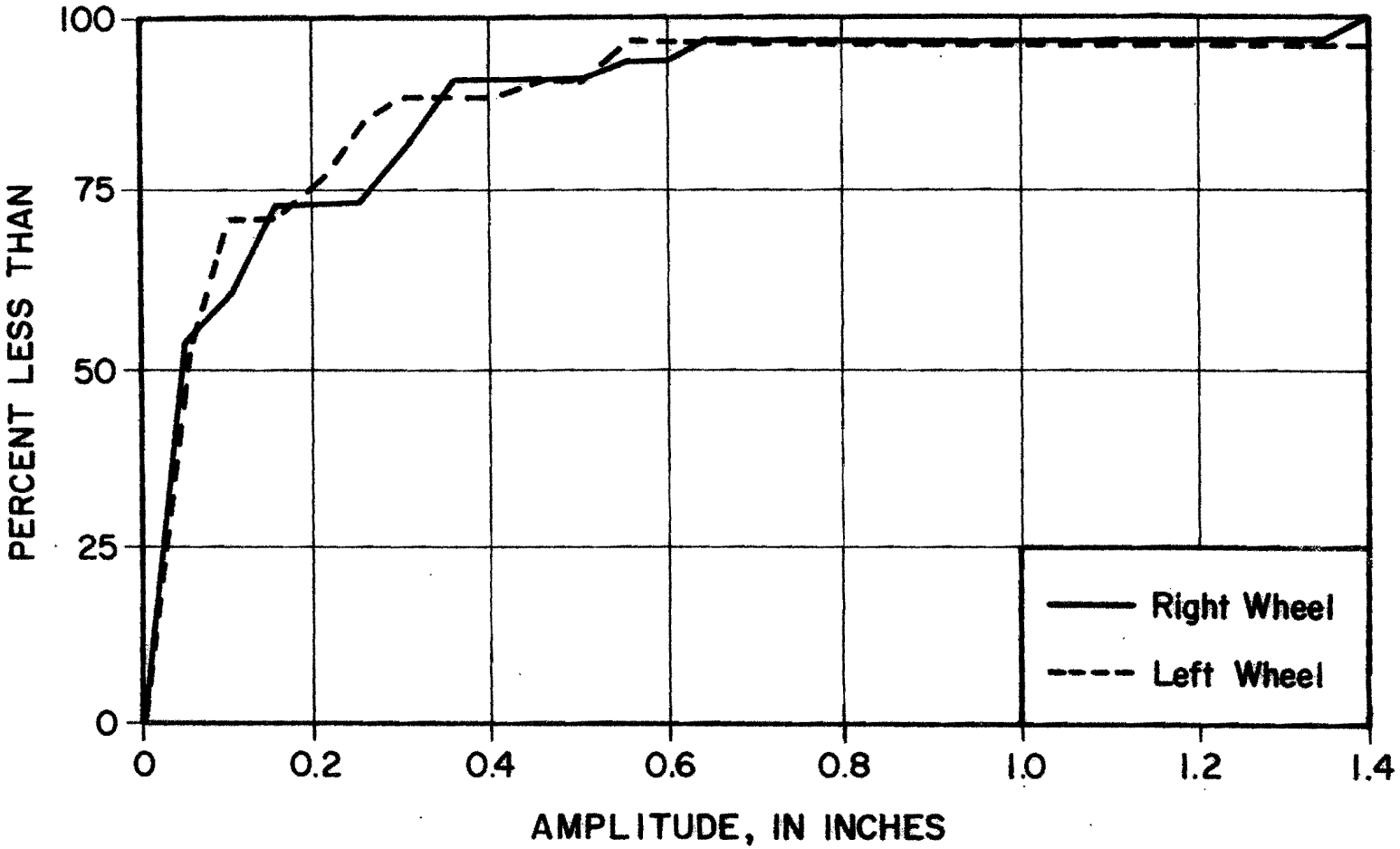

Figure X-32. Distribution of Amplitudes (Thrall 1)

The only missing part of this equation is the probability of finding a bump with spacing, s_i. Table X-3 shows the bump spacing for right and left wheelpaths on all of the pavement sections below which 25, 50, and 75 percent of all bump spacings fall. Assuming that this cumulative distribution of bump spacings has the equation

$$P(s) = e^{-K/s}$$

the probability of finding a bump in the range of bump spacing $s_i \pm \Delta s/2$ is

$$p(s_i) = \left[\frac{Kr}{s_i^{r+1}} \; e^{-K/s_i^r}\right] \Delta s$$

Values of K and r were determined from the data in Table X-3 and are recorded in Table X-4. The values of K for the Huntsville sections appear to be unreasonably large in comparison with the rest of the pavement sections. Thus, it is possible to compute quantities of required level-up material on a section of highway pavement using typical values of K and r to compute the probability of finding bumps of spacing s_i along the length of road along with the values of c and n determined previously. The procedure for making this estimate of materials quantities is as follows:

3. Compute the bump spacing increments by

$$\Delta s_i = \frac{s_{max}}{i^2 - 1} \qquad \text{for } i > 1$$

$$\Delta s_i = \frac{s_{max}}{2} \qquad \text{for } i = 1$$

Table X-3. Distribution of Bump Spacings

Section	Bump Spacings Greater Than, in Feet					
	Left Wheel			Right Wheel		
	25%	50%	75%	25%	50%	75%
Huntsville 1	15	22	29	14	20	27
Huntsville 2	18	24	32	15	23	32
Ben Arnold 1	23	40	68	15	28	56
Ben Arnold 2	18	29	81	15	30	78
Ben Arnold 3	23	40	71	14	22	46
Buckholts 1	21	48	84	16	24	54
Buckholts 2	12	33	70	14	32	57
Fairfield 1	18	31	56	12	22	48
Fairfield 2	14	29	57	13	27	49
Smithville 1A	12	15	28	13	19	34
Smithville 1B	17	34	45	19	34	48
Snook 1	13	30	51	17	26	49
OSR 1	14	31	68	13	24	47
OSR 2	15	27	45	14	24	35
OSR 3	10	15	24	13	22	39
Thrall 1	11	18	57	14	19	59
S. Antonio 410-1 (Nov. 79)	19	51	82	13	27	84
S. Antonio 37	26	43	69	21	40	69
S. Antonio 90-5 (Apr. 78)	18	31	49	18	36	54
S. Antonio 90-3 (Apr. 78)	15	31	66	15	32	63

Table X-4. Values of K and r for Left and Right Wheelpaths

Section	Left Wheelpath		Right Wheelpath	
	K	r	K	r
Huntsville 1	845	2.35	779	2.38
Huntsville 2	3855	2.73	381	2.05
Ben Arnold 1	135	1.45	35.9	1.20
Ben Arnold 2	24.0	1.02	18.0	0.95
Ben Arnold 3	113	1.40	45.7	1.30
Buckholts 1	43.7	1.11	42.8	1.26
Buckholts 2	13.1	0.88	27.0	1.10
Fairfield 1	78.0	1.39	23.2	1.13
Fairfield 2	27.6	1.12	29.8	1.18
Smithville 1A	96.6	1.76	87.0	1.63
Smithville 1B	105	1.50	188	1.64
Snook 1	26.4	1.12	89.1	1.48
OSR 1	19.8	0.99	32.7	1.22
OSR 2	68.8	1.43	127	1.69
OSR 3	88.2	1.80	55.9	1.43
Thrall 1	11.4	0.92	16.7	1.01
S. Antonio 410-1 (Nov. 79)	30.1	1.02	11.5	0.84
S. Antonio 37	272	1.61	79.6	1.31
S. Antonio 90-5 (Apr. 78)	133	1.56	81.6	1.38
S. Antonio 90-3 (Apr. 78)	25.2	1.06	27.9	1.09

1. Choose a maximum bump spacing, s_{max} that is twice as great as the 75 percent spacing given in Table X-3 and divide it into bump spacings given by

$$s_i = \frac{s_{max}}{i} \qquad i = 1, 2, 3, \ldots, m$$

The smallest spacing should be around 1 foot.

2. Compute the bump amplitudes a_i by

$$a_i = 2\ c\ s_i^{\ n}$$

3. Compute the bump spacing increments by

$$\Delta s_i = \frac{s_{max}}{1^2 - 1} \qquad \text{for } i > 1$$

$$\Delta s_i = \frac{s_{max}}{2} \qquad \text{for } i = 1$$

4. Compute the bump probability by

$$p(s_i) = \left[\frac{Kr}{s_i^{\ r+1}}\ e^{-K/s_i^{\ r}}\right] \Delta s_i$$

5. Compute the total quantity of level up material by

$$\text{Length} \times \text{Width} \times \sum_{i=1}^{m} a_i \times p(s_i)$$

If rutting has also ocurred on the pavement, an additional quantity of level-up material to fill up the ruts must be added to this quantity.

An expression that is somewhat more complicated may be used to estimate the quantities of material that may be removed by heater-planning or by roto-milling, each of which has a maximum depth of cut, d. The equation for the material removed by cutting to a depth, d, is as follows:

Total material removed

$$= \text{Width} \times \sum_{i=1}^{m} A_i \times p(s_i) \times \frac{\text{Length}}{s_i}$$

where A_i = the area of material removed in one bump spacing, s_i

The area depends upon the depth of cut, as follows:

1. If $d \geq 2a_i$, $A_i = a_i s_i$

2. If $d < 2a_i$, then

$$A_i = (a_i - d)\ (2_x d - s_i) + \frac{a_i s_i}{\pi} \sin \frac{2\pi}{s_i} x_d$$

where

$$x_d = \frac{s_i}{2\pi} \text{ arc cos } [\frac{d-a_i}{a_i}]$$

The computation may be done in the same five steps as outlined above for computing the total quantity of level-up material.